HOKKAIDO UNIVERSITY

Title	Titania photocatalysis : New insights in the photocatalytic mechanism and exemplary applications
Author(s)	王, 堃垒
Degree Grantor	北海道大学
Degree Name	博士(環境科学)
Dissertation Number	甲第13118号
Issue Date	2018-03-22
DOI	https://doi.org/10.14943/doctoral.k13118
Doc URL	https://hdl.handle.net/2115/77152
Type	doctoral thesis
File Information	Kunlei_WANG.pdf

Hokkaido University Collection of Scholarly and Academic Papers : HUSCAP

Titania photocatalysis:
New insights in the photocatalytic mechanism, and exemplary applications

酸化チタン系光触媒反応：
光触媒反応機構における新しい視点と典型的応用

2018

Kunlei WANG

Division of Environmental Materials Science,

Graduate School of Environmental Science,

Hokkaido University,

Sapporo, Japan

contents

Symbols and Abbreviations iv

Chapter I General introduction 1

1.1 Photocatalysis 3

1.1.1 History of photocatalysis study 3

1.1.2 Application of titania photocatalyst 6

1.2 Photocatalysts 9

1.2.1 Titania photocatalysts 10

1.2.2 Titania P25 19

1.3 Mechanism of photocatalytic reactions and improvement of photocatalytic activ 21

1.3.1 Volume modification (doping) 23

1.3.2 Surface modification 25

1.4 Purpose of this study 29

1.5 Reference 30

Chapter II P25——mixed-phase titania photocatalyst: Intrinsic high activity of crystalline phase vs "synergy" between crystalline phase 41

2.1 Introduction 43

2.2 Experimental details 50

2.2.1 Separation of anatase and rutile particles from P25 50

2.2.2 Characterization of isolated samples 53

2.2.3 Measurements of photocatalytic activity 57

2.3 Results and discussion 59

2.3.1 Physical isolation 59

2.3.2 Chemical isolation 61

2.4 Summary 74

2.5 References 75

Chapter III Interparticle electron transfer (IPET) 79

3.1 Introduction 81

3.2 Experimental details 84

3.3 Results and discussion 86

3.4 Summary 99

3.5 References 100

Chapter IV Size-controlled noble metal nanoparticles on titania support by modified photodeposition meth 103
4.1 Introduction 104
4.2 Experimental details 108
4.3 Results and discussion 110
4.4 Summary 120
4.5 References 121
Chapter V Exemplary applications of titania photocatalysts 125
5.1 Introduction 127
5.2 Experimental details 132
5.3 Results and discussion 136
5.3.1. Antifungal properties of titania photocatalysts prepared from P2 136
5.3.2. Decomposition of organic compounds and microorganism on titania samples modified with noble me 150
5.4 Summary 169
5.5 References 171
Chapter VI Concluding remarks 179
6.1 Concluding remarks 181
6.2 Future Aspects 185
6.3 Paper published 186
Acknowledgement 187

Symbols and Abbreviations

Ag	silver
ana	isolated-anatase sample
ANA	ISO-ana-200
AOPs	Advanced oxidation processes
AOTs	Advanced Oxidation Technologies
Au	gold
BET	Brunauer-Emmett-Teller equation used for estimation of specific surface area
CO_2	carbon dioxide
CO_2 system	reaction of photocatalytic decomposition of acetic acid
DRS	diffuse reflection spectrosopy
H_2 system	reaction of photocatalytic dehydrogenation of methanol
H_2O	water
H_2O_2	hydrogen peroxide
HomoP25	homogenized P25 titania
HT	hydrothermal process
IEQ	indoor environmental quality
IPCT	interparticle charge transfer
IPET	interparticle electron transfer
ISO	isolated
LSPR	localized surface plasmon resonance
MeOH	methanol
NaOH	sodium hydroxide
NM	noble metal
NP(s)	nanoparticle(s)
OAP	octahedral anatase particles
P25	commercial titania sample
Pt	platinum
RDB-PAS	reversed double-beam photoacoustic spectroscopy
rut	isolated-rutile sample
RUT	ISO-rut-NaOH-200
STEM	scanning transmission electron microscopic
Ti	titanum
TiO2	titania, titanium(IV) dioxide
TNWs	Potassium titanate nanowires
TRMC	resolved microwave conductivity
XPS	X-ray photoelectron spectroscopy
XRD	X-ray diffractometry
ZnO	zinc oxide

Chapter I

General Introduction

1.1 Photocatalysis

Braslavsky described a definition of photocatalysis in *Pure and Applied Chemistr*y, as follows: “Change in the rate of a chemical reaction or its initiation under the action of ultraviolet, visible, or infrared radiation in the presence of a substance — the photocatalyst — that absorbs light and is involved in the chemical transformation of the reaction partners”.[1] In generally, “photocatalysis” is an interdisciplinary science between catalysis and photochemistry, and the “photocatalysis” is the conceptual name for the photocatalytic reactions. Although, photocatalysis is often considered as part of catalysis, it should be pointed that there is crucial difference between both of them, i.e., in the case of catalysis, reaction is accelerated by catalyst (a decrease in an activation energy), whereas, in the case of photocatalysis, reaction usually does not proceed without photocatalyst at all.

1.1.1 History of photocatalysis study

One of the first findings on photocatalysis was noticed by Becquerel in 1839, who observed that sun-light exposed silver chloride (AgCl) electrode in an electrolyte solution could be a source of electricity, and resultant voltage was dependent on the wavelength of the incident light. Titanium(IV) oxide (titania) was developed in 19th century, and widely used as a pigment by artists. In the early 1920s, the phenomenon of pigment color fading was studied. It was suggested that titania could decompose organic dyes and binders of paints. This was probably the earliest time when the phenomenon of photocatalysis was described. In 1921, the first report on “photocatalysis” was published by Renz, in which it was described that titanium dioxide could be reduced by irradiation, resulting in dark coloration, and thus some photocatalytic reaction was suggested, as shown in **equation 1**:

$$TiO_2 + \text{light} \rightarrow Ti_2O_3 \quad \text{or} \quad TiO \qquad (1)$$

Baur et al. were first who obtained zero-valent silver from the silver salt by irradiation of zinc oxide (ZnO) photocatalyst. They suggested that oxidation and reduction reactions proceeded at the same time, as shown by the following mechanism (**equations 2-4**):

$ZnO + hv \rightarrow h+ + e-$ (2)

$h+ + OH- \rightarrow ¼\ O_2 + ½\ H_2O$ (3)

$e- + Ag+ \rightarrow Ag$ (4)

in which, *h:* Planck's constant, *v*: wave frequency, *hv*: photon energy (irradiation), h^+: positive hole; and e^-: the excited electron.

In 1927, the similar reaction mechanism in the reaction of photocatalytic generation of hydrogen peroxide (H_2O_2) on irradiated ZnO was proposed by Baur et al.. Whereas, five years later, Renz reported that metals could be formed on titania and niobium oxide (Nb_2O_2) by photocatalytic reduction.[2, 3] In 1938, Goodeve started the research on decomposition of pigments by TiO_2 powder, and measurements of the absorption spectra and quantum efficiency.[4-6] In that study, it was suggested that titania as catalyst could enhance photochemical oxidation. In 1949, Jacobsen tried to use the redox mechanism to explain the color fading of pigment.[7] It was proposed that the organic part of pigment could be oxidized and titania was reduced.

In 1950s, the study on photocatalysis was mainly focused on ZnO for H_2O_2 photogeneration, confirming the hypothesis of Baur.[8-11] On the other hand, TiO_2 was not famous in that time because the amount of H_2O_2 generated on its surface was relatively small. In 1955, Brattain and Garret found the photoelectric phenomenon through the study on germanium semiconductor electrodes, and from that time, the new field of science i.e., photoelectrochemistry, was started.[12] Filimonov in 1964 explained that dissociative chemisorption of alcohols adsorbed on titania and zinc oxide (ZnO) resulted in formation of alkoxide anions and surface -OH groups.[13, 14] Almost twenty years later, Matsuda and Kato found that photocatalytic activity of TiO_2 depended on crystalline phase, and the activity of anatase was higher than that of rutile.[15]

In 1972, Fujishima and Honda published a report for TiO_2 photoelectrode with ability of decomposition of H_2O to hydrogen and oxygen (electrochemical photolysis of water splitting), which is now called the Honda–Fujishima effect after its discovers.[16] Since this finding,

titania photocatalysis has been intensively studied both for mechanism explanation and possible applications. In 1970s, due to energy and environmental crisis, many studies were performed to solve these emergency problems. From that time, the use of titania as photocatalyst for environmental purification and energy conversion has been intensively investigated, e.g., for hydrogen generation.[17]

The brief history of titania photocatalysis is shown in **Figure 1.1**.[18, 19] Before 1990s, research on titania mainly focused on its possible application (purification of air and water) and improvement of photocatalytic activity, e.g., by deposition of co-catalyst and formation of composite structure (e.g., TiO_2/TS-1 photocatalyst).[20] For example, in 1976, Carey et al. studied the photocatalytic activity of TiO_2 for decomposition of organic compounds in wastewater.[21] In 1977, Frank and Bard reported the photocatalytic oxidization of cyanide ion (CN^-),[22] whereas Schrauzer and Guth studied the reduction of nitrogen (N_2) to ammonia (NH_3) on Fe/TiO_2.[23] In 1985, Matsunaga used TiO_2 as the antimicrobial agent to kill the *Lactobacillus acidophilus, Saccharomyces cerevisiae* and *Escherichia coli*.[24] In 1991, O'Regan and Graetzel used the nano-crystallite TiO_2 modified with dyes as the solar cell (dye sensitized solar cells, DSSCs) to convert the sun-light to the electricity.[25] Six years later, Fujishima group found the photogeneration of highly amphiphilic (both hydrophilic and oleophilic) titania surface and used it for the TiO_2-covered glass with self-cleaning and antifogging properties.[26] After 1990s, the main study on titania photocatalysis has focused on activation of TiO_2 under visible light irradiation by either doping or surface modification (as shortly presented in sections 1.3.1 and 1.3.2, and Chapter V).[27-29]

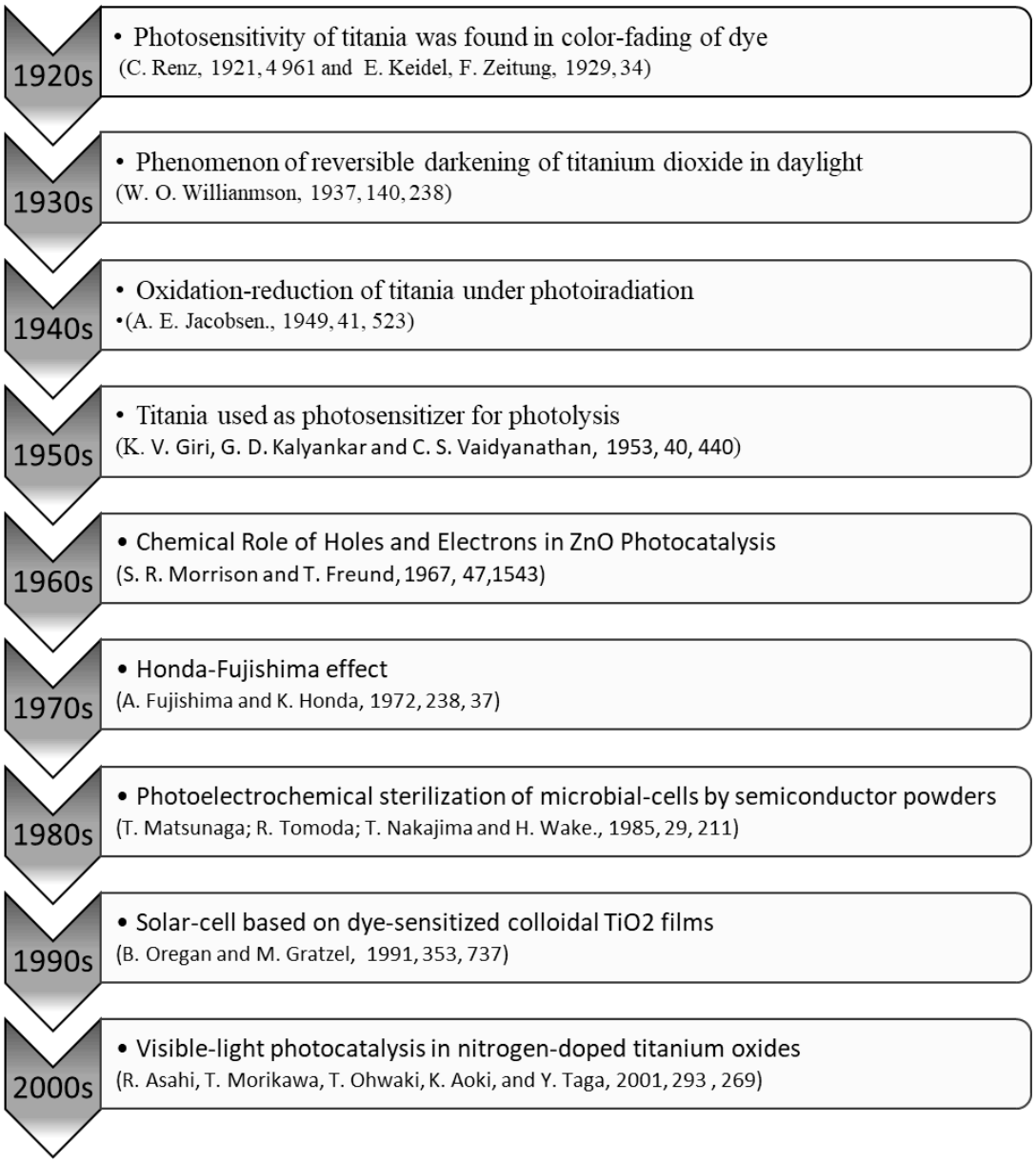


Figure. 1.1 Historical overview of heterogeneous photocatalysis in past 90 years. (since 1921).

1.1.2 Application of titania photocatalysis

Previously, titania was mainly used as a pigment for toothpaste, paints, plastics, textiles and sunscreen creams, due to high brightness and high refractive index. Presently, due to the high photocatalytic activity, chemical stability and low price, titania is used in many fields, e.g., for water and wastewater treatment,[30-36] air purification,[37-40] microorganisms killing,[41-44] self-cleaning surface,[45-49] solar energy conversion[25, 50-54] and so on.

Therefore, many researchers have been intensively studied titania photocatalysts. Especially in Japan, huge achievements in titania photocatalysis have been obtained, not only for fundamental studies, but also in application of titania as photocatalyst.[55] **Table 1.1**, shows some examples of TiO_2 applications, that are shortly discussed, as follows:

Table 1.1 Application of titania photocatalysis[56, 57]

FUNCTION	APPLICATION
self-cleaning	surface of wall, window lamp-chimney noise barrier, traffic mirrors
air purification	in-door air cleaning road, walls of building
Water/wastewater purification	surface/underground water sanitary/industrial sewage
cancer treatment	equipment/medicine
disinfection	indoor wall of hospital, medical uniforms, equipment, food, indoor surrounding

In 1997, Fujishima group found the photogeneration of a highly amphiphilic titania surface. The unique character of this surface is ascribed to the microstructured composition of hydrophilic and oleophilic phases, generated by ultraviolet irradiation.[58] As a result, TiO_2-coated glass with antifogging and self-cleaning, properties has been commonly prepared and commercially used, e.g., the front glass of Institute for Catalyst (ICAT) building.

Polluted indoor air possesses a significant health risk especially in developing countries. Titania under UV irradiation has strong ability to oxidize the organic compounds to CO_2 and H_2O (mineralization). Therefore, the photocatalysis can be used for removing the volatile organic compounds (VOCs), which are common pollutants of the indoor air, such as aldehydes and ketones.[37, 38, 40, 59-62] Moreover, it should be pointed that not only the organic compounds, but also the inorganic pollutant such as carbon monoxide (CO) and nitrogen oxides (NO and NO_2), can be removed by photocatalytic treatment.[63-66] On the other hand, another problem in indoor air is connected with its bad smell, resulting from smoking,

sweating and food spoilage. The main content of bad smell are originates from hydrogen sulfide (H_2S) and ammonia (NH_3). Photocatalysis can be used to remove bad smell by photooxidation of H_2S and NH_3 to sulfur dioxide (SO_2) and nitric acid (HNO_3) respectively.[67-73] Outdoor air pollution is also large environmental problem both in developing (mainly industrial pollution) and developed countries. For example, the number of motor vehicles has been increasing and the exhaust gasses contain various compounds, such as NO_x VOCs, CO, CO_2 and hydrocarbons. Photocatalysis can be used for purification of outdoor air, e.g., when the road and/or the walls near the road are covered by titania layer.[28, 74-81]

Microbiological pollutants are also very dangerous for environment and human. Among them, microscopic mould fungi are ubiquitous in both indoor and outdoor environment. Approximately 500 fungal species have been described as human pathogens. It has been noticed that the systematic human exposure to fungal spores results in an increase of allergies, asthma, respiratory problems, as well as mycoses in the lungs or on the skin. People may be exposed to mould either through inhalation or by skin contact with contaminated dust, and thus a certain level of exposure is inevitable. Although, the chemical compounds used for mould inhibition are quite effective for short-term antimicrobial purposes, their application is risky since they are often toxic. In recent years, numerous ecological and environmentally friendly methods have been extensively studied for the removal of various biological pollutants from air, water, wastewater and surfaces of technical materials. Among them photocatalytic oxidation on titanium dioxide is one of the best known. However, most of studies on the antimicrobial activity of titania were performed for bacteria and yeast. There are only a few studies focusing on the photocatalytic removal of potentially pathogenic fungi since they are much more persistent than simple bacteria organisms.[38, 42, 44, 82-97] Therefore, one of the aims of my thesis was to examine the influence of titania on few species of potentially pathogenic fungi.

1.2. Photocatalysts

In the case of heterogeneous photocatalysis, the "photocatalyst" is semiconductor, in which electron is excited from the conduction band (CB) to valence band (VB) under irradiation with energy equal or larger than its bandgap. The excited electron and positive hole (formed in VB) initiate reactions that cannot carry out spontaneously without photocatalyst, and, at the same time, photocatalyst is not changed.

For the semiconductor materials (often used as photocatalyst), the width of bandgap decides the photoabsorption properties, as show in **Figure. 1.2**.[98-109] The bandgaps of semiconductors are different, as well as the position of CB and VB. When the position of VB is more positive the ability of oxidation is higher; whereas when the position of CB is more negative the ability of reduction is higher. Therefore, the wide bandgap of semiconductor results in the efficient redox properties, (e.g., simultaneous reduction and oxidation of water), but also at the same, wide bandgap means inactivity under visible light. Titania with wide bandgap of ca. 3.0–3.2 eV is known from high photocatalytic activity, but also it is only active under UV irradiation. Accordingly, many studies have been performed to modify its structure, extending its working activity towards vis region of solar spectrum.[110-114]

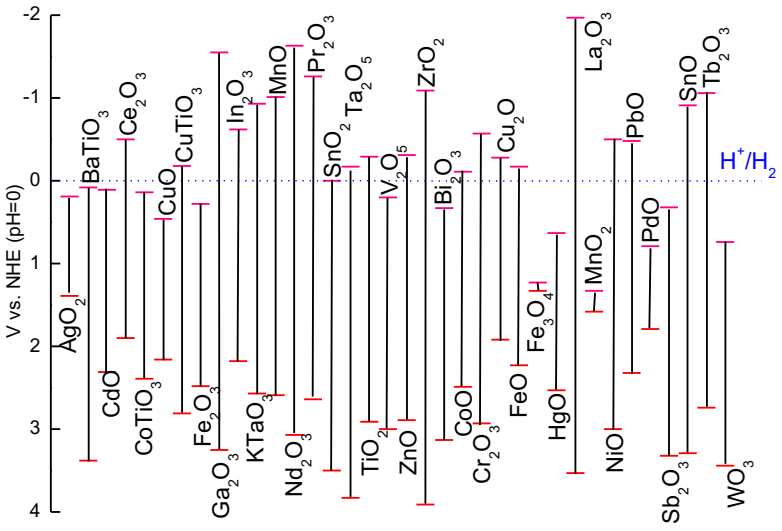


Figure.1.2 Examples of electronic properties of various semiconductors.

1.2.1 Titania photocatalysts

Photocatalytic reactions driven by the photoirradiated semiconducting materials, such as TiO_2, ZnO and tungsten oxide (WO_3), have attracted much attention owing to their availability for a wide range of applications. Among the candidates of photocatalyst for the mineralization of pollutants, it is well known that titania is the best and the sole material, though there are quite large variations in the photocatalytic activity of titania photocatalysts even if they are composed of same chemical composition. The merits of titania as photocatalyst are its photostability, sufficient redox ability, non-toxicity, and availability, as well as that their thin films are colorless and transparent to give no change in appearance of substrate materials (as shown in **Figure 1.3**). The last point should be also a demerit, since it means that titania can absorb only ultraviolet light, but not visible light, which is included mainly in the sunlight. Moreover, as in most of semiconductors, a high rate of recombination between electrons and holes results into low quantum efficiency. This is the reason that many studies have been focused on preparation of visible-light sensitive titania with low rate of charge carriers' recombination by various methods (as discussed in section 1.3 and Chapter V).

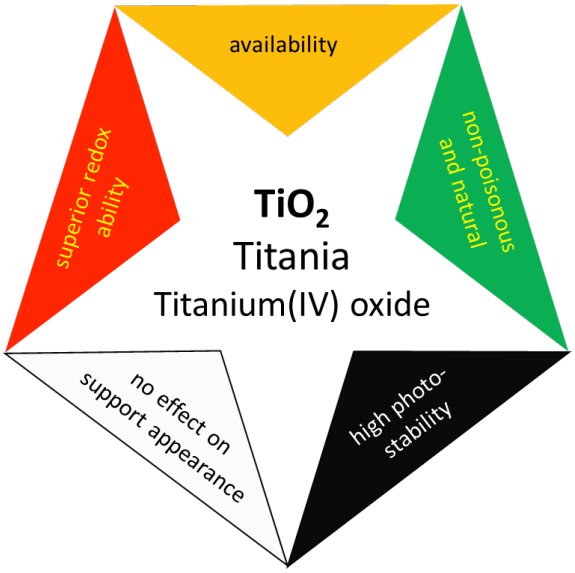


Figure.1.3 The advantage of titania as photocatalyst.

The photoabsorption property of titania is governed by its electronic structure, i.e., a width of band gap, 3.0–3.2 eV, between CB and VB, corresponds to the absorption-edge wavelength of

ca. 385-405 nm. Therefore, the reported strategies for preparation of visible-light sensitive titania can be categorized into two main groups. One is the addition of a small amount of chemical species, to modify the band structure itself to reduce the band-gap energy (cation or anion doping), and the other one is the addition of color compounds that absorb visible light as a sensitizer. In the former case, doping of nitrogen, sulfur, carbon or boron showed to be effective to activate titania under visible light irradiation. However, the doping may also result in formation of recombination centers in the crystalline lattice decreasing quantum yield under UV irradiation (also observed for self-doped titania, i.e., Ti^{3+}-rich titania). On the other hand, in the latter case, organic colored compounds have been often used and it has been clarified that most of those modifiers were decomposed more or less, due to their own photoreaction or photocatalysis by TiO_2. Therefore, noble metals have been used as surface modifiers, primarily because they accelerate the transfer of photoexcited electrons of titania to substrates, e.g. protons to evolve hydrogen (H_2), and recently due to ability of visible light absorption resulting from localized surface plasmon resonance (LSPR), as discussed in Chapter V.[115]

1.2.1.1 Properties of titania photocatalysts

Titania is naturally occurring oxide of titanium, including anatase, rutile and brookite, as shown in **Figure 1.4**. However, in nature titanium mainly appears in the form of various mixed oxides, e.g., ilmenite (titanium iron oxide mineral, $FeTiO_3$), rather than in the pure titania crystals.[116, 117]

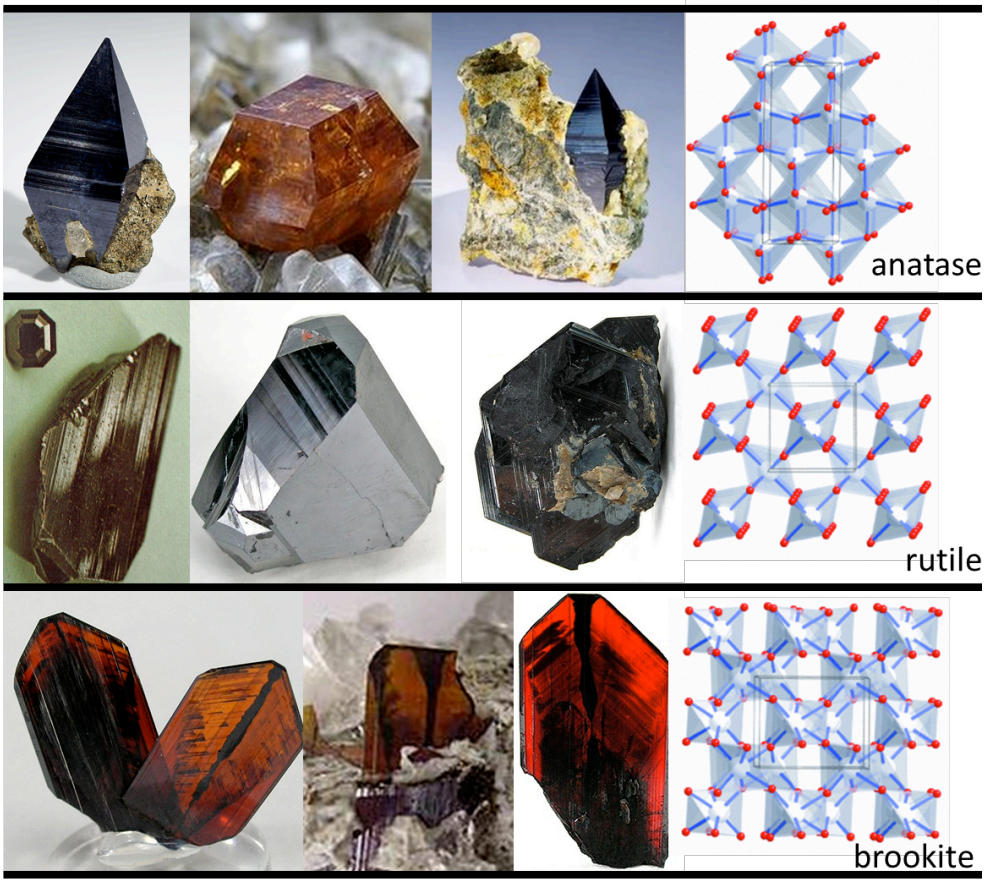


Figure 1.4 Photographs of natural titania minerals and crystallographic structures.

Anatase is usually found as small, isolated and sharply developed crystals, and like rutile, (a more commonly occurring form of titanium dioxide), it crystallizes in the tetragonal system. There are also important differences between the physical properties of anatase and rutile, as follows: the former is less hard (5.5–6 vs. 6-6.5 Mohs) and dense (specific gravity about 3.8 vs. 4.1). Moreover, anatase is optically negative whereas rutile is positive, and its luster is more strongly adamantine or metallic-adamantine than that of rutile. Rutile is the second most abundant mineral sand. Rutile found in primary rock cannot be extracted hence the deposits containing rutile sand can be mined, meaning a reduced availability to the high concentration ore.[55, 116, 118-120] Crude titania (in the form of rutile or synthetic rutile) is purified via converting to titanium tetrachloride in the chloride process.[117, 118]

Anatase and rutile belong to tetragonal system, whereas brookite to orthorhombic system, as shown in **Figure 1.4** and **Table 1.2**. Rutile is the most stable form of titania. Rutile has two

main crystal faces — (110) and (100) — with quite low energy. The most thermally stable is (110), and therefore it has been studied widely. It has rows of bridging oxygens (connected to just two Ti atoms). The corresponding Ti atoms are 6-coordinate. In contrast, the (110) surface also has alternating rows of bridging oxygen and 5-coordinate Ti atoms, but they exist in a different geometric relationship with each other. Brookite is the orthorhombic form of titanium dioxide. At temperatures above ca. 750 °C, brookite transforms to the rutile structure.[121-124] Amorphous titania, is not a crystalline phase (non-crystalline, (NC)). Although this form exhibits low photocatalytic activities, due to various defects working as recombination centers, in recent years, the study on amorphous titania has become more and more popular.[125-134] For example, it is proposed that defects site could be considered as interband energy levels allowing energy transfer from plasmonic noble metal to titania.

Table 1.2 Crystal structure parameter of rutile, anatase and brookite

	rutile	anatase	brookite
crystal structure	tetragonal	tetragonal	othorombic
lattice constants (Å)	a = 4.596	a = 4.596	a = 4.596
	b = 2.958	b = 9.515	b = 5.447
			c = 5.145
molecule /cell	2	4	8
density (g cm^{-3})	4.13	3.79	3.99
Ti-O bond length (Å)	1.949(4)	1.937(4)	1.87-2.04
	1.98(2)	1.965(2)	
O-Ti-O bond angle	81.2°	77.7°	77.0-105°
	90.0°	92.6°	

1.2.1.2 Preparation of titania photocatalysts

A variety of titania nanostructures have been prepared, such as nanoparticles, nanotubes, nanorods, nanofibers and nanoflowers for different applications. These structures can be made by various preparation methods, including commercial methods (industrial processes), such as sulfate and chloride processes, and laboratory methods, e.g., sol-gel, hydrothermal, microwave, reverse micelle and so on. Here, only the most important methods will be shortly described.

Industrial processes

TiO_2 is refined from ilmenite, rutile ore or titanium slag. The most often used methods of titania production are Sulfuric Acid Process and Chloride Process. In the middle of 1980s, the company of Degussa started to product titania nano-powder (named P25) by oxidizing of $TiCl_4$, as presented in **section 1.2.2**

The sulfate process needs simpler technology than the chloride route and is available for cheaper ores of lower grade. However, generally it has higher production costs, due to expensive apparatus for the acid treatment. In contrast, in the case of the chloride route, the construction of a chloroalkali unit may be required. The purer product with the tighter range of particle size could be produced by the chloride route, but anatase pigments could only be obtained by the sulfate route. The sulfate route is recognized as less environmentally friendly. However, considering acid recycling or neutralization, and developments of other byproducts, sulfate methods could be considered as good as the chloride route. Both methods are shortly presented below.

i) Sulfuric Acid Process

The Sulfuric Acid Process (sulfate route) consists of three main steps. The ore, generally an ilmenite, is dissolved in the sulfuric acid to obtain a mixture of sulfates (**equation 5**). The iron is removed from the solution and the color of the final product is not spoiled. The titanyl sulfate hydrolyses in solution to obtain insoluble, hydrated titanium dioxide (**equation 6**). Finally, the solid was heated in an oven to remove the water (**equation 7**) and decompose the residual sulfuric acid. The flowchart of the sulphate route is shown in **Figure 1.5**.

$$TiO_2 \cdot FeO + 2H_2SO_4 \rightarrow TiOSO_4 + FeSO_4 + 2H_2O \quad (5)$$

$$TiOSO_4 + 2H_2O \rightarrow TiO_2 \cdot H_2O + H_2SO_4 \quad (6)$$

$$TiO_2 \cdot H_2O \rightarrow TiO_2 + H_2O \quad (7)$$

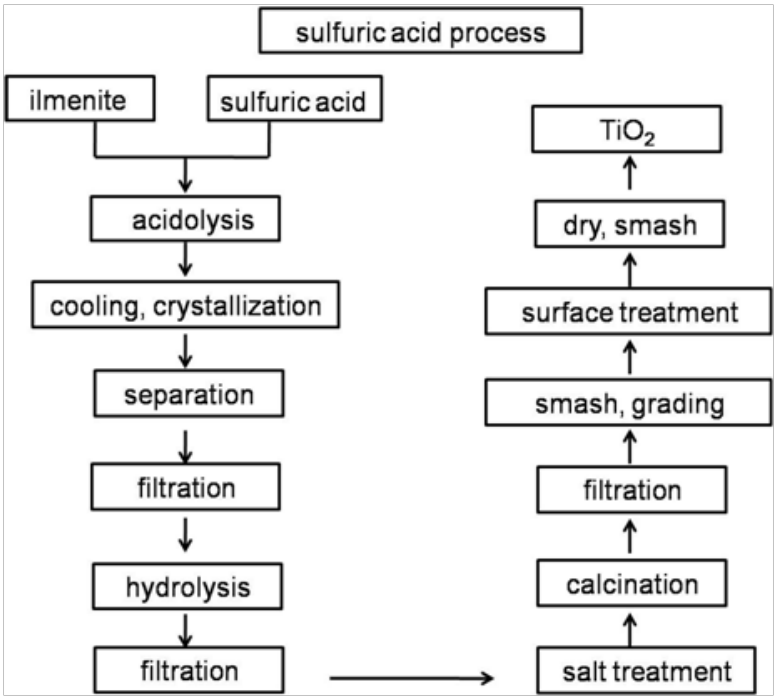


Figure 1.5 Flow chart of the sulfate process.[135]

ii) Chloride Process

The chloride process includes two main steps. At first, to make titanium chloride, dry ore is fed into a chlorinator combined with coke and chlorine (equation 8). The next step is the oxidation of titanium chloride, usually by burning (equation 9). The titanium(IV) oxide is obtained as a fine solid by adding seed crystals to a gas stream. The growth of the crystal is controlled by the nucleating agents. Finally, the products are washed and dried before milling and surface treatment. The flowchart of the chloride process is shown in **Figure 1.6**.

$$2TiO_2 + 3C + 4Cl_2 \rightarrow 2TiCl_4 + 2CO + CO_2 \quad (8)$$

$$TiCl_4 + O_2 \rightarrow TiO_2 + 2Cl_2 \quad (9)$$

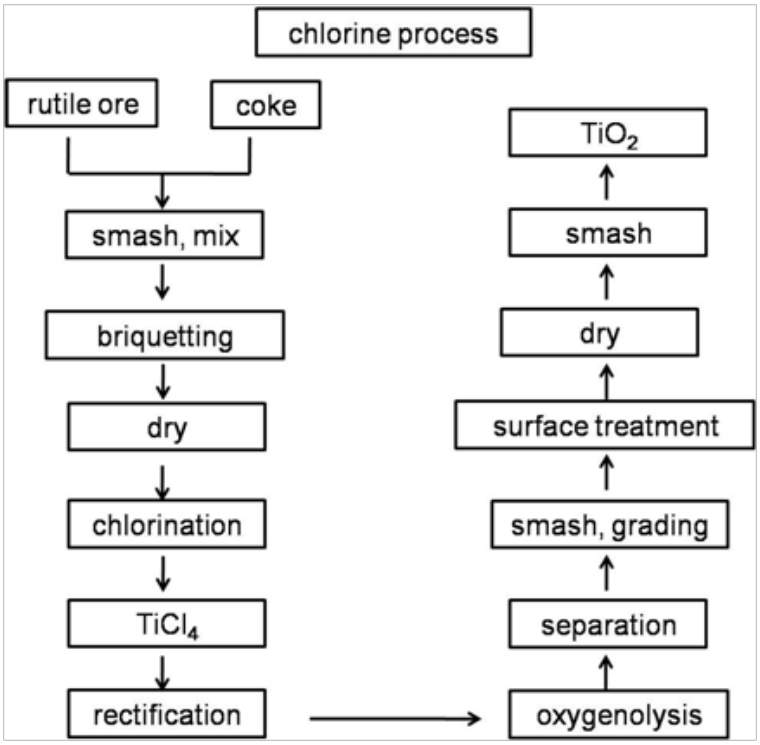


Figure 1.6 Flow chart of the chloride process.

Laboratory processes

The sol-gel method has created a large scope of interest in the preparation od inorganic ceramic and glass materials. This simple, cost effective and low temperature synthesis procedure has also been favored, and largely applied in catalyst preparation, due to its potential to fabricate catalysts by hydrolysis (equations 10-12) and polycondensation (equations 13-14), during which M-OH-M or M-O-M bridges are established between the metallic atoms M of the precursor molecules, resulting in oxides or hydroxides formation. The reaction mechanism is presented below (equations 10-14):

Hydrolysis reactions:

$$Ti(OR)_n + H_2O \rightarrow Ti(OH)(OR)_{n-1} + ROH \quad (10)$$

$$Ti(OH)(OR)_{n-1} + H_2O \rightarrow Ti(OH)_2(OR)_{n-2} + ROH \quad (11)$$

$$\text{The reactions continuously go on: } \rightarrow Ti(OH)_n. \quad (12)$$

Polycondensation reactions:

$$\text{-Ti-OH + HO-Ti} \rightarrow \text{-Ti-O-Ti- + } H_2O \quad (13)$$

$$\text{-Ti-OR + HO-Ti} \rightarrow \text{-Ti-O-Ti- + ROH} \quad (14)$$

The standard sol-gel method is a one-step process, i.e., simple addition of water to titanium alkoxides. However, this one-step process often results in formation of irregular and relatively big particles with low specific surface area (after calcination), and thus is barely used at present. Therefore, the sol-gel method has been improved to a two-step procedure which facilitates the preparation of bare and modified TiO_2 with controlled surface properties. Different elements, both metal and nonmetal (e.g., Ag, Cu, N, C and F), can be doped by introducing additional reactants during the sol-gel process. For example, it was found that doped anatase with Cu was active under visible irradiation, and due to improved separation of photogenerated electrons and holes, possessed also higher photocatalytic activity.[136-139]

The hydrothermal technique is another method for preparation of titania nanoparticles (NPs). Titania samples, prepared by hydrothermal method, show high homogeneity, purity, crystal symmetry, and narrow particle size distributions. The morphologies of titania depends on the process parameters, such as the structure of raw material (precursor), the concentration of alkaline solution (precursor), reaction temperature, pH value, reaction time, and the effect of post-treatment operations, such as acid/alkaline washing, grinding and heating. However, the process capacity is very low, as well as mixing in the reactor (which may cause blockages). Moreover, the difficulty in the scalability of the reactor for high volume throughput makes this method attractive only for small laboratory scale.

The solvothermal method is similar to the hydrothermal method, except that organic solvents are used instead of water. Recently this method has garnered lots of attention in preparation of ceramic materials, such as ZnO_2, CeO_2 and Fe_2O_3. It should be mentioned the temperature and pressure can be elevated much better than that during hydrothermal process. In particular, the solvothermal method is better to control the crystal phase and to obtain narrow size distribution and minimal aggregation.

The microwave-assisted method (microwave heating) has been utilized for material synthesis since late 1960s. It has received a large scope of attention, due to short reaction time and uniform heat distribution. The microwave heating method can be replaced by classical thermal heating to achieve similar temperature conditions. Nevertheless, the virtue of short reaction time and strong molecular oscillation cannot be achieved. However, microwave heating is only additional operation, but not synthesis method, and thus it must be combined with other methods, such as sol-gel, hydrothermal or solvothermal processes to get desired products.

The hard template method for preparation of nanomaterials entails the synthesis of monodisperse tubular or wire-like nanostructures within the pores of membranes or nanoporous solids, that have a preset morphology and porosity allowing the reverse duplication of their structures. The templates are usually anodic aluminum membranes (AAM), polymeric filter membranes, activated carbon, silica or ZnO, which can be removed via chemical etching or combustion after synthesis.

The metallic titanium can be also oxidized directly by oxidants such as O_2, H_2O_2 and O_3 to form TiO_2, all of that can be defined as direct oxidation. For example, TiO_2 nanorods can be obtained through direct oxidation by H_2O_2 at low temperature.[140-143] Moreover, electrochemical oxidation is also very popular for preparation of bare and modified titania nanotubes.[144-151]

The non-hydrolytic sol-gel method, a process based on different experimental conditions and reaction mechanisms, offers the possibility to better control the reaction pathways. A simple way to distinguish the aqueous sol-gel routes from the non-hydrolytic sol-gel routes is that the oxygen-supplied agent in the aqueous sol-gel route is originated from either the directly added water or water produced in situ, whereas, for the non-hydrolytic sol-gel process, the oxygen is provided by alkoxides, ethers, alcohols or anhydrides. Titania powders have been synthesized by non-hydrolytic sol-gel process starting from titanium(IV) chloride, titanium(IV) isopropoxide, carbon tetrachloride, and gelation has been performed in solvothermal conditions, at various temperatures, e.g., 140 °C or 160 °C and 500 °C.[152-156]

It was found that obtained products by non-hydrolytic sol-gel method were very active, e.g., powders obtained at 500 °C of calcination had higher activity than titania P25 for degradation of azo dye (Cl Reactive orange 16).[157, 158]

Gas-phase method is novel method of titania preparation, in which titania is synthesized from $TiCl_4$ and O_2 by rapid heating and quenching of gas reaction mixture, i.e., $TiCl_4$ is fed continuously to a pre-heated vaporizer through which argon passes to introduce $TiCl_4$ into an infrared furnace. Oxygen stream, coaxial with central $TiCl_4$ stream, is also fed to a furnace, in which only central part is heated to high temperature (> 1300 K). This method allows preparation of highly active faceted anatase samples (e.g., decahedral anatase particles (DAP) with eight (101) facets and two (001) facets).[159, 160] Although, this is very new method it has already been commercialized, and DAP titania should be available on the market soon.

1.2.2 Titania P25

Degussa (Evonik) P25 (P25), is a commercial titania photocatalyst, used widely because of its exceptionally high level of photocatalytic activity in many photocatalytic reaction systems. Actually, it is not easy to find a photocatalyst showing activity higher than that of P25. Therefore, P25 has been used as some de-facto standard titania photocatalyst.

1.2.2.1 Preparation of P25

P25 is produced in a similar manner to other AEROSIL processes by utilizing titanium chlorides as a raw material. During AEROSIL processes, $TiCl_4$, as high-purity liquid is vaporized and mixed with air and hydrogen as shown in **Figure. 1.7.** Immediately thereafter gases react at temperatures between 1000 and 2400 °C in a burner leading to the formation of pure and nanostructured titanium dioxide according the reaction (equations 15):

$$TiCl_4 + 2H_2 + O_2 \rightarrow TiO_2 + 4HCl \quad (15)$$

The properties of fumed titania products can be varied widely by adjusting the process parameters, e.g., temperature, duration and concentrations.

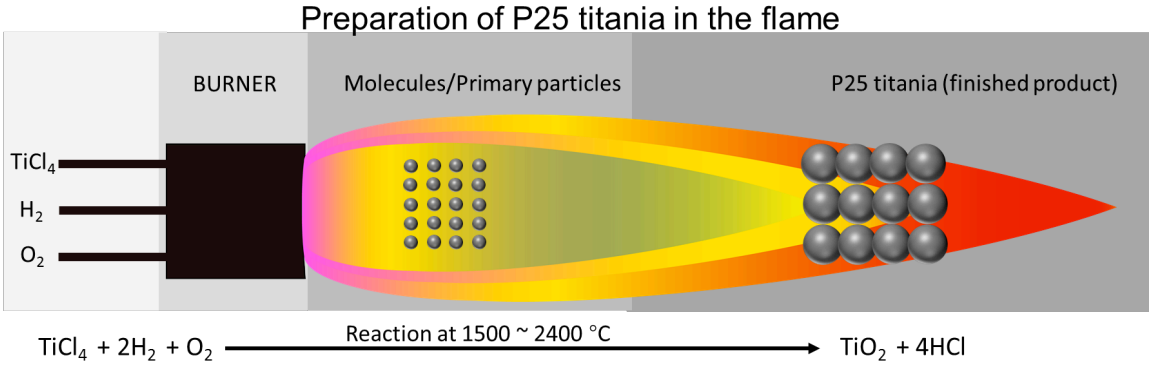


Figure 1.7 Schematic drawing of P25 preparation.

P25 is white powder with fine particles (ca. 25 nm) and hydrophilic character meaning it interacts well with water because the titania surface is coated with hydroxyl groups that can form hydrogen bonds with water molecules. In P25 powder fine particles join and form aggregates (where a number of primary particles are loosely bound together). The density of P25 is ca. 3.9 g cm^{-3} and the specific surface area (SSA) is ca. 50 m^2 g^{-1}. The P25 powder contains a mixture of anatase and rutile in an approximately 5.6:1 proportion. It has been proposed that the mixture of anatase and rutile in this proportion is important to ensure the best photocatalytic properties of titania.[161] Although, there are thousands of reports on P25, they differ significantly, even on the properties of P25. The most often reported ratio of anatase to rutile in P25 was 70:30 or 80:20, without an exact determination of crystalline composition.[162] Anatase, the main composite of P25 is usually the most photocatalytically active polymorph of titania, as shown in many reports.[163, 164] It was suggested that in P25, small crystals of anatase (ca. 25 nm) surround the large crystals of rutile.[162, 165-169] In many reports, rutile is described as low active phase of titania. In P25, its content does not extend ca. 30 %.[162, 165, 170-175] It should be mentioned that P25 consists also amorphous titania.[176] However, in many reports, amorphous phase has not been even considered in P25. Recently, some reports have discussed the photocatalytic activity of amorphous titania.[127, 130, 133, 177-185] The possible reasons of high photocatalytic activity of P25 are discussed in Chapters II and III.

1.3. Mechanism of photocatalytic reactions and improvement of photocatalytic activity

The chemical adsorption of molecule on a solid surface ("A" in **Figure 1.8**) involves a chemical interaction, which in many case determines a transfer of electrons within the adsorbent and the adsorbing species. The net effect is an energetic perturbation, more or less strong, of the electronic structure of the adsorbed molecule. When photons hit the surface of a solid, on which adsorbed species are present, chemical transformation of these species can occur via two different mechanisms, i.e.,[115]

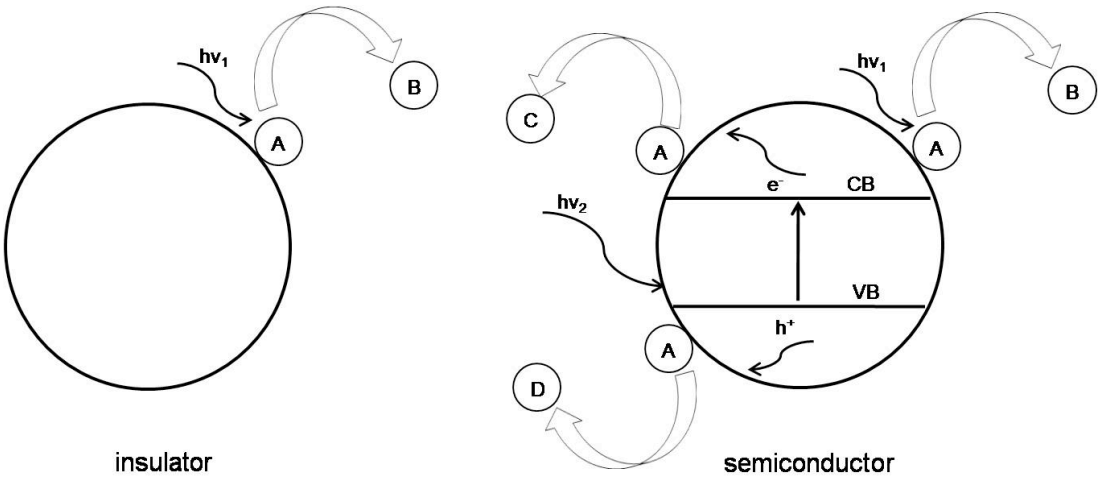


Figure 1.8 Schematic drawing of mechanisms of photolysis and photocatalysis of adsorbed species on insulator (left) and on semiconductor (right): A – adsorbate, A → B – photolysis, A → C – photocatalytic reduction, A → D – photocatalytic oxidation.

i) If the solid is an insulator compound, one or more adsorbed species may be excited by light of suitable energy and then may undergo chemical transformation, as show in **Figure 1.8**, left. This type of process is referred as "photolysis of adsorbed species".

ii) If the solid is a semiconductor compound, the light may also excite the solid, which photogenerates charge carriers' pairs, i.e., electrons and holes (e^-/h^+), as shown in **Figures 1.8**. The mechanism of semiconductor photocatalysis consists in i) excitation of semiconductor with light energy equal or larger than its band-gap energy ($E \geq E_g$), resulting in formation of pairs of charge carriers: electrons and holes (e^-/h^+), ii) charge carriers migration to the

semiconductor surface (or their recombination, "bulk recombination"), and (c) finally, reaction of charge carriers with adsorbed species (or their recombination, "surface recombination"), as shown in **Figure. 1.9**. In the presence of water and oxygen in the system, reactive oxygen species (ROS), such as superoxide ($^{\bullet}O_2^-$), hydrogen peroxide (H_2O_2), hydroxyl radicals ($^{\bullet}OH$), are formed and easily react with all organic and inorganic compounds. Hydroxyl radicals are known as the strongest oxidant, which could be used in water, and the processes/technologies, which use $^{\bullet}OH$ are known as Advanced Oxidation Processes/Technologies (AOPs/AOTs). It should be pointed that ROS are generated by both oxidation and reduction pathways when oxygen is present in the system, i.e., formation of $^{\bullet}O_2^-$ by scavenging of electrons by oxygen (as shown in **Figure. 1.9**).

It is worth noting that the processes which occur by the photolytic mechanism are possible when the solid is insulator and the role of the light is mainly that of exciting the adsorbed species. Whereas, for photocatalytic reactions occurring on the semiconductor, both mechanism can occur, i.e., photolysis of adsorbed species and photocatalysis.

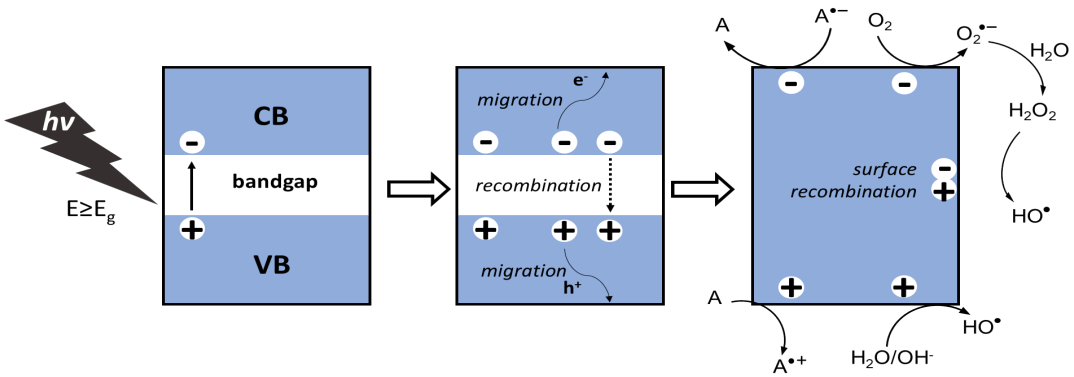


Figure 1.9 Schematic mechanism of semiconductor photocatalysis: (left) semiconductor excitation, (center) charge carriers migration to the surface and/or recombination, (right) reactions on semiconductor surface; CB - conduction band, VB - valence band, E_g - band-gap energy, e^- - electron, h^+ - hole, A - adsorbate.

The photocatalytic activity is controlled by various physical/structural properties, such as crystallinity, crystal size, particle size, specific surface area and morphology. Usually, large specific surface area, high crystallinity, small crystal size and anatase phase result in enhanced photocatalytic activity. However, it should be mentioned that also particular reaction, mobility

of electrons and distribution of electron traps influence the overall photocatalytic performance. Detailed studies on properties-governed activity, performed for 35 commercial titania samples, showed complexity of titania photocatalysis, and difficulty to find clear property-activity correlation (key-factor of high photocatalytic activity).[186] It should be pointed out that usually the change of one property during photocatalyst synthesis results in the simultaneous change of another property. Therefore, it is difficult to find the direct correlation between the photocatalytic activity and one certain property, even for self-prepared samples with well controlled properties. Despite all these difficulties and complexity of photocatalytic reactions, the structure-activity correlation is commonly used for understanding the principles of photocatalytic reactions.

As mentioned before, the improvement of photocatalytic activity of titania photocatalysts could be performed by two processes. One is reducing the recombination of charge carriers (both the surface recombination and bulk recombination), and another is improving the ability of light-absorption. Two main methods of activity improvement can be considered, i.e., surface modification and doping as shortly described below. Formation of heterojunctions, and thus interparticle charge transfer (discussed in Chapter III) could also result in activity improvement.

1.3.1 Volume modification (doping)

The doping of metal oxide materials (substitutional or interstitial) with metal or nonmetal elements is responsible for a change of the chemical nature in the solid, which is intrinsically connected with attractive and repulsive forces combined into a chemical bond.[187] Recently, many theoretical and experimental studies have been developed to investigate the metal (Fe, Cr, V Mo. Re, Ru, Mn, Co, Rh, Bi)[188-196] and nonmetal (N, S, B, C, F) doping effect on the electronic structure of titania photocatalysts.[111, 113, 197-199]

Vis activity of titania incorporated by doping can result from (a) a lower shift of conduction band minimum (CBM), (b) a higher shift of valence band maximum (VBM), and

(c) impurity states in the band gap, as shown in **Figure 1.10**. The following requirements have been defined for the doped photocatalysts:

1) the CBM should be higher than the H_2/H_2O level while the VBM lower than the O_2/H_2O level to ensure photoreduction and photooxidation activities for water splitting, respectively;

2) the states in the gap should be shallow or mixed with the band states of TiO_2 to transfer photo- or thermally excited carriers to reactive sites at the photocatalyst surface within their lifetime,[200]

Large number of studies reported that titania co-doped with different elements could exhibit much higher photocatalytic activity than singly doped photocatalyst, because of the synergistic effect between the doping elements promoting the vis absorption and facilitating the separation efficiency of photogenerated electron-hole pairs. For example, the tri-doped titania with N, F and Ta, prepared using NH_3 and TaF_5 as precursors, was efficient for phenol degradation under vis due to some increased surface area, increased hydroxyl radical generation and high vis absorption.[201]

Different from impurity doping, self-doping that produces Ti^{3+} species in TiO_2 has also been proven to be an effective way for extending the optical absorption of TiO_2 towards vis region. If a Ti^{4+} ion is changed to Ti^{3+} ion then the local electrostatic balance will be broken, and an oxygen vacancy will be introduced because of charge compensation. Ti^{3+} ions and oxygen vacancies can cause a visible light absorption, due to the induced mid-gap states within the band gap of TiO_2 resulting in the change of powder color from white to gray, yellow, blue or black.

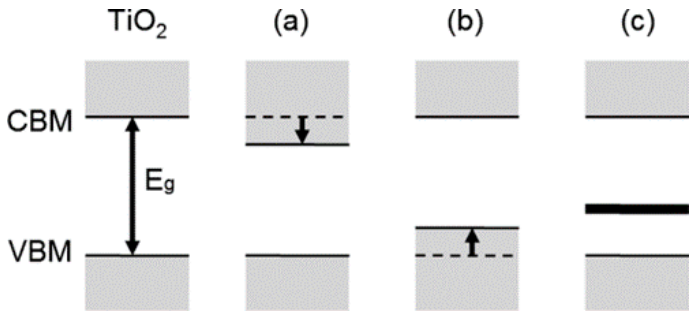


Figure 1.10 Three schemes of the band gap modifications for visible-light sensitization with lower shift of CBM (a), a higher shift of VBM (b), and impurity states (c).[200]

Copyright © 2014, American Chemical Society, all Rrights reserved

1.3.2 Surface modification

Surface modification is the process of modifying the surface of material by bringing physical, chemical or biological characteristics different from the ones originally found on the surface of a material. Various compounds could be used as surface modifiers, e.g., metals (in the form of metallic NPs (zero-valent metal) or chemical compounds), nonmetals (adsorbed anions or chemical compounds), organic compounds (colorless and color such as dyes). Finally, heterojunctions between semiconductors should be considered as another type of surface modification.

Many organic compounds have been used as surface modifiers. There are two main mechanisms of their action, i.e., (1) sensitization mechanism (usually for dyes, where dye is excited with visible light) or (2) formation of complex structure (organic compound-semiconductor) with ability of vis absorption. Modification of semiconductors with dyes has been extensively studied after the invention of dye sensitized solar cells (DSSCs) by O'Regan and Graetzel. First DSSCs with high efficiency was reported by aforementioned authors in 1991 for 10-μm-thick and transparent film of titania NPs of a few nanometers in size, coated with a monolayer of a charge-transfer dye (trimeric ruthenium complex: RuL2(μ-(CN)Ru(CN)L'2)2; where L – 2,2' bipyridine-4,4'-dicarboxylic acid and L' – 2,2'-bipyridine).[202]

Very interesting example was shown for titania modification with urea (usually such

modification was reported as resulting in titania N-doping) by D. Mitoraj and H. Kisch.106 It was proved that during thermal decomposition of urea, titania acted as thermal catalyst for the conversion of intermediate isocyanic acid to cyanamide, and then trimerization of cyanamide to melamine followed by polycondensation to melem- and melon-based poly(aminotri-s-triazine) derivatives, as shown in **Figure 1.11**. It was proposed that absorption at vis range is a charge-transfer band enabling an optical electron transfer from the polytriazine component to titania. This material showed an unique example of inorganic with and organic (polytriazine was present as a crystalline layer) semiconductor connected through Ti-N-C bond.[203]

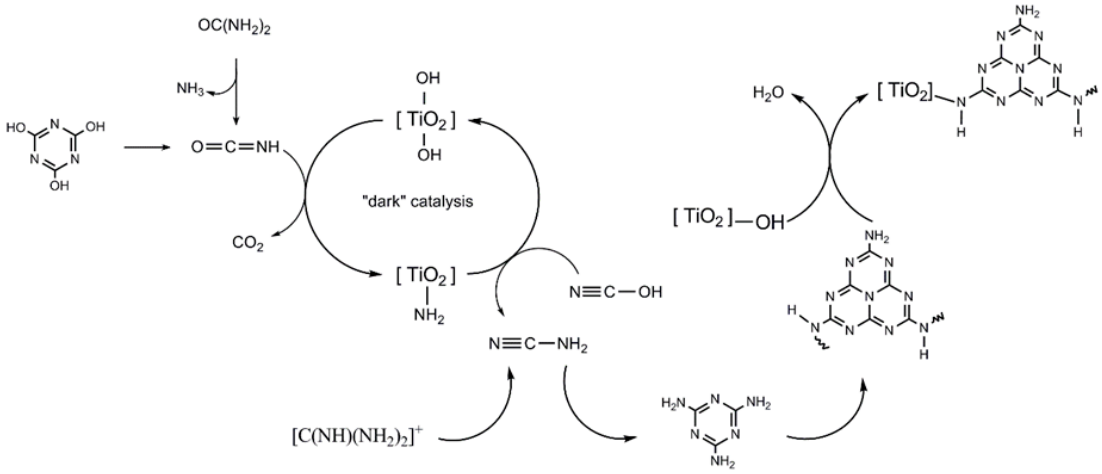


Figure 1.11 Mechanism of urea-induced titania modification.

The most frequently employed modification method for improving the photocatalytic activity of titania (or other photocatalysts) is its loading with NPs of metals (as shown in **Figure 1.12**). Various metals, such as Pt, Au, Ag and Cu have been employed for modification of titania by different methods, e.g., photodeposition, deposition-precipitation, ion-exchange, radiolysis and impregnation. It is well known that Schottky junction is formed on the interface metal-semiconductor.[204-206] As consequence, the high photocatalytic activity of metal-modified titania under UV irradiation is obtained, i.e., metal works as an electron pool resulting in inhibition of charge carriers' recombination. Besides, metal ions with a standard redox potential more positive than conduction band of titania can be photoreduced to the

low-valent states by photogenerated electron under UV irradiation, and then be deposited on the surface of titania (photodeposition method – commonly used for preparation of titania modified with noble metals).[207-213] Moreover, the noble metal (NM) NPs have the property of collective free electron resonance when excited by visible light, known as the localized surface plasmon resonance (LSPR).[209, 214-216] When these NMNPs are loaded on the titania surface, the plasmon-induced electrons are transferred from the plasmonic excited noble-metal NPs to the CB of titania. This results in appearance of visible light activity of NM-modified titania, and is known as "plasmonic photocatalysis". This mechanism is similar to titania sensitization by dyes (DSSCs), suggesting possible oxidation of noble metal. Therefore, application of sacrificial electron donors such as alcohols or Fe^{2+} have been proposed. It should be noted that the LSPR-induced photoeffect is significantly influenced by the property of TiO_2 support (size, shape, surface area, crystallinity).[217]

Various methods of preparation of NM-modified titania have been reported. Either firstly NM nanostructures are synthesized and then deposited on titania, or: i) titania is synthesized on NM nanostructures, ii) cations of NM are directly reduced on titania by chemical, photochemical, thermal and sonochemical methods, iii) NM is deposited on titania by other methods, e.g. electrophoretic and sintering, iv) NM and titania are synthesized simultaneously during hydrothermal method, laser pyrolysis and hydrolysis of titanium tetrabutoxide/isopropoxide followed by titania crystallization and formation of gold nanoparticles (NPs).[218] For example, Cameron et al. developed a facile method to prepare TiO_2/Au NPs, in which TiO_2 colloidal spheres serve as templates for the nucleation and growth of Au NPs in order to achieve controlled size distribution.[219, 220] On the other hand, if this interaction is weak, during the photocatalytic reaction, gold NPs may move on the surface of titania through Ostwald ripening, forming larger gold particles and losing their catalytic activity. Clearly, the developments of more facile strategies to prevent Au NPs from aggregation and improve the interaction with support are desirable to achieve highly efficient Au/TiO_2 photocatalysts.[221] Photodeposition method is commonly used for loading of noble metals on TiO_2 surface. This technique takes full advantage of photogenerated electrons for

reduction of metal cations and thus, formation of metal NPs. It has been proposed that metal NPs are formed on "reaction centers"/"defects" on the titania surface. This was proved when gold was deposited on 15 commercial titania samples, and fine titania with large content of defects (electron traps, ETs) stimulated formation of fine gold nanoclusters, whereas large titania with low content of ETs possessed large gold NPs (lack of nucleation sites resulting in gold aggregation).[222]

Although, activity of plasmonic photocatalysts has been proved for various reactions (decomposition of organic compounds, inactivation of microorganism, solar energy conversion), the overall activity (quantum yield) is still low and should be improved (for possible commercial applications), as discussed in Chapter V.

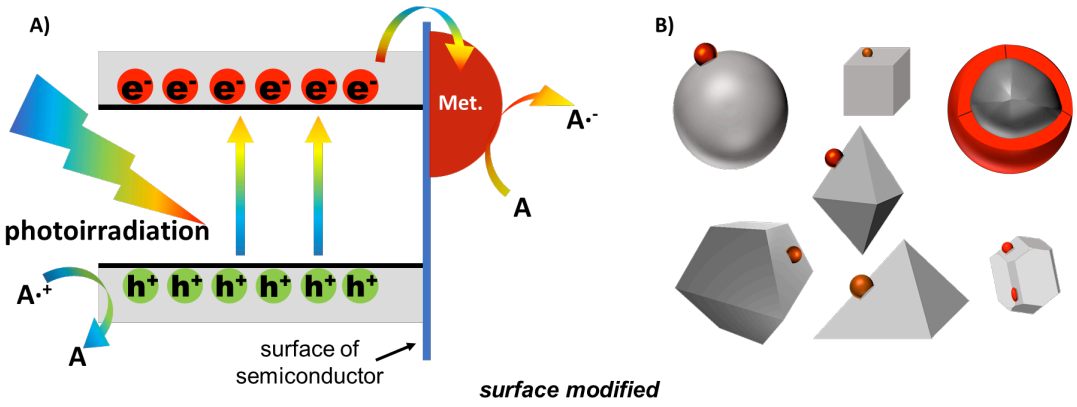


Figure.1.12 Schematic drawings of: A) electron transfer from semiconductor to metal NPs, and B) exemplary metal-titania nanostructures: grey-titania, red-metal.

1.4. Purpose of this study

Although, plenty of studies have been performed on titania photocatalysis, there are still many unanswered questions on photocatalytic performance of titania, e.g., the key-factors of photocatalytic activity and the mechanism of photocatalytic reactions. Of course, it is known that small particle size (and thus large specific surface area), high crystallinity and large bandgap (anatase presence) usually result in high photocatalytic activity. However, exceptionally high photocatalytic activity of P25 (mixed-phase titania) could not be simply explained by its properties. Therefore, various reasons of its activity have been presented, and mainly the "synergy" between anatase and rutile has been postulated. Although, recent study has rejected the "synergy" idea since it was found that intrinsic properties of isolated phases from P25 were responsible for high activity in various reaction systems, the efficiency of methanol dehydrogenation on P25 was much higher than that on rutile and anatase. It should be mentioned that in this reaction, Pt NPs have been used as co-catalyst. Therefore, not only the properties of titania, but also the properties of Pt deposits should be considered for explanation of photocatalytic performance (both the efficiency and the mechanism). Accordingly, the first aim of this thesis was to explain the reason of high activity of P25 for methanol dehydrogenation, considering the properties of both titania and platinum. During investigations, new findings on titania photocatalysis have been discovered, such as interparticle electron transfer (IPET) and preferential platinization of rutile. However, also some problems have been observed, such as aggregation of Pt NPs. Therefore, second aim of my study was to inhibit this aggregation. I have found new method of metal photodeposition on titania, which allows to control the properties of platinum (and other noble metals), and thus resultant photocatalytic activities. The final aim of my research was to propose/obtain the photoactive materials with ability to work under solar radiation (both UV and vis range of solar spectrum) for environmental applications, such as decomposition of organic compounds, evolution of hydrogen and inactivation of microorganisms (bacteria and fungi).

1.5. References

1. Braslavsky, S. E., *Pure and Applied Chemistry* **2007,** *79* (3), 293-465.
2. Renz, C., *Helvetica Chimica Acta* **1932,** *15*, 839-842.
3. Renz, C., *Helvetica Chimica Acta* **1932,** *15*, 1077-1084.
4. Goodeve, C. F., *Transactions of the Faraday Society* **1937,** *33*.
5. Goodeve, C. F.; Kitchener, J. A., *Transactions of the Faraday Society* **1938,** *34* (1), 0570-0579.
6. Goodeve, C. F.; Kitchener, J. A., *Transactions of the Faraday Society* **1938,** *34* (2), 0902-0908.
7. Jacobsen, A. E., *Industrial and Engineering Chemistry* **1949,** *41* (3), 523-526.
8. Rubin, T. R.; Calvert, J. G.; Rankin, G. T.; MacNevin, W., Photochemical Synthesis of Hydrogen Peroxide at Zinc Oxide Surfaces1. *Journal of the American Chemical Society* **1953,** *75* (12), 2850-2853.
9. Markham, M. C.; Laidler, K. J., A Kinetic Study of Photo-oxidations on the Surface of Zinc Oxide in Aqueous Suspensions. *The Journal of Physical Chemistry* **1953,** *57* (3), 363-369.
10. Calvert, J. G.; Theurer, K.; Rankin, G. T.; MacNevin, W. M., *Journal of the American Chemical Society* **1954,** *76* (9), 2575-2578.
11. Vail, C. B.; Holmquist, J. P.; White, L., *Journal of the American Chemical Society* **1954,** *76* (2), 624-625.
12 Garrett, C. G. B.; Brattain, W. H., *Physical Review* **1955,** *99* (2), 376-387.
13. Filimonov, V. N., *Doklady Akademii Nauk Sssr* **1964,** *154* (4), 922-&.
14. Filimonov, V. N., *Doklady Akademii Nauk Sssr* **1964,** *158* (6), 1408-&.
15. Matsuda, S.; Kato, A., *Applied Catalysis* **1983,** *8* (2), 149-165.
16. Fujishima, a.; Honda, K., *Nature* **1972,** *238*, 37.
17. Jitputti, J.; Suzuki, Y.; Yoshikawa, S., *Catalysis Communications* **2008,** *9* (6), 1265-1271.
18. Hashimoto, K.; Irie, H.; Fujishima, A., *Japanese Journal of Applied Physics Part 1-Regular Papers Brief Communications & Review Papers* **2005,** *44* (12), 8269-8285.
19. Serpone, N.; Emeline, A. V.; Horikoshi, S.; Kuznetsov, V. N.; Ryabchuk, V. K., *Photochem Photobiol Sci* **2012,** *11* (7), 1121-50.
20. Lu, G. X.; Gao, H. X.; Suo, J. H.; Li, S. B., *Journal of the Chemical Society-Chemical Communications* **1994,** (21), 2423-2424.
21. Carey, J. H.; Lawrence, J.; Tosine, H. M., *Bulletin of Environmental Contamination and Toxicology* **1976,** *16* (6), 697-701.
22. Frank, S. N.; Bard, A. J., *Journal of the American Chemical Society* **1977,** *99* (14), 4667-4675.
23. Schrauzer, G. N.; Guth, T. D., *J Am Chem Soc* **1977,** *99* (22), 7189-93.
24. Matsunaga, T.; Tomoda, R.; Nakajima, T.; Wake, H., *FEMS Microbiology Letters* **1985,** *29* (1-2), 211-214.
25. O'Regan, B.; Grätzel, M., *Nature* **1991,** *353*, 737.

26. Watanabe, T.; Nakajima, A.; Wang, R.; Minabe, M.; Koizumi, S.; Fujishima, A.; Hashimoto, K., *Thin Solid Films* **1999,** *351* (1-2), 260-263.
27. Wu, T. X.; Liu, G. M.; Zhao, J. C.; Hidaka, H.; Serpone, N., *Journal of Physical Chemistry B* **1998,** *102* (30), 5845-5851.
28. Khalil, L. B.; Mourad, W. E.; Rophael, M. W., *Applied Catalysis B-Environmental* **1998,** *17* (3), 267-273.
29. Zang, L.; Macyk, W.; Lange, C.; Maier, W. F.; Antonius, C.; Meissner, D.; Kisch, H., *Chemistry-a European Journal* **2000,** *6* (2), 379-384.
30. Hofstadler, K.; Bauer, R.; Novalic, S.; Heisler, G., *Environmental Science & Technology* **1994,** *28* (4), 670-674.
31. Davis, R. J.; Gainer, J. L.; Oneal, G.; Wu, I. W., *Water Environment Research* **1994,** *66* (1), 50-53.
32. Herrmann, J. M., *Catal Today* **1999,** *53* (1), 115-129.
33. Arslan, I.; Balcioglu, I. A.; Tuhkanen, T.; Bahnemann, D., *Journal of Environmental Engineering-Asce* **2000,** *126* (10), 903-911.
34. Banfield, J. F.; Zhang, H. Z., *Nanoparticles and the Environment* **2001,** *44*, 1-58.
35. Dunlop, P. S. M.; Byrne, J. A.; Manga, N.; Eggins, B. R., *Journal of Photochemistry and Photobiology a-Chemistry* **2002,** *148* (1-3), 355-363.
36. Gao, W. L.; Jin, R. C.; Chen, J. X.; Guan, X. X.; Zeng, H. S.; Zhang, F. X.; Liu, Z. G.; Guan, N. J., *Catalysis Letters* **2003,** *91* (1-2), 25-30.
37. Jacoby, W. A.; Blake, D. M.; Fennell, J. A.; Boulter, J. E.; Vargo, L. M.; George, M. C.; Dolberg, S. K., *Journal of the Air & Waste Management Association* **1996,** *46* (9), 891-898.
38. Goswami, D. Y.; Trivedi, D. M.; Block, S. S., *Journal of Solar Energy Engineering-Transactions of the Asme* **1997,** *119* (1), 92-96.
39. Peral, J.; Domenech, X.; Ollis, D. F., *Journal of Chemical Technology and Biotechnology* **1997,** *70* (2), 117-140.
40. Henschel, D. B., *Journal of the Air & Waste Management Association* **1998,** *48* (10), 985-994.
41. Markowska-Szczupak, A.; Wang, K. L.; Rokicka, P.; Endo, M.; Wei, Z. S.; Ohtani, B.; Morawski, A. W.; Kowalska, E., *J Photoch Photobio B* **2015,** *151*, 54-62.
42. Krishna, V.; Pumprueg, S.; Lee, S. H.; Zhao, J.; Sigmund, W.; Koopman, B.; Moudgil, B. M., *Process Safety and Environmental Protection* **2005,** *83* (B4), 393-397.
43. Long, T. C.; Saleh, N.; Tilton, R. D.; Lowry, G. V.; Veronesi, B., *Environmental Science & Technology* **2006,** *40* (14), 4346-4352.
44. Benabbou, A. K.; Derriche, Z.; Felix, C.; Lejeune, P.; Guillard, C., *Appl Catal B-Environ* **2007,** *76* (3-4), 257-263.
45. Lam, S. W.; Soetanto, A.; Amal, R., *Journal of Nanoparticle Research* **2009,** *11* (8), 1971-1979.
46. Quagliarini, E.; Bondioli, F.; Goffredo, G. B.; Licciulli, A.; Munafo, P., *Journal of Cultural Heritage* **2013,** *14* (1), 1-7.
47. Pinho, L.; Rojas, M.; Mosquera, M. J., *Applied Catalysis B-Environmental* **2015,** *178*, 144-154.

48. Moafi, H. F., Photocatalytic self-cleaning properties of lanthanum and silver co-doped TiO2 nanocomposite on polymeric fibers. *Iranian Journal of Catalysis* **2016,** *6* (3), 281-292.
49. Wu, H. Q.; Liu, Y. J.; Mao, L.; Jiang, C. H.; Ang, J. M.; Lu, X. H., *Journal of Membrane Science* **2017,** *532*, 20-29.
50. Scaife, D. E., *Solar Energy* **1980,** *25* (1), 41-54.
51. Kay, A.; Gratzel, M., *Solar Energy Materials and Solar Cells* **1996,** *44* (1), 99-117.
52. Park, N. G.; Schlichthorl, G.; van de Lagemaat, J.; Cheong, H. M.; Mascarenhas, A.; Frank, A. J., *Journal of Physical Chemistry B* **1999,** *103* (17), 3308-3314.
53. Park, N. G.; van de Lagemaat, J.; Frank, A. J., *Journal of Physical Chemistry B* **2000,** *104* (38), 8989-8994.
54. Chappel, S.; Chen, S. G.; Zaban, A., *Langmuir* **2002,** *18* (8), 3336-3342.
55. Fujishima, A.; Rao, T. N.; Tryk, D. A., *Journal of Photochemistry and Photobiology C: Photochemistry Reviews* **2000,** *1* (1), 1-21.
56. Nakata, K.; Fujishima, A., *Journal of Photochemistry and Photobiology C-Photochemistry Reviews* **2012,** *13* (3), 169-189.
57. Fujishima, A.; Zhang, X. T.; Tryk, D. A., *Surface Science Reports* **2008,** *63* (12), 515-582.
58. Wang, R.; Hashimoto, K.; Fujishima, A.; Chikuni, M.; Kojima, E.; Kitamura, A.; Shimohigoshi, M.; Watanabe, T., *Nature* **1997,** *388* (6641), 431-432.
59. Obee, T. N.; Brown, R. T., *Environmental Science & Technology* **1995,** *29* (5), 1223-1231.
60. Dreyer, M.; Lobban, L. L.; Newman, G.; Harwell, J. H., *Abstracts of Papers of the American Chemical Society* **2000,** *220*, U417-U417.
61. Pichat, P.; Disdier, J.; Hoang-Van, C.; Mas, D.; Goutailler, G.; Gaysse, C., *Catalysis Today* **2000,** *63* (2-4), 363-369.
62. Zhao, J.; Yang, X. D., *Building and Environment* **2003,** *38* (5), 645-654.
63. Ao, C. H.; Lee, S. C., *Journal of Photochemistry and Photobiology a-Chemistry* **2004,** *161* (2-3), 131-140.
64. Bianchi, C. L.; Pirola, C.; Galli, F.; Cerrato, G.; Morandi, S.; Capucci, V., *Chemical Engineering Journal* **2015,** *261*, 76-82.
65. Folli, A.; Campbell, S. B.; Anderson, J. A.; Macphee, D. E., *Journal of Photochemistry and Photobiology a-Chemistry* **2011,** *220* (2-3), 85-93.
66. Gandolfo, A.; Rouyer, L.; Wortham, H.; Gligorovski, S., *Applied Catalysis B-Environmental* **2017,** *209*, 429-436.
67. Aguilar-Romero, M.; Camposeco, R.; Castillo, S.; Marin, J.; Rodriguez-Gonzalez, V.; Garcia-Serrano, L. A.; Mejia-Centeno, I., *Fuel* **2017,** *198*, 123-133.
68. Ettireddy, P. R.; Ettireddy, N.; Mamedov, S.; Boolchand, P.; Smirniotis, P. G., *Applied Catalysis B-Environmental* **2007,** *76* (1-2), 123-134.
69. Li, L. L.; Zhang, L.; Ma, K. L.; Zou, W. X.; Cao, Y.; Xiong, Y.; Tang, C. J.; Dong, L., *Applied Catalysis B-Environmental* **2017,** *207*, 366-375.
70. Wang, Z. H.; Li, X. J.; Song, W. J.; Chen, J. F.; Li, T.; Feng, Z. P., *Reaction Kinetics Mechanisms and Catalysis* **2011,** *103* (2), 353-365.

71. Boyjoo, Y.; Su, H. Q.; Liu, J.; Pareek, V. K.; Wang, S. B., *Chemical Engineering Journal* **2017,** *310*, 537-559.
72. Canela, M. C.; Alberici, R. M.; Jardim, W. F., *Journal of Photochemistry and Photobiology a-Chemistry* **1998,** *112* (1), 73-80.
73. Vu, T. H. T.; Au, H. T.; Nguyen, T. T. T.; Do, M. H.; Pham, M. T.; Bui, D. H.; Phan, T. S.; Nguyen, D. L., *Journal of Sulfur Chemistry* **2017,** *38* (3), 264-278.
74. Busca, G.; Lietti, L.; Ramis, G.; Berti, F., *Applied Catalysis B-Environmental* **1998,** *18* (1-2), 1-36.
75. Khalil, L. B.; Rophael, M. W.; Mourad, W. E., *Applied Catalysis B-Environmental* **2002,** *36* (2), 125-130.
76. Son, G. S.; Yun, S. W.; Ko, S. H.; Song, J. W.; Lee, K. Y., *Journal of Advanced Oxidation Technologies* **2003,** *6* (1), 80-92.
77. Imoberdorf, G. E.; Irazoqui, H. A.; Alfano, O. M.; Cassano, A. E., *Chem Eng Sci* **2007,** *62* (3), 793-804.
78. Lim, M.; Zhou, Y.; Wang, L. Z.; Rudolph, V.; Lu, G. Q., *Asia-Pacific Journal of Chemical Engineering* **2009,** *4* (4), 387-402.
79. Anpo, M.; Che, M., In *Advances in Catalysis, Vol 44*, Haag, W. O.; Gates, B. C.; Knozinger, H., Eds. 1999; Vol. 44, pp 119-257.
80. Lasek, J.; Yu, Y. H.; Wu, J. C. S., *Journal of Photochemistry and Photobiology C-Photochemistry Reviews* **2013,** *14*, 29-52.
81. Maggos, T.; Bartzis, J. G.; Leva, P.; Kotzias, D., *Applied Physics a-Materials Science & Processing* **2007,** *89* (1), 81-84.
82. Poulios, I.; Spathis, P.; Grigoriadou, A.; Delidou, K.; Tsoumparis, P., *Journal of Environmental Science and Health Part a-Toxic/Hazardous Substances & Environmental Engineering* **1999,** *34* (7), 1455-1471.
83. Rincon, A. G.; Pulgarin, C., *Applied Catalysis B-Environmental* **2003,** *44* (3), 263-284.
84. Pekakis, P. A.; Xekoukoulotakis, N. P.; Mantzavinos, D., *Water Res* **2006,** *40* (6), 1276-1286.
85. Gumy, D.; Morais, C.; Bowen, P.; Pulgarin, C.; Giraldo, S.; Hajdu, R.; Kiwi, J., *Applied Catalysis B-Environmental* **2006,** *63* (1-2), 76-84.
86. Mitoraj, D.; Janczyk, A.; Strus, M.; Kisch, H.; Stochel, G.; Heczko, P. B.; Macyk, W., *Photochemical & Photobiological Sciences* **2007,** *6* (6), 642-648.
87. Sichel, C.; Tello, J.; de Cara, M.; Fernandez-Ibanez, P., *Catalysis Today* **2007,** *129* (1-2), 152-160.
88. Yang, X.; Wang, Y., *Building and Environment* **2008,** *43* (3), 253-257.
89. Murcia, J. J.; Avila-Martinez, E. G.; Rojas, H.; Navio, J. A.; Hidalgo, M. C., *Applied Catalysis B-Environmental* **2017,** *200*, 469-476.
90. Sun, D. S.; Tseng, Y. H.; Wu, W. S.; Wong, M. S.; Chang, H. H., *Nanomaterials* **2017,** *7* (1), 13.
91. Adan, C.; Marugan, J.; Mesones, S.; Casado, C.; van Grieken, R., *Chemical Engineering Journal* **2017,** *318*, 29-38.
92. Cruz-Ortiz, B. R.; Hamilton, J. W. J.; Pablos, C.; Diaz-Jimenez, L.; Cortes-Hernandez,

D. A.; Sharma, P. K.; Castro-Alferez, M.; Fernandez-Ibanez, P.; Dunlop, P. S. M.; Byrne, J. A., *Chemical Engineering Journal* **2017,** *316*, 179-186.

93. Paschoalino, M. P.; Jardim, W. F., *Indoor Air* **2008,** *18* (6), 473-479.

94. Chen, F. N.; Yang, X. D.; Wu, Q., *Environmental Science & Technology* **2009,** *43* (12), 4606-4611.

95. Markowska-Szczupak, A.; Ulfig, K.; Grzmil, B.; Morawski, A. W., *Polish Journal of Chemical Technology* **2010,** *12* (4), 53-57.

96. Le, T. S.; Ngo, Q. B.; Nguyen, V. D.; Nguyen, H. C.; Dao, T. H.; Tran, X. T.; Kabachkov, E. N.; Balikhin, I. L., *Advances in Natural Sciences-Nanoscience and Nanotechnology* **2014,** *5* (1).

97. Reddy, P. V. L.; Kavitha, B.; Reddy, P. A. K.; Kim, K. H., *Environmental Research* **2017,** *154*, 296-303.

98. Reddy, K. M.; Manorama, S. V.; Reddy, A. R., *Materials Chemistry and Physics* **2003,** *78* (1), 239-245.

99. Klein, C. A., *Journal of Applied Physics* **1968,** *39* (4), 2029-2038.

100. Wilson, B. A., *Bulletin of the American Physical Society* **1981,** *26* (3), 387-387.

101. Tiedje, T.; Abeles, B.; Persans, P. D.; Brooks, B. G.; Cody, G. D., *Journal of Non-Crystalline Solids* **1984,** *66* (1-2), 345-350.

102. Hamberg, I.; Granqvist, C. G.; Berggren, K. F.; Sernelius, B. E.; Engstrom, L., *Solar Energy Materials* **1985,** *12* (6), 479-490.

103. Horan, P.; Blau, W., *Contemporary Physics* **1987,** *28* (1), 59-68.

104. Zolper, J. C.; Shanabrook, B. V., *Proceedings of the Ieee* **2002,** *90* (6), 939-941.

105. Hurum, D. C.; Gray, K. A.; Rajh, T.; Thurnauer, M. C., *Journal of Physical Chemistry B* **2004,** *108* (42), 16483-16487.

106. Sotnikov, A. E.; Chernikov, M. A.; Ryabushkin, O. A.; Trubenko, P.; Moshegov, N.; Ovtchinikov, A., *Quantum Electronics* **2004,** *34* (9), 871-874.

107. Zhong, X. H.; Knoll, W., B*Abstracts of Papers of the American Chemical Society* **2006,** *231*.

108. Valencia, S.; Marín, J. M.; Restrepo, G., *The Open Materials Science Journal* **2010,** *4* (1), 9-14.

109. Beaulac, R., *Abstracts of Papers of the American Chemical Society* **2013,** *246*.

110. Wang, L. J.; Zhang, X.; Gao, H. Q.; Hu, J. H.; Mao, J.; Liang, C. H.; Zhang, P.; Shao, G. S., 3 *Science of Advanced Materials* **2016,** *8* (6), 1256-1262.

111. Sun, S. C.; Zhang, J. J.; Gao, P.; Wang, Y.; Li, X. B.; Wu, T. T.; Wang, Y. B.; Chen, Y. J.; Yang, P. P., *Applied Catalysis B-Environmental* **2017,** *206*, 168-174.

112. Babu, B.; Kadam, A. N.; Ravikumar, R. V. S. S. N.; Byon, C., *Journal of Alloys and Compounds* **2017,** *703*, 330-336.

113. Salehi-Abar, P.; Kazempour, A., *Chemical Physics Letters* **2017,** *673*, 56-61.

114. Khan, M.; Yi, Z.; Gul, S. R.; Wang, Y. Z.; Fawad, U., *Journal of Materials Science* **2017,** *52* (10), 5634-5640.

115. Schiavello, M., *Electrochimica Acta* **1993,** *38* (1), 11-14.

116. Lazzeri, M.; Vittadini, A.; Selloni, A., *Physical Review B* **2001,** *63* (15), 9.

117. Diebold, U., *Applied Physics a-Materials Science & Processing* **2003,** *76* (5), 681-687.
118. Diebold, U., *Surface Science Reports* **2003,** *48* (5-8), 53-229.
119. Samat, M. H.; Taib, M. F. M.; Hassan, O. H.; Yahya, M. Z. A.; Ali, A. M. M., *Materials Research Express* **2017,** *4* (4), 7.
120. Bickley, R. I.; Gonzalez-Carreno, T.; Lees, J. S.; Palmisano, L.; Tilley, R. J. D., *Journal of Solid State Chemistry* **1991,** *92* (1), 178-90.
121. Tomita, K.; Petrykin, V.; Kobayashi, M.; Shiro, M.; Yoshimura, M.; Kakihana, M., *Angewandte Chemie-International Edition* **2006,** *45* (15), 2378-2381.
122. Vequizo, J. J. M.; Matsunaga, H.; Ishiku, T.; Karnimura, S.; Ohno, T.; Yamakata, A., *Acs Catalysis* **2017,** *7* (4), 2644-2651.
123. Stengl, V.; Szatmary, L.; Subrt, J.; Lukac, J.; Murafa, N.; Niznansky, D.; Cizek, K.; Jirkovsky, J.; Petrova, N., *Journal of Materials Chemistry* **2006,** *16* (18), 1709-1716.
124. Dambournet, D.; Belharouak, I.; Amine, K., *Chemistry of Materials* **2010,** *22* (3), 1173-1179.
125. Li, X. L.; Mao, Y.; Leng, K. Y.; Ye, G.; Sun, Y. Y.; Xu, W., *Microporous and Mesoporous Materials* **2017,** *254*, 114-120.
126. Sharma, V.; Harith, G.; Kumar, S.; Sharma, R.; Reddy, K. L.; Bahuguna, A.; Krishnan, V., *Materials Technology* **2017,** *32* (8), 461-471.
127. Lebedev, V. A.; Kozlov, D. A.; Kolesnik, I. V.; Poluboyarinov, A. S.; Becerikli, A. E.; Grunert, W.; Garshev, A. V., *Applied Catalysis B-Environmental* **2016,** *195*, 39-47.
128. Deng, X. Q.; Zhu, X. B.; Sun, Z. G.; Li, X. S.; Liu, J. L.; Shi, C.; Zhu, A. M., *Chemical Engineering Journal* **2016,** *306*, 1001-1009.
129. Piccinini, F.; Levi, M.; Turri, S., *Progress in Organic Coatings* **2013,** *76* (9), 1265-1272.
130. Wu, S. L.; Hu, W. T.; Luo, X. B.; Deng, F.; Yu, K.; Luo, S. L.; Yang, L. X.; Tu, X. M.; Zeng, G. S., *Environmental Technology* **2013,** *34* (15), 2285-2290.
131. Abedi, S.; Karimi, B.; Kazemi, F.; Bostina, M.; Vali, H., *Organic & Biomolecular Chemistry* **2013,** *11* (3), 416-419.
132. Kimling, M. C.; Scales, N.; Hanley, T. L.; Caruso, R. A., *Environmental Science & Technology* **2012,** *46* (14), 7913-7920.
133. Kasar, S.; Kumar, S.; Kar, A.; Krishnan, K.; Kulkarni, N. K.; Tomar, B. S., *Journal of Radioanalytical and Nuclear Chemistry* **2012,** *294* (1), 103-107.
134. Kanna, M.; Wongnawa, S.; Buddee, S.; Dilokkhunakul, K.; Pinpithak, P., *Journal of Sol-Gel Science and Technology* **2010,** *53* (2), 162-170.
135. Manufacturing process of Titanium Dioxide. *network knowledge*. http://guichon-valves.com/faqs/titanium-dioxide-ti-o2-manufacturing-process-of-titanium-dioxide/
136. Wu, S. X.; Ma, Z.; Qin, Y. N.; He, F.; Jia, L. S.; Zhang, Y. J., *Acta Physico-Chimica Sinica* **2003,** *19* (10), 967-969.
137. Sakthivel, S.; Janczarek, M.; Kisch, H., *J. Phys. Chem. B* **2004,** *108* (50), 19384-19387.
138. Di Valentin, C.; Pacchioni, G.; Selloni, A., *Chemistry of Materials* **2005,** *17* (26),

6656-6665.
139. Wu, X. Y.; Liao, B.; Liang, H.; Zhang, X.; Liu, A. D., *Chinese Journal of Structural Chemistry* **2011,** *30* (9), 1332-1340.
140. Lee, K. S.; Park, I. S., *Scripta Materialia* **2003,** *48* (6), 659-663.
141. Moon, I. S.; Seo, H. S.; Kim, K. J.; Jang, S. H.; Jeong, W. J.; Moon, S. L.; Lee, H. R.; Chung, M. C.; Choi, S. K.; Jung, S. C.; Ahn, H. G., *Journal of Nanoscience and Nanotechnology* **2011,** *11* (8), 7382-7385.
142. Schmidt-Stein, F.; Thiemann, S.; Berger, S.; Hahn, R.; Schmuki, P., *Acta Materialia* **2010,** *58* (19), 6317-6323.
143. Park, T. E.; Choe, H. C.; Brantley, W. A., *Surface & Coatings Technology* **2013,** *235*, 706-713.
144. Mor, G. K.; Varghese, O. K.; Paulose, M.; Mukherjee, N.; Grimes, C. A., *Journal of Materials Research* **2003,** *18* (11), 2588-2593.
145. Varghese, O. K.; Gong, D. W.; Paulose, M.; Grimes, C. A.; Dickey, E. C., *Journal of Materials Research* **2003,** *18* (1), 156-165.
146. Mor, G. K.; Varghese, O. K.; Paulose, M.; Grimes, C. A., *Advanced Functional Materials* **2005,** *15* (8), 1291-1296.
147. Mor, G. K.; Shankar, K.; Paulose, M.; Varghese, O. K.; Grimes, C. A., *Nano Letters* **2006,** *6* (2), 215-218.
148. Shankar, K.; Bandara, J.; Paulose, M.; Wietasch, H.; Varghese, O. K.; Mor, G. K.; LaTempa, T. J.; Thelakkat, M.; Grimes, C. A., *Nano Letters* **2008,** *8* (6), 1654-1659.
149. Wu, N. Q.; Wang, J.; Tafen, D.; Wang, H.; Zheng, J. G.; Lewis, J. P.; Liu, X. G.; Leonard, S. S.; Manivannan, A., *Journal of the American Chemical Society* **2010,** *132* (19), 6679-6685.
150. Ma, Q.; Liu, S. J.; Weng, L. Q.; Liu, Y.; Liu, B., *Journal of Alloys and Compounds* **2010,** *501* (2), 333-338.
151. Li, X. Y.; Hou, Y.; Zhao, Q. D.; Chen, G. H., *Langmuir* **2011,** *27* (6), 3113-3120.
152. Miyakawa, M.; Murakami, S.; Yasuda, T.; Kohno, M.; Onoue, S.; Kera, Y.; Ohtani, B., *Physical Chemistry Chemical Physics* **2001,** *3* (13), 2697-2703.
153. Yin, S.; Aita, Y.; Komatsu, M.; Wang, J. S.; Tang, Q.; Sato, T., *Journal of Materials Chemistry* **2005,** *15* (6), 674-682.
154. Huang, D. G.; Liao, S. J.; Liu, J. M.; Dang, Z.; Petrik, L., *Journal of Photochemistry and Photobiology a-Chemistry* **2006,** *184* (3), 282-288.
155. Yang, H. G.; Liu, G.; Qiao, S. Z.; Sun, C. H.; Jin, Y. G.; Smith, S. C.; Zou, J.; Cheng, H. M.; Lu, G. Q., *Journal of the American Chemical Society* **2009,** *131* (11), 4078-4083.
156. Yang, G.; Jiang, Z.; Shi, H.; Jones, M. O.; Xiao, T.; Edwards, P. P.; Yan, Z., *Applied Catalysis B: Environmental* **2010,** *96* (3-4), 458-465.
157. Lucarelli, L.; Nadtochenko, V.; Kiwi, J., *Langmuir* **2000,** *16* (3), 1102-1108.
158. Lachheb, H.; Puzenat, E.; Houas, A.; Ksibi, M.; Elaloui, E.; Guillard, C.; Herrmann, J. M., *Applied Catalysis B-Environmental* **2002,** *39* (1), 75-90.
159. Janczarek, M.; Kowalska, E.; Ohtani, B., *Chem Eng J* **2016,** *289*, 502-512.
160. Amano, F.; Prieto-Mahaney, O. O.; Terada, Y.; Yasumoto, T.; Shibayama, T.; Ohtani,

B., *Chemistry of Materials* **2009,** *21* (13), 2601-2603.
161. Ohtani, B.; Prieto-Mahaney, O. O.; Li, D.; Abe, R., *Journal of Photochemistry and Photobiology A: Chemistry* **2010,** *216* (2-3), 179-182.
162. Sarukawa, K.; Tokieda, K.; Matsumura, M., *Journal of Catalysis* **2001,** *203* (1), 82-86.
163. Liu, P. X.; Chen, J.; Zheng, N. F., *Chinese Journal of Catalysis* **2017,** *38* (9), 1574-1580.
164. van der Meulen, T.; Mattson, A.; Osterlund, L., *Journal of Catalysis* **2007,** *251* (1), 131-144.
165. Ohno, T.; Sarukawa, K.; Matsumura, M., *New Journal of Chemistry* **2002,** *26* (9), 1167-1170.
166. Hurum, D. C.; Gray, K. A.; Rajh, T.; Thurnauer, M. C., *J. Phys. Chem. B* **2005,** *109* (2), 977-980.
167. Li, G. H.; Ciston, S.; Saponjic, Z. V.; Chen, L.; Dimitrijevic, N. M.; Rajh, T.; Gray, K. A., *Journal of Catalysis* **2008,** *253* (1), 105-110.
168. Ohtani, B.; Azuma, Y.; Li, D.; Ihara, T.; Abe, R., *Trans. Mater. Res. Soc. Jpn* **2007,** *32* (2), 401.
169. Apopei, P.; Catrinescu, C.; Teodosiu, C.; Royer, S., *Applied Catalysis B: Environmental* **2014,** *160–161*, 374-382.
170. Howard, C. J.; Sabine, T. M.; Dickson, F., *Acta Crystallographica Section B-Structural Science* **1991,** *47*, 462-468.
171. Sanjines, R.; Tang, H.; Berger, H.; Gozzo, F.; Margaritondo, G.; Levy, F., *Journal of Applied Physics* **1994,** *75* (6), 2945-2951.
172. Bourikas, K.; Hiemstra, T.; Van Riemsdijk, W. H., *Langmuir* **2001,** *17* (3), 749-756.
173. Egerton, T. A.; Mattinson, J. A., *Journal of Photochemistry and Photobiology A: Chemistry* **2008,** *194* (2-3), 283-289.
174. Shiraishi, Y.; Hirakawa, H.; Togawa, Y.; Sugano, Y.; Ichikawa, S.; Hirai, T., *ACS Catalysis* **2013,** *3* (10), 2318-2326.
175. Rajashekhar, K. E.; Devi, L. G., *Journal of Molecular Catalysis a-Chemical* **2013,** *374*, 12-21.
176. Hurum, D. C.; Agrios, A. G.; Gray, K. A.; Rajh, T.; Thurnauer, M. C., *Journal of Physical Chemistry B* **2003,** *107* (19), 4545-4549.
177. Hsu, L. S.; Rujkorakarn, R.; Sites, J. R.; She, C. Y., *J Appl Phys* **1986,** *59* (10), 3475-80.
178. Ohtani, B.; Ogawa, Y.; Nishimoto, S.-i., *The Journal of Physical Chemistry B* **1997,** *101* (19), 3746-3752.
179. Kisch, H.; Zang, L.; Lange, C.; Maier, W. F.; Antonius, C.; Meissner, D., *Angewandte Chemie-International Edition* **1998,** *37* (21), 3034-3036.
180. Yanagisawa, K., *Chemistry of Materials* **1999,** *11* (10), 2770-2774.
181. Plappert, E. C.; Dahmen, K. H.; Hauert, R.; Ernst, K. H., *Chemical Vapor Deposition* **1999,** *5* (2), 79-85.
182. Chen, J. H.; Kohls, D.; Beaucage, G., *Abstracts of Papers of the American Chemical Society* **2000,** *220*, U241-U241.

183. Macyk, W.; Kisch, H., *Chemistry-a European Journal* **2001,** *7* (9), 1862-1867.
184. Shi, D. P.; Li, Z. Q.; Zhang, Y.; Kou, X. L.; Wang, L. W.; Wang, J. T.; Li, J. G., *Nanoscience and Nanotechnology Letters* **2009,** *1* (3), 165-170.
185. Sobczyk-Guzenda, A.; Owczarek, S.; Szymanowski, H.; Gazicki-Lipman, M., *Vacuum* **2015,** *117*, 104-111.
186. Prieto-Mahaney, O.-O.; Murakami, N.; Abe, R.; Ohtani, B., *Chemistry Letters* **2009,** *38* (3), 238-239.
187. A. P. Ribeiro, R.; R. de Lazaro, S.; R. de Oliveira, C., *Current Physical Chemistry* **2016,** *6* (1), 22-27.
188. Chen, J.; Li, Y. Z.; Fang, S. M.; Yang, Y.; Zhao, X. J., *Chemical Engineering Journal* **2018,** *332*, 205-215.
189. Babu, B.; Kadam, A. N.; Ravikumar, R.; Byon, C., *Journal of Alloys and Compounds* **2017,** *703*, 330-336.
190. Aviles-Garcia, O.; Espino-Valencia, J.; Romero, R.; Rico-Cerda, J. L.; Arroyo-Albiter, M.; Natividad, R., *Fuel* **2017,** *198*, 31-41.
191. Razali, M. H.; Noor, A. F. M.; Yusoff, M., *Science of Advanced Materials* **2017,** *9* (6), 1032-1041.
192. Xu, C. Y.; Zhang, Y. W.; Chen, J. C.; Lin, J. Y.; Zhang, X. H.; Wang, Z. H.; Zhou, J. H., *Applied Catalysis B-Environmental* **2017,** *204*, 324-334.
193. Sharma, A.; Varshney, M.; Shin, H. J.; Lee, B. H.; Chae, K. H.; Won, S. O., *Materials Chemistry and Physics* **2017,** *191*, 129-144.
194. Ilkhechi, N. N.; Ghobadi, N.; Akbarpour, M. R., *Journal of Materials Science-Materials in Electronics* **2017,** *28* (9), 6426-6434.
195. Zhang, P. F.; Li, X. W.; Wu, X. K.; Zhao, T. X.; Wen, L. S., *Journal of Alloys and Compounds* **2016,** *673*, 405-410.
196. Gao, M. Y.; Jiang, D.; Sun, D. K.; Hou, B.; Li, D. B., *Acta Chimica Sinica* **2014,** *72* (10), 1092-1098.
197. Wang, S. B.; Zhang, X. W.; Li, S.; Fang, Y.; Pan, L.; Zou, J. J., *Journal of Hazardous Materials* **2017,** *331*, 235-245.
198. Zhao, X. G.; Huang, L. Q., *Ceramics International* **2017,** *43* (5), 3975-3980.
199. Islam, S. Z.; Nagpure, S.; Kim, D. Y.; Rankin, S. E., *Inorganics* **2017,** *5* (1), 43.
200. Asahi, R.; Morikawa, T.; Irie, H.; Ohwaki, T., *Chem Rev* **2014,** *114* (19), 9824-52.
201. Wang, W.; Lu, C.; Ni, Y.; Su, M.; Huang, W.; Xu, Z., *Applied Surface Science* **2012,** *258* (22), 8696-8703.
202. O'Regan, B.; Grätzel, M., *Nature* **1991,** *353* (6346), 737-740.
203. Mitoraj, D.; Kisch, H., *Angew Chem Int Ed Engl* **2008,** *47* (51), 9975-8.
204. Lu, Y.; Chen, S.; Quan, X.; Yu, H. T., *Chinese Journal of Catalysis* **2011,** *32* (12), 1838-1843.
205. Wang, M. Z.; Liang, F. X.; Nie, B.; Zeng, L. H.; Zheng, L. X.; Lv, P.; Yu, Y. Q.; Xie, C.; Li, Y. Y.; Luo, L. B., *Particle & Particle Systems Characterization* **2013,** *30* (7), 630-636.
206. Devi, L. G.; Kavitha, R., *Applied Surface Science* **2016,** *360*, 601-622.
207. Kumbhar, A.; Chumanov, G., *Journal of Nanoscience and Nanotechnology* **2004,** *4* (3),

299-303.
208. Chumanov, G.; Kumbhar, A., *Abstracts of Papers of the American Chemical Society* **2004,** *227*, U1246-U1246.
209. Manera, M. G.; Cozzoli, P. D.; Curri, M. L.; Leo, G.; Rella, R.; Agostiano, A.; Vasanelli, L., *Synthetic Metals* **2005,** *148* (1), 25-29.
210. Kowalska, E.; Abe, R.; Ohtani, B., V *Chem Commun* **2009,** (2), 241-243.
211. Wang, J.; Wang, L. Y.; Sun, Y.; Zhu, X. N.; Cao, Y. B.; Wang, X. H.; Zhang, H. Q.; Song, D. Q., *Colloids and Surfaces B-Biointerfaces* **2010,** *75* (2), 520-525.
212. Son, M. S.; Im, J. E.; Wang, K. K.; Oh, S. L.; Kim, Y. R.; Yoo, K. H., *Applied Physics Letters* **2010,** *96* (2).
213. Silva, C. G.; Juarez, R.; Marino, T.; Molinari, R.; Garcia, H., *Journal of the American Chemical Society* **2011,** *133* (3), 595-602.
214. Lin, H. Y.; Chen, C. T.; Chen, Y. C., *Analytical Chemistry* **2006,** *78* (19), 6873-6878.
215. Sun, Y.; Bi, N.; Song, D. Q.; Bai, Y.; Wang, L. Y.; Zhang, H. Q., *Sensors and Actuators B-Chemical* **2008,** *134* (2), 566-572.
216. Zhang, Y.; Yuwono, A. H.; Li, J.; Wang, J., *Microporous and Mesoporous Materials* **2008,** *110* (2-3), 242-249.
217. Wei, Z. S.; Rosa, L.; Wang, K. L.; Endo, M.; Juodkazis, S.; Ohtani, B.; Kowalska, E., *Applied Catalysis B-Environmental* **2017,** *206*, 393-405.
218. Kowalska, E., In *Gold Nanoparticles for Physics, Chemistry and Biology*, 2nd ed.; Louis, C.; Pluchery, O., Eds. World Scientific: Singapore, 2017; pp 319-364.
219. Cameron, D.; Holliday, R.; Thompson, D., *Journal of Power Sources* **2003,** *118* (1-2), 298-303.
220. Froschl, T.; Hormann, U.; Kubiak, P.; Kucerova, G.; Pfanzelt, M.; Weiss, C. K.; Behm, R. J.; Husing, N.; Kaiser, U.; Landfester, K.; Wohlfahrt-Mehrens, M., *Chemical Society Reviews* **2012,** *41* (15), 5313-5360.
221. Baur, E.; Perret, A., *Helvetica Chimica Acta* **1924,** *7*, 910-915.
222. Kowalska, E.; Mahaney, O. O. P.; Abe, R.; Ohtani, B., *Physical Chemistry Chemical Physics* **2010,** *12* (10), 2344-2355.

Chapter II

P25 — mixed-phase titania photocatalyst:

Intrinsic high activity of crystalline phases

vs

“synergy” between crystalline phases

2.1. Introduction

2.1.1. P25 — mixed-phase titania photocatalyst

P25 has been widely used as photocatalyst due to high photocatalytic activity in various photocatalytic reaction systems[1], such as:

i) decomposition of organic compounds (e.g., phenols (nitro-, chloro-), dyes, acids (formic, oxalic, salicylic, hydroxybenzoic and humic), herbicides (isoproturon, simazine and propazine), pharmaceuticals, chloromethane, catechol, dioxane, aromatic aminocompounds)[2-6] and inorganic compounds (e.g., arsenic)[7] in water and/or wastewater,

ii) degradation of gas-phase pollutants, such as carbon tetrachloride, carbon oxide, acetylene, ethanol, 2-propanol, acetone, trichloroethylene, NO_x,[8-12]

iii) purification of indoor environment (e.g., removal of mite allergens),[13]

iv) inactivation of microorganisms,[14-17]

v) self-cleaning surface (cotton textiles, cementitious and cellulose materials[18-20]),

vi) solar energy conversion.[21]

Complete degradation (100%) of various compounds (often resulting in their mineralization–complete oxidation) has been frequently reported. For example,

(1) textile dyes (Reactive Yellow 17 (RY17&, Reactive Red 2 (RR2) and Reactive Blue 4 (RB4)) were completely decomposed (mineralized) in the suspension of P25 (1 g/L) during 3-12 h of UV irradiation, and during longer time (> 12 h) of solar radiation,[2]

(2) pharmaceutical drugs were more efficiently decomposed and mineralized on P25 than on Merck anatase under UV irradiation reaching complete mineralization for 22 h and 28 h, respectively[22],

(3) P25 showed the highest photocatalytic activities among forty commercial titania photocatalysts for oxidative decomposition of acetic acid.[23]

Therefore, P25 was used as a “gold standard” photocatalyst not only as powder sample, but

also deposited onto glass as a film.[6, 16, 24-33,34] The number of the published papers using "P25" and "photocatalysis" as keywords is more than ten thousand papers per year, as shown in **Figure 2.1.**

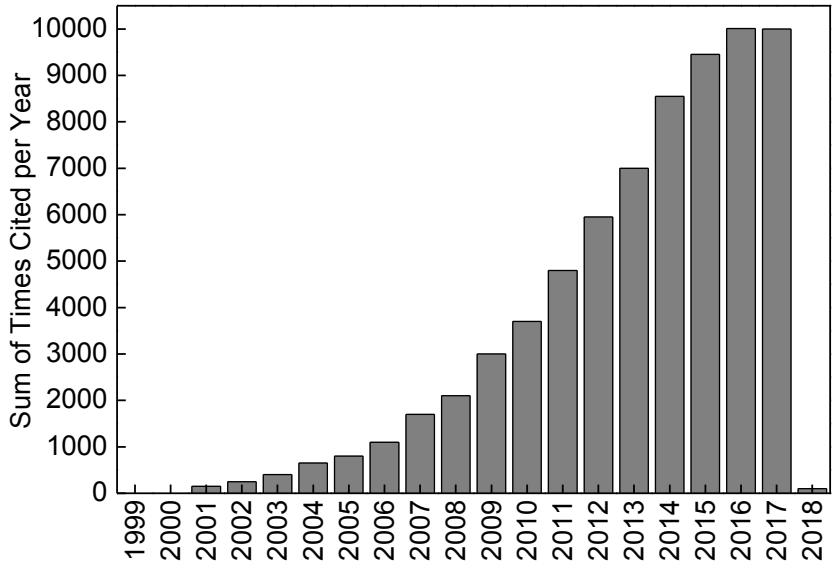


Figure 2.1 The sum of times cited per year of published reports for "P25" and "photocatalysis" as keywords (*web. of science*, Nov. 2017).

There are many possible explanations for the reason why P25 shows high photocatalytic activity in various photocatalytic reactions, such as small particle size and thus large specific surface area, high crystallinity, specific crystalline composition (anatase-rutile mixture), etc. However, it should be pointed out that, P25 titania does not have the best surface properties among various titania photocatalysts,[23] but usually it has better photocatalytic activities (for both oxidation and reduction reactions) than other photocatalysts even those with better surface properties (larger specific surface area, smaller crystallites, larger crystallinity, better morphology, e.g., faceted nanoparticles).[35, 36] Therefore, high photocatalytic activity of P25 could not be simply explained by surface properties, and various reasons have already been proposed, as follows:

1. co-presence of some impurity in the crystal lattice of titania, e.g., Fe^{3+}, which may retard charge carriers' recombination,[37]

2. enrichment of titania surface with OH groups resulting in enhanced formation of hydroxyl radicals under irradiation,[38-40]

3. presence of amorphous titania (usually inactive form of titania due to fast recombination of charge carriers), which could participate in transfer of charge carriers between different phases (anatase ↔ amorphous ↔ rutile (various combination of electrons and holes migrations between two or three phases have been proposed),[41] due to the existence of localized Anderson states at the band edges of the amorphous phase creating tails into the bandgap),[41]

4. co-existence of anatase and rutile, e.g., the overlayer of rutile on anatase crystal,[41] resulting in electron transfer between them, and thus retardation of charge carriers' recombination.

The last reason (4) is the most often used for explanation of the high photocatalytic activity of P25,[26, 41-43] where usually the transfer of electrons from anatase to rutile have been proposed, due to more negative potential of conduction band (CB) of anatase (larger bandgap) than rutile.[44-51] In contrast, some reports proposed opposite direction of electron transfer from rutile to anatase, e.g., migration of holes from anatase core to the rutile overlayer and adverse transfer of electrons,[41] and transfer of electrons from rutile to anatase lattice trapping sites.[26, 29] Schematic diagram showing five possible band alignments in mixed-phase titania is shown in **Figure 2.2**. For example, Type V (conduction bands being aligned) was suggested as the most probable structure for anatase-rutile composites, based on transient infrared absorption-excitation energy scanning spectroscopy.[52] Therefore, it has been proposed that the electron migration direction is controlled by dynamic factors, such as particle size, presence of electron/hole scavengers on either the surface of anatase or rutile phases, or both.

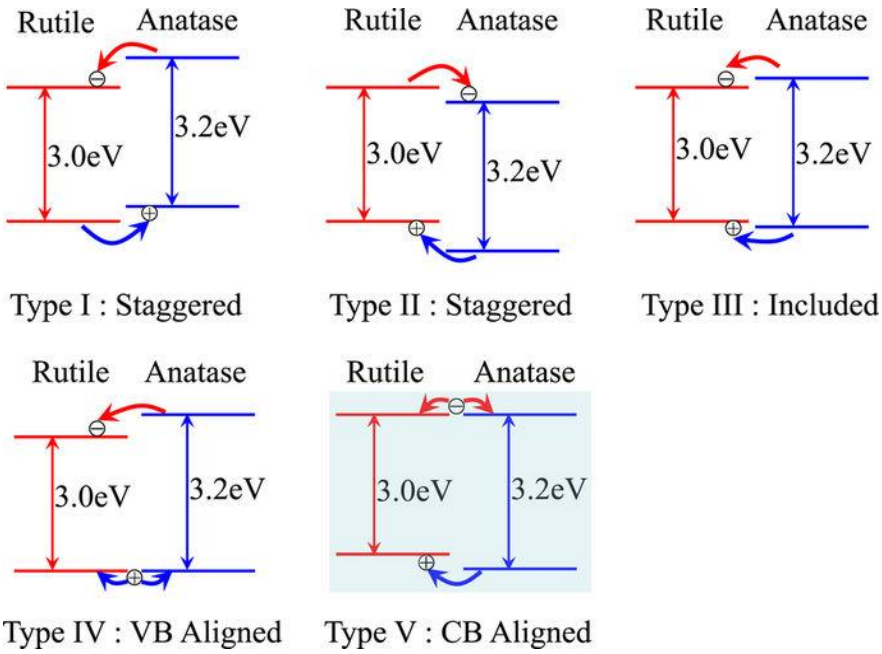


Figure 2.2 Schematic diagram showing five possible band alignments between anatase and rutile.[52]

Copyright © 2015, Springer Nature, all rights reserved

Although, the results of some investigations suggest the electron transfer between anatase and rutile in P25 (e.g., by EPR spectroscopy),[26, 29] the reference samples of anatase and rutile have not been the same as those in P25. Therefore, it is impossible to conclude that high photocatalytic activity of P25 is caused by transfer of charge carriers between crystalline phases.

In 1991, Bickley et al. suggested that high activity of P25 (and other mixed-phase titania photocatalysts) was caused by the enhancement in "the magnitude of the space-charge potential" as a result of the contact between different phases and by the presence of localized electronic states in amorphous phase.[41] Although, it is unknown who first used the term of "synergy" or "synergistic effect" for explanation of high activity of P25, many reports have used it interchangeable for interparticle charge transfer (IPCT) to explain the reason of high activity of P25 and other mixed-phase titania photocatalysts.[1,46, 53-56] However, usually no experimental evidence has been shown, and "synergy" has been only speculated based on results showing higher activity of P25 than that of single titania phase (anatase and rutile). Moreover, in many cases, the activity of P25 was only slightly higher than that of most active

phase (usually anatase), but not higher than the simple sum of its parts ("synergy" — "synergistic effect"). Therefore, even the term of "synergy" has been often used incorrectly.

To confirm "synergistic effect" (or/and IPCT), usually physical methods have been used, such as mixing and thermal treatment. Phase mixing can be performed either in the aqueous suspension of two or three kinds of titania particles or by grinding. Higher activity of the mixed-phase sample than that of sole anatase or rutile was explained as a proof for "synergistic effect". For example, Ohno et al. in 2003 suggested "synergism" between rutile and anatase in photocatalytic oxidation of naphthalene for titania samples prepared by two methods: mixing of anatase and rutile and thermal treatment of anatase.[57] The synergetic effect was found in both kinds of samples (activity higher than the simple sum of its parts), and it was proposed that IPCT was responsible for this synergy. Moreover, the activity of the most active mixed-phase titania was similar to that of P25. Based on these data, similar "synergy" was proposed for P25, i.e., electron transfer between anatase and rutile, resulting in its high photocatalytic activity.

Investigation on "synergy" by thermal treatment method (applied also by Ohno et al, in the study discussed above) uses the intrinsic properties of titania, i.e., the stability. It is known that metastable anatase and brookite phase convert irreversibly to rutile upon heating. Therefore, during thermal treatment the mixture of anatase and rutile can be easily obtained, e.g., anatase particle can be loaded with rutile particle. For example, Jing et al. reported that anatase-rutile mixed sample were prepared by calcination of titania, prepared by precipitation method.[58] However, in that study, the La_2O_3 was additionally loaded on the surface of titania samples, and thus, possible synergy between anatase and rutile could not be directly confirmed.

Moreover, it should be pointed that thermal treatment can change not only the composition of samples (anatase/rutile ratio), but also all other properties, such as particle size, specific surface area, morphology, ET's content, etc. In some studies, "synergy" in P25 was suggested in comparison to anatase and rutile that did not originated from P25, and thus with quite different properties than that in P25. Additionally, some photocatalytic activity tests

were carried out in the presence of loaded co-catalyst and thus properties of co-catalyst could be more decisive for overall activity than that of titania components.

In the previous studies performed in Ohtani laboratory, anatase and rutile particles were successfully isolated from P25 by chemical method, and photocatalytic activity of isolated titania particles and re-built P25 (R-P25, same anatase/rutile ratio as in original P25 titania) was tested in four kinds of photocatalytic reactions, e.g., (a) oxidative decomposition of acetic acid under aerobic conditions, (b) oxidative decomposition of acetaldehyde in air, (c) dehydrogenation of methanol in a deaerated aqueous solution and (d) oxygen liberation from a deaerated aqueous silver sulfate solution. It was confirmed that amorphous titania was almost inactive in all tested reactions (Unfortunately, amorphous titania was not isolated from P25 since it is impossible by chemical dissolution method. Therefore, other methods, e.g., vibration, have been tried to isolate amorphous titania from P25 in my study. Anyhow, it is not expected that the influence of amorphous phase on overall activity could be significant, due to its low content and negligible activity independently on preparation procedure (large content of defects as charge carriers' recombination sites),), as shown in **Figure. 2.3**. Anatase showed highest activity for oxidative decomposition of acetic acid (a) and acetaldehyde (b), probably due to its larger bandgap than that of rutile (more negative CB allowing one-electron reduction of oxygen).[1] In contrast, rutile showed the highest activity for oxygen evolution, which could be caused by co-presence of silver sulfate as electron acceptor and narrower bandgap (UV/vis light harvesting). It should be pointed that in three reaction systems (a, b and d) P25 and re-build P25 did not show the highest activity, and thus high activity of P25 could not be explained due to "synergy" or any IPCT between anatase and rutile, but by intrinsic high activities of it components (anatase and rutile) in different reaction systems. However, in the case of methanol dehydrogenation, P25 and R-P25 samples showed higher activity than that of anatase and rutile suggesting some interaction (e.g., IPCT) between two phases or between crystalline phases and amorphous titania. Therefore, this system has been investigated in my study, i.e., to explain the reason of high activity of P25 for hydrogen evolution.

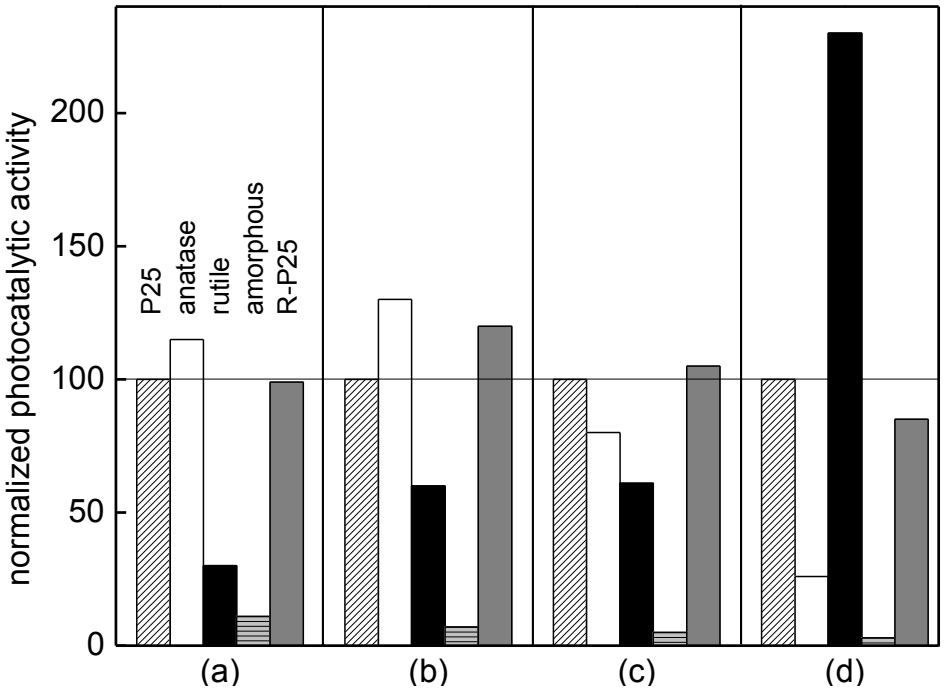


Figure. 2.3 The photocatalytic activity of P25, isolated-phases and re-constructed samples in four kinds of reaction. P25 was used as reference calculated the photocatalytic activity as 100%.
(a) oxidative decomposition of acetic acid;
(b) oxidative decomposition of acetaldehyde in air;
(c) dehydrogenation of methanol in a deaerated aqueous solution;
(d) oxygen liberation from a deaerated aqueous silver sulfate solution.

Copyright © 2010 Elsevier B.V., all rights reserved, license number: 4296200653292

Although, it was found that chemical methods, used for anatase and rutile isolation from P25, were efficient, the possibility of existence of some impurities on the surface of isolated phases (due to chemical etching) has caused that other methods — physical methods (vibration, sonication) have been also applied for crystalline phase separation in my studies. Moreover, it was thought that physical methods could result in obtaining original amorphous titania. In addition, purification of crystalline phases, prepared by chemical methods have been applied in my study. Both procedures of phase isolation are presented in this chapter.

2.2. Experimental details

2.2.1. Separation of anatase and rutile particles from P25

2.2.1.1 Physical separation

Physical separation was carried out by vibration treatment. P25 was supplied by Nippon Aerosil in a scale of 1 kg. A 1-kg portion of sample (original-P25, without any treatment) was mechanically vibrated (from the bottom) in a plastic measuring cylinder equipped with 18 sampling holes at different position from the bottom, as shown in **Figure. 2.4**. The SHAKER HM-162, (ca.20 Hz of frequency, 1.5 mm of amplitude) was used as the vibrator. Moreover, in some experiments additional sonication was used. An ultrasonication probe, supplied by SONICS & MATERIALS INC (VCX 130, 20 kHz of frequency), was immersed in the top part of powder, and the sample was ultrasonically agitated simultaneously.

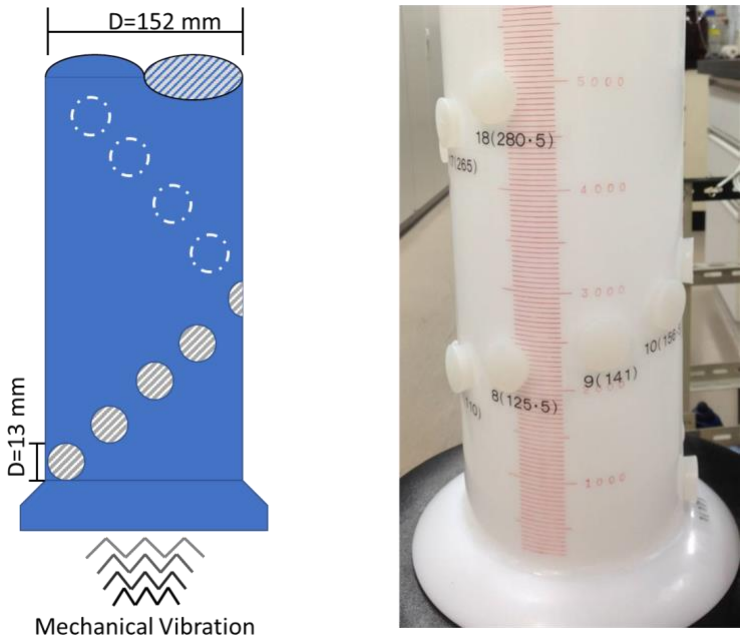


Figure. 2.4 A mechanical vibration set-up for P25.
(left) schematic drawing, (right) photograph of experimental set-up.

2.2.1.2 Chemical separation

Because P25 is non-uniform (due to wide temperature range in the flame during synthesis of P25, as shown in **Figure 1.7**), original P25 was homogenized first, i.e., P25 was suspended in Milli-Q water under mechanical stirring for 24 h and then dried by freeze-drying as shown in **Figure 2.5**.



Figure 2.5 Photographs of homogenization of P25: (left) mechanical stirring, (right, top) freeze-drying, and (right bottom) obtained product (HomoP25).

Anatase isolation

Anatase particles (ISO-ana) were obtained from HomoP25 by selective dissolution of rutile phase in hydrogen peroxide-ammonia mixture (H_2O_2-NH_3) under magnetic stirring for 15 h at 25 °C, as was proposed by Ohtani et al. in 2007.[59] The residual titania was washed several times with Milli-Q water, centrifuged under 15,000 rpm, and dried by freeze-drying and named as ISO-ana (isolated-anatase), as shown in **Figure 2.6**. The color of the isolated sample was light-yellow (**Figure 2.6** right). The yellow coloration of TiO_2 after treatment with H_2O_2 could arise from the presence of surface titanium peroxo complexes. Indeed, titanium

peroxide complexes in solution are known to produce an intense yellow color.[60, 61] Boonstra et al. noted the appearance of a yellow coloration after exposure of TiO_2 to H_2O_2 vapors, whereas illumination of the sample in the presence of dioxygen (i.e., formation of the ionic O_2-Ti^{4+} system) did not produce the same coloration.[62] The yellow color was attributed to the presence of pertitanic acid moieties on the oxide surface (Ti–OOH). In order to remove impurities, originated from the isolation process, annealing, was applied. Annealing was carried out at 120 ºC, 200 ºC, 300 ºC and 500 ºC in a rotary furnace for 2.5 h. The samples were named respectively to annealing temperature, i.e., ISO-ana-[200] means ISO-ana sample annealed at 200 ºC.



Figure 2.6 Photograph of: (left) set-up for isolation of anatase, and (right) ISO-ana sample.

Rutile isolation

Rutile particles were isolated from HomoP25 by selective dissolution of anatase phase in a diluted hydrofluoric acid (HF) solution under magnetic stirring for 24 h at room temperature, as was proposed by Ohno et al. in 2001.[42] The residual titania was washed several times with Milli-Q water, centrifuged under 4,500 rpm, and dried by freeze drying and named as ISO-rut (isolated-rutile), as shown in **Figure 2.7**. In contrast to ISO-ana (slight yellow), ISO-rut was white (**Figure 2.7**, right) — similar to original P25 and HomoP25. It was proposed that, the selective dissolution of anatase by hydrofluoric acid originate from its lower stability than that of rutile.[42] Similar to anatase samples, to remove impurities, originated from the isolation process, annealing, was applied. Annealing was carried out at

120 ºC, 200 ºC, 300 ºC and 500 ºC in a rotary furnace for 2.5 h. The samples were named respectively to annealing temperature, i.e., ISO-rut-[300] means ISO-rut sample annealed at 300 ºC. In addition, to remove hydrofluoric acid from the surface of isolated rutile (ISO-rut) and to avoid formation of F-modified titania (during annealing), ISO-rut was washed with aqueous solution of NaOH (1 M) by magnetic stirring for 30 min, and then annealed. Samples were named respectively to annealed temperature, such as ISO-rut-NaOH-200 means ISO-rut sample washed with NaOH and annealed at 200 ºC.



Figure 2.7 Photograph of: (left) set-up for isolation of rutile, and (right) ISO-rut sample.

2.2.2. Characterization of isolated samples

Various methods were used for sample characterization, such as X-ray diffraction (XRD), X-ray photoelectron spectroscopy (XPS), diffuse reflectance spectroscopy (DRS), time-resolved microwave conductivity (TRMC), scanning transmission electron microscopy (STEM) and reversed double-beam photoacoustic spectroscopy (RDB-PAS), which are shortly described, as follows:

XRD was used for measuring the crystalline size and crystalline composition of samples. The crystallinity was estimated by the internal standard method, with a highly crystalline nickel oxide (NiO) as the standard, as shown in **Figure 2.8**. In brief, 40 mg NiO (20.0 wt%) was mixed thoroughly with a 160 mg titania sample (80.0 wt%) by grinding in an agate mortar. XRD analysis was performed using a Rigaku intelligent X-ray diffraction system SmartLab, equipped with a sealed tube X-ray generator (a copper target; operated at 40 kV and 30 mA), a D/teX high-speed position sensitive detector system and an ASC-10 automatic

sample changer. XRD analysis was performed for 2Θ range of 10~90°, scan speed of 1.0° min^{-1} and scan step of 0.008°. The obtained XRD patterns were analyzed by Rigaku PDXL, a crystal structure analysis package including Rietveld analysis, installed in a computer controlling the diffractometer **(Figure. 2.9)**. Since a Rietveld analysis gives composition of each crystal among total crystal content, the composition of the standard (formally 20.0 wt%) is measured to be larger, if the sample contains non-crystalline phase, composition is estimated by re-calculation to make the standard composition to be 20.0 wt% (**Figure 2.8**).

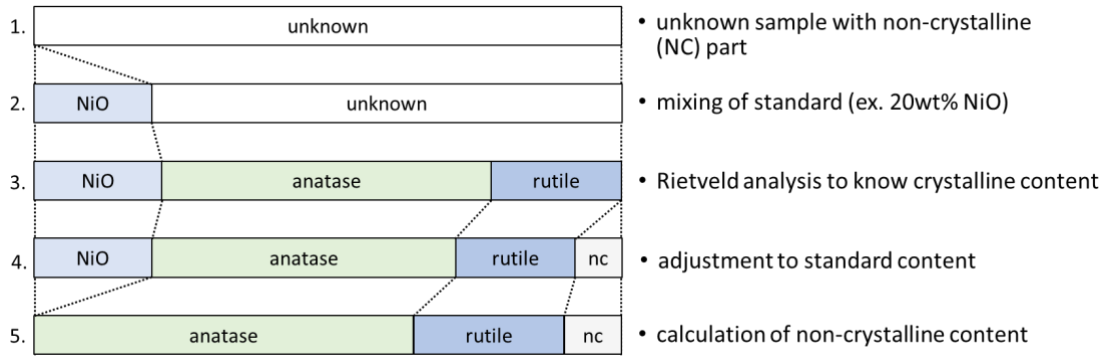


Figure.2.8 Schematic drawing of the calculation method used for crystallinity estimation in titania samples with NiO as an internal standard.



Figure.2.9 Photograph of XRD instrument for checking the crystalline composition of titania samples: (left) full view and, (right) interior view photograph of XRD instrument.

Specific surface area (SSA) of samples was estimated using the Brunauer-Emmett-Teller (BET) equation by nitrogen adsorption at 77 K by Quantachrome NOVA 1200e (**Figure. 2.10**). The samples were dried by freeze-drying before measurement. During the pretreatment,

the samples were thermally treated at 423 K for 2 h (degas process). A suitable amount of sample (100–150 mg) was taken for each test.



Figure. 2.10 Photograph of BET equipment for measurement of specific surface area of samples (SSA).

To characterize the photoabsorption properties of titania samples, diffuse reflectance spectra (DRS) were recorded. The measurements were carried out on Jasco V-670 spectrophotometer equipped with a PIN-757 integrating sphere (**Figure. 2.11**). The baseline was recorded using $BaSO_4$ as a reference. In the case of modified titania samples, respective bare titania samples were also used as a reference.

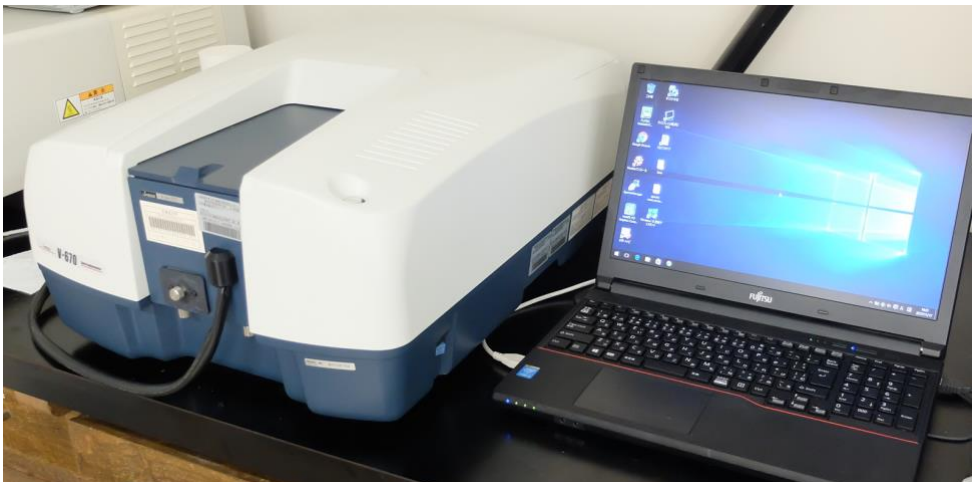


Figure. 2.11 Photograph of DRS equipment for measurement of photoabsorption properties.

The morphology of samples was measured by scanning transmission electron microscopy (STEM, HITACHI HD-2000). STEM images were acquired at a wide range of magnifications (1500–1500000), for 200-kV accelerating voltage and 20-A emission current. The powders were dispersed in ethanol in an ultrasonic bath for one minute, and the suspension droplets were deposited on a carbon-covered copper microgrid and then the images were recorded. More than 500 NPs of titania and 300 NPs of Pt were counted for evaluation of distribution of particles' sizes. It should be pointed that for evaluation of Pt NPs' size, only the width of single NP was measured, but not the length of formed aggregates.

X-ray photoelectron spectroscopy (XPS; JEOL JPC-9010MC) was used for studying the surface content of element in sample and their oxidation states. Usually, 50 scans were carried out and average data were used for analysis. Considering that the amount of F and noble metals (Chapter III, IV and V) in the samples was low, 100 scans for F and noble metals (Pt, Au, Ag and Cu) were performed. During the measurements, the main chamber pressure was kept below 5.0×10^{-6} Pa.

The lifetimes of charge carriers were estimated by time-resolved microwave conductivity (TRMC) method. The incident microwaves were generated by a Gunn diode of the Ka band and the tests were done at 36.8 GHz. The pulsed light source was a Nd: YAG laser providing IR irradiation at a wavelength of 1064 nm. The full width at half maximum of one pulse was 10 ns; the repetition frequency of the pulses was 10 Hz. UV light (355 nm) was obtained by tripling the IR radiation.[63]

Reversed double-beam photoacoustic spectroscopy (RDB-PAS), was used for measuring the energy-resolved distribution of electron traps of titania powders. In RDB-PAS measurement, electrons in the valence band of a powder sample are directly excited to electron traps (ETs) and accumulate in the ETs from the deeper side (anodic) to the shallower side (cathodic) side by wavelength-scanned continuous light, and the increase of photoabsorption of electron-filled ETs is measured by modulated light as a fix wavelength by PAS.[64, 65]

2.2.3. Measurements of photocatalytic activity

Photocatalytic activity was tested under UV/vis irradiation in two reaction systems: 1) oxidative decomposition of acetic acid under aerobic conditions, and 2) dehydrogenation of methanol under anaerobic conditions.

In the case of oxidative decomposition of acetic acid (CO_2 system), photocatalytic activity was examined by measuring the amount of evolved carbon dioxide (CO_2) from continuously stirred suspensions of a sample (50 mg) in aqueous solution of acetic acid (5.0 mL, 5.0 vol%) under UV/vis irradiation according to equation 11. During the irradiation, a portion (0.2 mL) of the gas phase of reaction mixture was withdrawn with a syringe and subjected to gas chromatographic analysis of carbon dioxide by gas chromatography (TCD-GC, Shimadzu GC-8A-IT). The experimental set-up is shown in **Figure 2.12**.

$$CH_3COOH + 2O_2 \xrightarrow[UV]{TiO_2/e^-/h^+} 2CO_2 + 2H_2O \qquad (11)$$



Figure. 2.12 Photographs of: (left) set-up for photocatalytic activity tests, and (right) gas chromatograph (GC) for measurement of the amount of evolved CO_2.

In the case of methanol dehydrogenation (H_2 system), different to the CO_2 system, reaction was performed under anaerobic conditions, according to **equation 12**. The photocatalytic activities in H_2 system were examined by measuring the amount of evolved H_2 from

continuously stirred (1000 rpm) suspensions of a sample (50 mg) in a deaerated (15-min Ar pre-bubbling) aqueous methanol solution (5.0 mL, 50 vol%) containing chloroplatinic acid (corresponding to 2.0 wt% (as platinum) of a sample) for in-situ platinum photodeposition.

$$CH_3OH \xrightarrow[UV]{TiO_2/e^-/h^+} HCHO + H_2 \qquad (12)$$

The same irradiation set-up was used as that in CO_2 system (**Figure** 2.12). The procedure of platinum in situ photodeposition during methanol dehydrogenation is shown in **Figure 2.13**.

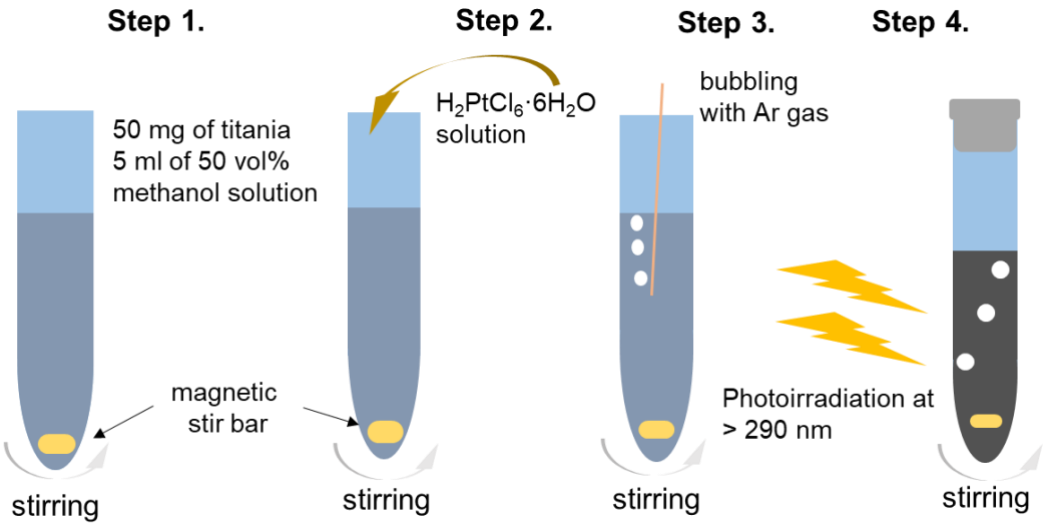


Figure. 2.13 Process of platinum photodeposition.

2.3. Results and discussions

2.3.1 Physical isolation

Mechanical vibration (24 h) resulted in only slight change in crystalline composition, as shown in **Figure 2.14** (Sample were taken from different position of cylinder, as shown in **Figure 2.4** (left).). Interestingly, it was found that during vibration, the volume of sample decreased significantly, as shown in **Figure 2.15**. It is clear that during first 5 min of vibration, the volume of P25 decreased fast, due to a decrease in a space between particles. Further decrease in P25 volume was observed till 1000 min which could be caused by aggregation of particles during the vibration process. Indeed, large aggregates, i.e., balls of millimeter size were formed during vibration, as shown in **Figure 2.16**. It has been reported that, during mechanic vibration, vibration energy could be transfer to the particles resulting in their easy aggregation by van der Waals force between particles.[66-71] After 1000 min of vibration, the volume did not change suggesting that aggregation was completed. It should be pointed that aggregation of particles makes separation of crystalline phases almost impossible.

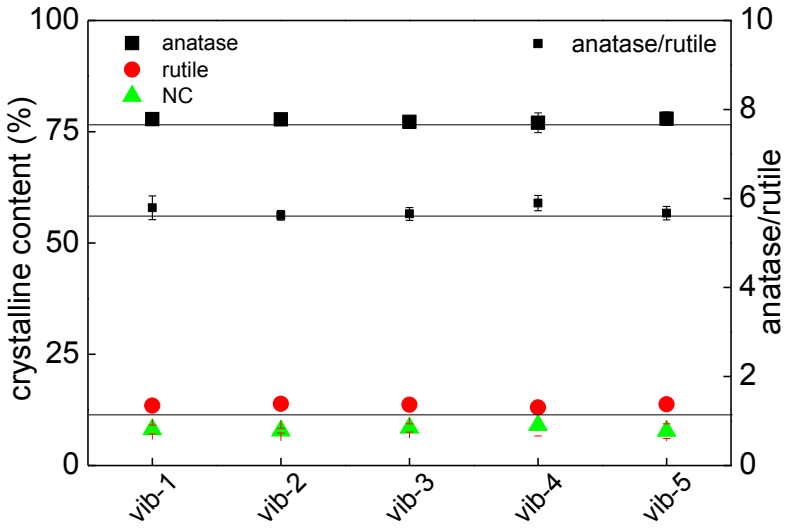


Figure. 2.14 The crystalline composition of vibrated samples.

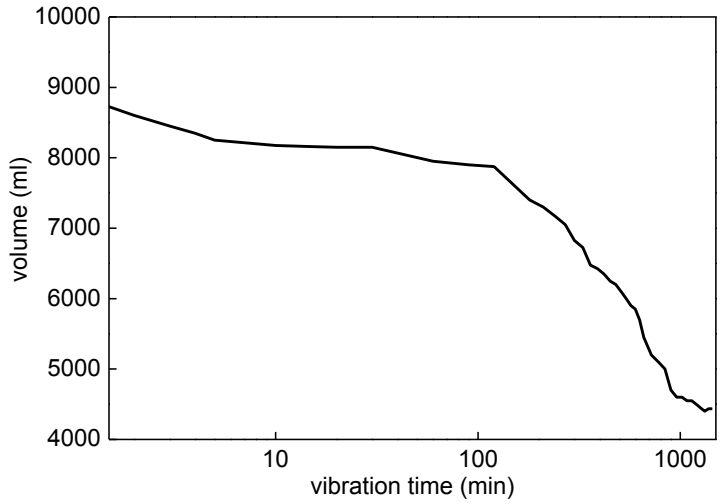


Figure. 2.15 The volume change of 1 kg of P25 powder during vibration.

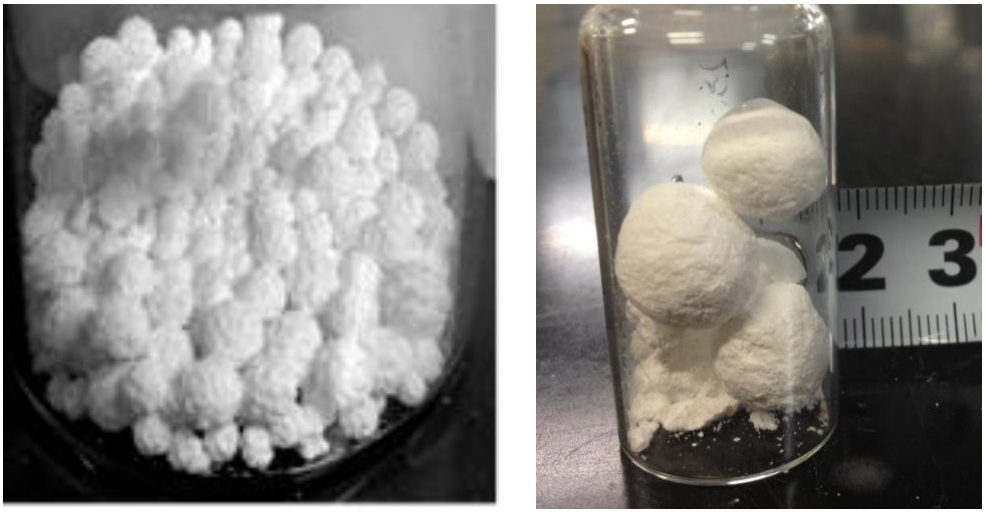


Figure. 2.16 Photographs of aggregated balls of millimeter size.

Therefore, to the avoid the aggregation of particles during the vibration, ultrasonic agitation was additionally applied. Indeed, sonication inhibited the formation of aggregated balls during mechanical vibration. Moreover, partial phase separation was observed for short vibration time (till 4 h), as shown in **Figure. 2.17**. However, longer time of vibration resulted in mixing of all particles again due to the movement of all particle in the cylinder, as has been already reported.[71] Therefore, vibration and vibration-sonication could not separate mixed-phase titania well, and thus, other methods, such as chemical separation, light-assisted separation (now under study), have been used for efficient separation.

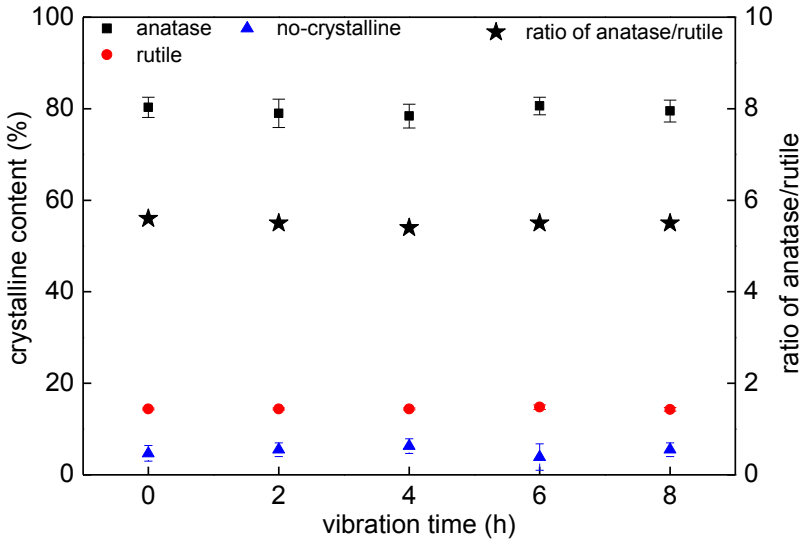


Figure. 2.17 Crystalline composition and anatase/rutile ratio of mechanically vibrated samples during ultrasonic-assisted vibration.

2.3.2 Chemical isolation

Before chemical isolation, P25 sample was homogenized first, because it is highly nonuniform, as shown in **Table 2.1** (Composition depends on sampling position.). It was found that proposed homogenization method was very efficient, and homogenized samples contained of ca. 78% anatase, 14% rutile and 8% non-crystalline phase, as confirmed by XRD analysis for three samples (**Table 2.2**). The HomoP25 sample was used as the source of titania for phase isolation (rutile and anatase) and as the standard (reference) sample for photocatalytic activity tests.

Table 2.1 Crystalline composition of original P25

original·P25·(OP25)

sample	crystalline·composition·(%)		
	Anatase	rutile	NC
1	76	13	11
2	77	14	9
3	76	13	11
4	79	14	7
5	80	14	6
6	79	15	6
SD·(%)	1.7	0.8	2.3

Copyright © 2017 Elsevier B.V., all rights reserved

Table 2.2 Crystalline composition of HomoP25

HomoP25

sample	crystalline·composition·(%)		
	anatase	rutile	NC
1	78·	14·	8·
2	78·	14·	8·
3	77·	14·	9·
SD·(%)	0.3	0.1	0.8

SD:·Standard·Deviation

Copyright © 2017 Elsevier B.V., all rights reserved

Chemical dissolution methods resulted in efficient isolation of crystalline phases, as shown in **Table 2.3**. The specific surface area (SSA) of ISO-RUT and ISO-ANA were 32 m^2/g and 61 m^2/g, respectively. Based on relation between the size of spherical particles and specific surface area (**equation 13**):

$$1500=SSA*D \quad (13)$$

in which: 1500 is a constant, SSA is the specific surface area of sample (m^2/g) and D is the particle size of sample (nm),

the average particle size of ISO-ana and ISO-rut samples were estimated to be ca. 25 nm and ca. 47 nm, respectively. Considering the content of rutile phase and anatase phase in P25, the estimated SSA of P25 (SSA_{P25}), without considering NC phase, could be calculated, as follow:

$$SSA_{P25} = SSA_{ana} * w_{ana} + SSA_{rut} * w_{rut} \quad (14)$$

in which,

SSA_{ana} is the specific surface area of anatase particle (m^2/g), w_{ana} is the content of anatase phase in P25 (%), SSA_{rut} is the specific surface area of rutile particle (m^2/g) and w_{rut} is the content of rutile phase in P25 (%).

Here, the SSA_{P25} = 61 * 78% + 28 * 14% (m^2/g) = 51.5 m^2/g.

This calculated SSA_{P25} is almost the same as the measured value of SSA (52 m^2/g), that confirms efficiency of isolation processes.

Table 2.3 Properties of HomoP25 and isolated phases

sample	Crystal composition and crystallite sizes (XRD analysis)					SSA (BET)	Particle size/nm (STEM)	
	anatase phase		rutile phase		NC part			
	content (%)	size /nm	content (%)	size /nm	content (%)	/m^2g^{-1}	average	mean
HomoP25	78	25.3	14	39.6	8	52	27.5	22.5
ANA	86	23.7	1	-	13	61	23.3	19.5
RUT	0	-	98	39.5	2	28	40.2	32.4

NC–non-crystal, SSA–specific surface area

Copyright © 2017 Elsevier B.V., all rights reserved

Morphology of samples was investigated by STEM observation, and exemplary STEM images are shown in **Figure 2.18**. The presence of nanoparticles (NPs) of different sizes (from 15 to 150 nm) was observed in HomoP25 sample. The comparison with isolated samples allowed to conclude that rutile and anatase had larger and smaller sizes, respectively, which was also confirmed by XRD analysis (**Table 2.3**). The particle size of rutile varied from 20 to 150 nm, whereas anatase from 15 to 60 nm. The existence of rutile and anatase in the form of larger and smaller NPs, respectively, is not surprising since usually rutile forms larger NPs, as the result of its preparation at higher temperatures.

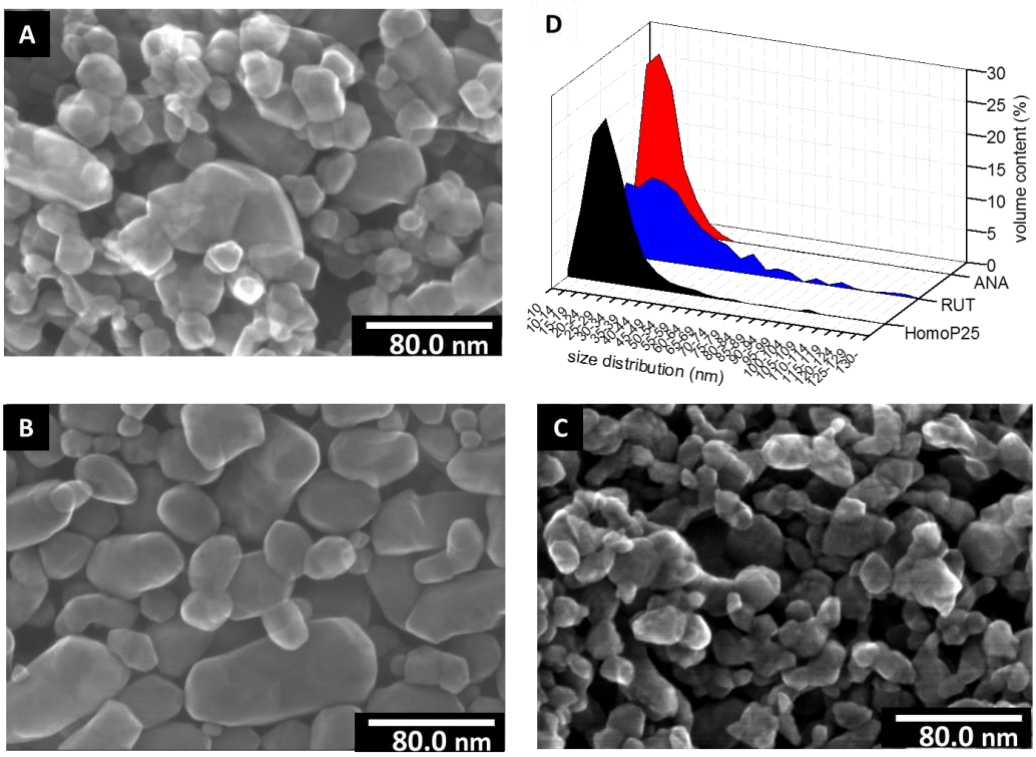


Figure. 2.18 STEM (SE mode) images of HomoP25 (A), ISO-rut (B) and ISO-ana (C), and distribution of NPs' sizes (D).

Copyright © 2017 Elsevier B.V., all rights reserved

Photoabsorption properties of HomoP25 and isolated samples are shown in **Figure. 2.19** (left) and **Figure. 2.20** (left). It is clearly observed that isolation resulted in shift of absorption edge to shorter and longer wavelengths for ISO-ana and ISO-rut, as a result of efficient removal of rutile and anatase, respectively. The stronger absorption of ISO-ana at visible range (400-500 nm) was not surprising since this sample was slightly yellow. The possible reason of this absorption could result from the presence of the impurities from isolation process, i.e., inclusion of nitrogen from ammonia or surface peroxy species from hydrogen peroxide during the isolation process. The nitrogen-modified titania or H_2O_2 adsorbed titania samples usually exhibit such photoabsorption properties and are yellow colored.[60, 61, 72, 73] The photoabsorption by ISO-rut was practically only bathochromically shifted in comparison to HomoP25, proving anatase removal (Rutile has slightly narrower bandgap than anatase.). The slight higher photoabsorption at visible range at 400-700 nm did not result in any change of sample color, and thus, higher light scattering on large rutile NPs was initially considered as the reason of this photoabsorption. The XRD patterns of HomoP25, ISO-ana and ISO-rut are shown in **Figure. 2.19** (right) and **Figure. 2.20** (right). The lack of anatase and rutile peaks in XRD patterns of ISO-rut and ISO-ana, respectively, suggests that applied isolation process was efficient and removed anatase and rutile crystallites almost completely. For ISO-ana and ISO-rut, the width of the most intense anatase and rutile peaks (**Figure. 2.19** (right) and **Figure. 2.20** (right)), reflecting the crystallite size, was almost the same as that of these peaks in HomoP25, indicating that the crystallite sizes did not change during the isolation processes (**Table 2.3**), as has already been reported.[59] The analysis of crystalline sizes confirmed that sizes of anatase and rutile practically did not change, as shown in **Table 2.3**. The slight decrease in anatase size, i.e., from 25.3 nm to 23.7 nm, for HomoP25and ISO-ana, respectively, suggests the possible dissolution of anatase crystallites together with rutile during titania treatment with hydrogen peroxide-ammonia mixture, and thus proving the suggested mechanism of dissolution of both crystalline phase. Though crystalline phases could be removed efficiently, non-crystalline (NC) components were

included in the samples as shown in **Table 2.3**. The increase in NC content could result from: i) dissolution of titania crystallites during isolation process with subsequent re-formation into amorphous titania particles; and ii) formation of NC phase during selective isolation process from HF, NH_3, H_2O_2, amorphous titania, and compounds formed during titania dissolution.

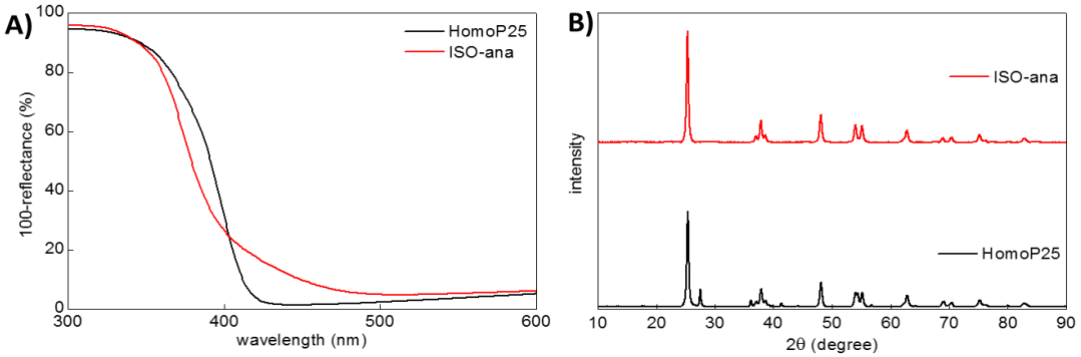


Figure. 2.19 The photoabsorption properties (a) and the XRD patterns (b) of ISO-ana and HomoP25.

Copyright © 2017 Elsevier B.V., all rights reserved

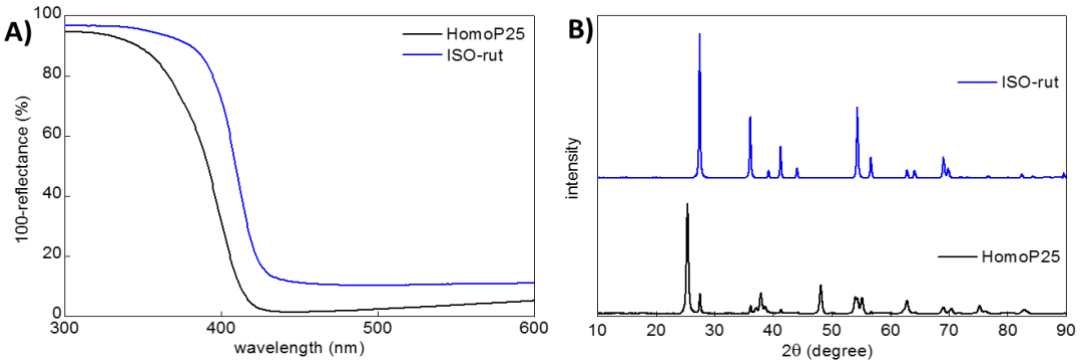


Figure. 2.20 The photoabsorption properties (a) and the XRD patterns (b) of ISO-rut and HomoP25.

Copyright © 2017 Elsevier B.V., all rights reserved

The photocatalytic activity of isolated phases was checked for oxidative decomposition of acetic acid (CO_2 system) and dehydrogenation of methanol (H_2), and compared with data form HomoP25 (100%), as shown in **Figure 2.21**. ISO-rut and ISO-ana showed low activity in the H_2 system, but ISO-ana exhibited higher activity in the CO_2 system than HomoP25 similarly to reported data previously (**Figure. 2.3**). Higher activity of ISO-ana than that of HomoP25 and ISO-rut is probably caused by slightly more negative position of CB of anatase (wider band gap) than that of rutile, as shown in **Figure 2.22**.[64, 65, 74-76] Much higher activity of HomoP25 in H_2 system than that of single crystalline phase could suggest "synergy" between

two phases (the activity of P25 is higher than the sum of activities of ISO-ana and ISO-rut), e.g., IPCT. However, it should be reminded that chemical isolation method may result in surface impurity, that cannot be easily detect by XRD measurements. Indeed, photoabsorption properties of ISO-ana (**Figure 2.19**) suggest the presence of some impurifies, (due to NH_3 and H_2O_2 treatment) resulting in visible-absorption (300-500 nm).

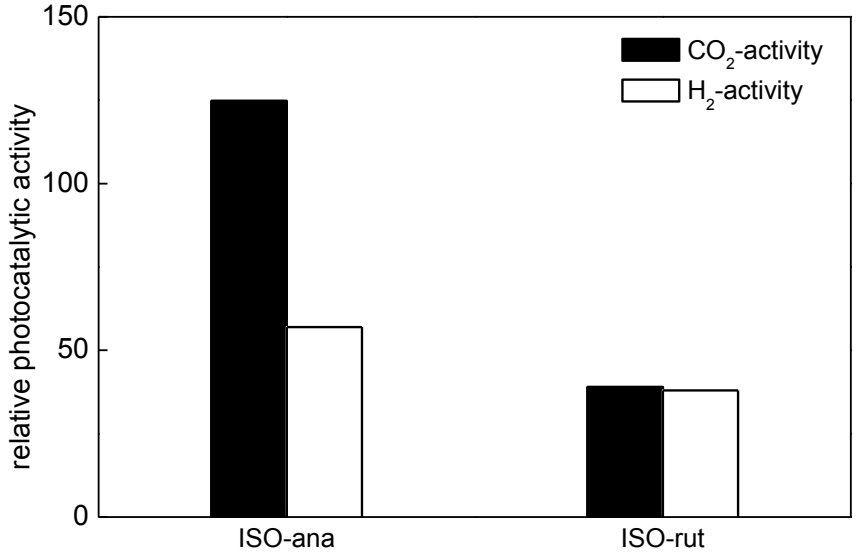


Figure. 2.21 Photocatalytic activities of isolated samples related to that of Homo-P25 as reference (100%).

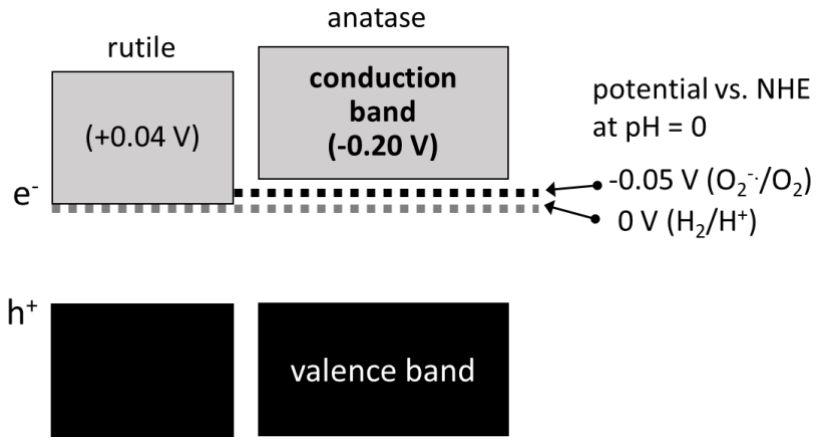


Figure. 2.22 Schematic drawing of bandgap structure of anatase and rutile.[77]

In order to remove impurities, originated from the isolation process, the post-treatment operation, i.e., annealing, was applied. The DRS data for the annealed samples are shown in **Figure. 2.23** (left) and **Figure. 2.24** (left). It was found that annealing resulted in

disappearance of visible-light absorption of ISO-ana indicating efficient removal of contaminants. It should be pointed that crystalline properties (composition, crystalline size) did not change by the post-treatment, indicating that calcination removed only the impurities from the isolated samples. Whereas, quite different behavior was noticed for annealed ISO-rut, as shown in **Figure 2.24**. The shapes of DRS spectra, especially for samples annealed at 120 ºC and 200 ºC, highly differed from DRS of ISO-rut, showing significant photoabsorption in the visible range, as clearly observed by sample color change from white to light brown. It is proposed that a shoulder at 400-800 nm could originate from either trivalent titanium species or titania modified with adsorbed hydrofluoric acid.

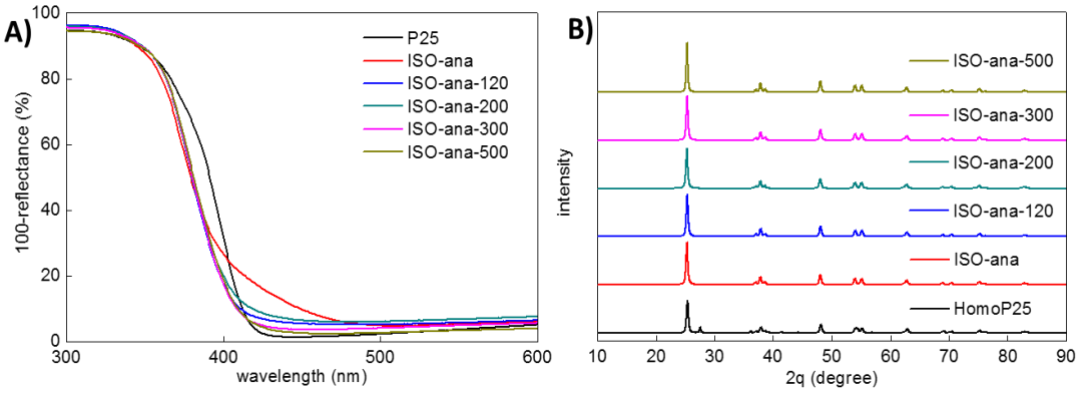


Figure. 2.23 The photoabsorption properties (a) and the XRD patterns (b) of ISO-ana-[temp] samples and HomoP25.

Copyright © 2017 Elsevier B.V., all rights reserved

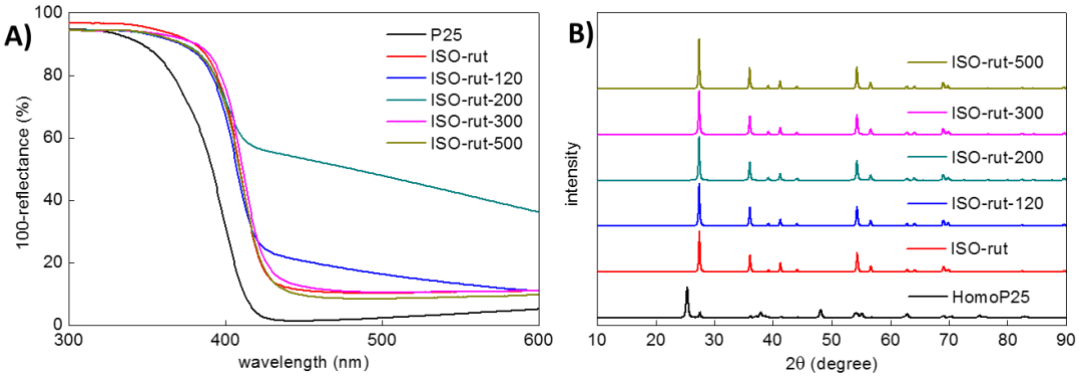


Figure. 2.24 The photoabsorption properties (a) and the XRD patterns (b) of ISO-rut-[temp] samples and HomoP25

Copyright © 2017 Elsevier B.V., all rights reserved

Post-treatment annealing caused the change of crystalline composition, as shown in **Tables 2.4** and **2.5**. Surprisingly, after annealing at 120 and 200 ºC, the NC content in ISO-rut increased. It is proposed that HF etching resulted in dissolution of titania crystals and simultaneous formation of F-modified amorphous titania. The further increase in annealing temperature to 300 ºC and 500 ºC resulted in preparation of samples with much higher amount of NC than ISO-rut, i.e., 23 and 28 % for 300 and 500 ºC, respectively. It is proposed that HF present on the surface of titania could react with crystalline rutile causing its dissolution, and thus new amorphous compounds containing titanium, fluorine, hydrogen and oxygen could be formed. Different tendency was obtained for annealed ISO-ana, for which annealing caused disappearance of visible light absorption for all samples and also decrease of NC content for ISO-ana-120 and ISO-ana-300. The increase in annealing temperature to 500 ºC resulted in an increase in NC content, which could be caused by similar mechanism as was proposed for annealed rutile, i.e., chemical compounds used for anatase isolation (NH_3, H_2O_2), adsorbed on titania surface, could react with crystalline anatase at high temperature causing its dissolution and formation of new amorphous compounds consisting titanium, oxygen, nitrogen and hydrogen.

Table 2.4 Crystalline composition of HomoP25 and isolated-anatase annealed at different temperature

Sample	Crystalline Composition (%)		
	Anatase	Rutile	NC
Homo-P25	78	14	8
ISO-ana	86	1	13
ISO-ana-120	84	4	12
ISO-ana-200	86	1	13
ISO-ana-300	90	3	7
ISO-ana-500	82	0	17

Table 2.5 Crystalline composition of HomoP25 and isolated-rutile annealed at different temperature

Sample	Crystalline Composition (%)		
	Anatase	Rutile	NC
Homo-P25	78	14	8
ISO-rut	0	89	11
ISO-rut-120	0	84	16
ISO-rut-200	0	79	21
ISO-rut-300	1	76	23
ISO-rut-500	1	72	28

To remove hydrofluoric acid from the surface of isolated rutile (ISO-rut) and to avoid formation of F-modified titania (during annealing), ISO-rut was washed with aqueous solution of NaOH, and then annealed. It was found that removing HF by NaOH washing was very efficient, and the surface content of fluorine, measured by XPS, was reduced from 9% to less than 1% (**Table 2.6**). Moreover, high vis photoabsorption of isolated rutile sample after NaOH washing disappeared, as shown in **Figure 2.25**. The crystalline compositions of washed samples annealed at different temperatures are shown in **Table 2.7**. The content of NC phase in washed samples was lower than that of unwashed ones for all annealed samples, proving the removal of absorbed HF from the surface of the ISO-rut. Only not annealed sample (ISO-rut-NaOH) possessed higher amount of NC than unwashed sample (ISO-rut), suggesting that not only acidic, but also alkali treatment may cause dissolution of crystalline phase and formation of amorphous compounds. After purification of isolated titania samples, the purified anatase sample was named as ANA (ISO-ana-200) and purified rutile sample was named as RUT (ISO-rut-NaOH-200).

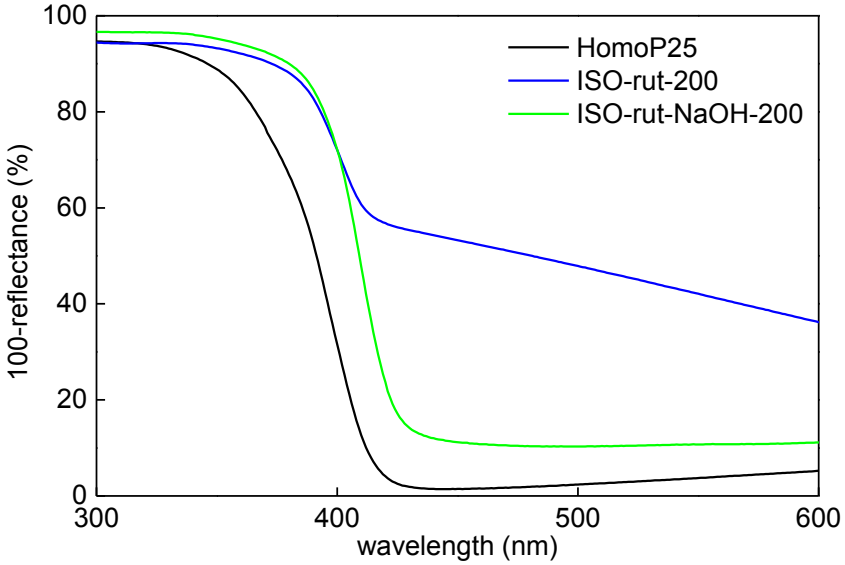


Figure 2.25 Photoabsorption of ISO-rut-200, ISO-rut-NaOH-200 and HomoP25.

Table 2.6 Content of adsorbed fluorine measured by XPS

Sample	F/Ti (%)
ISO-rut-200	9.2
ISO-rut-NaOH-200	0.9

Table 2.7 Crystalline composition of washed samples

Sample	Crystalline Composition (%)		
	Anatase	Rutile	NC
Homo-P25	78	14	8
ISO-rut-NaOH	0	84	16
ISO-rut-NaOH-120	0	89	11
ISO-rut-NaOH-200	1	97	2
ISO-rut-NaOH-300	0	80	19
ISO-rut-NaOH-500	0	84	16

Purification methods did not change overall activities significantly in CO_2 system, i.e., similarly to not-treated samples, anatase sample was the most active (**Figure 2.26**), due to more negative position of CB, and thus, the ability of one-electron reduction of oxygen. Interestingly, ISO-rut-200 with the strongest vis-absorption showed the highest activity among rutile samples, which could be caused by titania modification with fluorine. Some

recent reports have indicated that such modification enhanced photocatalytic activity.[78, 79] Moreover, purification of isolated rutile by NaOH washing resulted in slight decrease in activity of all rutile samples, which could be caused by sodium presence. It is well known that sodium decreases photocatalytic activity of titania, being recombination center.[14, 80] In contrast, for methanol dehydrogenation both isolated samples (independently on annealing conditions) shows lower activity than that of P25, which could suggest some IPCT ("synergy") between anatase and rutile in P25. However, purified rutile sample by NaOH washing and annealing at 120 and 200 ºC exhibited higher activity than that of P25 (The small content of sodium did not inhibit the activity significantly.). Therefore, it was found that high photocatalytic activity of P25 was not caused by "synergy" between anatase and rutile, but by intrinsic high activities of both crystalline phases in different reaction system, i.e., anatase for oxidative decomposition of acetic acid and rutile for dehydrogenation of methanol.

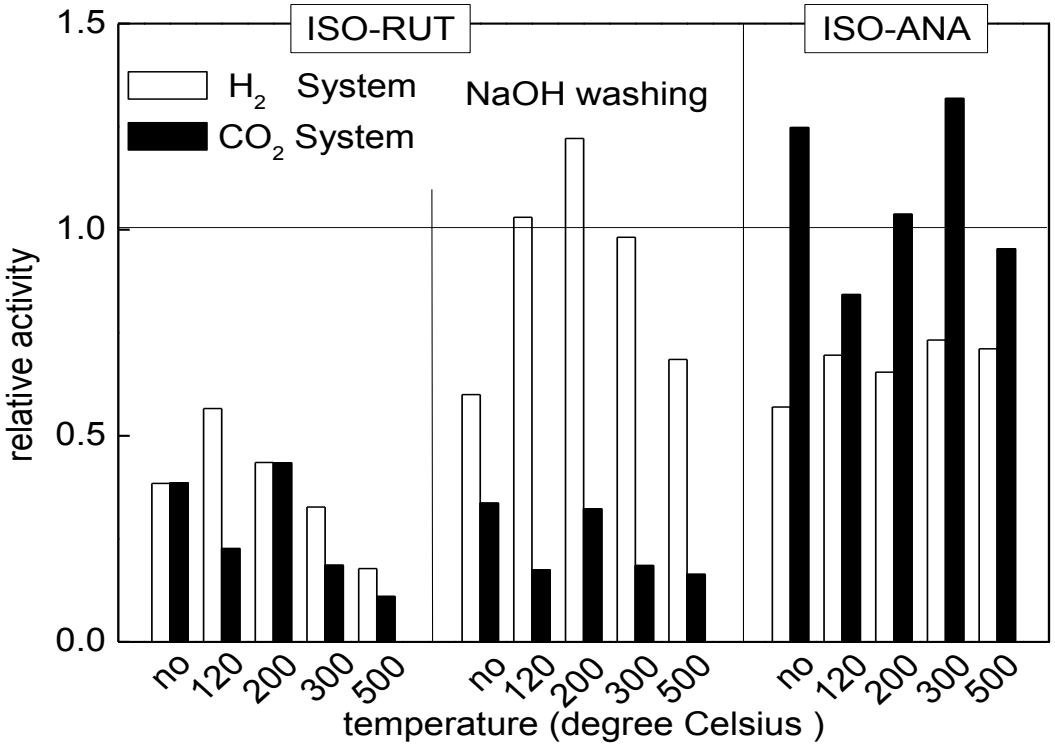


Figure. 2.26 The photocatalytic activity of isolated samples in two system related to Homo-P25 as reference (100%).

TRMC measurements were performed to investigate the mobility of charge carriers, and obtained data are shown in **Figure 2.27**. More intensive TRMC signal (I_{max}) for ISO-ana than

that for HomoP25, ISO-rut and ISO-rut-200 confirmed that anatase is responsible for high photocatalytic activity. The similar decay for ISO-anatase and HomoP25 confirms high activity of P25, due to anatase presence. Lower I_{max} and faster decay for ISO-rut and ISO-rut-200 indicate that photogenerated electrons are trapped fast at recombination centers. Therefore, it is proposed that higher activity of anatase than rutile for oxidative decomposition of acetic acid is not only caused by more negative position of CB, but also the intrinsic properties of both crystalline phases, i.e., larger content of deep electron traps (ETs) in rutile than that in anatase. Preliminary RDB-PAS experiments confirmed larger content of shallow ETs in isolated anatase samples and larger content of deep ETs in isolated rutile samples.

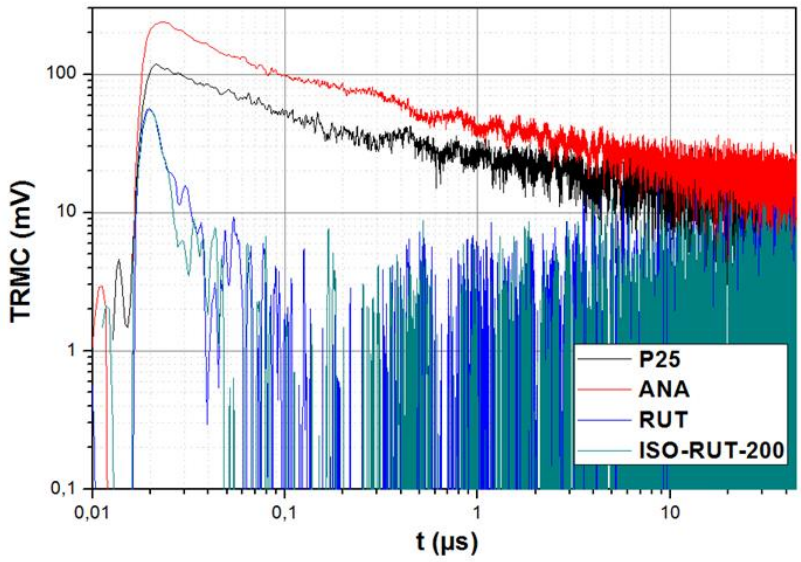


Figure 2.27 The TRMC results of HomoP25, ANA and RUT samples.

Therefore, it is difficult to explain surprisingly high activity of rutile sample in H_2 system, that could not be simply explained by mobility and lifetime of electrons, as well as distribution of ETs. However, it should be reminded that in H_2 system, Pt NPs are used as co-catalyst (for hydrogen formation). Moreover, Pt NPs also retard recombination between electrons and holes. Indeed, TRMC measurements, taken for Pt-modified titania, showed significant decreased in I_{max}, as shown in **Figure 2.28**. It should be pointed that a decrease in TRMC signal after loading with Pt is not caused by fast charge carriers' recombination, but

because of electron scavenging by Pt, as already reported,[81] and thus, retardation of their recombination with holes.

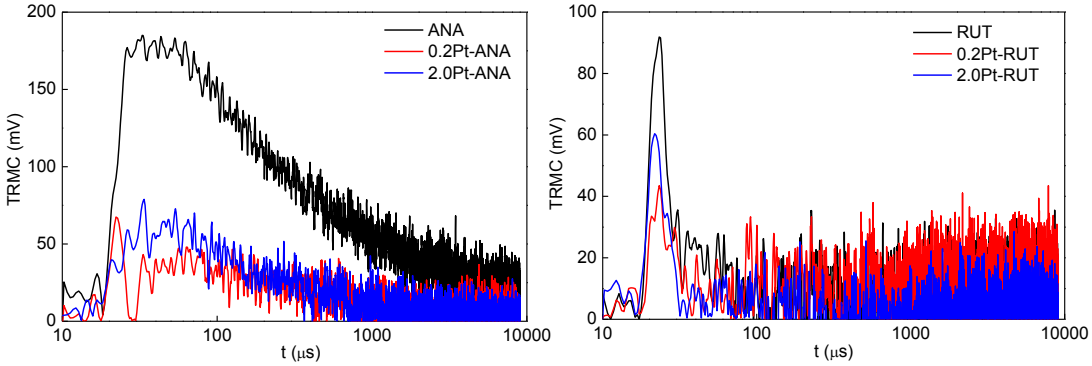


Figure 2.28 The TRMC results of bare and Pt-modified ANA (left) and RUT (right) samples: 0.2 and 2 wt% Pt was used for modification (as presented in Chapter III).

2.4. Summary

Rutile particles and anatase particles were successfully isolated from P25 by chemical dissolution method. Purification of isolated samples by thermal treatment and alkali washing (for rutile) resulted in efficient removal of adsorption species, such as ammonia/peroxy species and hydrofluoric acid from anatase and rutile surface, respectively. Unfortunately, it was impossible to remove all non-crystalline phase (mainly amorphous titania) since during chemical isolation, strong chemical etching could dissolve not only crystalline titania, but also initiate formation of amorphous titania (It is possible that amorphous titania layer could partly surround anatase and rutile crystals.). TRMC experiments confirmed that anatase in P25 is responsible for higher photocatalytic activity for reactions involving one-electron reduction of oxygen, due to high mobility of photogenerated electrons. Whereas, for dehydrogenation of methanol, rutile is responsible for high activity of P25, due to ability of photoabsorption of more photons (narrow bandgap). It should be reminded that in H_2 system, Pt NPs deposited on the titania surface played double function: 1) as hydrogen evolution site, and 2) inhibition of charge carriers' recombination (confirmed by TRMC measurements). Therefore, it is thought that properties of Pt NPs could be crucial for overall activity, and thus this issue has been studied in detail, as presented in Chapter III and Chapter IV.

2.5. References

1. Ohtani, B.; Prieto-Mahaney, O. O.; Li, D.; Abe, R., W*J. Photochem. Photobiol., A* **2010,** *216*, 179.
2. Neppolian, B., *Journal of Hazardous Materials* **2002,** *89* (2-3), 303-317.
3. Mills, A.; Morris, S., *Journal of Photochemistry and Photobiology a-Chemistry* **1993,** *71* (1), 75-83.
4. Mozia, S.; Tomaszewska, M.; Morawski, A. W., *Applied Catalysis B: Environmental* **2005,** *59* (1-2), 131-137.
5. Toepfer, B.; Gora, A.; Li Puma, G., *Applied Catalysis B-Environmental* **2006,** *68* (3-4), 171-180.
6. Grzechulska, J.; Morawski, A. W., *Applied Catalysis B: Environmental* **2003,** *46* (2), 415-419.
7. Ferguson, M. A.; Hering, J. G., *Environmental Science & Technology* **2006,** *40* (13), 4261-4267.
8. Yao, Z. X.; Wang, M. Q.; Sun, S. H.; Jia, R. B.; Li, H., *Journal of Inorganic and Organometallic Polymers and Materials* **2014,** *24* (2), 315-320.
9. Jiao, Y. C.; Jiang, H. L.; Chen, F., *Acs Catalysis* **2014,** *4* (7), 2249-2257.
10. Thevenet, F.; Guillard, C.; Rousseau, A., *Chemical Engineering Journal* **2014,** *244*, 50-58.
11. Sakai, H.; Kubota, Y.; Yamaguchi, K.; Fukuoka, H.; Inumaru, K., *Journal of Porous Materials* **2012,** *20* (4), 693-699.
12. Toma, F.-L.; Bertrand, G.; Chwa, S. O.; Meunier, C.; Klein, D.; Coddet, C., *Surface and Coatings Technology* **2006,** *200* (20-21), 5855-5862.
13. Nishikawa, N.; Kaneco, S.; Katsumata, H.; Suzuki, T.; Ohta, K.; Yamazaki, E.; Masuyama, K.; Hashimoto, T.; Kamiya, K., *Fresenius Environmental Bulletin* **2007,** *16* (3), 310-314.
14. Markowska-Szczupak, A.; Wang, K. L.; Rokicka, P.; Endo, M.; Wei, Z. S.; Ohtani, B.; Morawski, A. W.; Kowalska, E., *J Photoch Photobio B* **2015,** *151*, 54-62.
15. Krishna, V.; Pumprueg, S.; Lee, S. H.; Zhao, J.; Sigmund, W.; Koopman, B.; Moudgil, B. M., *Process Safety and Environmental Protection* **2005,** *83* (B4), 393-397.
16. Long, T. C.; Saleh, N.; Tilton, R. D.; Lowry, G. V.; Veronesi, B., *Environmental Science & Technology* **2006,** *40* (14), 4346-4352.
17. Benabbou, A. K.; Derriche, Z.; Felix, C.; Lejeune, P.; Guillard, C., *Appl Catal B-Environ* **2007,** *76* (3-4), 257-263.
18. Bozzi, A.; Yuranova, T.; Guasaquillo, I.; Laub, D.; Kiwi, J., *Journal of Photochemistry and Photobiology A: Chemistry* **2005,** *174* (2), 156-164.
19. Smits, M.; Chan, C. k.; Tytgat, T.; Craeye, B.; Costarramone, N.; Lacombe, S.; Lenaerts, S., *Chemical Engineering Journal* **2013,** *222*, 411-418.
20. Vero, N.; Hribernik, S.; Andreozzi, P.; Sfiligoj-Smole, M., *Fibers and Polymers* **2009,** *10* (5), 716-723.
21. Antoniadou, M.; Lianos, P., Production of electricity by photoelectrochemical oxidation

of ethanol in a PhotoFuelCell. *Applied Catalysis B-Environmental* **2010,** *99* (1-2), 307-313.
22. Yurdakal, S.; Loddo, V.; Augugliaro, V.; Berber, H.; Palmisano, G.; Palmisano, L., *Catalysis Today* **2007,** *129* (1-2), 9-15.
23. Ohtani, B.; Mahaney, O. O. P.; Amano, F.; Murakami, N.; Abe, R., *Journal of Advanced Oxidation Technologies* **2010,** *13* (3).
24. Zielinska, B.; Grzechulska, J.; Grzmil, B.; Morawski, A. W., *Applied Catalysis B-Environmental* **2001,** *35* (1), L1-L7.
25. O'Regan, B.; Lenzmann, F.; Muis, R.; Wienke, J., *Chemistry of Materials* **2002,** *14* (12), 5023-5029.
26. Hurum, D. C.; Agrios, A. G.; Gray, K. A.; Rajh, T.; Thurnauer, M. C., *Journal of Physical Chemistry B* **2003,** *107* (19), 4545-4549.
27. Demeestere, K.; Dewulf, J.; Van Langenhove, H.; Sercu, B., *Chemical Engineering Science* **2003,** *58* (11), 2255-2267.
28. Hurum, D. C.; Gray, K. A.; Rajh, T.; Thurnauer, M. C., *Journal of Physical Chemistry B* **2004,** *108* (42), 16483-16487.
29. Hurum, D. C.; Gray, K. A.; Rajh, T.; Thurnauer, M. C., *J. Phys. Chem. B* **2005,** *109* (2), 977-980.
30. Teoh, W. Y.; Madler, L.; Beydoun, D.; Pratsinis, S. E.; Amal, R., *Chemical Engineering Science* **2005,** *60* (21), 5852-5861.
31. Kirchnerova, J.; Cohen, M. L. H.; Guy, C.; Klvana, D., *Applied Catalysis a-General* **2005,** *282* (1-2), 321-332.
32. Yu, J. G.; Yu, H. G.; Cheng, B.; Zhou, M. H.; Zhao, X. J., *Journal of Molecular Catalysis a-Chemical* **2006,** *253* (1-2), 112-118.
33. Janus, M.; Morawski, A. W., *Applied Catalysis B-Environmental* **2007,** *75* (1-2), 118-123.
34. Mills, A.; Lee, S.-K., *Journal of Photochemistry and Photobiology A: Chemistry* **2002,** *152* (1), 233-247.
35. Amano, F.; Yasumoto, T.; Mahaney, O. O. P.; Uchida, S.; Shibayama, T.; Terada, Y.; Ohtani, B., *Topics in Catalysis* **2010,** *53* (7-10), 455-461.
36. Wei, Z.; Kowalska, E.; Ohtani, B., *Molecules* **2014,** *19* (12), 19573-87.
37. Zhang, Z. B.; Wang, C. C.; Zakaria, R.; Ying, J. Y., *Journal of Physical Chemistry B* **1998,** *102* (52), 10871-10878.
38. Fang, Y. F.; Huang, Y. P.; Chen, H. C.; Luo, G. F.; Liu, X. L.; Liu, L. M., *Chinese Journal of Analytical Chemistry* **2006,** *34*, S83-S86.
39. Kaewgun, S.; Nolph, C. A.; Lee, B. I.; Wang, L. Q., *Materials Chemistry and Physics* **2009,** *114* (1), 439-445.
40. Di Paola, A.; Bellardita, M.; Palmisano, L.; Barbierikova, Z.; Brezova, V., *Journal of Photochemistry and Photobiology a-Chemistry* **2014,** *273*, 59-67.
41. Bickley, R. I.; Gonzalez-Carreno, T.; Lees, J. S.; Palmisano, L.; Tilley, R. J. D., *Journal of Solid State Chemistry* **1991,** *92* (1), 178-90.
42. Ohno, T.; Sarukawa, K.; Tokieda, K.; Matsumura, M., *Journal of Catalysis* **2001,** *203* (1), 82-86.

43. Ohtani, B., *Chemistry Letters* **2008,** *37* (3), 216-229.
44. Boehme, M.; Ensinger, W., *Nano-Micro Letters* **2011,** *3* (4), 236-241.
45. van der Meulen, T.; Mattson, A.; Osterlund, L., *Journal of Catalysis* **2007,** *251* (1), 131-144.
46. Su, R.; Bechstein, R.; Sø, L.; Vang, R. T.; Sillassen, M.; Esbjörnsson, B.; Palmqvist, A.; Besenbacher, F., *The Journal of Physical Chemistry C* **2011,** *115* (49), 24287-24292.
47. Zhu, Q.; Qian, J. S.; Pan, H.; Tu, L.; Zhou, X. F., *Nanotechnology* **2011,** *22* (39), 9.
48. Wang, Q. Z.; Lian, J. H.; Bai, Y.; Hui, J.; Zhong, J. B.; Li, J. Z.; An, N.; Yu, J.; Wang, F. P., *Materials Science in Semiconductor Processing* **2015,** *40*, 418-423.
49. Rui, Z. B.; Wu, S. R.; Peng, C.; Ji, H. B., *Chemical Engineering Journal* **2014,** *243*, 254-264.
50. Zhang, J.; Xu, Q.; Feng, Z.; Li, M.; Li, C., *Angew Chem Int Ed Engl* **2008,** *47* (9), 1766-9.
51. Scanlon, D. O.; Dunnill, C. W.; Buckeridge, J.; Shevlin, S. A.; Logsdail, A. J.; Woodley, S. M.; Catlow, C. R.; Powell, M. J.; Palgrave, R. G.; Parkin, I. P.; Watson, G. W.; Keal, T. W.; Sherwood, P.; Walsh, A.; Sokol, A. A., *Nat Mater* **2013,** *12* (9), 798-801.
52. Mi, Y.; Weng, Y. X., *Sci Rep-Uk* **2015,** *5*.
53. Jiang, X. Z.; Manawan, M.; Feng, T.; Qian, R. F.; Zhao, T.; Zhou, G. D.; Kong, F. T.; Wang, Q.; Dai, S. Y.; Pan, J. H., *Catalysis Today* **2018,** *300*, 12-17.
54. Xiong, Z.; Wu, H.; Zhang, L.; Gu, Y.; Zhao, X. S., *Journal of Materials Chemistry A* **2014,** *2* (24).
55. Li, A.; Wang, Z.; Yin, H.; Wang, S.; Yan, P.; Huang, B.; Wang, X.; Li, R.; Zong, X.; Han, H.; Li, C., *Chemical Science* **2016,** *7* (9), 6076-6082.
56. Jiang, D.; Zhang, S.; Zhao, H., *Environmental Science & Technology* **2007,** *41* (1), 303-308.
57. Ohno, T.; Tokieda, K.; Higashida, S.; Matsumura, M., *Applied Catalysis, A: General* **2003,** *244* (2), 383-391.
58. Zhang, J.; Li, M. J.; Feng, Z. C.; Chen, J.; Li, C., *Journal of Physical Chemistry B* **2006,** *110* (2), 927-935.
59. Ohtani, B.; Azuma, Y.; Li, D.; Ihara, T.; Abe, R., *Trans. Mater. Res. Soc. Jpn* **2007,** *32* (2), 401.
60. Carati, A.; Flego, C.; Previde Massara, E.; Millini, R.; Carluccio, L.; Parker, W. O.; Bellussi, G., *Microporous and Mesoporous Materials* **1999,** *30* (1), 137-144.
61. Wu, P.; Komatsu, T.; Yashima, T., *The Journal of Physical Chemistry B* **1998,** *102* (46), 9297-9303.
62. Boonstra, A. H.; Mutsaers, C. A. H. A., *The Journal of Physical Chemistry* **1975,** *79* (18), 1940-1943.
63. Hai, Z.; El Kolli, N.; Uribe, D. B.; Beaunier, P.; José-Yacaman, M.; Vigneron, J.; Etcheberry, A.; Sorgues, S.; Colbeau-Justin, C.; Chen, J., *J. Mater. Chem. A* **2013,** *1*, 10829.
64. Nitta, A.; Takase, M.; Takashima, M.; Murakami, N.; Ohtani, B., *Chem Commun (Camb)* **2016,** *52* (81), 12096-12099.
65. Nitta, A.; Takashima, M.; Murakami, N.; Takase, M.; Ohtani, B., *Electrochimica Acta*

2017.

66. Zhang, F. W.; Wang, L.; Liu, C. P.; Wu, P.; Zhan, S., *Physics Letters A* **2014,** *378* (18-19), 1303-1308.

67. Han, Y.; Li, Q.; Liu, W.; He, Y., Effect of *Metallurgical and Materials Transactions A* **2012,** *43* (5), 1400-1404.

68. Valverde, J. M.; Castellanos, A., *AIChE Journal* **2006,** *52* (5), 1705-1714.

69. Perera, V.; Jackson, A. P.; Asphaug, E.; Ballouz, R. L., *Icarus* **2016,** *278*, 194-203.

70. Liao, C. C.; Hsiau, S. S., T *Kona Powder and Particle Journal* **2016,** (33), 109-126.

71. Mobius, M. E.; Lauderdale, B. E.; Nagel, S. R.; Jaeger, H. M., *Nature* **2001,** *414* (6861), 270.

72. Dolat, D.; Moszynski, D.; Guskos, N.; Ohtani, B.; Morawski, A. W., *Applied Surface Science* **2013,** *266*, 410-419.

73. Yap, P. S.; Cheah, Y. L.; Srinivasan, M.; Lim, T. T., *Applied Catalysis a-General* **2012,** *427*, 125-136.

74. Reddy, K. M.; Manorama, S. V.; Reddy, A. R., *Materials Chemistry and Physics* **2003,** *78* (1), 239-245.

75. Valencia, S.; Marín, J. M.; Restrepo, G., *The Open Materials Science Journal* **2010,** *4* (1), 9-14.

76. A. P. Ribeiro, R.; R. de Lazaro, S.; R. de Oliveira, C., *Current Physical Chemistry* **2016,** *6* (1), 22-27.

77. Ohtani, B., *Journal of Photochemistry and Photobiology C: Photochemistry Reviews* **2010,** *11* (4), 157-178.

78. Dozzi, Maria V.; Selli, E., *Materials Science in Semiconductor Processing* **2016,** *42*, 36-39.

79. Khoa Le, T.; Flahaut, D.; Foix, D.; Blanc, S.; Hung Nguyen, H. K.; Xuan Huynh, T. K.; Martinez, H., *Journal of Solid State Chemistry* **2012,** *187*, 300-308.

80. Diebold, U., *Surface Science Reports* **2003,** *48* (5-8), 53-229.

81. Kowalska, E.; Remita, H.; Colbeau-Justin, C.; Hupka, J.; Belloni, J., *Journal of Physical Chemistry C* **2008,** *112* (4), 1124-1131.

Chapter III

Interparticle electron transfer

(IPET)

3.1 Introduction

Surface modification of titania with noble metal is one of the most efficient methods for improving the photocatalytic activity of titania photocatalysts (as already discussed in section 1.3.2 of Chapter I). When metal NPs are deposited on the surface of titania, not only the surface properties of titania are changed, but also (photo)catalytic performance, by e.g.,

1) improvement of activity by retardation of charge carriers' recombination (noble metal as an electron pool),[1-3]

2) increasing the wavelength response range (light harvesting, e.g., due to surface plasmon resonance),[4-6]

3) changing the selectivity and yield of products.

It should be reminded that for titania (and other semiconductors) photocatalytic activity depends on the mobility and lifetime of charge carriers. In this sense, the migration of charge carriers to the surface, where they can react with adsorbed reagents, is the key-factor of the high photocatalytic activity. Even though, there are many methods for improving the photocatalytic activity of titania by reducing the recombination of charge carriers during photoirradiation, the mechanism of migration of electrons and holes of titania during photoirradiation is still not clear (especially for the charge migration between titania particles, i.e., interparticle charge transfer (IPCT)[7, 8]). In conventional sense, the charge carriers' migration means the electron and/or hole transfer to the surface of titania for reaction with adsorbed species. However, transfer of charges between particles (IPCT)[9, 10] should be also considered. For example, IPCT was proposed as the main reason of high activity of P25 (as already discussed in Chapter II). It should be reminded that various kinds of IPCT were proposed even for one titania photocatalyst–P25. For example, it was suggested that IPCT occurred between three types of titania in P25, i.e., anatase-amorphous-rutile with various combinations of electrons and holes migrations between two or three phases, due to the existence of localized states at the band edges of the amorphous phase creating tails into the bandgap.[9] Usually transfer of electron from anatase to rutile is proposed, due to more negative

potential of CB of anatase than rutile (**Figure 2.22**). However, some reports have proposed an opposite direction of electron transfer, i.e., (i) from rutile to anatase, e.g., migration of holes from anatase to the rutile overlayer and adverse transfer of electron, (ii) from rutile to anatase lattice trapping sites,[9] and (iii) electron transfer in both directions (in the case of the same position of CB, as shown in **Figure 2.2**) depending on dynamic factors (not thermodynamics), such as particle size, co-existence of adsorbed scavengers, etc.[11] Although, the results of some investigations suggest the electron transfer between anatase and rutile in P25 (e.g., by EPR spectroscopy,[12, 13] transient infrared absorption-excitation energy scanning spectroscopy[11]) the reference samples of anatase and rutile have not been the same as those in P25. Therefore, it is impossible to conclude that high photocatalytic activity of P25 is caused by transfer of charge carriers between crystalline phases. Indeed, my study has shown that intrinsic properties of both crystalline phases (anatase and rutile), i.e., high activity in different reaction systems are responsible for high activity of P25 (Chapter II), as was proposed by Ohtani et al. in 2010.[14]

It should be pointed that despite many reports on the migration of charge carries in titania particles have already been published, most of them only proposed that electrons are transferred to metal NPs changing the Fermi level, but difference in titania crystalline phase (anatase/rutile) are usually not even mentioned. Polymorphic forms of titania are different, i.e., they have different structure (**Figure 1.4**), different bandgap (**Figure 2.22**), and even in some mixed-phase titania (such as P25) anatase and rutile crystallites differ significantly, e.g., crystalline size (**Table 2.3**), surface charge (zeta potential). Therefore, it must be expected that these differences should result in different migration of charge carries for anatase and rutile. Moreover, it is also clear that properties of deposited metal, as well as charge carriers' migration from titania to deposited metal could depend on titania kind. Of course, there are some reports on the influence of Pt properties and amount on the photocatalytic activity, but these reports are mainly for narrow range of platinum loading (0.5 wt% - 2.0 wt%) and not for different titania samples.[3, 15-17] To the best of my knowledge, there is no detailed study on the influence of platinum loading on the photocatalytic activity of P25 and isolated phases from

P25. Moreover, my study on methanol dehydrogenation clearly indicates that rutile is more active than anatase (Chapter II), despite worse mobility of photogenerated electrons (TRMC data, **Figure 2.27**). There are two main possible reasons of higher activity of rutile than anatase for methanol dehydrogenation: (1) better photoabsorption properties (narrower bandgap), (2) better distribution/deposition of Pt NPs (with double functions: inhibition of charge carriers' recombination and hydrogen evolution site). Therefore, platinum-deposited titania (both mixed-phase—P25 and single phase—anatase and rutile) have been investigated in detail (loading amount and action spectra), and obtained data are presented in this chapter.

3.2 Experimental details

To explain the mechanism of methanol dehydrogenation on platinum-modified titania, three titania samples were studied, i.e., HomoP25, ANA and RUT (ANA and RUT were isolated from P25, as described in Chapter II.). In addition, reference sample—HomoP25 annealed at 473 K (in the presence of air, the same conditions as those used for ANA and RUT preparation) was prepared, and named as HomoP25-200.

The photocatalytic activity of samples was evaluated for methanol dehydrogenation on platinized titania samples by measurement of the amount of liberated hydrogen in two reaction systems, i.e., (1) under polychromatic irradiation (UV/vis), and (2) under monochromatic irradiation (action spectrum (AS) analysis). For polychromatic irradiation (1), the Pt NPs were photodeposited in situ under anaerobic conditions (as described in Chapter II). For AS analysis (2), first Pt was deposited on titania and then apparent quantum yield was measured. The procedure was the same as that described for deposition of Pt on titania, with the exception of: i) the volume of testing tubes (55 mL), ii) the volume of methanol (25 mL), iii) the amount of weighted titania (500 mg). In brief, Pt photodeposition was carried out under UV/vis irradiation (400-W high-pressure mercury arc, $\lambda > 290$ nm) on 500 mg of titania suspended in aqueous methanol (50 vol%, 25 mL). Aqueous solution of chloroplatinic acid (H_2PtCl_6, used as Pt source) was added to the test tube (55-mL pyrex glass containing the suspension of titania) under continuous stirring (to enable uniform distribution of metal NPs on titania). Then, air from the tube was purged by argon bubbling (ca. 15 min), the tube was sealed with a rubber septum, and the absence of oxygen was checked by gas-chromatography (TCD-GC, Shimadzu GC-8A-IT). The suspension was irradiated under continuous stirring (1,000 rpm) at 298 K in a thermostated water bath, and the amount of evolved hydrogen was checked each 15 min by TCD-GC. After irradiation, the samples were centrifuged, washed with methanol (3 times) and water (5 times), and freeze-dried. The irradiation set-up was very similar to that shown in **Figure 2.12** (the same lamp), except for test-tube holder (larger tubes were used). Pt-modified samples were named accordingly deposited amount of platinum, e.g.,

0.5@HomoP25 means that 0.5 wt% Pt was deposited on HomoP25.

For action spectra (AS) analysis, 30 mg of photocatalyst was suspended in 3 mL of aqueous methanol (50 vol%), air was removed from a quartz cell by argon bubbling (ca. 15 min), and a cell was sealed with a rubber septum. Then, a cell was irradiated for 1 h using a diffraction grating type illuminator (JASCO CRM-FD), equipped with a 300-W xenon lamp (Hamamatsu Photonics C2578-02). The intensity of irradiation, measure by a Hioki 3664 optical power meter, was in the range of 6.19–7.63 mW. During the irradiation, a portion (0.2 mL) of the gas phase was withdrawn from the reaction mixture with a syringe and injected into a gas-chromatograph. Apparent quantum yield (Φ_{app}) was calculated as the ratio of the rate of electron consumption (from the rate of hydrogen generation) to the flux of incident photons, assuming that two photons were required. The experimental set-up is shown in **Figure. 3.1**.

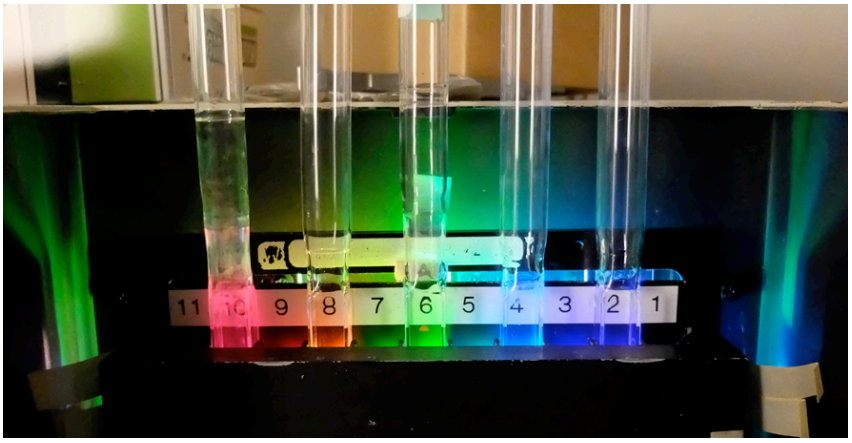


Figure. 3.1 Photograph of experimental set-up for AS analysis.

3.3 Results and discussions

It was confirmed that platinum was necessary to evolve hydrogen, as shown in **Figure 3.2**. It was found that deposition of platinum resulted in 17-fold activity increase for HomoP25 sample. Then, the influence of Pt amount (0.005–2 wt%) on the photocatalytic activity was investigated, and the obtained data are shown in **Figure. 3.3**. It was found that the amount of platinum highly influenced the photocatalytic activity. Obviously, with an increase in Pt amount, the photocatalytic activities increased for all tested samples, confirming that Pt NPs are necessary for efficient hydrogen evolution. RUT sample showed the highest photocatalytic activity independently on the loading amount of platinum, probably due to broader photoabsorption than that of anatase (narrower band-gap), as shown in the **Figure. 3.4.**

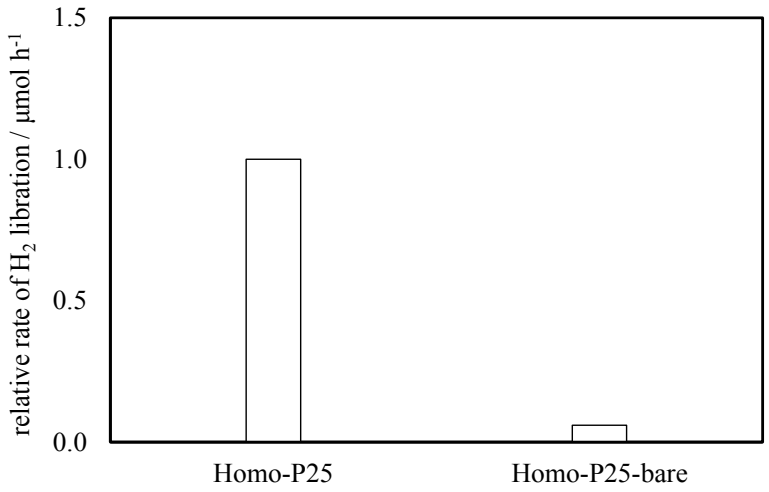


Figure. 3.2 The photocatalytic activity of HomoP25 (loaded with 2.0 wt% of Pt and

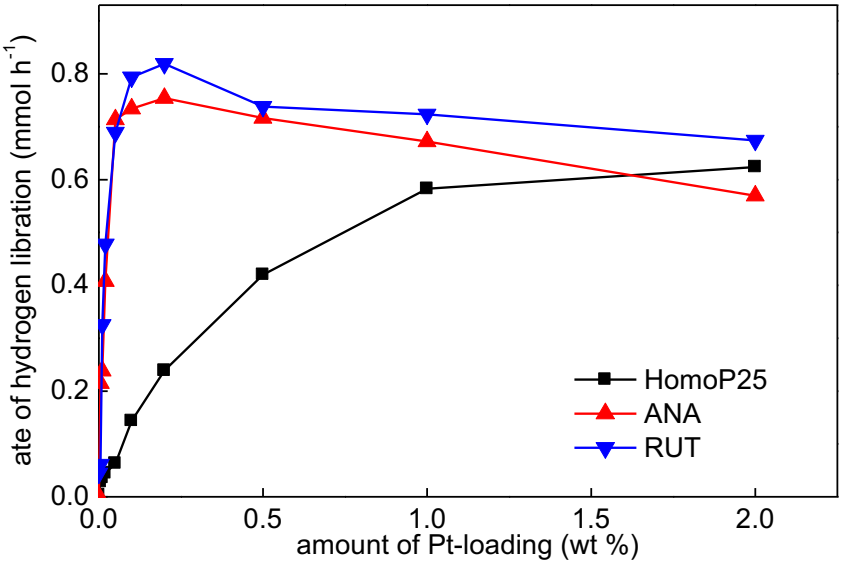


Figure. 3.3 Dependence of photocatalytic activity on the amount of Pt loading.

Copyright © 2017 Elsevier B.V., all rights reserved

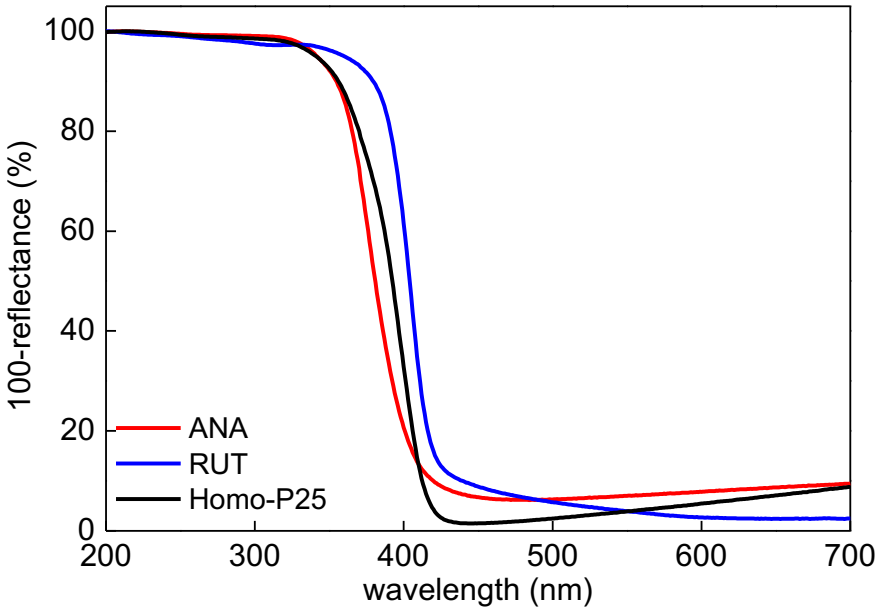


Figure. 3.4 Relative DRS of HomoP25, ANA and RUT

Copyright © 2017 Elsevier B.V., all rights reserved

Although, the lower level of conduction band (CB) of rutile has been reported as the main reason of its lower photocatalytic activity than that of anatase (poor reduction ability of photogenerated electrons),[18-20] the presence of Pt NPs (as a co-catalyst and an electron pool)

compensates it, and the broader photoabsorption results in enhanced overall photocatalytic activity. For larger amount of loaded-platinum (2 wt%), the activities of all samples seemed to saturate (were almost the same), and slight decrease at the higher loadings are attributable to the shielding of light by Pt deposits. The saturation can be interpreted by the expectation that at least one Pt NP was deposited on each titania particle (all titania particles were modified), on the basis of assumption that only Pt-deposited particles are active for photocatalytic hydrogen evolution and the activity does not depend on the number of Pt NPs if at least one Pt NP is deposited, as has been suggested previously.[2] In the lower Pt content range (0.005–0.2 wt%), the photocatalytic activities of RUT and ANA are significantly (few times) larger than that of HomoP25. It should be reminded that isolated samples were annealed at 473 K (for sample purification). Although this relatively low temperature should not cause NPs sintering (what was confirmed by STEM observations where only a few larger rutile NPs could be observed (**Figure. 2.18**)), it is proposed that the interface between NPs was increased allowing enhanced electron transfer between two (or more) NPs. In this regard, much lower amount of Pt could be sufficient for high photocatalytic activity, i.e., one Pt NP on one titania aggregate (as shown in **Figure. 3.5**). In other words, interparticle electron transfer (IPET) must occur within those aggregates/agglomerates formed by relatively low-temperature heating. Slight decrease in photocatalytic activity for larger than 0.2 wt% content of Pt for ANA and RUT is possibly caused by Pt aggregation (increase in Pt size with loading amount was observed, e.g., as shown for HomoP25 sample in **Figure. 3.6**) or “inner filter effect” (as Pt NPs are dark limiting photon absorption by titania, as shown in **Figure 3.7**).

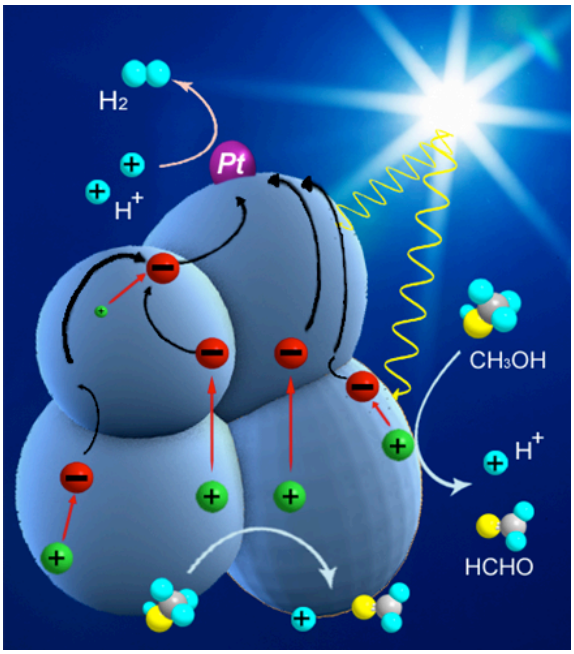


Figure. 3.5 Schematic drawing of IPET for Pt-modified aggregated titania particles.

Copyright © 2017 Elsevier B.V., all rights reserved

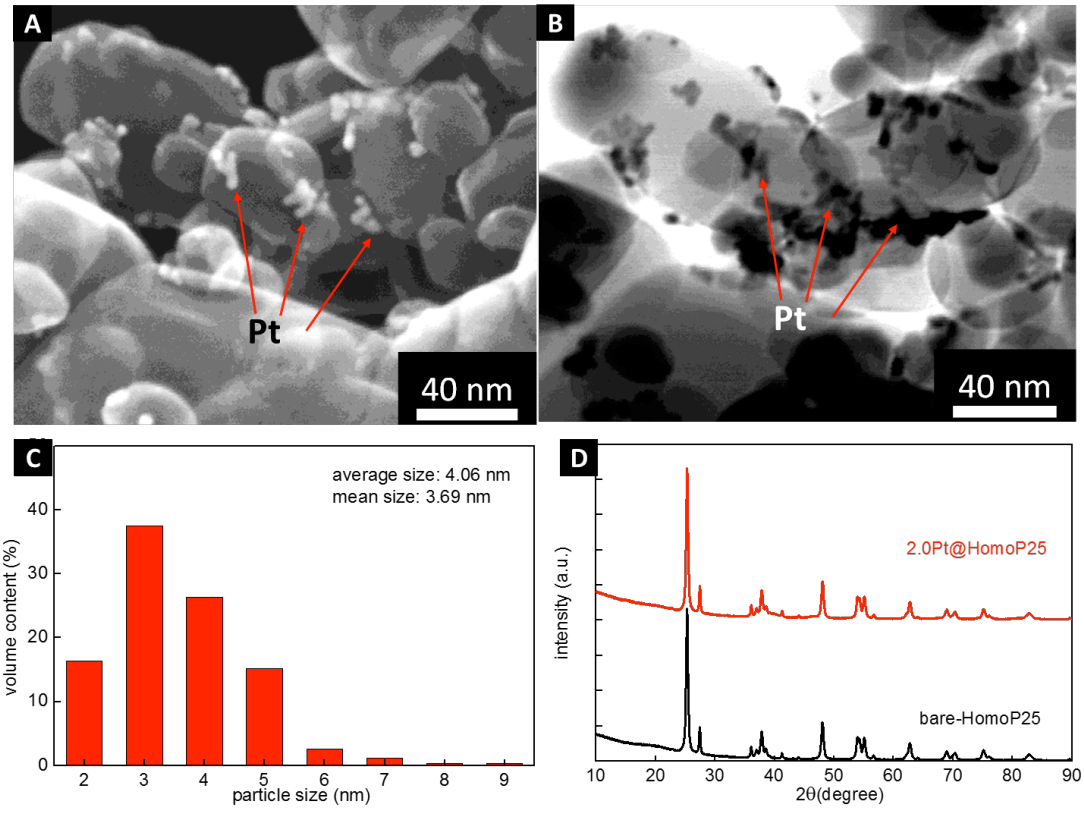


Figure.3.6 (A-B) STEM images of HomoP25 modified with 2 wt% of Pt NPs: (A) SE-mode, and (B) TEM-mode, (C) distribution of Pt NPs' sizes, and (D) XRD patterns for bare and modified titania.

Copyright © 2017 Elsevier B.V., all rights reserved

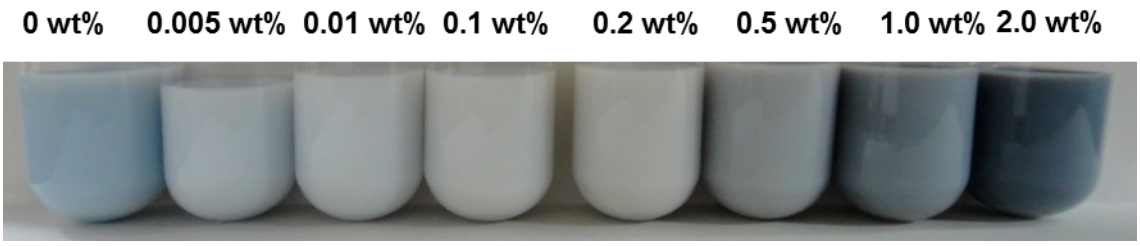


Figure.3.7 Photographs of HomoP25 samples after activity tests for different amounts of in situ Pt loading (0.005-2.o wt%).

To confirm that enhanced photocatalytic activity could be obtained by titania NPs aggregation by annealing, HomoP25 was also annealed at the same temperature as ANA and RUT (473 K), and obtained data for this sample (HomoP25-200) are shown in **Figure. 3.8**. It was found, that lower amount of Pt was sufficient to cause the same photocatalytic activity for annealed sample (HomoP25-200) as that for HomoP25 e.g., the same photocatalytic activities for both samples were obtained for 0.2 wt% (HomoP25-200) and 0.5 wt% (HomoP25) of Pt loading. By the heating at 473 K in air, the activity of HomoP25-200 at the lower Pt amount region was slightly improved compared with that of P25, i.e., the amount of Pt deposits required for activation of titania particles was reduced by heating, but was lower than those of ANA and RUT. This may be also explained by the aggregation/agglomeration of titania particles by the relatively low-temperature heating to make photoexcited electrons be transferred within aggregates/agglomerates (IPET), and the effective size of HomoP25-200 aggregates/agglomerates for IPET is smaller than those of ANA and RUT (Note that even though the heating temperature at the final stage of isolation of ANA and RUT was similar to that of HomoP25, ANA and RUT isolation processes must modify their surface structure affecting the size and connection of aggregate/agglomerates.). The explanation of mechanism needs further study, which is now in progress. One of the most valuable methods to investigate the mechanism of photocatalytic reactions is action spectrum analysis.

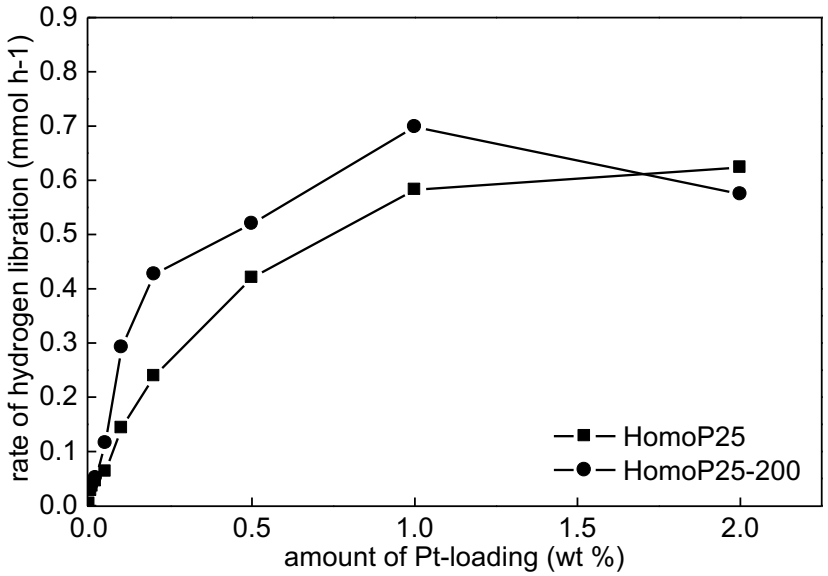


Figure. 3.8. Dependence of photocatalytic activity on the amount of Pt loading for HomoP25 and HomoP25-200.

For action spectra (AS), platinum was first deposited on three titania samples: HomoP25, ANA and RUT. Platinum was efficiently deposited on all samples, as shown in **Figures 3.9-3.13**. XRD patterns of Pt-loaded HomoP25 confirm that photodeposition did not influence the crystalline properties of titania (lack of shift in anatase and rutile position), as shown in **Figure 3.9**. Since the content of platinum was low and crystallite sizes were very small, it is difficult to detect any platinum peaks in these patterns. Therefore, XRD patterns after subtraction of titania peaks are also shown in **Figure 3.10**. The clear peaks of platinum have been observed, that correspond to Pt facets of (111), (200), (220), (311) and (222) at 40.25°, 46.81°, 68.36°, 82.42° and 86.96°, respectively. It was found that crystallite size of Pt did not depend on Pt-loading amount, as shown in **Figure 3.11**. Therefore, it is proposed that during aggregation (at larger loading content), platinum forms long aggregates (as shown in **Figure 3.6**), which are composed of small (2-3 nm) nanocrystals of Pt.

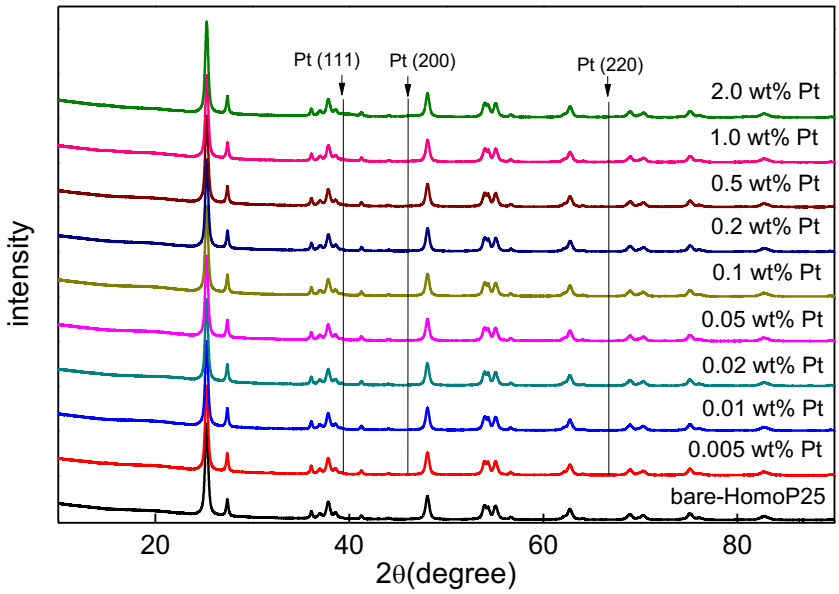


Figure.3.9 The XRD patterns of Pt-loaded HomoP25

Copyright © 2017 Elsevier B.V., all rights reserved

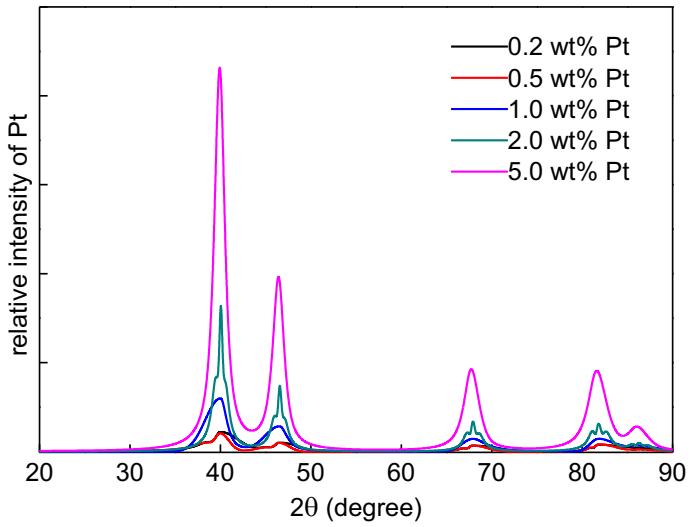


Figure.3.10 The XRD patterns of Pt-loaded HomoP25 after titania subtraction.

Copyright © 2017 Elsevier B.V., all rights reserved

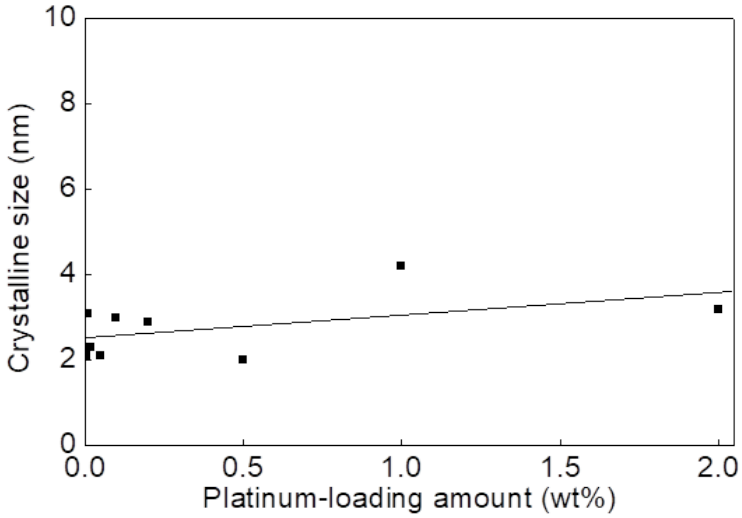


Figure 3.11 The crystalline size of Pt loaded on HomoP25.

Copyright © 2017 Elsevier B.V., all rights reserved

Modification of titania with platinum resulted in greyish coloration of all samples, as shown for five HomoP25 samples in **Figure 3.12**. DRS spectra confirm enhancement in vis-absorption with Pt-loading amount (**Figure 3.13**). Photoabsorption properties of platinized titania depend on the optical properties of platinum, titania and the volume fraction of the metal in the composite mixture. Driessen et al. showed that the photoabsorption of Pt/TiO_2 in vis range, predicted by Maxwell-Garnett theory, increased as a function of platinum volume fraction.[21]

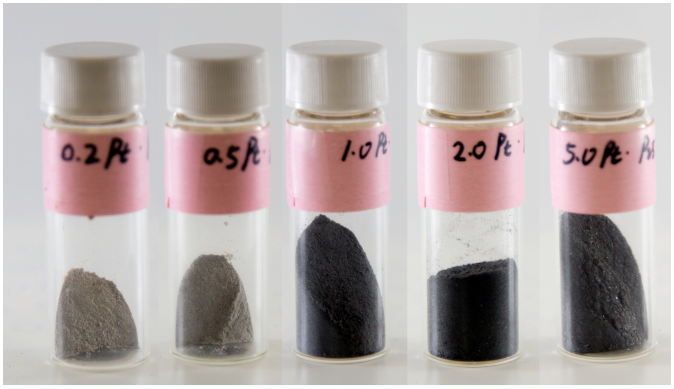


Figure 3.12 Photographs of Pt@HomoP25 samples with various amounts of loaded Pt.

Copyright © 2017 Elsevier B.V., all rights reserved

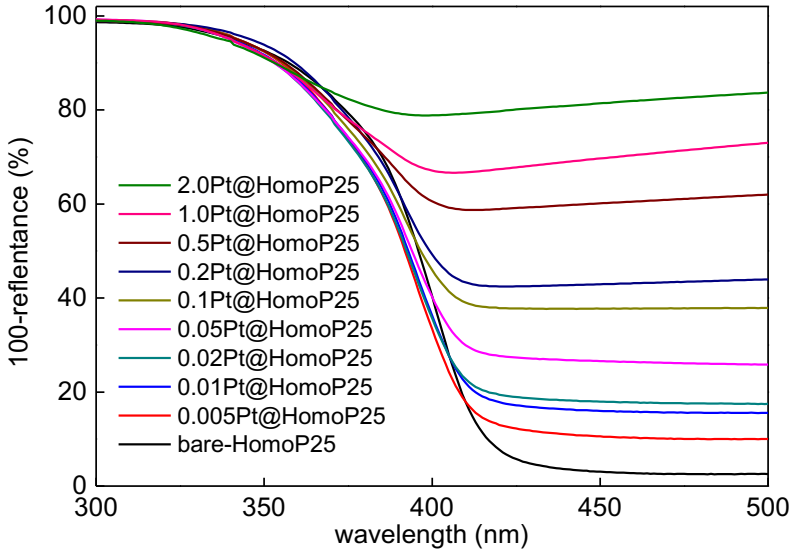


Figure 3.13 DRS of Pt@HomoP25 samples with various amounts of loaded Pt.

Copyright © 2017 Elsevier B.V., all rights reserved

Action spectra of methanol dehydrogenation on bare and platinized-samples (for 0.2 wt% of Pt) were investigated, and obtained data are shown in **Figure 3.14 A**. The necessity of Pt NPs' presence was confirmed since bare ANA and bare RUT sample were practically inactive in this reaction system. At short UV range (350–365 nm), the apparent quantum efficiency (Φapp) of platinized samples correlates with the overall photocatalytic activity of those samples (**Figure. 3.14 A**), i.e., Pt@RUT > Pt@ANA > Pt@HomoP25. Much lower photocatalytic activity of Pt@HomoP25 was caused by insufficient amount of Pt in that sample (non-aggregated titania NPs), as has been discussed above. The shape of action spectra of Pt@ANA and Pt@RUT resembles respective absorption spectra (**Figure. 3.14 B** and **Figure. 3.14 C**). Interestingly, the photocatalytic activity of Pt@HomoP25 was higher than that of Pt@ANA at UV range of 380-395 nm. It should be reminded that at this UV range mainly rutile absorbs light (especially at 395 nm). Therefore, higher photocatalytic activity of Pt@HomoP25 than that of Pt@ANA indicates that rutile was platinized first, especially taking into consideration much lower content of rutile than anatase in HomoP25 (14% vs. 78%). To confirm this assumption, various composition of samples (physical mixtures) were prepared and tested, i.e., (a) 15% Pt(0.2 wt%)/RUT and 85% ANA; (b) 50%

Pt(0.2 wt%)/RUT and 50% ANA; (c) 15% RUT and 85% Pt(0.2 wt%)/ANA; (d) 15% RUT and 85% Pt(0.1 wt%)/ANA; (e) 15% Pt(0.2 wt%)/RUT and 85% Pt(0.2 wt%)/ANA; (f) 15% Pt(0.1 wt%)/RUT and 85% Pt(0.1 wt%)/ANA. Firstly, larger content of platinized sample in the mixture resulted in enhanced photocatalytic activity, i.e., (b) > (a), (c) > (d), and (e) > (f). At short wavelengths, the mixtures of both platinized phases ((e) and (f)) showed higher photocatalytic activities than that of mixtures composed of one bare and one modified phase, which is not surprising since both platinized phases showed high photocatalytic activities (as shown in **Figure. 3.14**). It should be pointed that all those mixtures had lower activity than that of Pt@RUT. However, the Φ_{app} of (e) sample (Φ_{app}=73%, containing platinized anatase and rutile) was higher than that of Pt@ANA (Φ_{app}=69%) confirming that rutile was more active phase in this system. The most interesting is the shape of action spectra of (a) and (b) samples containing only platinized rutile with the sharp peak at 395 nm. The explanation is like that used for explanation of higher photocatalytic activity of Pt@HomoP25 than Pt@ANA (**Figure. 3.14**) and re-built sample (**Figure. 3.15**), i.e., at this wavelength only rutile can absorb light, whereas at shorter wavelength (380 nm) both phases absorb light. Therefore, a decrease in Φapp (at 380 nm) was caused by the competition between two phases: active (Pt@RUT) and inactive (ANA), about photon absorption. Interestingly, re-estimated absorption spectrum (from the DRS measurements of ANA and RUT) clearly shows characteristic peak (**Figure. 3.16**) observed at action spectrum. The characteristic peak in the spectrum is clearly caused by the difference in photoabsorption properties between anatase and rutile, due to the difference in the bandgap of rutile (3.0 eV) and anatase (3.2 eV),[22] i.e., i) at the wavelengths shorter than ca. 390 nm both anatase and rutile can absorb photons; ii) at 390–400 nm the absorption properties of anatase are decreasing, and iii) at the wavelength longer than ca. 400 nm only rutile can absorb photons. In addition, HomoP25 with larger content of platinum (0.5 wt%) was also tested and characteristic peak at 395 nm was obtained (**Figure. 3.17**); the same as for (a) and (b) samples), confirming that rutile phase was platinized first. Therefore, it was shown that rutile is more active form of titania for methanol dehydrogenation in the presence of platinum as a co-catalyst. Moreover, at first rutile was

platinized, despite larger content of anatase in P25. One of the possible reasons is preferable adsorption of Pt precursor, hexachloroplatinum(IV) ions on rutile particles in P25, as confirmed by Zeta-potential analysis (**Table 3.1**). As a general trend, it has been often reported that rutile particles tend to exhibit higher photocatalytic activity for deposition of metal such as silver than anatase particles.[23, 24] Another possible reason is preferable electron transfer from anatase particles, as a major component absorbing light, to rutile particles, which has often been claimed in the literature, since the conduction-bottom position of rutile is reported to be slightly lower than that of anatase.[25]

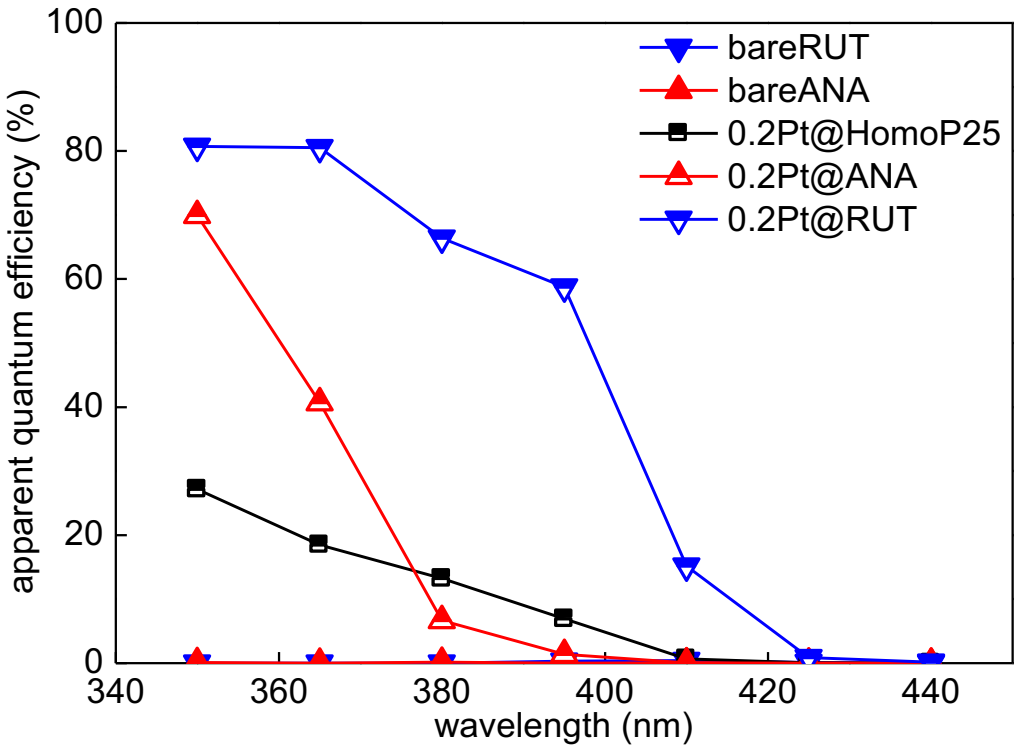


Figure.3.14 Action spectra of samples.

Copyright © 2017 Elsevier B.V., all rights reserved

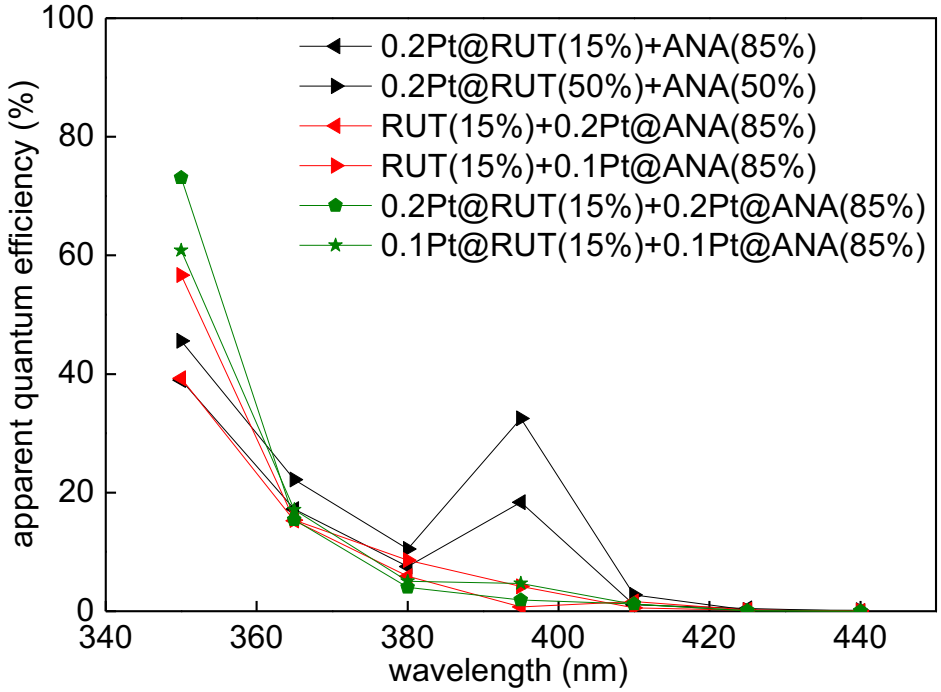


Figure.3.15 Action spectra of samples composited by Pt modified titania and bare titania.

Copyright © 2017 Elsevier B.V., all rights reserved

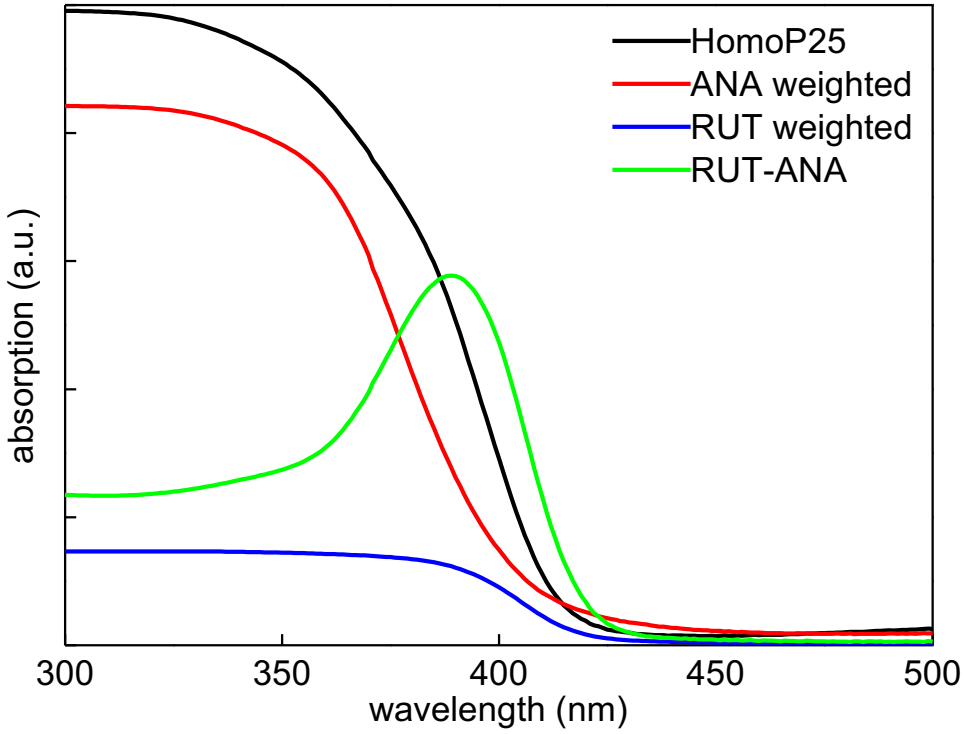


Figure.3.16 weighted absorption spectra of RUT and ANA considered them contents in HomoP25.

Copyright © 2017 Elsevier B.V., all rights reserved

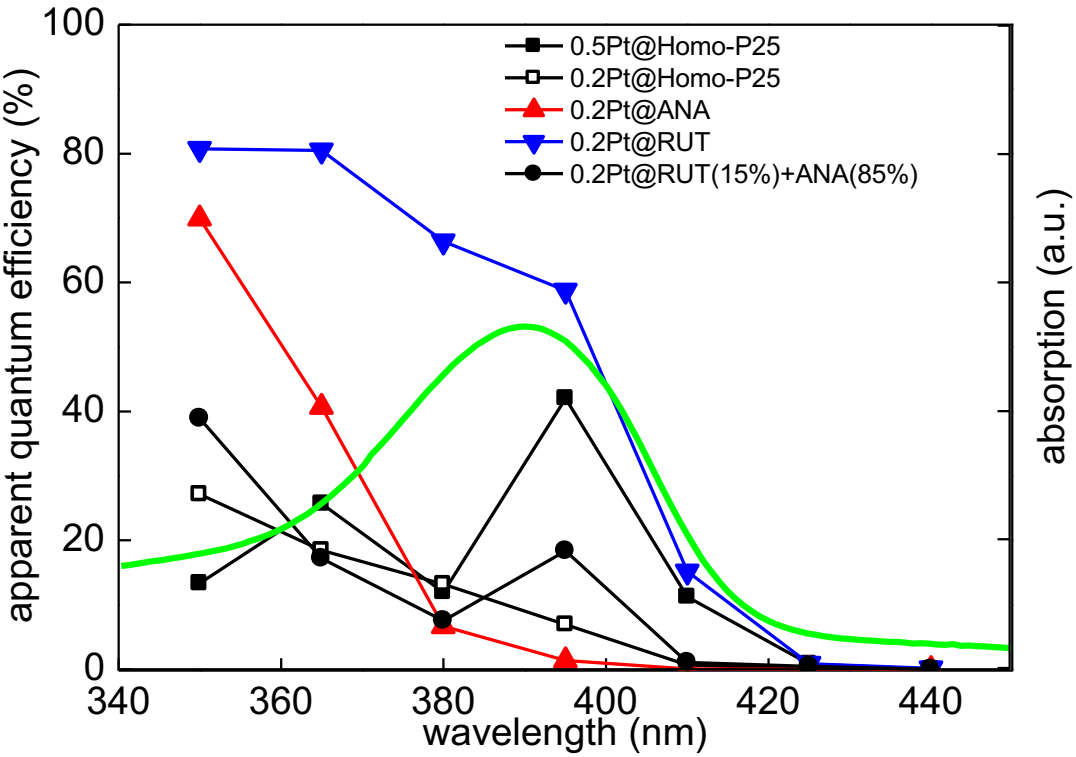


Figure.3.17 Action spectra and absorption spectra of samples:

Copyright © 2017 Elsevier B.V., all rights reserved

Table 3.1 Zeta-potential of ANA, RUT and HomoP25 sample

	Zeta-potential (mV)
HomoP25	41.1
ANA	16.9
RUT	-29.7

Copyright © 2017 Elsevier B.V., all rights reserved

3.4. Summary

It was found that platinized rutile was more active than platinized anatase and platinized HomoP25, probably due to ability of photoabsorption of more photons (narrower band gap). Therefore, proposed in literature an electron transfer between two polymorphic forms of titania as the main reason of high photocatalytic activity of P25 has been discarded. Moreover, it was found that in P25 sample rutile was platinized first, probably due to positively charged surface allowing easy adsorption of chloroplatinate ions.

Although, there are many reports claiming interparticle electron transfer (IPET) in heterogeneous photocatalytic systems, especially preferable transfer from anatase to rutile particles in P25, which seemed consistent with the experimental results and is attractive for the researchers in the field of photocatalysis. However, within my knowledge, there seemed to be no direct evidence for IPET. Therefore, I propose that for P25 photocatalysis, no synergetic effect due to IPET between anatase and rutile is required for interpretation of high photocatalytic activity of P25. My results suggest that IPET may occur not only between anatase and rutile (hetero-IPET), but also between single anatase particles and single rutile particles when isolated ANA and RUT are heated at relatively low temperature to form aggregates/agglomerates (homo-IPET). This may be the first evidence for IPET of titania particles.

3.5. References

1. Hope, G. A.; Bard, A. J., *J. Phys. Chem.* **1983,** *87*, 1979-1984.
2. Ohtani, B.; Iwai, K.; Nishimoto, S.; Sato, S., *Journal Of Physical Chemistry B* **1997,** *101* (17), 3349-3359.
3. Kowalska, E.; Remita, H.; Colbeau-Justin, C.; Hupka, J.; Belloni, J., *J. Phys. Chem. C* **2008,** *112* (4), 1124-1131.
4. Tian, Y.; Tatsuma, T., *J Am Chem Soc* **2005,** *127* (20), 7632-7637.
5. Kowalska, E.; Abe, R.; Ohtani, B., V *Chem Commun* **2009,** (2), 241-243.
6. Ueno, K.; Misawa, H., *J. Photoch. Photobio. C* **2013,** *15*, 31-52.
7. Chan, D.; Perram, J. W.; White, L. R.; Healy, T. W., *J. Chem. Soc., Faraday Trans. 1* **1975,** *71* (5), 1046-57.
8. Serpone, N.; Borgarello, E.; Pelizzetti, E., *J. Electrochem. Soc.: Electrochem. Sci. Technol.* **1988,** *135* (11), 2760-2766.
9. Bickley, R. I.; Gonzalez-Carreno, T.; Lees, J. S.; Palmisano, L.; Tilley, R. J. D., *Journal of Solid State Chemistry* **1991,** *92* (1), 178-90.
10. Ohno, T.; Tokieda, K.; Higashida, S.; Matsumura, M., *Applied Catalysis, A: General* **2003,** *244* (2), 383-391.
11. Mi, Y.; Weng, Y. X., *Sci Rep-Uk* **2015,** *5*.
12. Hurum, D. C.; Agrios, A. G.; Gray, K. A.; Rajh, T.; Thurnauer, M. C., *Journal of Physical Chemistry B* **2003,** *107* (19), 4545-4549.
13. Hurum, D. C.; Gray, K. A.; Rajh, T.; Thurnauer, M. C., *J. Phys. Chem. B* **2005,** *109* (2), 977-980.
14. Ohtani, B.; Prieto-Mahaney, O. O.; Li, D.; Abe, R., *J Photoch Photobio A* **2010,** *216* (2-3), 179-182.
15. Siuzdak, K.; Sawczak, M.; Klein, M.; Nowaczyk, G.; Jurga, S.; Cenian, A., *Phys Chem Chem Phys* **2014,** *16* (29), 15199-15206.
16. Pichat, P.; Mozzanega, M. N.; Disdier, J.; Herrmann, J. M., *Nouv. J. Chim.* **1982,** *6* (11), 559-64.
17. Kandiel, T. A.; Dillert, R.; Robben, L.; Bahnemann, D. W., *Catal Today* **2011,** *161* (1), 196-201.
18. Luttrell, T.; Halpegamage, S.; Tao, J. G.; Kramer, A.; Sutter, E.; Batzill, M., *Scientific Reports* **2014,** *4*, 8.
19. Reyes-Coronado, D.; Rodriguez-Gattorno, G.; Espinosa-Pesqueira, M. E.; Cab, C.; de Coss, R.; Oskam, G., *Nanotechnology* **2008,** *19* (14), 10.
20. Pfeifer, V.; Erhart, P.; Li, S.; Rachut, K.; Morasch, J.; Brötz, J.; Reckers, P.; Mayer, T.; Rühle, S.; Zaban, A.; Mora Seró, I.; Bisquert, J.; Jaegermann, W.; Klein, A., *The Journal of Physical Chemistry Letters* **2013,** *4* (23), 4182-4187.
21. Driessen, M. D.; Grassian, V. H., Photooxidation of Trichloroethylene on Pt/TiO2. *J. Phys. Chem. B* **1998,** *102* (8), 1418-1423.
22. Scanlon, D. O.; Dunnill, C. W.; Buckeridge, J.; Shevlin, S. A.; Logsdail, A. J.; Woodley, S. M.; Catlow, C. R.; Powell, M. J.; Palgrave, R. G.; Parkin, I. P.; Watson, G. W.; Keal, T. W.;

Sherwood, P.; Walsh, A.; Sokol, A. A., *Nat Mater* **2013,** *12* (9), 798-801.
23. Ohtani, B.; Okugawa, Y.; Nishimoto, S.; Kagiya, T., *The Journal of Physical Chemistry* **1987,** *91* (13), 3550-3555.
24. Nishimoto, S.-I.; Ohtani, B.; Kajiwara, H.; Kagiya, T., *Journal of the Chemical Society, Faraday Transactions 1: Physical Chemistry in Condensed Phases* **1983,** *79* (11), 2685.
25. Kavan, L.; Gratzel, M.; Gilbert, S. E.; Klemenz, C.; Scheel, H. J., *Journal of the American Chemical Society* **1996,** *118* (28), 6716-6723.

Chapter IV

Size-controlled noble metal nanoparticles on titania by modified photodeposition method

4.1 Introduction

Noble metals (NM: Pt, Au, Ag, Ir, Pd) in the form of either adsorbed complexes[1-3] or metallic deposits[3-7] have been used for improvement of photocatalytic activity of semiconductors for more than 40 years (as shortly mentioned in Chapter I). Enhancement of photoactivity originates from prolongation of lifetime of charge carriers (photogenerated electrons and holes),[3] since NM serves as an electron sink, and thus accelerating the transfer of electrons from titania to substrates, e.g., protons to evolve hydrogen.[8, 9] Surface modification of titania with NMNPs results in electrons transfer from titania to the modifiers forming the Schottky barrier .[10] The transfer of electrons from titania to NMNPs has been confirmed in various studies, e.g., by detected decrease in photoluminescence (electron de-excitation across band gap to recombine with holes),[11-15] cathodic shift of flatband potential position and increase of photocurrent quantum yield,[16] reduced lifetime of mobile electrons (by time resolved microwave conductivity (TRMC) measurements),[17] generation of various reactive oxygen species (ROS) (by electron paramagnetic resonance (EPR) measurements).[18, 19] Moreover, there are plenty of examples indirectly proving an electron transfer from titania to NM by enhancement of photocatalytic activity after semiconductor modification in both oxidation and reduction pathways.[20] For example, an efficient separation of electrons and holes after gold NPs deposition on titanate-loaded silica (SBA-15) resulted in enhancement of photocatalytic activities in both reduction (hydrogen evolution from methanol) and oxidation (hydroxylation of terephthalic acid) reactions, respectively.[21]

However, scavenging of electrons by NMNPs could also result in a decrease in photocatalytic activity, especially for reduction reactions occurring on titania surface (not on NM), because of decrease in number of available electrons, due to their transfer from titania to

deposited NMNPs. For example, immersing of Au/Ag NPs inside titania film caused an enhancement of activity for photo-oxidation reactions (e.g., oxidation of model dye (methylene blue, MB) and water, due to electron sinking inside Au/Ag), but also lowering activity for photo-reduction reactions (i.e., reduction of adsorbed model dye (resazurin dye) on titania surface).[22] Similarly, a decrease in photocurrent was observed when gold was deposited on titania surface of a TiO_2/FTO (fluorine doped tin oxide) electrode (Au/TiO_2/FTO), due to the electron transfer from titania to gold, instead of to an FTO electrode.[23]

The properties of both semiconductor and noble metal nanoparticles (NMNPs) strongly influence the resultant properties of NMNPs, such as specific surface area, crystallinity, crystalline size, photoabsorption properties, morphology, and thus resultant photocatalytic activities. Kind and structure of the support (semiconductor), as well as the method of NM deposition highly influence the properties of the resultant NM deposits. For example, larger NMNPs were formed on larger titania NPs[24, 25] and on pure anatase than on anatase-rutile mixture, [26] pores in titania film nanostructure limited the size of deposited gold NPs,[23] the smallest gold NPs were formed by deposition-precipitation, then sol-immobilization and finally by photodeposition method.[19] Moreover, post-treatment operations of NM-modified semiconductor have been also used for various purposes such as: i) titania crystallization, ii) reduction of cations of NM, iii) removal of adsorbed impurities like Cl^- (from NM precursor), capping[27] and stabilizing[23] agents of NM colloids, iv) enhancement of interaction between NM and support,[23, 28] v) and NM aggregation.[23, 29] The conditions during activity testing could also change properties of photocatalysts, e.g., due to NM reshaping, as a result of temperature increase[30] or irradiation.[31] Although, photodeposition method results in formation of large and non-uniform NPs, it is one of the best methods for preparation of NM-modified titania for few reasons: (1) fast and simple (depending on NM, e.g., less than 1 min and 5 min is sufficient to

deposit 2 wt% of platinum and gold on titania,[32-34] (2) no need to use any organic solvents and stabilizing/capping agents, which are difficult to be removed from photocatalysts surface (influencing an overall activity), (3) polydispersity of formed NMNPs could be also advantageous, e.g., for plasmonic photocatalysis (under visible light irradiation, shortly presented in Chapter V) due to broad photoabsorption properties (light harvesting).[32]

Therefore, photodeposition method has been used in my study. However, since NMNPs aggregate during fast photodeposition process, the interface between NM and titania is not large. To inhibit aggregation of NMNPs (to enhance NM-titania interface), and thus overall activity, NMNPs have been deposited on titania by modified photodeposition method (to slow down photodeposition speed), as shortly presented in this chapter.

4.2 Experimental details

Photodeposition was performed in the same set-up as that described in Chapter II. For preparation of metal-modified titania samples, the solutions of chloroplatinic acid ($H_2PtCl_6 \cdot 6H_2O$), chloroauric acid ($HAuCl_4 \cdot 6H_2O$), copper sulfate ($CuSO_4 \cdot 5H_2O$) and silver nitrate ($AgNO_3$) were used as metal precursors. 500 mg of titania was used for each photodeposition, the amount of each metal was calculated to be 0.2-2 wt% to titania. The weighted titania powder was put into a Pyrex glass tube equipped with a magnetic stirrer, to which 25 mL of methanol aqueous solution (50 vol%) was added. Then, the aqueous solution of metal salts was slowly dropped while being stirred. The suspension was argon-sparged for 15 min. The tube was sealed with a rubber septum and photoirradiation with magnetic stirring (500 rpm) by a 400-W high-pressure mercury lamp (Eiko-sha) under thermostatic control at 298 K. The thus-obtained photocatalyst was centrifuged, washed with methanol and three times with distilled water, freeze dried, and then the products were collected for the further study.

To control solely the size of NMNPs, modified photodeposition method was used for titania samples. Three modified photodeposition systems were used: (1) without Ar pre-bubbling (initial aerobic conditions): MeOH/air sample and (2) for O_2-saturated MeOH suspension (15-min O_2 pre-bubbling): MeOH/O_2 sample; in those two systems (MeOH/air and MeOH/O_2) photogenerated electrons were firstly consumed by O_2 hindering formation of gold NPs, and (3) in the presence of 2-propanol (IPA; 50 vol%) as a hole scavenger (instead of methanol) under Ar atmosphere: IPA/Ar sample. The NM-modified sample prepared at standard conditions (under Ar from deaerated MeOH suspension) was named as MeOH/Ar (for easier comparison between those four samples).

Two kinds of highly-active titania samples were used for this study, i.e., Homo-P25 and

faceted anatase titania (octahedral anatase particle, OAP) with eight equivalent (101) facets. Potassium titanate nanowires (TNWs; Earthclean Tohoku Co. Ltd) were used as the precursor for fabrication of the titania samples containing OAPs. TNWs (100-1067 mg) were ultrasonically dispersed in Milli-Q water (30-40 mL) for 1 h, and then suspension was put into a 100-mL sealed Teflon bottle into which, an additional portion of Milli-Q water (20 or 40 mL) was added, when necessary. The bottle was put into an outer sleeve of a stainless autoclave and then heated in an oven for 6 h at 433 K. The obtained suspension was dispersed by ultrasonication for 10 min and then centrifugally separated (12000 rpm, 20 minutes). The white precipitates were collected and dried overnight under vacuum (353 K, 12 h). HT processes were performed for five weights of TNWs (200, 267, 400, 533 and 1067 mg) and two volumes of water of 60 and 80 mL. The codes of the samples were defined as follow: TNWs amount/water volume. For example, 267/80 sample was prepared with 267 mg of TNWs and 80 mL of water.

4.3 Results and discussion

Both titania samples (Homo-P25 and OAP) possesses very high activity for oxidative decomposition of acetic acid ((CO_2 system, the most active titania samples). However, OAP showed surprisingly low activity for dehydrogenation of methanol. It was proposed that although this faceted titania is highly active in CO_2 system (due to preferential distribution of shallow than deep electron traps, ETs, as suggested from TRMC and PAS measurements[35]), low activity for methanol dehydrogenation originated from possible aggregation of Pt NPs on very fine OAP nanocrystals (ca. 15-18 nm). Therefore, modified photodeposition method was used to obtain highly active OAP sample in both reaction systems (CO_2 and H_2). First, OAP samples (prepared by various conditions of hydrothermal reaction) were modified with platinum by photodeposition method (MeOH/Ar) and modified photodeposition method (MeOH/O_2).

Indeed, modified photodeposition method resulted in significant enhancement (2.0-2.6x) of hydrogen evolution rate for all OAP samples, as shown in **Figure 4.1**(A) Enhancement in activity clearly correlates with the change of properties of platinum NPs, i.e., formation of smaller platinum NPs, uniformly distributed on OAP (**Figure 4.1**(B and D))

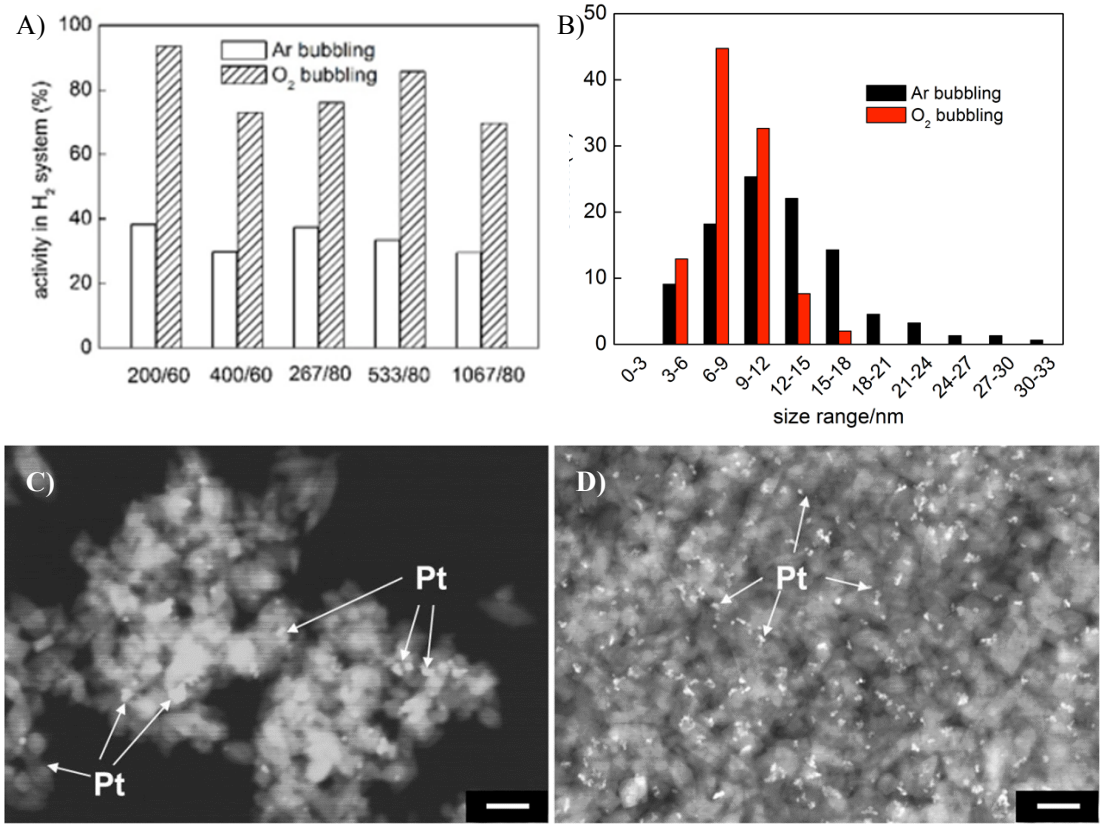


Figure 4.1 (A) Photocatalytic activity of Pt loaded OAPs; (B) size distribution of Pt loaded with OAPs samples; (C) and (D) the STEM images of Pt loaded OAPs

Copyright © 2016 Elsevier B.V., all rights reserved

Activities of Homo-P25 was also improved by application of modified photodeposition method, especially at larger amount of platinum loading (1-2 wt%), as shown **in Figure 4.2**. However, this improvement was not so high as in the case of OAP. It is not surprising since P25 possesses both anatase and rutile NPs, Pt NPs are preferentially adsorbed on rutile phase, and platinized-rutile is much more active than platinized-anatase (as was discussed in Chapter III). Microscopic observation clearly indicates that Pt aggregation was inhibited by modified photodeposition method. Detailed study on correlation between properties of Pt NPs, their deposition site (depending on their amount and photodeposition conditions) on overall photocatalytic activity is under study.

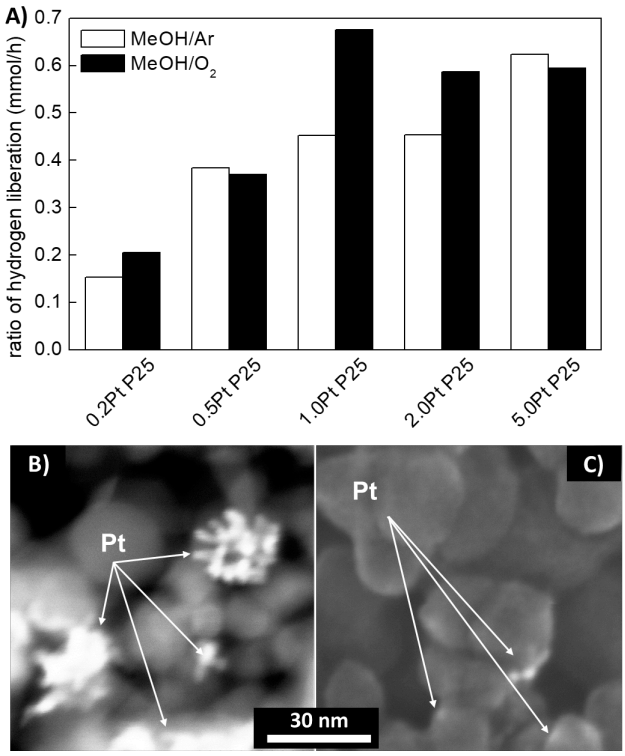


Figure 4.2 (A) Photocatalytic activity of Pt modified HomoP25 under aerobic/ anaerobic conditions (Ar for anaerobic and O_2 for aerobic condition);
STEM image for 2.0 wt% loaded HomoP25 under anaerobic condition (B) and under aerobic condition (C).

In the next step, photodeposition of other NMNPs on OAP sample was also performed to check usefulness of modified photodeposition method to control the properties of NMNPs and thus overall activity. As expected, oxygen presence significantly hindered reduction of metal cations and deposition of metallic NPs on OAPs, as shown in **Figure 4.3**.

The induction period (intersection with x-axis) during which NPs of noble metals are formed, depends on properties of metal and titania (e.g., amount, kind and distribution of electron traps). In the case of platinum and gold deposition under deaerated conditions is very fast and a few minutes is sufficient to reduce all metallic cations and form NPs. This is evident by linear evolution of hydrogen at constant rate.[32, 36, 37] In previous studies the complete photodeposition of Au was confirmed for a wide range of gold content from 0.05 to 10 wt% by

atomic absorption spectroscopy.[36] Similarly, in the present study, photodeposition of Au and Pt was very fast and less than 5 min was sufficient to deposit them on OAPs. Whereas, deposition of Cu and Ag needed longer time, i.e., ca. 8 and 45 min, respectively. The rate of methanol dehydrogenation correlated with reduction facility of metal cations (induction period), i.e., the shorter the induction period was, the higher was the rate of hydrogen generation. It is suggested that rates of formation of metallic deposits and methanol dehydrogenation correlate with the difference between the work function of metal (Ag=4.26 eV, Cu=4.7 eV, Au=5.1 eV, Pt=6.35 eV) and titania (4.0 eV), i.e., the electronic potential barrier (the Schottky barrier) generated by the band alignment at the metal-semiconductor heterojunction.

Under aerated conditions, much longer induction periods were needed for metal photodeposition and linear evolution of hydrogen, i.e., ca. 180, 215, 230 and >300 min for Pt, Cu, Au and Ag, respectively. At first, excited electrons were mainly captured by oxygen and only slightly reduced metal cations, as shown in the **Figure 4.3** (right).

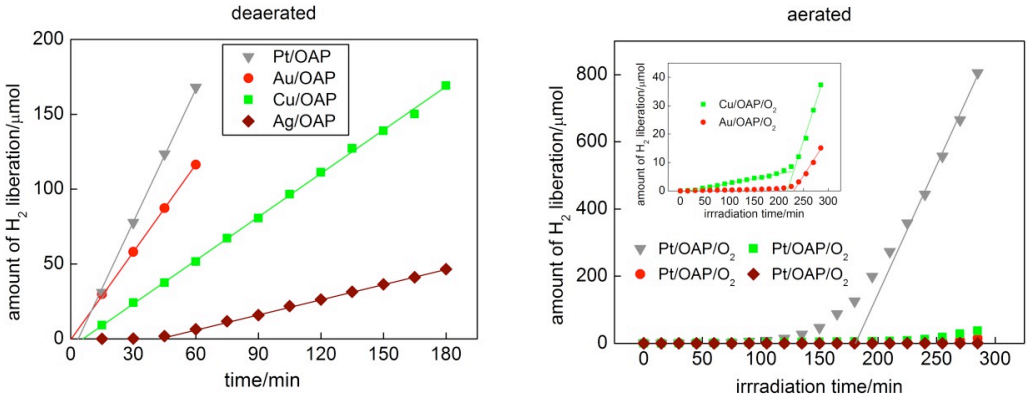


Figure 4.3 Methanol dehydrogenation during metal photodeposition on OAPs under (left) deaerated and (MeOH/Ar) and (right) aerated conditions ($MeOH/O_2$).

Copyright © 2018, Copyright Clearance Center, Inc., Creative Commons Attribution License (CC BY), All rights reserved

An oxygen consumption (shown in **Figure 4.4**) correlates with observed induction periods, i.e., the fastest oxygen consumption was achieved after 120 min during Pt deposition. Interestingly,

photodeposition performed under aerated conditions showed different tendency, i.e., shorter induction period for Cu than Au (the inset of **Figure 4.3** (right)), which suggested that probably instead of Cu, copper oxide (CuO, 5.3-eV work function) was firstly deposited on OAPs. Interestingly, in the case of Cu and Ag, two reaction rates of hydrogen evolution could be observed: (1) after shorter induction period (initial induction period, ca. 40-50 min) linear evolution of hydrogen was observed at very low rate (ca. 0.04 and 0.002 μmol min^{-1} for Cu and Ag, respectively), and then (2) significant increase in reaction rate was observed when oxygen was consumed. Therefore, it is proposed that at first oxides of Ag and Cu are formed under aerated conditions, and then they are reduced to zero-valent metal under deaerated conditions.

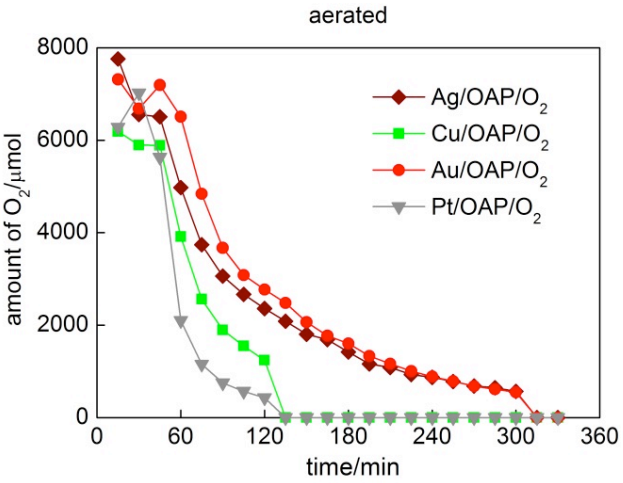


Figure 4.4 Oxygen consumption during metal deposition under aerated conditions (MeOH/O_2).

Copyright © 2018, Copyright Clearance Center, Inc., Creative Commons Attribution License (CC BY), All rights reserved

Photodeposition (MeOH/Ar) and modified photodeposition (MeOH/O_2) methods resulted in preparation of two kinds of samples, with different properties and activities (exemplary activities are shown in next chapter). However, two kinds of samples could be only prepared. Therefore, additional modifications were applied to obtain samples of much different properties, i.e., by use of another hole scavenger (2-propanol instead of methanol; IPA/Ar) and air instead of O_2 or Ar

(MeOH/air). As a result, gold NPs were deposited on the surface of OAP by photodeposition method under four different conditions (MeOH/Ar, MeOH/air, MeOH/O_2 and IPA/Ar). In–situ photodeposition of gold on OAPs caused dehydrogenation of alcohols, and the fastest hydrogen evolution (almost without induction period) was observed for methanol as a hole scavenger under Ar atmosphere (MeOH/Ar), as shown in **Figure 4.5**. In the presence of O_2 in the system (MeOH/air, MeOH/O_2), the induction period (ca. 15 min and 60 min, respectively), during which photogenerated electrons were mainly consumed by oxygen (inset in **Figure 4.5**) instead of reducing gold(III), was observed. The change of hole scavenger from MeOH to IPA resulted in significant decrease in efficiency of hydrogen evolution, possibly due to lower polarity of IPA than that of MeOH. It was reported that efficiency of hydrogen evolution was highly dependent on properties of hole scavenger such as polarity, the number of hydroxyl groups, the number of alpha-hydrogens and standard oxidation potential.[11]

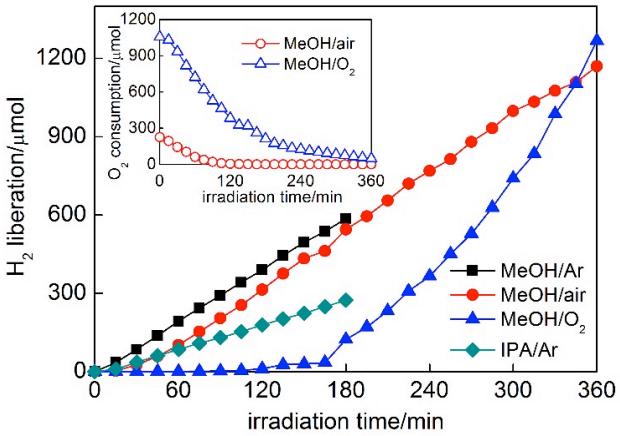


Figure 4.5 Hydrogen evolution and disappearance of oxygen (inset) during gold photodeposition on OAP for four kinds of photodeposition method.

Copyright © 2018, Copyright Clearance Center, Inc., Creative Commons Attribution License (CC BY), All rights reserved

Au-OAPs samples exhibited dark violet color indicating the presence of spherical gold NPs of few nm.[32] Diffuse reflectance spectra of all samples did not differ significantly with λ_{max} of LSPR at ca. 545 nm **(Figure 4.6)**, and slight stronger scattering at longer wavelengths

(800-1200 nm) for samples prepared under Ar suggesting the presence of larger size of gold NPs in those samples.[38]

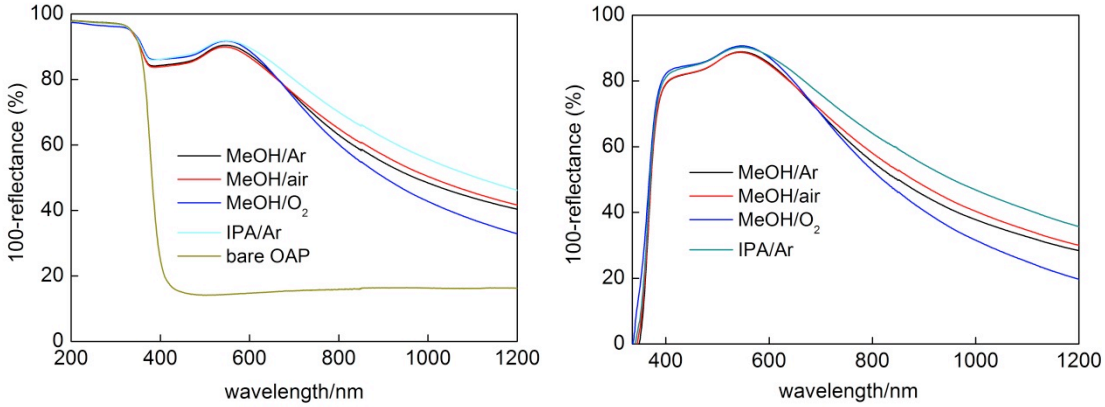


Figure 4.6 Diffuse reflectance spectra of Au/OAP (DRS colors correspond to the **Figure 4.5**).

Copyright © 2018, Copyright Clearance Center, Inc., Creative Commons Attribution License (CC BY), All rights reserved

Here, by modification of only photodeposition conditions of gold NPs on the same titania sample (OAPs prepared at the same conditions of US-HT), it was possible to obtain the impurity-free products (without surfactants and capping/stabilizing agents of gold NPs), which differed by only properties of gold NPs (**Figure 4.6** and **Figure 4.7**). As expected, gold NPs were the most polydispersed in Au/OAPs sample prepared under Ar in the presence of MeOH as a hole scavenger (MeOH/Ar), due to very fast gold(III) reduction and formation of gold NPs (as show in **Figure 4.5**). The presence of larger molecule as a hole scavenger (IPA instead of MeOH, IPA/Ar) or O_2 as an electron scavenger (MeOH/air and MeOH/O_2) retarded the gold growth significantly. The content of large Au NPs (> 30 nm) in the final product decreased in the order: MeOH/Ar (30-80 nm) > IPA/Ar (36-39 nm) > MeOH/O_2 (33-36 nm) ≥ MeOH/air (27-30 nm).

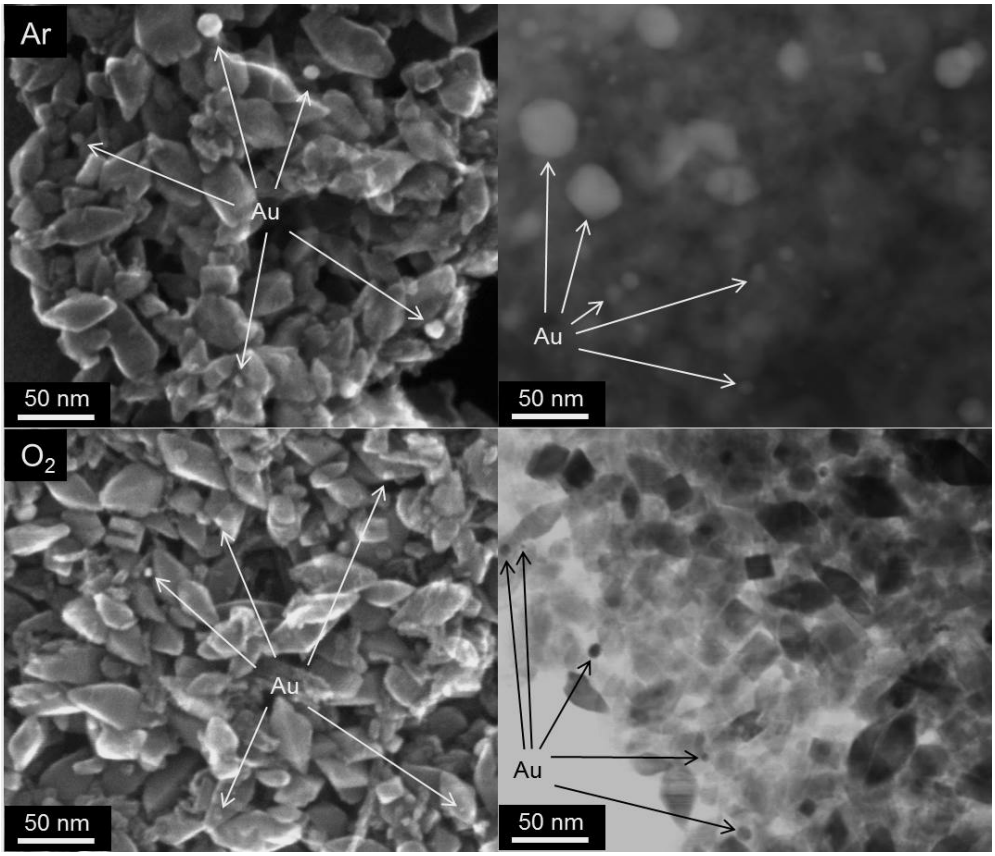


Figure 4.6 STEM images of Au/OAP samples: MeOH/Ar (top) and MeOH/O_2 (bottom).

Copyright © 2018, Copyright Clearance Center, Inc., Creative Commons Attribution License (CC BY), All rights reserved

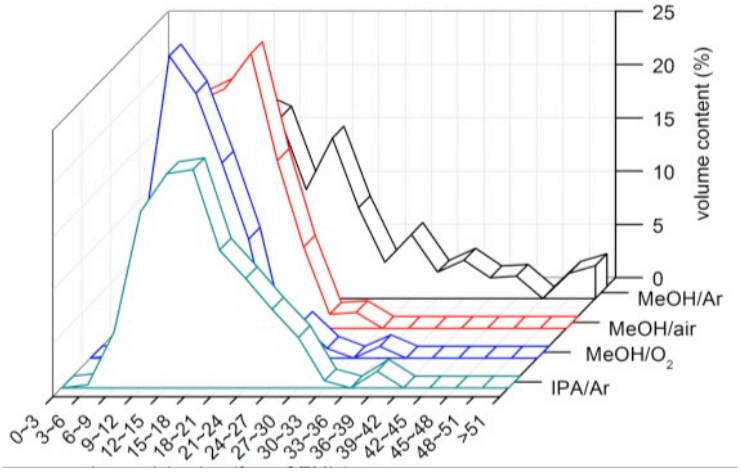


Figure 4.7. Distribution of gold NPs' size for Au/OAPs samples prepared under different conditions of gold photodeposition.

Copyright © 2018, Copyright Clearance Center, Inc., Creative Commons Attribution License (CC BY), All rights reserved

Photocatalytic activity under UV/vis irradiation was tested for (1) oxidative decomposition of acetic acid (CO_2 system), and (2) MeOH dehydrogenation under deaerated conditions (15-min Ar prebubbling (H_2 system)). Modification of OAPs with gold NPs resulted in significant enhancement of photocatalytic activity (as already reported [32]), being ca. 1.5-1.6 (CO_2 system) and 6.6-8.3 (H_2 system) times higher than that of bare OAPs (**Figure 4.8**). Interestingly, similar photocatalytic activity of Au/OAPs samples tested in the presence of the same hole scavenger (MeOH (H_2 system); 2.57 and 2.94 μmol min^{-1} for samples prepared in the presence of IPA (IPA/Ar) and MeOH (MeOH/Ar), respectively, **Figure 4.8** (right)) confirms that the kind of a hole scavenger is decisive for efficient hydrogen evolution (as compared with more than twice faster hydrogen evolution from MeOH than IPA suspension during gold photodeposition, as shown in **Figure 4.5**).

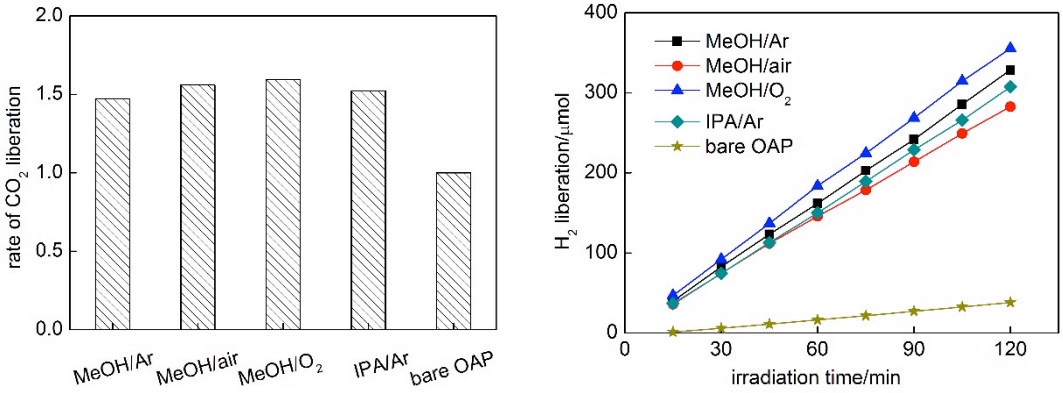


Figure 4.8 Photocatalytic activity under UV/vis irradiation for Au/OAPs samples for (left) oxidative decomposition of acetic acid, and (right) MeOH dehydrogenation under anaerobic conditions.

Copyright © 2018, Copyright Clearance Center, Inc., Creative Commons Attribution License (CC BY), All rights reserved

It must be pointed that differences in UV/vis-activity of those Au/OAPs samples in both tested systems (CO_2 and H_2) are not large (< 8% and < 20%, respectively, as shown in **Figure 4.8**), indicating that size and distribution of gold NPs is not decisive for UV/vis-photocatalytic

activity, where primary function of gold is mainly to inhibit the recombination of charge carriers (but not to activate titania as it is under vis excitation of LSPR). Larger differences in photocatalytic activity between modified samples in H_2 system than in CO_2 system originate from an additional function of gold deposits in the latter system, i.e., as co-catalyst on which hydrogen evolution takes place. The highest UV-activity is observed for the smallest gold NPs, and thus more uniformly distributed on OAP (less content of bare titania of neglected activity in the final product). The significant difference between photocatalytic activity of Au/OAP samples is observed only under vis irradiation confirming that the size of gold NPs or/and their distribution are decisive for vis activity.[39]

4.4 Summary

Modified photodeposition method allows to prepare photocatalysts with different properties, i.e., sizes and distribution of NMNPs, and thus different photocatalytic activity. In the case of methanol dehydrogenation, platinum (or other NM) is usually used as co-catalyst. However, aggregation of Pt NPs during fast photodeposition (anaerobic conditions and in the presence of methanol as hole scavenger) could result in low photocatalytic activity for hydrogen evolution since deposition of large aggregates of Pt NPs on titania (or in some cases these aggregates are surrounded by fine titania NPs) results in co-presence of many un-modified titania particles (with negligible activity), which compete with Pt-modified titania for photon absorption (as was suggested by AS experiments in Chapter III). Therefore, preparation of NM-modified titania by novel photodeposition method, allowing to slow down photodeposition speed (e.g., in the initial presence of oxygen as electron scavenger), enables to obtained photocatalysts with more-uniform NM NPs, and thus well distributed on titania support. Moreover, preparation of NM-modified titania by changing the conditions of photodeposition enables to prepare photocatalysts with much different surface properties, and thus overall photocatalytic activities by fast and simple method (without the use of surfactants, stabilizers, capping agents).

4.5 References

1. Zang, L.; Lange, C.; Abraham, I.; Storck, S.; Maier, W. F.; Kisch, H., *J. Phys. Chem. B* **1998,** *102* (52), 10765-10771.

2. Ohtani, B.; Nishimoto, S.-i., *J. Phys. Chem. B* **1993,** *97*, 920-926.

3. Kowalska, E.; Remita, H.; Colbeau-Justin, C.; Hupka, J.; Belloni, J., *J. Phys. Chem. C* **2008,** *112* (4), 1124-1131.

4. Sclafani, A.; Mozzanega, M.-N.; Herrmann, J. M.,. *Journal of Catalysis* **1997,** *168*, 117-120.

5. Banmwenda, G. R.; Tsubota, S.; Nakamura, T.; Haruta, M., *J. Photochem. Photobiol. A-Chem.* **1995,** *89*, 177-189.

6. Ohtani, B.; Kakimoto, M.; Miyadzu, H.; Nishimoto, S.; Kagiya, T., *J. Phys. Chem.* **1988,** *92*, 5773-5777.

7. Kowalska, E., In *Gold Nanoparticles for Physics, Chemistry and Biology*, 2nd ed.; Louis, C.; Pluchery, O., Eds. World Scientific: Singapore, 2017; pp 319-364.

8. Pichat, P.; Herrmann, J. M.; Disdier, J.; Courbon, H.; Mozzanega, M. N., *Nouv. J. Chim.* **1981,** *5* (12), 627-636.

9. Ohtani, B.; Ogawa, Y.; Nishimoto, S.-i., *J. Phys. Chem. B* **1997,** *101* (19), 3746-3752.

10. Han, C. H.; Yang, X. Z.; Gao, G. J.; Wang, J.; Lu, H. L.; Liu, J.; Tong, M.; Liang, X. Y., *Green Chemistry* **2014,** *16* (7), 3603-3615.

11. Chen, W. T.; Chan, A.; Al-Azri, Z. H. N.; Dosado, A. G.; Nadeem, M. A.; Sun-Waterhouse, D.; Idriss, H.; Waterhouse, G. I. N., *Journal of Catalysis* **2015,** *329*, 499-513.

12. Dosado, A. G.; Chen, W. T.; Chan, A.; Sun-Waterhouse, D.; Waterhouse, G. I. N., *Journal of Catalysis* **2015,** *330*, 238-254.

13. Yu, J. G.; Yue, L.; Liu, S. W.; Huang, B. B.; Zhang, X. Y., *J Colloid Interf Sci* **2009,** *334* (1), 58-64.

14. Li, F. B.; Li, X. Z., *Appl. Catal. A.-Gen.* **2002,** *228* (1-2), 15-27.

15. Mkhalid, I. A., *J. Alloy Compd.* **2015,** *631*, 298-302.

16. Smirnova, N.; Vorobets, V.; Linnik, O.; Manuilov, E.; Kolbasov, G.; Eremenko, A., *Surface and Interface Analysis* **2010,** *42* (6-7), 1205-1208.

17. Carneiro, J. T.; Savenije, T. J.; Mul, G., *Physical Chemistry Chemical Physics* **2009,** *11* (15), 2708-2714.

18. Caretti, I.; Keulemans, M.; Verbruggen, S. W.; Lenaerts, S.; Van Doorslaer, S., *Topics in Catalysis* **2015,** *58* (12-13), 776-782.

19. Priebe, J. B.; Radnik, J.; Lennox, A. J. J.; Pohl, M. M.; Karnahl, M.; Hollmann, D.; Grabow, K.; Bentrup, U.; Junge, H.; Beller, M.; Bruckner, A., *Acs Catal* **2015,** *5* (4), 2137-2148.

20. Mei, B.; Wiktor, C.; Turner, S.; Pougin, A.; van Tendeloo, G.; Fischer, R. A.; Muhler, M.; Strunk, J., *ACS Catal.* **2013,** *3* (12), 3041-3049.

21. Kowalska, E.; Rosa, L.; Rau, S.; Juodkazis, S.; Ohtani, B., Preparation of titania/Au/titania nanoparticles with improved photoactivity and stability for visible-light application. **in preparation**.

22. Kundu, S.; Kafizas, A.; Hyett, G.; Mills, A.; Darr, J. A.; Parkin, I. P., *J Mater Chem* **2011,** *21* (19), 6854-6863.

23. Brennan, L. J.; Purcell-Milton, F.; Salmeron, A. S.; Zhang, H.; Govorov, A. O.; Fedorov, A. V.; Gun'ko, Y. K., *Nanoscale Res. Lett.* **2015,** *10*, 1-12.

24. Bokhimi, X.; Zanella, R.; Morales, A., *J Phys Chem C* **2007,** *111* (42), 15210-15216.

25. Kowalska, E.; Wei, Z.; Karabiyik, B.; Herissan, A.; Janczarek, M.; Endo, M.; Markowska-Szczupak, A.; Remita, H.; Ohtani, B., *Catal Today* **2015,** *252*, 136-142.

26. Cojocaru, B.; Neatu, S.; Sacaliuc-Parvulescu, E.; Levy, F.; Parvulescu, V. I.; Garcia, H., *Appl. Catal. B-Environ.* **2011,** *107* (1-2), 140-149.

27. Bowker, M.; Morton, C.; Kennedy, J.; Bahruji, H.; Greves, J.; Jones, W.; Davies, P. R.; Brookes, C.; Wells, P. P.; Dimitratos, N., *Journal of Catalysis* **2014,** *310*, 10-15.

28. Menegazzo, F.; Signoretto, M.; Marchese, D.; Pinna, F.; Manzoli, M., *Journal of Catalysis* **2015,** *326*, 1-8.

29. Manzoli, M.; Menegazzo, F.; Signoretto, M.; Cruciani, G.; Pinna, F., *Journal of Catalysis* **2015,** *330*, 465-473.

30. Liu, Y.; Mills, E. N.; Composto, R. J., *J Mater Chem* **2009,** *19* (18), 2704-2709.

31. Al-Sherbini, E.-S. A. M., *Materials Chemistry and Physics* **2010,** *121* (1-2), 349-353.

32. Kowalska, E.; Mahaney, O. O. P.; Abe, R.; Ohtani, B., V *Phys. Chem. Chem. Phys.* **2010,** *12* (10), 2344-2355.

33. Wei, Z.; Endo, M.; Wang, K.; Charbit, E.; Markowska-Szczupak, A.; Ohtani, B.; Kowalska, E., *Chem. Eng. J.* **2017,** *318*, 121-134.

34. Wei, Z.; Kowalska, E.; Wang, K.; Colbeau-Justin, C.; Ohtani, B., *Catal Today* **2017,** *280*, 29-36.

35. Wei, Z.; Kowalska, E.; Verrett, J.; Colbeau-Justin, C.; Remita, H.; Ohtani, B., *Nanoscale* **2015,** *7* (29), 12392-12404.

36. Kowalska, E.; Rau, S.; Ohtani, B., *Journal of Nanotechnology* **2012**, 1-11.

37. Kowalska, E.; Janczarek, M.; Rosa, L.; Juodkazi, S.; Ohtani, B., *Catal Today* **2014,** *230*, 131-137.

38. Zheng, S.; Wei, Z.; Yoshiiri, K.; Braumuller, M.; Ohtani, B.; Rau, S.; Kowalska, E., *Photochemical & Photobiological Sciences* **2016,** *15*, 69-79.

39. Wei, Z.; Rosa, L.; Wang, K.; Endo, M.; Juodkazi, S.; Ohtani, B.; Kowalska, E., *Appl.*

Catal. B: Environ. **2017,** *206*, 393-405.

Chapter V

Exemplary applications of titania photocatalysts

5.1 Introduction

Titania is probably the most widely studied and commonly applied heterogenous photocatalyst for both environmental purification (water/wastewater treatment, air purification, surface cleaning)[1] and solar energy conversion (e.g., DSSCs), as already mentioned in Chapter I. In this chapter, some possible applications of titania photocatalysts will be shortly presented, considering important aspects discussed in previous chapters, such as influence of (1) the impurities present on titania surface and applied purification methods (Chapter II), (2) interparticle electron transfer (IPET; Chapter III), and (3) properties of deposited noble metals (Chapter IV) on the resultant photocatalytic activity.

Exemplary applications, presented in this Chapter, are focused on the most urgent problems focusing humanity, i.e., microbiological pollution and low quantum yield of heterogeneous photocatalysis under solar radiation. Therefore, titania photocatalysts, prepared during this research, have been applied for inactivation of microorganisms (bacteria and fungi) and decomposition of organic pollutants under visible light (vis) irradiation. Of course, photocatalytic activity under UV/vis irradiation was also checked for hydrogen evolution and acetic acid decomposition, but main data for these "standard" reactions have already been shown in previous chapters.

An enormous amount and kinds of various indoor and outdoor pollutants are released during people's everyday lives affecting their health. Both chemical and microbiological pollutants are very dangerous, e.g., traffic-related air pollution was associated with prevalence of childhood asthma, the acute effect on respiratory symptoms and peak expiratory flow rate of fungus spores was found for *Cladosporium* sp. and *Epicoccum* sp., everyday exposure to multiple chemicals was associated with asthma, allergy, autism, medically unexplained

symptoms[2, 3], poisoning, neurobehavioral disorder,[4] chronic cough,[5] risk of cancer and death.[6] Although environmental contaminations by chemical pollutants is usually well-monitored and controlled, especially in developed countries (due to strict environmental regulations, e.g., by EC and USEPA),[7-9] microbiological pollution is often accidental resulting in out-of-control spreading of microorganisms. In addition, microorganisms, in contradistinction to chemical pollutants, can grow very fast without their continuous release to the environment, e.g., some bacteria and fungi can rapidly reproduce on the surface of building materials such as wood, paper, gypsum, ceramic, mineral, paints and plastics.[10] Moreover, positive, negative or neutral interactions between various bacteria and fungi *via* infochemicals produced by them,[11, 12] as well as between microorganisms and chemical pollutants, may have crucial impact on an environment. For example, it was found that pathogenic bacteria *Pseudomonas aeruginosa* or compounds possessing 12-carbon chain length (dodecanol, C12-acyl homoserine lactone) inhibited transition of fungal cells (*Candida albicans*) from non-virulent to virulent.[13] Similarly, significant improvement of degradation and mineralization of polycyclic aromatic hydrocarbons was observed by fungal-bacterial co-cultures in comparison with poor activities of single cultures of fungi (*Penicilum janthinellum*) and bacteria (*Stenotrophomonas maltophilia*).[14] The cooperation of bacteria and fungi was also found for degradation of alkylphenols since the former assimilated the aromatic ring and the latter attacked the aliphatic chain.[15] Whereas, biosorption of heavy metals by microorganisms (*Micrococcus* sp. and *Aspergillus* sp.)[16] could have an inconsistent effect on an environment, i.e., (i) positive by removal of heavy metals from environment, and (2) negative by their subsequent (out-of-control) release into environment. Based on all of these studies it is clear that interactions between microorganisms, chemical compounds and an environment are highly complex and unpredictable, thus development of environmentally-friendly techniques, which are simultaneously efficient in degradation of

pollutants is highly important and urgent.

Reducing exposure to chemicals and bioaerosols at home, school and in the workplace as a preventative action can lead to improvement of indoor environmental quality (IEQ) and simultaneously to better people health. In order to improve the air quality, the producers of building materials are obligated to develop new technological solutions, i.e., novel materials with reduced content of hazardous chemical compounds, and with chemical compounds possessing antimicrobial properties. Semiconductor photocatalysts are considered as such materials, which at the same time are safe for human and may improve IEQ. Heterogeneous photocatalysis is considered as one of the best methods for environmental purification because additional chemical compounds such as strong oxidants (ozone, hydrogen peroxide, chlorine)[17-24] are not introduced into an environment.[1, 25] The energy consumption is also much lower than in the case of other Advanced Oxidation Processes, AOPs, e.g., wet air oxidation,[26] supercritical water oxidation,[27] H_2O_2/UV-C,[28] because UV-A lamps or even free solar radiation could be used for photocatalyst activation.[29] Titania is one of the most widely used heterogeneous photocatalysts, due to its high chemical and thermal stability, non-toxicity, and high photocatalytic activity.[30-33] It should be clarified that the meaning of "non-toxicity" of titania originates from its chemical properties, but not from its physical structure, and as such nanoparticles of titania (and all other nanomaterials) are considered as potentially toxic, due to ability to go through the biological barriers causing damage to various organs.[34] Three polymorphic forms of titania are known, i.e., anatase, rutile and brookite (as discussed in Chapter I). Anatase and brookite are metastable, while rutile is thermodynamically stable. Brookite has been seldom studied, due to more complicated synthetic methods of its preparation, which often need application of highly concentrated acids or high temperature and pressure.[35] Titania in rutile form is widely used for whitening of commercial products such as paints,

lacquers, plastic, paper and gum. While, anatase is mainly used as photoactive coating material, due to its self-cleaning and superhydrophilicity properties.[30, 36, 37] These properties are induced by UV light irradiation of the photocatalyst and subsequent generation of reactive oxygen species (ROS) oxidizing adsorbed pollutants.[38] Superhydophilicity causes also enhancement of cleaning effect, due to easily removing of dirt with rainwater.[39, 40] Since the first report by Matsunaga *et al.* in 1985 on the application of TiO_2 photocatalysis for destruction of *Lactobacillus acidophilus*, *Escherichia coli* and *Saccharomyces cerevisiae*[41] much interest in use of heterogeneous photocatalysis for water and air disinfection has been noticed. Most of studies on the antimicrobial activity of titania were perform with simple microorganisms, such as bacteria, viruses and prions.[42-46] Up to now extensive research has been done in the area of antibacterial action of TiO_2, i.e., on explanation of the mechanism of action and on the influence of various factors, such as irradiation (type, range, intensity), titania (amount, surface properties, content of dopants/modifiers), photocatalyst immobilisation, process conditions (temperature, water turbidity), on the efficiency of photocatalytic process.[47-49] Whereas the antifungal capability of titania photocatalyst was confirmed only for few species of yeast and mould fungi.[50-53] Recent report on inactivation of pathogenic fungi indicated that irradiated titania P25 highly inhibited growth of fungi *Pseudallescheria-Scedosporium*, while the strains of *Aspergillus versicolor* were mainly resistant.[54] The antifungal activities have been usually tested on anatase or anatase-rutile mixture (e.g., P25) and there are no reports on the effect of pure rutile on growth of fungi. Thus, the aim of the present study was to examine the influence of polymorphs of titania, rutile and anatase, on growth a few species of mould fungi. P25, its isolated polymorphs, i.e., anatase and rutile, and also faceted anatase (OAP) have been used for the study. [55]

It should be reminded that titania is inactive under vis irradiation, which limits its common

application to world regions of high intensity of solar radiation. Moreover, recombination between electrons and holes (typical for all semiconducting materials) results in low quantum yield. Therefore, plenty of studies have been performed to improve titania performance by its surface modification, doping and preparation of coupled nanostructures.[56-65] Modification with metals (metallic nanoparticles and clusters,[66-70] metal complexes[71, 72]) has been one of the most often used methods, both for enhancement of activity under UV light (as already mentioned in Chapter IV), and titania activation towards visible light irradiation. It is well known that under UV irradiation metallic deposits works as an electron sink inhibiting the recombination of charge carriers. Whereas, under visible light irradiation, either narrowing of band-gap[73-75] or energy/electron transfer from modifier to titania[76-78] causes the visible response. Recently, modification of titania with NPs of NM possessing visible light absorption (due to LSPR) has been very extensively studied, and such obtained materials are called plasmonic photocatalysts. Although, contrary reports have been published concerning the mechanism of their action, i.e., transfer of energy,[79] transfer of charge carriers,[80, 81] plasmonic heating,[82] their photocatalytic activity at very broad ranges of irradiation makes them very promising materials for environmental purification and energy conversion. In addition, antibacterial properties of silver and copper extend their possible application towards dark conditions. It is thought that the mechanism could strongly depend on surface properties and morphology of these photocatalysts, i.e., on the properties of semiconductor, noble metal and interaction between them.

5.2 Experimental details

Environmental applications of titania photocatalysis have been examined for titania samples prepared during my PhD research (Chapters II-IV), i.e., original P25, HomoP25, single phase titania (anatase and rutile) samples isolated from HomoP25 and faceted anatase (OAP). For vis activity, titania samples were modified with NMNPs to obtain plasmonic photocatalysts, as presented in Chapter IV. Photocatalytic activities were tested under UV/vis irradiation for oxidative decomposition of acetic acid (CO_2 system) and anaerobic dehydrogenation of methanol (H_2 system), as presented in Chapter II. The visible light activity for oxidation of 2-proponol was evaluated by determination of the amount of acetone generated. Fifty mg of the photocatalyst was suspended in 5 mL of 2-propanol (5 vol%) and irradiated under magnetic stirring in a photoreactor equipped with a 300-W xenon lamp (CX-04E Inotech, Japan), cold mirror, water filter and cut-off filter (Y45 ($\lambda > 420$ nm), Asahi Techno Glass). Dark reactions in a testing tube (the same as used for photoirradiation experiments) thoroughly covered with aluminum foil were also carried out. The photoreactor was described in detail and shown in published papers.[80, 83] The generated acetone was analyzed in liquid phase, after its filtration through a syringeless filter (Whatman Mini-UniPrep, PVDF), by gas chromatography (Shimadzu GC-14B, equipped with a flame ionization detector). Antimicrobial activity was tested for selected microorganisms (bacteria and fundi), as described below.

The antifungal activity of titania samples prepared from P25 was investigated by agar plate method on standard Czapek Yeast Agar (CYA; BTL). The basal medium was supplemented with 20 g/L of titania samples: original P25, and isolated polymorphic forms (anatase and rutile) from P25. The antifungal activities were tested for the following fungi strains isolated from air, *Penicillium chrysogenum*, strain ZUT1; *Aspergillus versicolor*, strains: ZUT130, ZUT110;

Aspergillus flavus, strain ZUT2; *Aspergillus melleus*, strain ZUT3; *Pseudallescheria boydii*, strain ZUT25; *Pseudallescheria ellipsoidea*, ZUT12; *Scedosporium apiospermum*, strain ZUT11; *Scedosporium aurantiacum*, strain ZUT4, and from damp walls: *Stachybotrys chartarum*, strain ZUTST. Ten-day old fungal cultures on MEA slants at 25 °C were used for preparation of spore suspensions. 5 ml of sterile physiological saline were added to each slant. The slants were then vigorously shaken by a vortex for 3 min. Each plate was centrally inoculated with 5 µl of spore suspension. Due to limited amount of photocatalysts for experiments carried out on *P. chrysogenum* and *A. mellus* three symmetrical places of each plate were inoculated with spore suspension (as shown for 4-day incubated samples in **Figure** 5.5c). It must be pointed that even for these experiments at least 2 g of photocatalyst had to be prepared for tests of one fungal strain in the dark and light conditions. One part of the plates was incubated in the dark, while another part was exposed to natural indoor light (intensity of ca. 120 W m^{-2}). The irradiation was daily intensified by 8-hour exposition to halogen light (intensity of ca. 1300 W m^{-2}) from three halogen lamps (50 W/each) mounted ca. 50 cm above plates. The UV light intensity was negligible (ca. 0.3 W m^{-2}). The incubation was carried out for 10 days at 25 °C. The colony diameters were measured after 2, 4, 6, 8 and 10 days of incubation. The daily growth rates (mm/day) were calculated from the linear regression equation (**equation. 15**):

$$r = a \cdot t + b, \qquad (15)$$

where “r” is colony radius (mm); “t” is incubation time (day), “a” is daily growth rate, and “b” is growth retardation time (lag phase; λ).

According to Dantigny *et al.*[84] the lag time calculated from macroscopic observations of mycelium has no biological significance, and thus the analysis of b values has been abandoned in present study.[3]

Antifungal experiments were performed for seven titania samples obtained from P25, i.e., i) homogenized P25 (homo-P25), ii) thermally post-treated homo-P25 at 200 and 500 °C (homo-P25-200, homo-P25-500), iii) isolated anatase (A), iv) isolated rutile (R), v) isolated anatase thermally post-treated at 200 °C (A-200), vi) isolated rutile washed with NaOH and thermally post-treated at 200°C (R-200), and vii) isolated anatase washed with NaOH (A_{Na}), as discussed in Chapter II. In brief, P25 sample of 20 g was suspended in 0.2-L Milli-Q water for 12 h under 500 rpm and then freeze-dried at -80°C and 10 Pa for 24 h (homo-P25). Anatase particles (A) were obtained from homo-P25 (6 g) by selective dissolution of rutile phase in a mixture of hydrogen peroxide (30 wt%, 200 mL) and ammonia (25 wt%, 6 mL) under magnetic stirring for 15 h at 25 °C.[85] The residual anatase titania was washed with Milli-Q water and centrifuged under 15,000 rpm several times, and freeze-dried. Thermal post-treatment at 200 °C for 2.5 h was applied for sample purification and the resultant sample was labelled as A-200. Rutile particles were isolated from P25 by selective dissolution of anatase phase from homo-P25 (9 g) in a diluted hydrofluoric acid (10 wt%, 200 mL) under magnetic stirring for 24 h at room temperature.[86] The residual titania was washed several times with Milli-Q water, centrifuged under 4000 rpm, dried by the freeze-drying process and labelled as R. For further sample purification, the sample was additionally washed with aqueous sodium hydroxide (to remove HF), freeze-dried and thermally post-treated at 200 °C for 2.5 h. The resultant sample was labelled as R_{Na}-200. To study the possible influence of thermal treatment on surface properties of titania P25, e.g., aggregation and sintering, and thus on resultant antifungal properties, homo-P25 was also thermally treated at 200 and 500 °C and obtained samples were

labelled as homo-P25-200 and homo-P25-500. In addition, the possible influence of sodium on antifungal properties was also investigated for anatase sample (A) washed with aqueous sodium hydroxide, freeze-dried and labelled as A_{Na}.

Faceted anatase particles (OAP) were modified with noble metals (as described in Chapter IV) and applied for antimicrobial tests and decomposition of acetic acid (under UV), dehydrogenation of methanol (under UV) and vis decomposition of 2-propanol. Antimicrobial properties of NM-modified OAP were investigated in the dark (control) and under irradiation with UV and/or visible light. The xenon lamp with UV-35 ($\lambda > 350$ nm) or Y-45 ($\lambda > 450$ nm) cut-off filter, respectively, was used. A 50 mg of photocatalyst and 7 mL of microorganisms suspensions in sterile 0.9% saline solution (NaCl) were applied. The following microorganisms were used: bacteria *Escherichia coli* K12 from ATCC29425 and fungi *Candida albicans* isolated from patients with the poor immune system (throat smear). The bacteria and yeast density was 0.5 in McFarland standard, which corresponds to ca. 1.5×10^8 colony-forming unit (CFU) mL^{-1}. The antimicrobial tests were performed by the plate counting methods, as follows: 0.5 mL of suspension was taken after 0.5, 1, 2 and 3 h of reaction. The serial dilutions were prepared and spread over agar media PCA (Plate Count Agar from Becton, Dickinson and Company) for *E. coli*, and MEA (Malt Extract Agar from Merck Millipore Corporation) for *C. albicans*. The plates were incubated overnight at 310 K. After this period, the number of colonies were counted to determine the number of viable cells (as log N/N_0).

5.3 Results and discussion

5.3.1. Antifungal properties of titania photocatalysts prepared from P25

P25 is composed of two polymorphic forms of titania, i.e., anatase and rutile, and non-crystalline (NC) part in the amount of 73-85, 14-17 and 0-13%, respectively, as already presented in Chapter II. In this regard, it is impossible to judge which part of P25 or if the interaction between its components is responsible for antifungal properties. Thus, isolated polymorphic forms, i.e., A (anatase) and R (rutile), were used for detailed studies. It must be reminded that P25 is non-uniform, and thus homogenized samples of P25 were used as starting material (homo-P25). The composition of titania samples, i.e., homo-P25 and isolated phases without and with thermal post-treatment (homo-P25, homo-P25-200, homo-P25-500, A, A_{Na}, A-200, R and R_{Na}-200) is shown in **Table 5.1** and exemplary XRD patterns are presented in the left part of **Figure 5.1**.

Table 5.1. Phase composition of titania samples

Sample code name		Composition (%)			Crystalline size (nm)	
		anatase	rutile	NC phase	anatase	rutile
homo-P25	sample 1	77.6	14.1	8.3	25.3	39.6
	sample 2	77.6	14.4	8.0	28.7	33.9
	sample 3	77.1	14.0	8.9	30.2	36.1
	average	77.4	14.2	8.4	28.1	36.5
homo-P25-200		74.8	13.6	11.6	30.5	35.2
homo-P25-500		71.3	18.8	9.9	34.1	52.4
A		86.6	0	13.4	25.9	-
A_{Na}		80.5	0	19.5	22.3	-
A-200		85.9	0	14.1	23.7	-
R		0	88.6	11.4	-	38.6
R_{Na}-200		0	97.1	2.9	-	39.5

Copyright © 2015 Elsevier B.V., all rights reserved

Homogenization resulted in preparation of uniform titania samples of ca. 77% of anatase, 14% of rutile and 8% of NC, as confirmed by three XRD analyses (samples 1-3 in **Table 5.1**). Thermal treatment of homo-P25 at 500 °C resulted in slight increase of rutile content up to 18.8%, due to thermally induced crystallization of amorphous titania and phase transition from anatase to rutile. Isolated samples (A, A_{Na}, A-200, R, R_{Na}-200) contained only one crystalline phase of anatase and rutile with minority of NC phase, as shown in the left part of **Figure 5.1**. It is expected that NC part contains small amount of adsorbed water (<3% based on thermogravimetry measurements) and amorphous titania. XRD patterns proved crystalline purity of isolated samples, i.e., disappearance of anatase and rutile peaks for R/R_{Na}-200 and A/A_{Na}/A-200 samples, respectively. The size of anatase and rutile crystallites equalled to 28.1 and 36.5 nm, respectively, in homo-P25. Isolation process only slightly reduced crystalline size of anatase, probably due to chemical etching. Crystalline sizes increased by thermal treatment, especially at higher temperature of 500 °C reaching 34.1 and 52.4 nm for anatase and rutile phases, respectively.

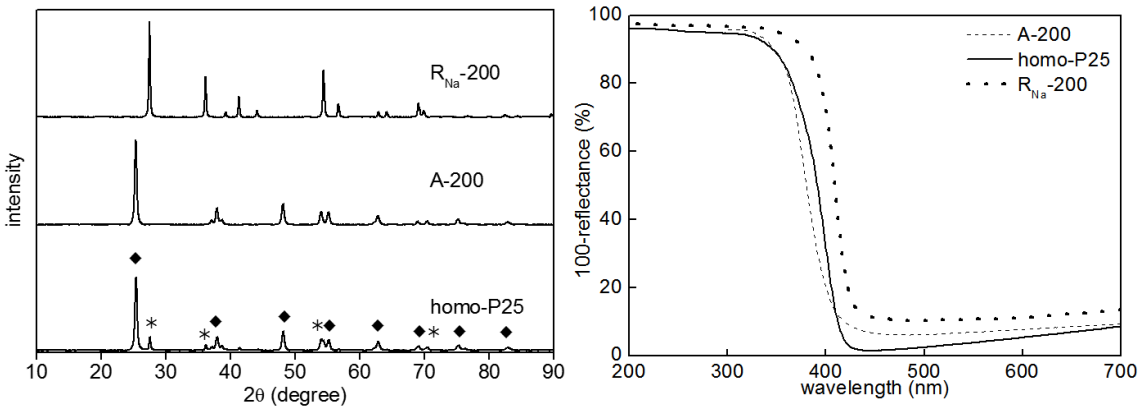


Figure 5.1. (left) XRD patterns and (right) DRS spectra of homo-P25, A-200 and R_{Na}-200: ♦ anatase, ∗ rutile

Copyright © 2015 Elsevier B.V., all rights reserved

The absorption properties of samples were studied by DRS, and exemplary data are shown in the right part of **Figure 5.1**. The observed hypsochromic and bathochromic shifts of photoabsorption for A-200 and R_{Na}-200 samples, respectively, in comparison with homo-P25, were expected, due to narrower band-gap of rutile (ca. 3.0 eV) than anatase (ca. 3.2 eV). The surface purity of rutile samples was also examined by XPS analysis, i.e., the efficiency of post-treatment operation during rutile photocatalysts washing. Five main elements were analyzed in details by narrow XPS scanning, i.e., titanium, oxygen, carbon, fluorine and sodium, and obtained data are summarized in **Table 5.2**. It was found that isolated rutile sample unwashed with NaOH (R) possessed large content of fluorine on the surface reaching 8.35 mol% (in relation to titanium). Whereas R-200 sample, R washed with NaOH and thermally treated at 200 °C, contained much lower amount of fluorine on the surface of 2.26 mol%. Both samples possessed excess of carbon on the surface, i.e., 26.1 and 50.5 mol% for R_{Na}-200 and R, respectively. The atomic ratio of oxygen to titania for R sample slightly exceeded stoichiometric value of 2.0 reaching 2.2. Whereas for R_{Na}-200 the lack of oxygen was notice since 1.72% of O/Ti ratio was obtained. It is thought that sample washing with NaOH removed adsorbed fluorine, carbon and oxygen (in the form of hydroxyl groups). It must be pointed that though some adsorbents were washed out from titania surface, washing with NaOH caused adsorption of sodium on the surface. After deconvolution of titanium and oxygen peaks (**Figure. 5.2**), it was found that titanium in R and R_{Na}-200 samples existed mainly in oxidized form of Ti^{+4} (97.2% and 95.7%, respectively), as shown in **Table 5.3**. O 1s region could be deconvoluted for three peaks at BE of 529.3-529.5 eV, 531.3-531.8 eV and 533.4-533.8 eV. The first peak can be attributed to oxygen in crystalline lattice of TiO_2, the second peak to OH group binding with two Ti atoms or Ti_2O_3, while the third peak to surface oxygen in Ti-OH.[87, 88] Oxygen mainly

occurred in the form of TiO_2, reaching 65% and 79% for R and R-200, respectively, which confirms that alkali washing resulted in desorption of hydroxyl groups from the surface.

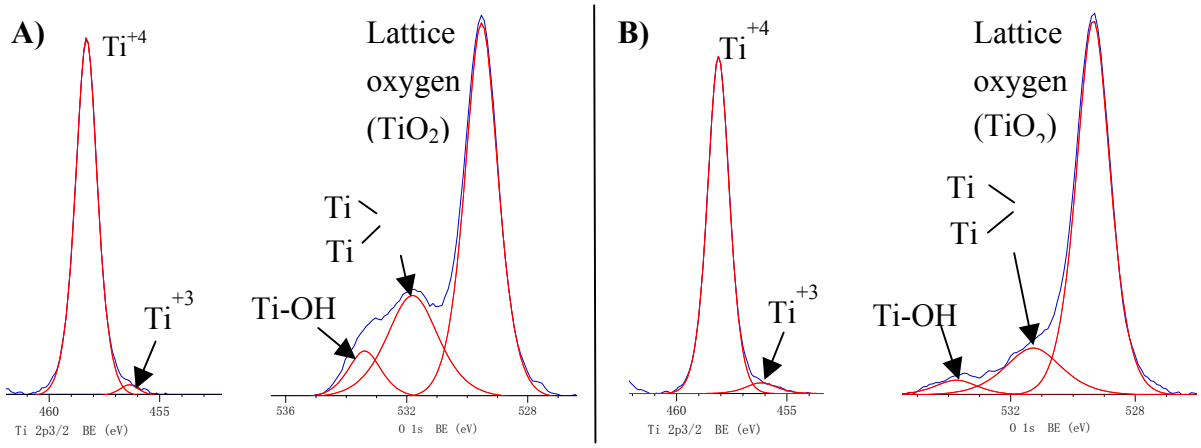


Figure 5.2. XPS spectra of (left) Ti 2p and (right) O 1s regions for rutile samples: R (A) and R_{Na}-200 (B).

Copyright © 2015 Elsevier B.V., all rights reserved

Table 5.2. Chemical composition of rutile photocatalysts based on XPS analysis

Sample	Ti mol%	O mol%	O:Ti	C mol%	C:Ti	F mol%	F:Ti	Na mol%	Na:Ti
R	15.09	33.16	2.2	50.49	3.3	1.26	0.08	-	-
R_{Na}-200	22.59	38.94	1.7	26.1	1.2	0.51	0.02	11.86	0.5

Copyright © 2015 Elsevier B.V., all rights reserved

Table 5.3. Oxidation state of titanium and oxygen in rutile samples based on XPS analysis

Sample	Ti 2p (%)		O 1s (%)		
	Ti^{+4}	Ti^{+3}	-OH	$(-OH)_2$, Ti_2O_3	TiO_2
R	97.2	2.8	8.0	27.5	64.5
R_{Na}-200	95.7	4.3	3.9	16.7	79.4

Copyright © 2015 Elsevier B.V., all rights reserved

Morphology of samples was studied by STEM and exemplary images of A, R and homo-P25 are shown in **Figure 5.3**. Similar to XRD data, slightly smaller NPs were detected for anatase (**Figure 5.3**, bottom, right) than for rutile (**Figure 5.3**, bottom, left) samples of 20-40

nm and 30-60 nm, respectively. Therefore, it is proposed that larger and smaller NPs detected in homo-P25 (**Figure 5.3**, top) correspond to rutile and anatase crystallites, respectively. Large aggregates of 100-200 nm were noticed only in isolated rutile and mixed sample indicating that mainly rutile crystallites formed these aggregates.

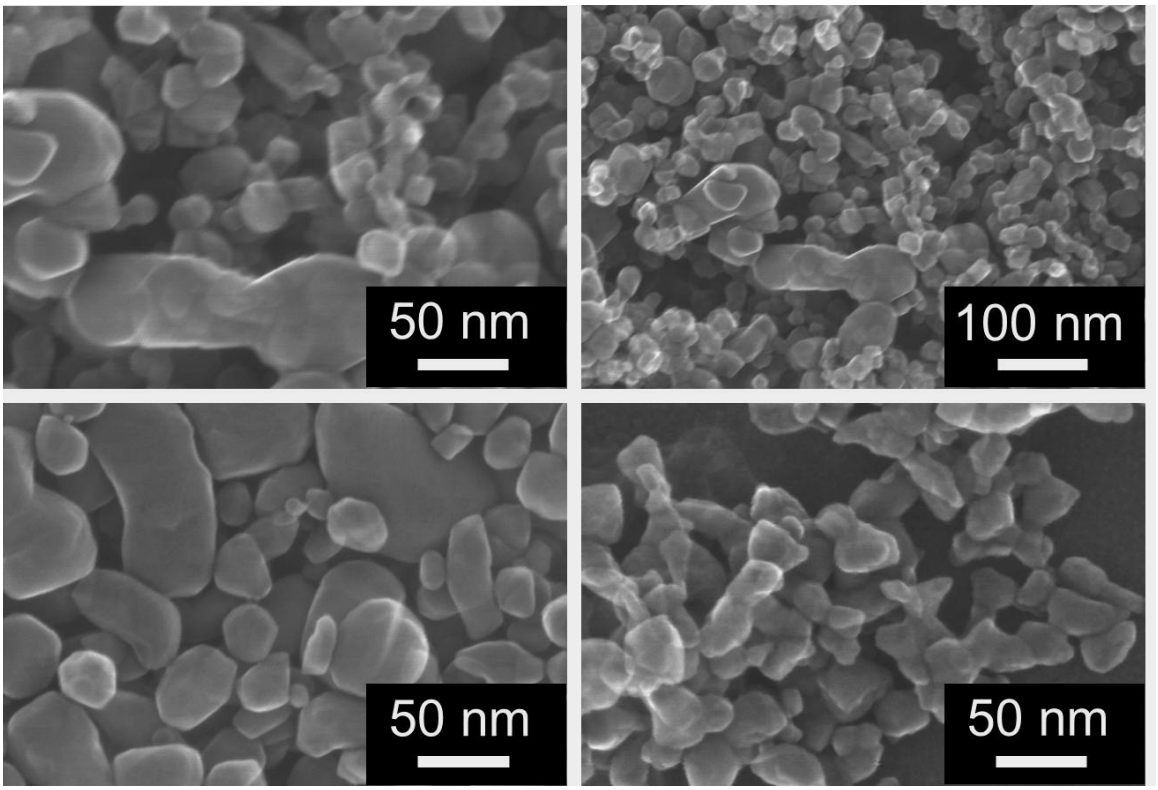


Figure 5.3. STEM images of homo-P25 (top), R (bottom, left) and A (bottom, right).

Copyright © 2015 Elsevier B.V., all rights reserved

Raw titania (A and R) samples (without purification)

At first antifungal properties were tested for following fungi: *Pseudallescheria boydii* (ZUT25), *Scedosporium apiospermum* (ZUT11), *Pseudallescheria ellipsoidea* (ZUT12), *Scedosporium aurantiacum* (ZUT4), *Aspergillus versicolor* (ZUT130, ZUT110), *Aspergillus flavus* (ZUT2) and *Stachybotrys chartarum* (ZUTST). The rates of fungal daily growth during experiments performed in the dark (D) and under light (L) on isolated phases (A and R) are shown in **Figure 5.4**.

The complete inhibition of growth was achieved for only one strain *Pseudallescheria boydii* (ZUT25) on media supplemented with anatase under irradiation (**Figure 5.4a**). The light also inhibited fungal growth on anatase for ZUT 110 and ZUT2, and slightly for ZUT12, ZUT4, ZUT130 and ZUTST. However, the simulative effect of light on fungal growth was observed for ZUT 11. Almost all observed differences were statistically significant (ZUT25, ZUT11, ZUT12, ZUT4, ZUT110, ZUT2, ZUTST). The indoor light (photolysis, but not photocatalysis) mostly inhibited fungal growth what was observed on control media (without titania). It should be pointed that presence of anatase accelerated growth of ZUT2, ZUT4, ZUT12 and ZUTST under irradiation, and inhibited growth of all tested fungi in the dark (except ZUTST). This indicates that irradiated anatase positively changed fungal environment, possibly due to change of water accessibility (superhydrophilicity) and thus stimulated fungal growth. The free water is essential for normal activity of extracellular enzyme in a process known as absorptive nutrition. The enzymes, which are released by fungi, break down complex (polymer) substances in building materials. Then, the simple compounds are dissolved in water and absorbed by the fungi. The recent report on antifungal properties of P25 for various water activity (a_w=0.850-0.999) has indicated that titania stimulated fungal growth in the lack of accessible water (however, mainly in the dark).[54] The inhibition of fungal growth by non-irradiated anatase could be cause by its adsorption on fungal surface, which could result in inhibition of sporulation. According to Calvo *et al.*[89] interactions between sporulation and mycotoxin production in relation to environmental factors are not understood at a genetic level. It is possible, however, that some compounds have subtle effects on sporulation (decrease in asexual spore production is not detectable by the unaided eye), but exhibit a decrease mycotoxin production. For example, simple sugars such as glucose, fructose, sucrose, and sorbitol support high fungal growth, sporulation, and aflatoxin production. In contrast, peptone and the

more-complex sugars like galactose, xylose, mannitol, do not support aflatoxin production well.[89]

Rutile showed similar action to anatase for *P. boydii* (ZUT25) and *A. versicolor* (ZUT130, ZUT110), but inhibition of growth of ZUT25 and ZUT130 in the dark was 3-4 times lower than that on anatase, which could be caused by large particles of rutile and thus lower interface between titania and fungus. Whereas, activity of rutile under irradiation was two times higher than that of anatase for *A. versicolor* (ZUT110), probably due to its broader photoabsorption (≤ 420 nm for rutile and ≤ 400 nm for anatase, **Figure 5.1**, right), which is crucial for present studies performed under daily light (not UV lamps). In the dark and under irradiation rutile stimulated growth of fungi which growth was accelerated by irradiation of anatase, i.e., ZUT12, ZUT4, ZUT2 and ZUTST. All differences between samples tested under irradiation in the presence and absence of rutile were statistically significant (**Figure 5.4b**). Though used amount of photocatalyst (20 g × dm^{-3}) was not sufficient for complete elimination of mould fungi, the further experiments were continued for the same conditions for clear analysis (comparison) of data.

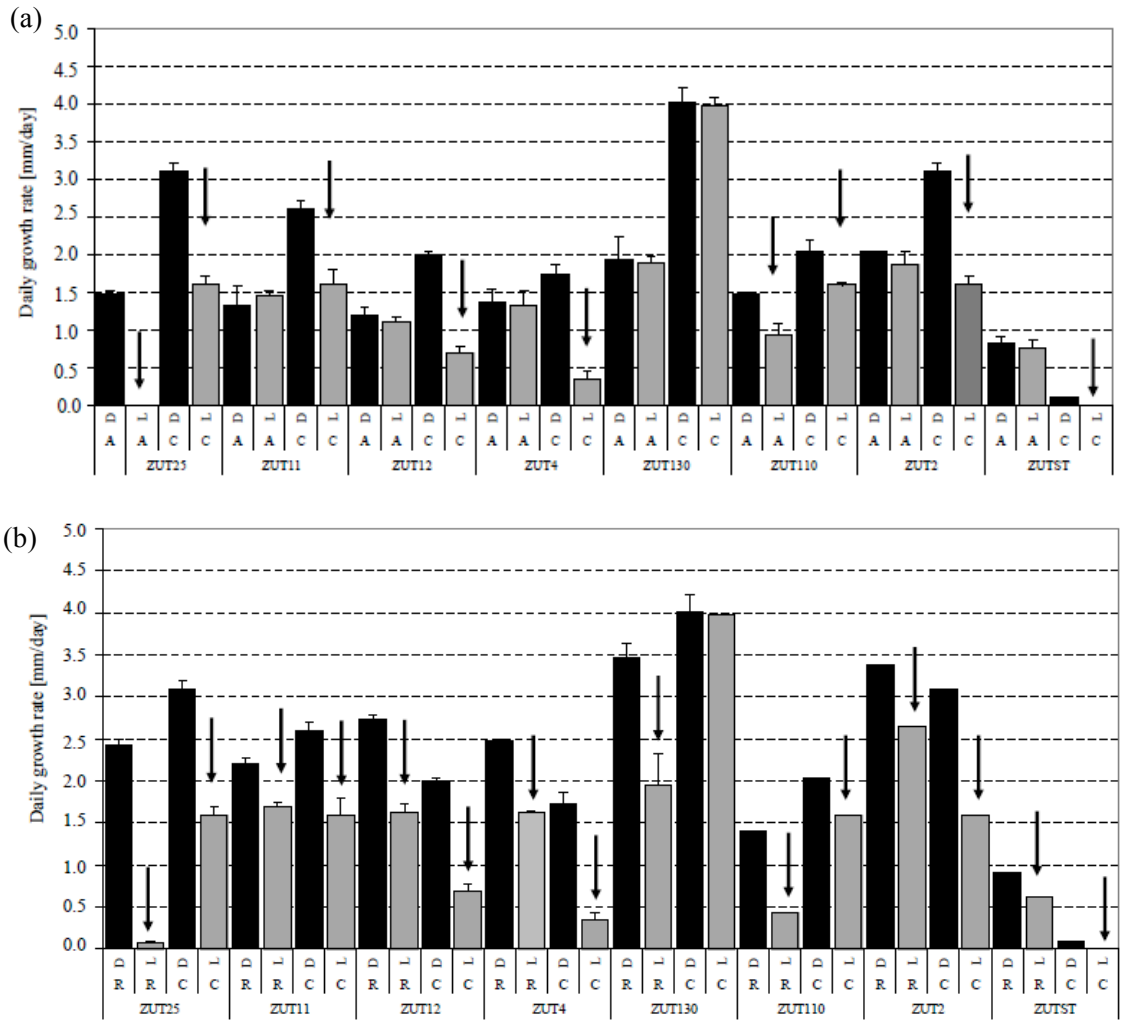


Figure 5.4 Mean daily radius growth of selected mould on media supplemented with 20 g x dm^{-3} of (a) anatase and (b) rutile incubated in dark (D) and light (L) conditions; A – anatase (A), R – rutile (R), C - control (without photocatalyst), strains of fungi: ZUT25 - *P. boydii*, ZUT11 - *S. apiospermum,* ZUT12 - *P. ellipsoidea,* ZUT4 - *S. aurantiacum,* ZUT130 and ZUT 110 - *A. versicolor,* ZUT2 - *A. flavus,* ZUTST - *S. chartarum*; black bars mean standard deviations between replications, black arrows mean statistically significant differences between daily growth rate in light and dark at $p \leq 0.05$.

Copyright © 2015 Elsevier B.V., all rights reserved

Summarizing, it must be pointed that though surface properties of both crystalline forms were similar (particle size), they differed significantly by resultant antifungal properties. Activity of rutile was highly accelerated by light, due to its ability of absorption of more

photons than anatase (narrower band-gap). While, irradiated anatase stimulated fungal growth possibly as a result of its superhydrophilic properties which could influence water accessibility by fungi. In addition, it was found that antifungal properties of titania depended significantly on structure of examined fungi, and thus either enhancement or inhibition of fungal growth was noticed.

Purified titania samples (A-200, R_{Na}-200)

It must be pointed that isolation process was performed by chemical etching, and thus isolated anatase and rutile (A, R) possessed chemical impurities adsorbed on titania surface, e.g., nitrogen, fluorine, sodium (as has been proved by XPS data), which could influence the resultant antifungal properties. In this regard, purification of samples by alkali washing (only for rutile to remove HF) and thermal treatment (for both samples) was carried out, and antifungal properties of purified samples, i.e., A-200 and R_{Na}-200, was tested and data are presented in **Figure 5.5(a-b)**. Sample purification resulted in enhancement of antifungal properties of anatase under irradiation for four fungal strains, i.e., *S. apiospermum* (ZUT11), *P. ellipsoidea* (ZUT12), *S. aurantiacum* (ZUT4), *A. flavus* (ZUT2). However, antifungal properties of anatase for *P. boydii* (ZUT25) and *A. versicolor* (ZUT130) decreased. In the dark antifungal properties of anatase worsened for five fungal strains, i.e., *S. apiospermum* (ZUT11), *P. ellipsoidea* (ZUT12), *S. aurantiacum* (ZUT4), *A. versicolor* (ZUT130, ZUT110), which could be caused by decrease of interface between titania and fungus, due to particle aggregation under thermal treatment (in contrast to more efficient evolution of hydrogen at lower Pt-loading amount, as discussed in Chapter III (IPET)).

Due to limited amount of purified rutile, tests were conducted only for two strains of fungi: *P. boydii* (ZUT25) and *S. chartarum* (ZUTST). In comparison with non-purified rutile

(**Figure 5.4b**), the daily growth rates of examined fungi by purified rutile increased slightly in the dark and increased highly under irradiation. It is suggested that removal of HF by washing with NaOH resulted in change of rutile surface (XPS data shown in **Tables 5.2** and **5.3**), and adsorbed sodium on titania surface could:

(i) (under irradiation) work as recombination centers for photogenerated charge carriers (e^-/h^+) resulting in decrease of photocatalytic activity;[90, 91] it is also possible that during thermal treatment photocatalytically inactive sodium titanate could be formed),[92]

(ii) (in the dark) accelerate fungal growth (sodium as nutrient) which was also suggested by already mentioned decrease in antifungal properties in the dark. There is partial evidence from the literature of significant influence of NaCl and $CaCl_2$ on the fungal growth.[93]

It is clear that fungal growth rates are dependent on both the purity of photocatalysts and a strain of fungi.

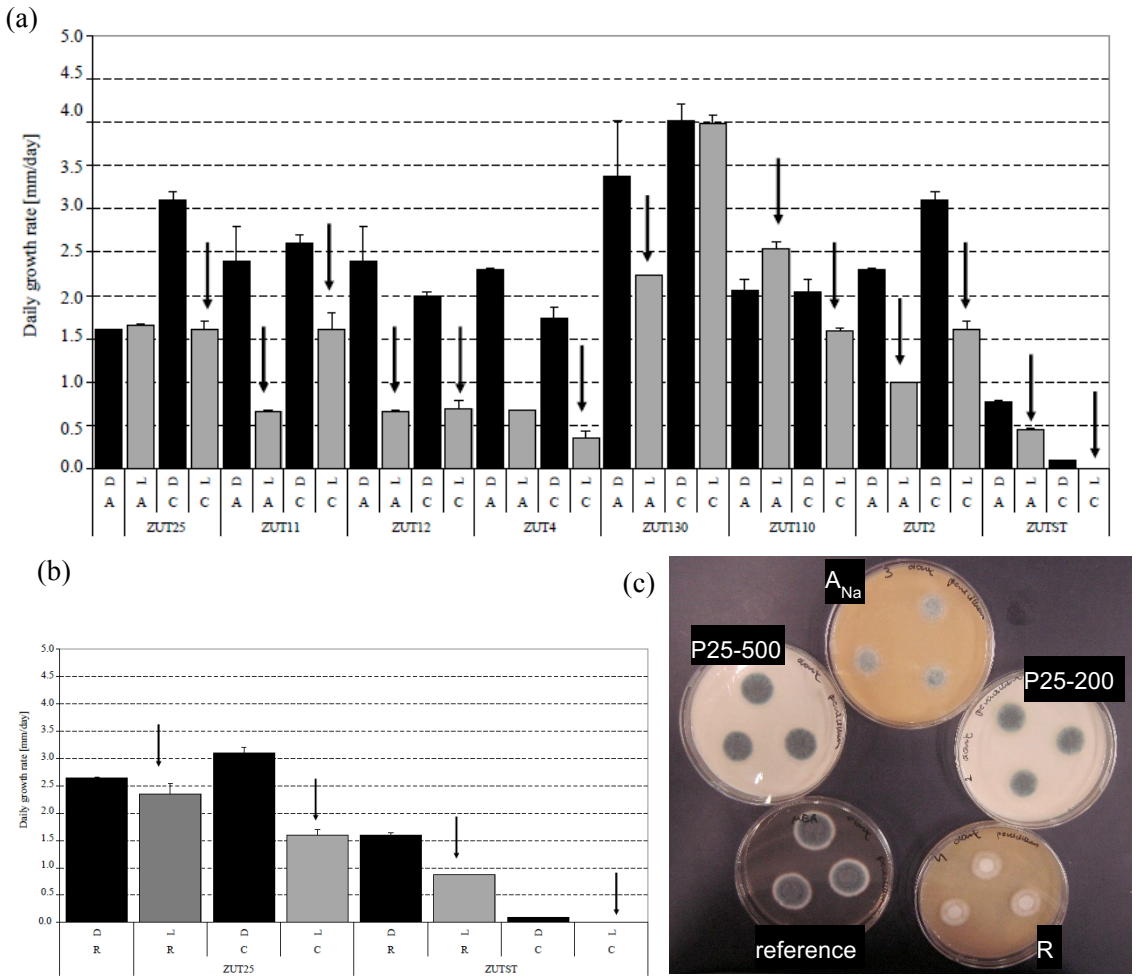


Figure 5.5. (a and b) Mean daily radius growth of selected mould on media supplemented with 20 g x dm^{-3} of purified (a) anatase (A-200) and (b) rutile (R_{Na}-200) incubated in dark (D) and light (L) conditions; A – anatase (A-200), R – rutile (R_{Na}-200), C - control (without photocatalyst), strains of fungi: ZUT25 - *P. boydii*, ZUT11 - *S. apiospermum,* ZUT12 - *P. ellipsoidea,* ZUT4 - *S. aurantiacum,* ZUT130 and ZUT 110 - *A. versicolor,* ZUT2 - *A. flavus,* ZUTST - *S. chartarum*; black bars mean standard deviations between replications, black arrows mean statistically significant differences between daily growth rate in light and dark at $p \leq 0.05$; (c) photograph of mycelium growth of *P. chrysogenum* ZUT1 after 4-day incubation in the dark on reference (without titania) and on titania samples: P25-500, P25-200, A_{Na}, R (antifungal data shown in **Figure 5.6**).

Copyright © 2015 Elsevier B.V., all rights reserved

To further investigate an influence of thermal treatment and presence of impurities on titania surface, antifungal properties for two additional strains of fungi: *Penicillum chrysogenum*

(ZUT1) and *Aspergillus melleus* (ZUT21) were examined on P25 thermally treated at 200°C (P25-200) and 500°C (P25-500) and on isolated anatase washed with NaOH (A_{Na}) and isolated rutile (R). It was found that growth of fungi was strongly inhibited by presence of titania both under irradiation and in the dark, as shown in **Figures 5.5c** and **5.6.** It is suggested that rutile phase is mainly responsible for titania activity under irradiation, due to narrower band-gap, and thus ability of visible light absorption (similar to methanol dehydrogenation, discussed in Chapter III). In addition, presence of adsorbed fluoride on rutile surface could both i) activate titania towards visible light by e.g., generation of localized state in the band-gap creating surface oxygen vacancies, and ii) inhibit recombination of charge carriers.[94] In the case of *P. chrysogenum*, the same antifungal activity in the dark for P25-200 and A_{Na} was not surprising since P25 was mainly composed of anatase. Slight decrease in antifungal activity for P25-500 could be caused by sintering and aggregation of titania NPs at higher temperature, and thus due to decrease of interface between titania and fungus. The highest antifungal activity of rutile in the dark could be caused by the presence of fluoride on titania surface. Similar to inhibition of fungal growth in the dark on non-purified rutile sample as is evident by comparison of data from **Figure**s **5.4b (R)** and 5.5b (R_{Na}-200). Much worse activity of anatase than rutile under irradiation and in the dark could be caused by sodium presence, similarly as was proposed for alkali washed rutile sample (R_{Na}-200), i.e., enhanced recombination of charge carriers and nutrient promoted fungal growth, respectively. According to recent studies of Boumaaza *et al.*[93] sodium presence in various concentrations can promote or reduce the in vitro mycelial growth and sporulation. In contradistinction to *P. chrysogenum*, P25-200 exhibited the highest antifungal properties under irradiation against *A. melleus*. It is possible that synergism between anatase and rutile, i.e., transfer of charge carriers between two polymorphs, could result in higher photocatalytic activity as was previously proposed for decomposition of chemical

compounds.[86, 95] However, it is expected that for both fungal strains the same synergism should be observed. The lack of synergism for *P. chrysogenum* indicates that other factors could be crucial for resultant antifungal activities, e.g., presence of impurities on titania surface. It is proposed that fluorine and sodium may inhibit fungal growth, but this inhibition highly depends on fungal structure. The worse activity of P25-500 than P25-200 under irradiation for both fungal strains is possibly caused by creating new recombination centers for aggregated titania nanoparticles. Though statistically significant difference between incubation under light and in the dark was not noticed, and thus influence of light could not be clearly confirmed by simple growth of mycelium, it must be pointed that sporulation and mycotoxin generation (observed as formed droplets, which most probably should consist mycotoxins since mycotoxin production is associated with sporulation and has been been documented in several mycotoxigenic genera, for example *Aspergillus*)[89] was highly inhibited under irradiation, as shown in the right part of **Figure 5.7**. The reduction of spores' content presented in air is crucial for preventing impact of mycotoxins on human health. Only slight difference in sporulation and mycotoxin generation was observed between control sample and that supplemented with photocatalyst by simple visual observations. In this regard, further studies on counting of generated spores and mycotoxin production (qualitative and quantitative analyses) are presently under investigation.

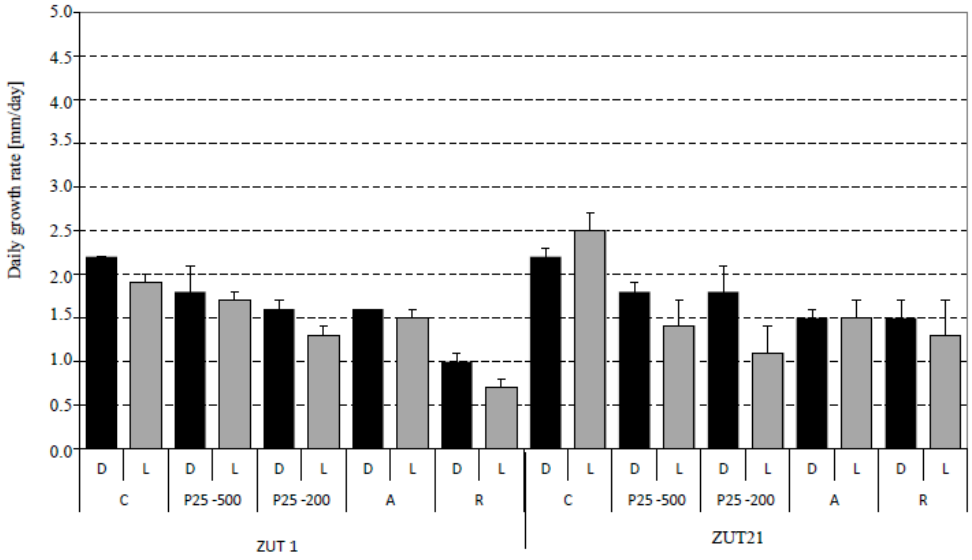


Figure 5.6 Mean daily radius growth of *Penicillium chrysogenum* (ZUT1) and *Aspergillus melleus* (ZUT21) in dark (D) and light (L) conditions on media supplemented with 20 g x dm^{-3} of photocatalyst; A – anatase washed with NaOH (A_{Na}), R – rutile (R), P25-200 – homogenized P25 thermally post-treated at 200°C, P25-500 – homogenized P25 thermally post-treated at 500°C, C - control (without photocatalyst); black bars mean standard deviations between replications.

Copyright © 2015 Elsevier B.V., all rights reserved

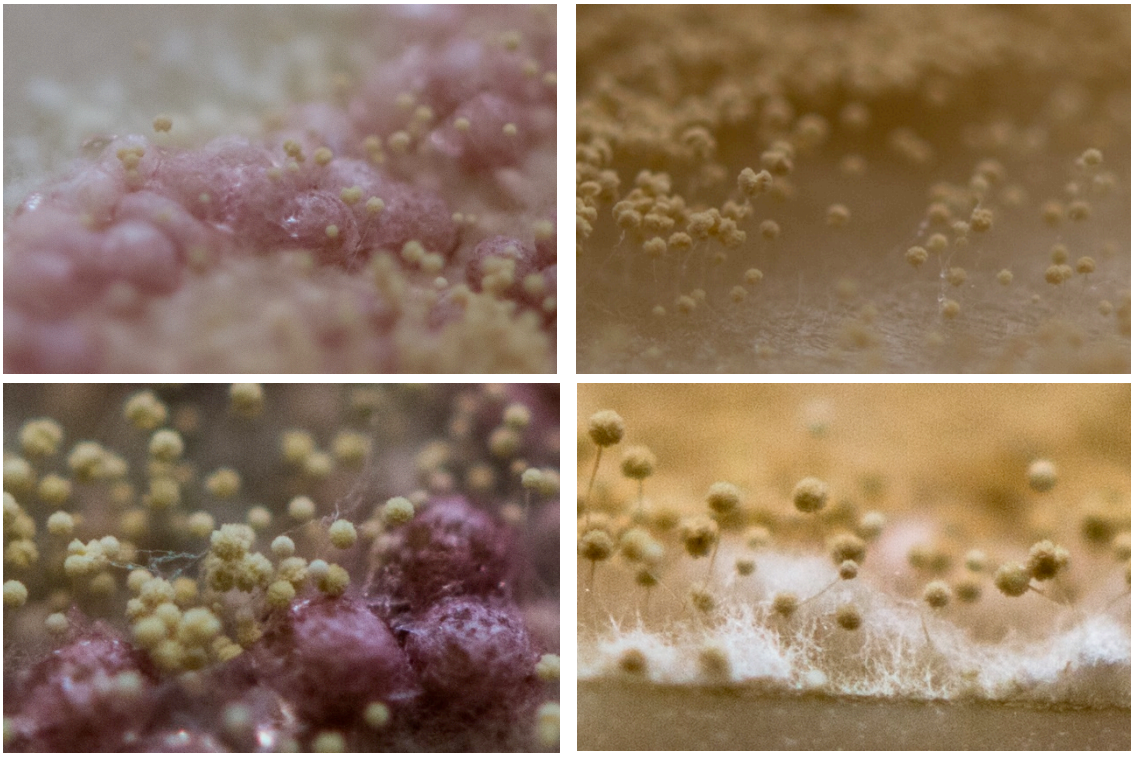


Figure 5.7. Images of 3-day growth of *A. melleus* (left) in the dark and (right) under irradiation without (top) and in the presence of homo-P25 (bottom).

Copyright © 2015 Elsevier B.V., all rights reserved

5.3.2. Decomposition of organic compounds and microorganism on titania samples modified with noble metals

OAP sample was modified with NMNPs by photodeposition, as shown in Section 4.2. Absorption properties (DRS) and photographs of all modified samples are shown in **Figure 5.8** Since LSPR position of Pt and Ag is near band edge of titania, DRS spectra were taken with bare OAPs as a reference (to eliminate titania absorption properties). It should be pointed that position of LSPR of noble metals depends on kind of noble metal, properties of NPs such as their size and shapes, and environment (diffractive index). In general, LSPR at shorter wavelengths is observed for spherical and small NPs, and change in NPs shape or increase in NPs size results in bathochromic shift of LSPR. For example, LSPR of spherical NPs of Pt, Ag,

Au and Cu appears at ca. 400 nm,[96] 430 nm,[97] 540 nm[98] and 560 nm,[99] respectively.

It must be also reminded that Pt and Au are chemically stable and their exposition to an ambient environment after preparation does not change their surface properties. In contrary, Ag and Cu are easily oxidized, and their oxides are usually observed on the surface of NPs, independently on preparation method.[100, 101] For example, titania modification by strong radiolytic reduction of Cu^{2+} resulted in formation of CuO/TiO_2,[102] and oxidation of Cu NPs even by oxygen diffusion into water was also reported.[99] In this regard, it is expected that both metallic and oxidized forms of Ag and Cu could be detected during their characterization.

In my study, contrary results were obtained for particular metals by change of photodeposition method from deaerated to aerated conditions, i.e., increase in photoabsorption intensity was observed for Au and Ag samples, and slight decrease for Pt and Cu samples. The shape of DRS spectra practically did not change for Au and Pt, slightly changed for Cu and significantly changed for Ag. The broadening of LSPR of silver indicated that aerated conditions resulted in formation of more polydispersed silver NPs. It should be reminded that DRS spectra consisted of both absorption and scattering. Therefore, less intensive DRS spectra of Pt/OAPs at longer wavelengths could confirmed the findings that smaller Pt NPs were formed under aerated conditions (Chapter IV). In the case of Au, LSPR practically did not change, the intensity was stronger, but less scattering at longer wavelengths could suggest formation of less content of larger NPs. In contrary, no LSPR peak could be observed for Cu/TiO_2, which confirmed its easy oxidation in ambient environment (after preparation) resulting in the characteristic absorption band of CuO at near IR.[102-104] Slight green color of Cu/OAPs prepared under deaerated conditions suggests that Cu could exist also in the form of $[Cu(OH)]_2CO_3$ (or less possible CuO_2, due to its instability). It should be pointed that just after photodeposition (under aerated and deaerated conditions), the color of Cu samples was violet,

which confirmed that metallic copper was formed on titania. Interestingly, in the case of deposition under aerated conditions, at first black deposits of CuO were noticed, and then after oxygen consumption the zero-valent copper (violet color) was formed.

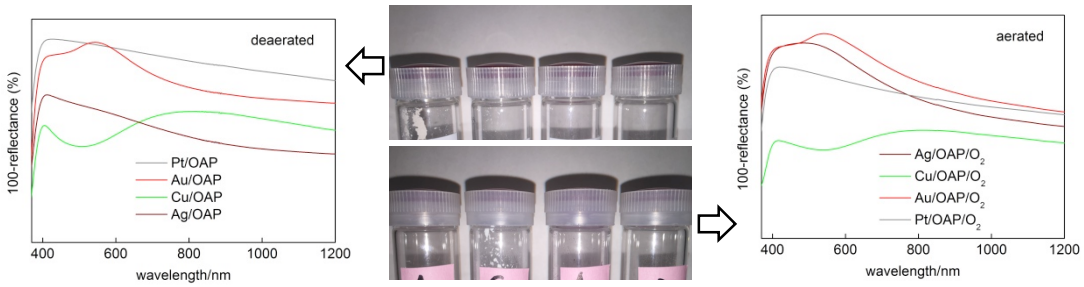


Figure 5.8 Photoabsorption properties of modified OAP samples prepared under (left) deaerated and (right) aerated conditions; bare OAP used as reference.

Copyright © 2018, Copyright Clearance Center, Inc., Creative Commons Attribution License (CC BY), All rights reserved

To determine crystalline composition and crystallite sizes of metallic deposits, XRD was performed and obtained data are summarized in **Table 5.4.** Since low amount of metals was used for modification (0.5 wt%) and their sizes were very small, no clear XRD peaks for metallic deposits could be observed, except for Au/OAPs prepared under aerated conditions, which showed characteristic gold features. Similarly, during previous study, Ag peak could not be clearly observed even for much larger amount of deposited metal (2 wt%), when fine anatase NPs (of similar sizes to OAPs) were used as a support.[100] Therefore, Rietveld refinement was used for detailed data analysis. In the case of Pt and Au, zero-valent deposits were clearly identified, while less noble metals (Ag and Cu) existed mainly in the form of their oxides (Ag_2O and CuO), as was suggested from photodeposition data (Chapter IV, **Figure 4.3**, right). Preparation method influenced sizes of metallic deposits, i.e., slightly smaller sizes of Pt and much larger sizes of other metals were obtained. Increase in crystallite sizes is quite surprising since slowing down deposition process by oxygen presence should result in formation of

smaller metallic deposits, as has been observed for Au deposition on various commercial titania samples (unpublished data). It is proposed that here, due to special properties of OAP (i.e., octahedron morphology, high crystallinity, low amount of deep electron traps and small crystallite size), the growth of crystallites is predominant instead of formation of new crystallites and their dispersion on OAP. In addition, it must be pointed that under aerated conditions less noble metals (Ag and Cu) formed first oxides, but not metallic deposits as under deaerated conditions. Therefore, it is concluded that deaerated conditions result in formation of fine zero-valent deposits, which further are partly oxidized (on the surface) under contact with ambient atmosphere. Whereas, under aerobic conditions, much larger metallic oxides (and also zero-valent metals) are obtained - directly formed under irradiation. It must be also reminded that DRS data reflect mainly the sizes of NPs, but not crystallites. Therefore, lack of influence of an increase in gold crystallite size (by aerated method) on LSPR position indicates that deposition method does not influence the size of resultant NPs, where only larger crystallites have been predominantly formed on OAPs.

Table 5.4. XRD analysis of metallic deposits in modified OAPs

Code	Pt/OAP	Au/OAP	Cu/OAP			Ag/OAP		
main component	Pt	Au	CuO			Ag_2O		
other components	-	-	Cu		Cu_2O	Ag		AgO
deaerated conditions								
crystallite size/nm	5.0	5.1	Cu	Cu_2O	CuO	Ag	Ag_2O	AgO
			1.8	10.9	4	n.d.	1.9	n.d
aerated conditions								
crystallite size/nm	4.5	11.7	Cu	Cu_2O	CuO	Ag	Ag_2O	AgO
			4.1	n.d.	15.2	n.d.	9.4	n.d.

n.d. – not determined

Copyright © 2018, Copyright Clearance Center, Inc.,
Creative Commons Attribution License (CC BY), All rights reserved

To characterize surface composition of the samples, oxygen, titanium, carbon and metals (Au, Ag, Pt and Cu) were analyzed by XPS method. It was found that ratio of oxygen to titanium exceeded those of chemical formula of titania (O:Ti = 2) reaching ca. 2.5. Various studies showed an excess of oxygen on titania surface, e.g., 4.6 ratio was reported for titania samples prepared by microemulsion method[87] and 2.5 ratio for titania prepared by laser ablation.[105]

Oxidation states of all elements were analyzed by deconvolution of XPS peaks. Exemplary spectra for bare OAP sample are shown in **Figure 5.9**. Titanium existed mainly in Ti^{+4} form (97.3%). Carbon 1s region was deconvoluted for three peaks at binding energies (BE) of ca. 284.8, 286.1 and 288.6 eV, which could be assigned to C-C, C-OH and C=O states and obtained contents were 67.0%, 23.9% and 9.1%, respectively. Carbon originates from the atmosphere during preparation of samples for XPS measurements and is always detected in all titania samples.[106] According to literature reports, O 1s peak could be composed of three to five different oxygen species such as Ti-O bonds in TiO_2 and Ti_2O_3, H-O bonds in hydroxyl groups, carbon bonds (C-O and C=O) and adsorbed water.[107] In this study, three peaks were observed after deconvolution of O 1s peak in all samples at BE of ca. 529.4, 531.6 and 533.2 eV, and respective contents equaled to 60.1%, 23.3% and 16.6%. The first peak is related to oxygen in the crystal lattice of TiO_2, the second peak to C=O, Ti_2O_3, and/or OH groups bounded with two titanium atoms, and the third peak mainly to hydroxyl groups bound to titanium and carbon (Ti-OH, C-OH).[88]

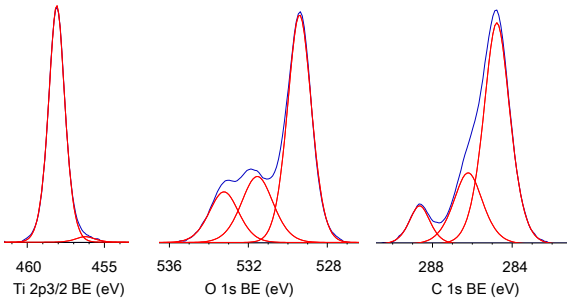


Figure 5.8. XPS results for Ti $2p_{3/2}$, O 1s, C 1s of bare OAP.

Copyright © 2018, Copyright Clearance Center, Inc., Creative Commons Attribution License (CC BY), All rights reserved

The presence of metals was confirmed in all modified samples, as shown in **Figure 5.10**. The content of metals exceeded the amount used for deposition (0.5 wt%) reaching ca. 3.5, 2.5, 2.2 and 3.1 wt% for Pt, Au, Cu and Ag, respectively, for samples prepared under deaerated conditions. The enrichment of titania surface with metals was expected and previously reported,[101] since metals were deposited on titania surface and XPS analysis measured the surface composition of samples. Interestingly, the content of metals changed when photodeposition was performed under aerated conditions, and larger amounts of Pt and Au (4.2 and 4.7, respectively), but smaller amounts of Cu and Ag (1.3 and 1.4 wt%, respectively) were obtained. This confirms previous data (DRS, photodeposition and partly XRD), suggesting that Pt and Au formed smaller NPs under aerated conditions (higher covering of titania surface, stronger XPS peaks of metals), but on the surface of less noble metals (Ag and Cu) oxides layer was formed (lower XPS peaks of metals). In addition, this hypothesis is also confirmed by XPS data of oxygen peak, as shown in **Figure 5.10**. Oxygen forms did not significantly differ between samples prepared under deaerated conditions (top line), but Au and Pt modified OAPs prepared under aerated conditions possessed huge amount of hydroxyl groups on titania surface (bottom line), similar to extended time of HT. In contradiction, hydroxyl groups were not additionally formed on OAPs modified with Ag and Cu, since oxygen formed metallic oxides

on the surface of these less noble metals. Deconvolution of Pt,[108-110], Au,[87] Cu[102, 111] and Ag [87, 101, 102] peaks confirmed that metal deposition under deaerated conditions resulted in formation of mainly zero-charged Au and Pt (ca. 90 and 61%, respectively) deposits, and oxidized forms of Ag and Cu (**Table 5.5**). Change in preparation method to aerated conditions resulted in formation of NPs with more positive charges, even for Pt and Au. Therefore, it is proposed that hydroxyl groups could be adsorbed on both titania surface and metallic deposits. The method of deposition practically did not influence an oxidation state of Cu, and only slightly more Cu^{2+} was formed than Cu^{1+} under aerated conditions (23.9% under deaerated and 28.4% under aerated conditions). Interestingly, preparation of Ag/OAP under aerated conditions resulted in formation of Ag^{2+} (besides predominant Ag^{1+}) and larger amount of zero-charged Ag(0), which explains the stable brown color of this sample even after drying.

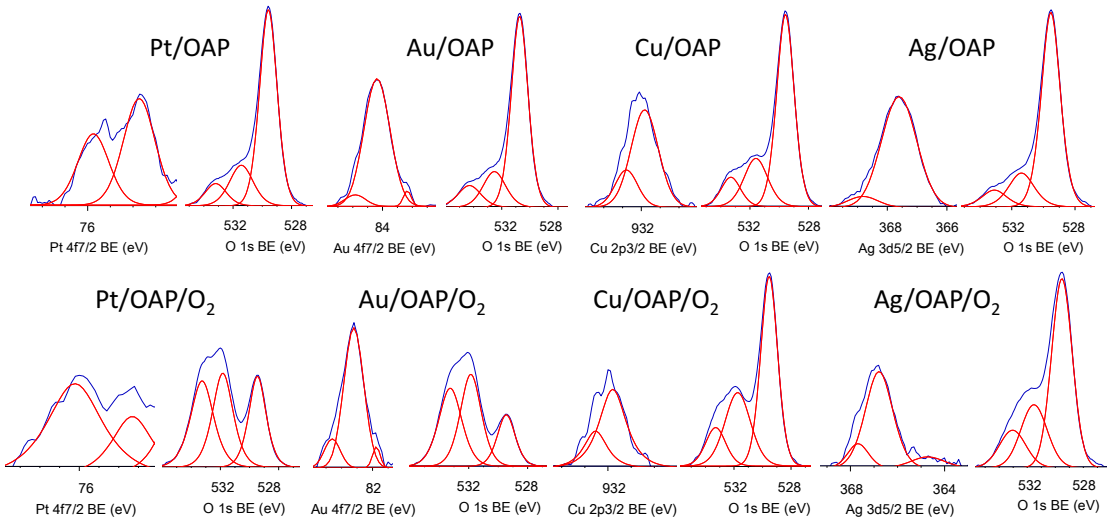


Figure 5.9. XPS results for Pt $4f_{7/2}$, Au $4f_{7/2}$, Cu $2p_{3/2}$, Ag $3d_{5/2}$ and O 1s for samples prepared under (top) deaerated and (bottom) aerated conditions.

Copyright © 2018, Copyright Clearance Center, Inc., Creative Commons Attribution License (CC BY), All rights reserved

Table 5.5 Fraction of oxidation states of Pt, Au, Au and Ag from deconvolution of XPS peaks of Pt $4f_{7/2}$, Au $4f_{7/2}$, Cu $2p_{3/2}$ and Ag $3d_{5/2}$

Sample	Pt/OAP		Au/OAP			Cu/OAP		Ag/OAP		
Form	Pt(δ+)	Pt(0)	Au(δ+)	Au(0)	Au(δ-)	Cu^{2+}	Cu^{+}	Ag^{2+}	Ag^{+}	Ag(0)
OAPs modified with metals under deaerated conditions										
Content (%)	39.1	60.9	6.4	90.3	3.3	23.9	76.1	0	92.4	7.6
OAPs modified with metals under aerated conditions										
Content (%)	67.8	32.2	13.4	81.9	4.7	28.4	71.6	10.9	74.5	14.6

Copyright © 2018, Copyright Clearance Center, Inc.,
Creative Commons Attribution License (CC BY), All rights reserved

Photocatalytic activity of bare and modified OAP samples was tested for two reaction systems under UV/vis irradiation (anaerobic dehydrogenation of methanol and oxidative decomposition of acetic acid) and for oxidation of 2-propanol under visible light irradiation ($\lambda >$ 450 nm). Photoactivity tests for methanol dehydrogenation were carried out similarly to photodeposition of metals under deaerated conditions, but in smaller test tubes (as described in experimental part, Chapter IV), i.e., at first oxygen was removed from the system by argon bubbling. Since metallic deposits were already present on titania surface, almost no induction period was observed for Pt and Au, and shorter induction periods for Ag and Cu than during their deposition (**Figure 4.3**), as shown in **Figure 5.10**. It should be pointed that induction periods for Pt, Au and Ag were longer for samples prepared under aerated than deaerated conditions, i.e., 0.9, 1.9, 9.4 min, and 0.4, 0.7 and 7.5 min, respectively, suggesting that at first positive charge on metallic deposits should be neutralized and then proton could be reduced on the surface of zero-charged metal. Interestingly, the same induction periods were observed for Cu modified samples (ca. 5.6 min), which is not surprised since surface properties of both Cu/OAPs and Cu/OAPs/O_2 photocatalysts were almost the same (**Table 5.5**), where Cu existed mainly in the form of its oxides.

It was confirmed that bare titania was inactive for hydrogen evolution and the presence of

metallic co-catalyst was necessary. It is known that the rate of hydrogen evolution depends on kind of metallic co-catalyst and also on structural properties of titania. For example, it was reported that the highest activities were observed for large rutile and fine anatase samples after their modification with gold. Considering metallic deposits, Pt is the most active for hydrogen evolution, then Au, Cu and Ag. Similar results have already been reported for Au, Ag and Pt modified titania,[68, 112] and Au, Cu and Ag modified titania.[113] It has been proposed that the lowest activity of silver modified titania originated from its smallest work function, since the greater the difference between the metal work function and that of titania is, the higher is the electronic potential barrier (the Schottky barrier) generated by the band alignment at the metal-semiconductor heterojunction. The higher the Schottky barrier is, the higher is the transfer and trapping of photogenerated electron by metal,[114] and thus the higher is hydrogen generation rate. Therefore, the work function of Ag, Cu, Au, Pt and titania of 4.26, 4.7, 5.1, 6.35 eV and 4.0 eV,[115] respectively, correlated with their efficiency for hydrogen generation. Moreover, activation overpotential for hydrogen evolution on the surface of co-catalyst should be also considered. Indeed, the values of overpotential correlate with resultant activities, where smallest values of -0.05 V are for Pt, then -0.24 V for Au, and the largest for less active metals, i.e., -0.48 V for Ag and Cu. It must be reminded that Cu is mainly present in oxides form, and therefore overpotential for hydrogen evolution on Cu_2O and CuO should be considered. The co-catalytic function of CuO (electron scavenging, similar to zero-valent noble metals) has already been reported for CuO/WO_3 photocatalysts, where multiple-electron reaction on CuO was proposed.[116] In addition, the participation of Cu oxides (CuO and Cu_2O) in hydrogen evolution should be also considered since activity of these semiconductors has already been reported for ethanol dehydrogenation.[117]

Interestingly, all rates of hydrogen evolution for photocatalysts prepared under aerated

conditions are slightly lower than that under deaerated conditions (**Figures 5.11**). It is proposed that the presence of adsorbed oxygen (hydroxyl groups, **Figure 5.10**) on both titania and metallic deposits hindered methanol and proton adsorption, and thus their reactions with photogenerated holes and electrons, respectively.

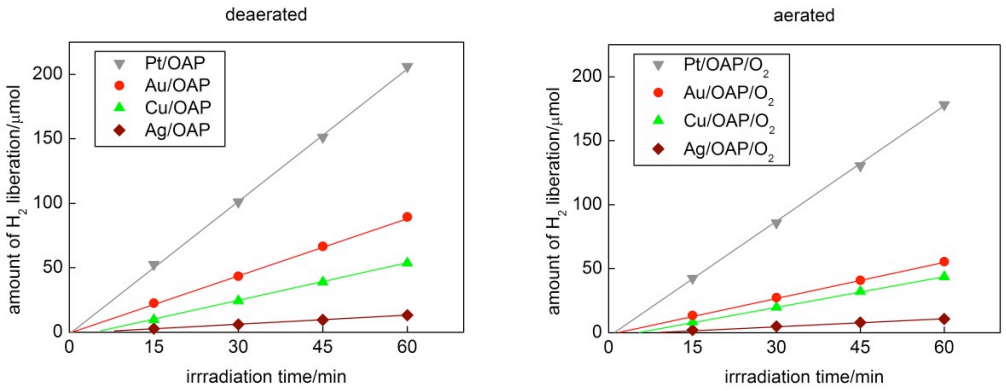


Figure 5.11. Anaerobic UV/vis dehydrogenation of methanol on OAPs modified with metals under (left) anaerobic and (right) aerobic conditions.

Copyright © 2018, Copyright Clearance Center, Inc., Creative Commons Attribution License (CC BY), All rights reserved

The photocatalytic activities of bare and modified OAPs in another reaction system, oxidative decomposition of acetic acid, is shown in **Figure 5.12**. It is clear that OAPs modification with noble metals resulted in significant enhancement of photocatalytic activity. Interestingly, enhancement in activity did not correlate with work function of metals, suggesting that not only the formation of Schottky barrier, but also other properties were crucial. Previous study indicated that the content of surface hydroxyl groups influenced the photocatalytic activity, as a source of reactive oxygen species (ROS).[118, 119] Therefore, the highest photocatalytic activity of Cu/OAPs correlated well with the largest amount of hydroxyl groups on its surface. It must be pointed that in contradiction to methanol dehydrogenation, decomposition of acetic acid was performed in aerobic conditions, and thus it is highly probable that less noble metals (Ag and Cu) existed mainly in their oxides forms. Therefore, it is proposed that heterojunction

between two/three oxides, i.e., titania and CuO/Cu_2O and titania and Ag_2O/AgO could result in inhibition of recombination of charge carriers, as has already been reported for this kind of coupled semiconductors.[102, 103, 120, 121]

Interestingly, samples prepared under aerated conditions possessed much higher photocatalytic activity than those prepared under deaerated conditions, and correlation between enhancements of photocatalytic activities after metal deposition by both preparation methods was linear. It is proposed that surface enrichment with oxygen and hydroxyl groups, and thus more efficient generation of ROS is responsible for high photocatalytic activity of samples prepared under aerobic conditions, as has recently been proposed for titania modified with rare earth elements.[118]

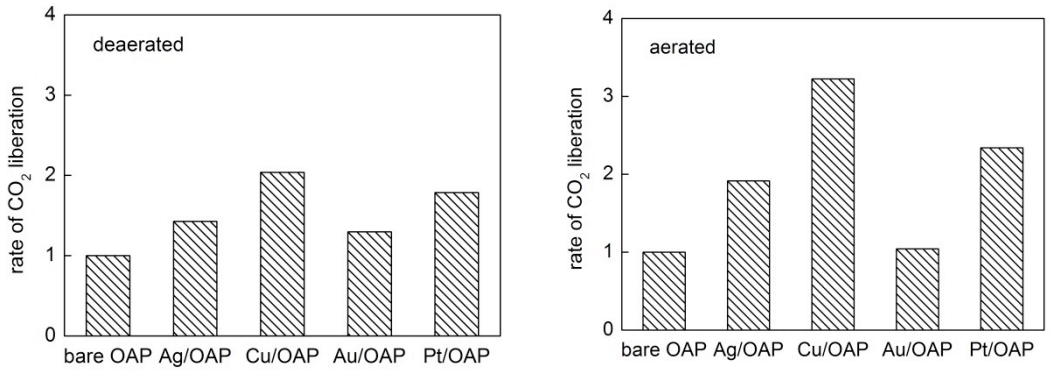


Figure 5.12. Aerobic UV/vis decomposition of acetic acid on OAPs modified with metals under (left) anaerobic and (right) aerobic conditions.

Copyright © 2018, Copyright Clearance Center, Inc., Creative Commons Attribution License (CC BY), All rights reserved

All modified photocatalysts showed activity under visible light irradiation and inactivity in the dark with the exception of Pt/OAP. Pt/OAP showed extremely high activity (ca. 2 orders higher than that of Au/OAP), mainly, due to its "dark" catalytic activity (> 90% activity). The dark activity of Pt/OAP is very interesting matter for further detailed study, but is not included in this thesis (not to make discussion too complex and confusing). Therefore, only

photocatalytic activities of bare OAP and modified with Au, Cu and Ag are presented in **Figure 5.13**. The visible activity of titania modified with Au and Ag (due to activation of their plasmon resonance (LSPR)) is well known and at present under extensive study. It was proposed that light absorption at broader wavelengths (wide LSPR) resulted in enhanced photocatalytic activity since more photons (of different energy) could be absorbed, and then efficiently participated in overall photocatalytic activity.[80] Therefore, change of deposition conditions (from anaerobic to aerobic) resulting in enhanced photocatalytic activity of Ag/OAP and lower activity of Au/OAP correlates well with photoabsorption properties, i.e., broader LSPR for Ag/TiO_2 and lower scattering for Au/TiO_2. Much lower photocatalytic activity of Ag/OAP than Au/OAP could be caused by applied experimental conditions, i.e., irradiation with wavelengths longer than 450 nm (to ensure inactivity of bare titania) and thus cutting of large part of LSPR of Ag.

The visible activity of Cu/OAP should result from excitation of Cu oxides possessing much narrower band-gap than titania (2.0-2.2 eV for Cu_2O and 1.3-1.6 eV of CuO)[122], due to lack of characteristics of zero-valent Cu (LSPR at ca. 560 nm and Cu(0) by XPS). It was also proposed that electrons in the valence band of titania could be excited to Cu^{II} species through interfacial charge transfer (IFCT) process.[123] The photocatalytic activity under visible light irradiation of single Cu oxides (CuO and Cu_2O),[117] hybrid CuO-Cu_2O arrays,[122] and coupled Cu oxides with other semiconductors (Cu_xO/TiO_2,[123, 124] CuO/TiO_2[102]) has already been reported for hydrogen evolution and oxidation of organic compounds. The lower photocatalytic activity of $Cu/OAP/O_2$ prepared under aerated conditions could result from slight different content of Cu_2O and CuO in these samples, which could influence the transfer of excited electron from Cu_2O to CuO/TiO_2.[103, 122] It is also probable that different composition of Cu/OAP sample prepared under deaerated conditions (green color, due to $[Cu(OH)]_2CO_3$ or CuO_2 incorporated in surface layer of OAP)

could be responsible for this visible activity. Further research on this matter is presently under study.

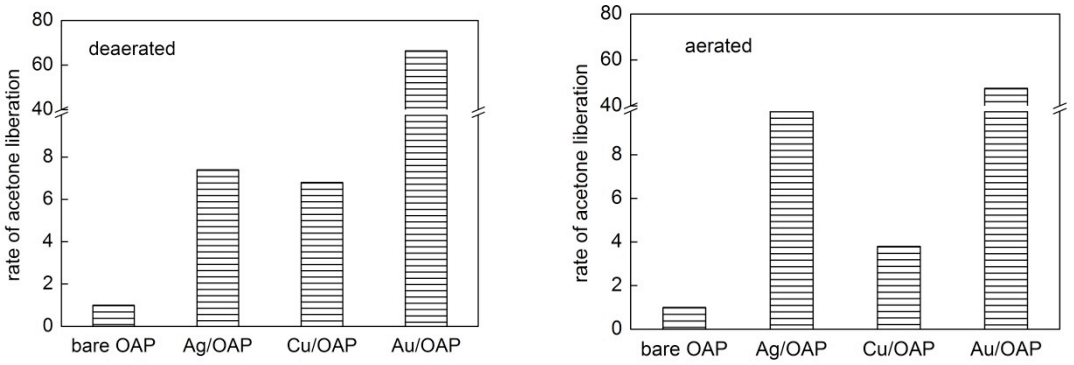


Figure 5.13. Aerobic vis oxidation of 2-propanol on OAP modified with metals under (left) anaerobic and (right) aerobic conditions.

Copyright © 2018, Copyright Clearance Center, Inc., Creative Commons Attribution License (CC BY), All rights reserved

Antibacterial (against *E coli*) properties of bare OAP samples, prepared by various durations of hydrothermal reaction (3-24 h) was tested in the dark and under irradiation with UV/vis (λ > 350 nm), and obtained data are shown in **Figure 5.14** (top). For comparison activities of those samples for acetic acid decomposition and dehydrogenation of methanol (in the presence of *in-situ* deposited Pt) under UV/vis are also shown in the bottom part of **Figure 5.14**. It is clear that bare OAP samples do not have significant activity in the dark, while under irradiation an anatase is activated by UV irradiation and formed ROS are responsible for bacteria inactivation, as has already been reported for other titania samples [47]. The SEM images of healthy and destroyed bacteria cells before and after 1-h irradiation in the presence of OAP prepared for 6-h HT are shown in **Figure 5.15.**

Under UV/vis the antibacterial activity of titania is directly correlated with its structural properties, which is confirmed by similar tendency in two other systems (**Figure 5.14**, bottom). The lowest activities in all tested reaction systems showed OAPs samples prepared for

shortest time of HT, which is not surprising as this sample contained larger content of unreacted TNW. With increase in HT duration, completion of HT increased, which resulted in the highest activity of samples prepared for 24 h. It should be pointed that for HT process the optimal conditions, resulting in high crystallinity and sufficient surface area of samples, are obtained for various temperatures and durations of HT depending on precursor properties. [3]it is clear that the best properties of OAPs are obtained for samples prepared for 12 and 24-h HT (the same activities for methanol dehydrogenation and acetic acid decomposition). However, antibacterial properties of these two samples differed and the best activity was obtained for samples prepared at the longest duration of HT. The crystallite sizes of these two samples did not differ significantly, but aspect ratio of 24hOAP sample was smaller than 12hOAP sample. Therefore, it can suggest that the presence of additional (001) facet could be beneficial for bacteria inactivation, which is reasonable due to different distribution of charges on (101) and (001) facets. This hypothesis will be investigated in detail in my future study, i.e., the influence of facet content on antibacterial properties.

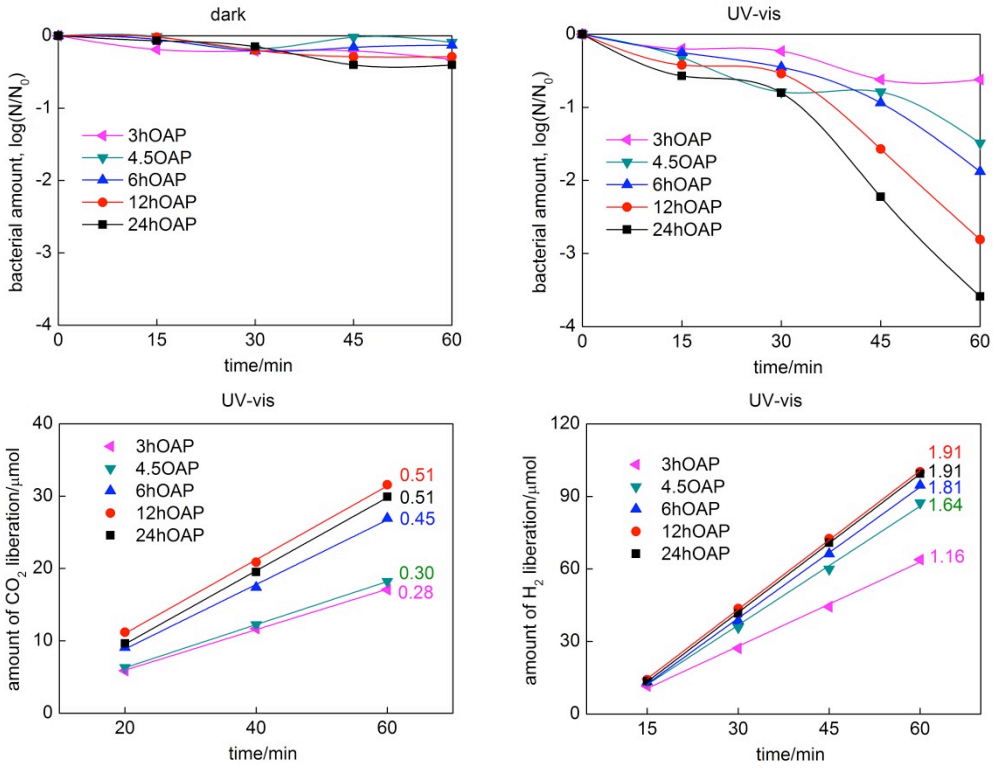


Figure 5.14. Activity of bare OAP samples prepared at various durations of hydrothermal (HT) reaction, for: (top) *E. coli* (left) in the dark and (right) under UV/vis irradiation (Y35 filter), (bottom, left) acetic acid under UV/vis and (bottom, right) methanol under UV/vis (2 wt% of Pt *in-situ* deposited).

Copyright © 2018, Copyright Clearance Center, Inc., Creative Commons Attribution License (CC BY), All rights reserved

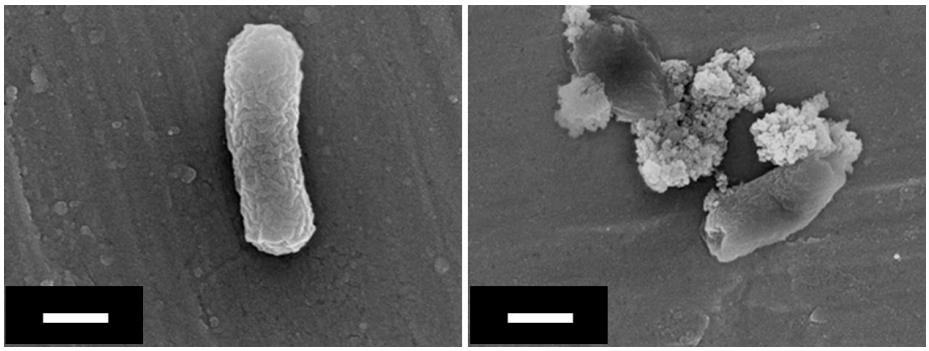


Figure 5.15. SEM images of *E. coli* (left) before and (right) after 1 h of UV/vis irradiation in the presence of OAP. Scale bars: 500 nm.

Copyright © 2018, Copyright Clearance Center, Inc., Creative Commons Attribution License (CC BY), All rights reserved

The antibacterial activities of OAP samples modified with noble metals (modification under deaerated conditions) in the dark and under irradiation with UV and/or vis are shown in **Figure. 5.16** (top). In the dark, only Ag/OAP showed antibacterial properties, which is not surprising due to excellent antimicrobial properties of Ag known since ancient times.[125, 126] Various studies have been performed to explain the mechanism of silver action, e.g., it is proposed that especially in the case of Gram-negative bacteria (e.g., *E. coli*), Ag NPs could adsorb and accumulate on outer membrane, creating the gaps in the integrity of the bilayer, which results in permeability increase and finally in bacteria cell death.[127] It has been proposed that smaller size of NPs and positive zeta potential promote interactions allowing penetration of NPs in bacteria membranes. In addition, the release of Ag cations from Ag NPs in water or during penetration of NPs into cells has been suggested.[128] Although NPs have higher antibacterial activity than the free ions of Ag, the overall antibacterial properties are attributed to both the physical properties of NPs and the elution of Ag cations.[126]

Under UV/vis irradiation only OAP modified with Cu showed significant enhancement of antibacterial properties. Antibacterial properties of Cu modified titania has recently been reported, and different mechanisms have been proposed. For example, the damage of the outer cell by generated ROS on irradiated titania with simultaneous Cu ions infiltration across the cell membrane was reported.[129, 130] In contradiction, Qiu et al. reported inactivity of free Cu ions (Cu^{+} and Cu^{2+}) and claimed that only titania modified with solid-state Cu_xO nanoclusters (possessing Cu^{I}) showed enhanced activity in the dark and under irradiation with visible light.[123] The ratio of Cu^{I} to Cu^{II} in Cu_xO nanoclusters of 1.3 was proposed as an optimal for the best antibacterial properties. Therefore, to check how Cu properties influence antibacterial properties Cu/OAP/O_2 (prepared under aerated conditions) was also tested, and data are shown in **Figure 5.16** (bottom, left). Interestingly, this sample possessed also

antibacterial properties in the dark, and two orders higher activity under UV/vis irradiation, which probably resulted from larger content of Cu^{I} in this sample (**Table 5.5**). The further study on the influence of properties of Cu deposits on antibacterial properties are presently under investigation. It is also possible that similar to bare OAP samples prepared for various HT durations, where antibacterial properties correlate with their activity for oxidation of acetic acid (**Figure 5.14**), more efficient separation of charge carriers, and thus generation of ROS is responsible for the best activity of Cu modified OAPs.

In contradiction to Qiu study, Cu/OAP did not show antibacterial activity under visible light irradiation, where only Ag modified samples could inactivate bacteria. It should be reminded that dark activity of Ag NPs participated in resultant activity under visible light irradiation. However, activity under visible light was two orders higher than in the dark. It is proposed that under visible light irradiation, Ag oxidation and release of Ag cations occurs (under LSPR, an electron transfer from silver to CB of titania). Therefore, free Ag cations could penetrate membrane cells resulting in bacteria killing. Antibacterial tests for Ag sample prepared under aerated conditions ($Ag/OAP/O_2$) were also performed and data are shown in **Figure 5.16** (bottom, right). Interestingly, the shape of curves in the dark and under irradiation for $Ag/OAP/O_2$ was different than for Ag/OAP sample. $Ag/OAP/O_2$ sample was almost inactive during first hour of irradiation and then after 2 h of irradiation an acceleration of activity was observed. There are two possibilities for such behavior: (1) type of bacteria, and (2) properties of photocatalyst. Benabbou et al.[131] and Bui et al.[132] suggested that bacteria inactivation proceeded in several steps, due to complex structure of outer liposaccharide (LPS) membrane, which was not easy to be oxidized even by photocatalytic process. However, in the present case, properties of photocatalyst seems more crucial as activities of both Ag modified samples differed significantly. It is proposed that during first 2 h of irradiation an active form of

photocatalyst was formed. However, at present it is difficult to evaluate either more efficient release of Ag or better photoabsorption properties (broader LSPR) of this sample are responsible for enhanced inactivation of bacteria.

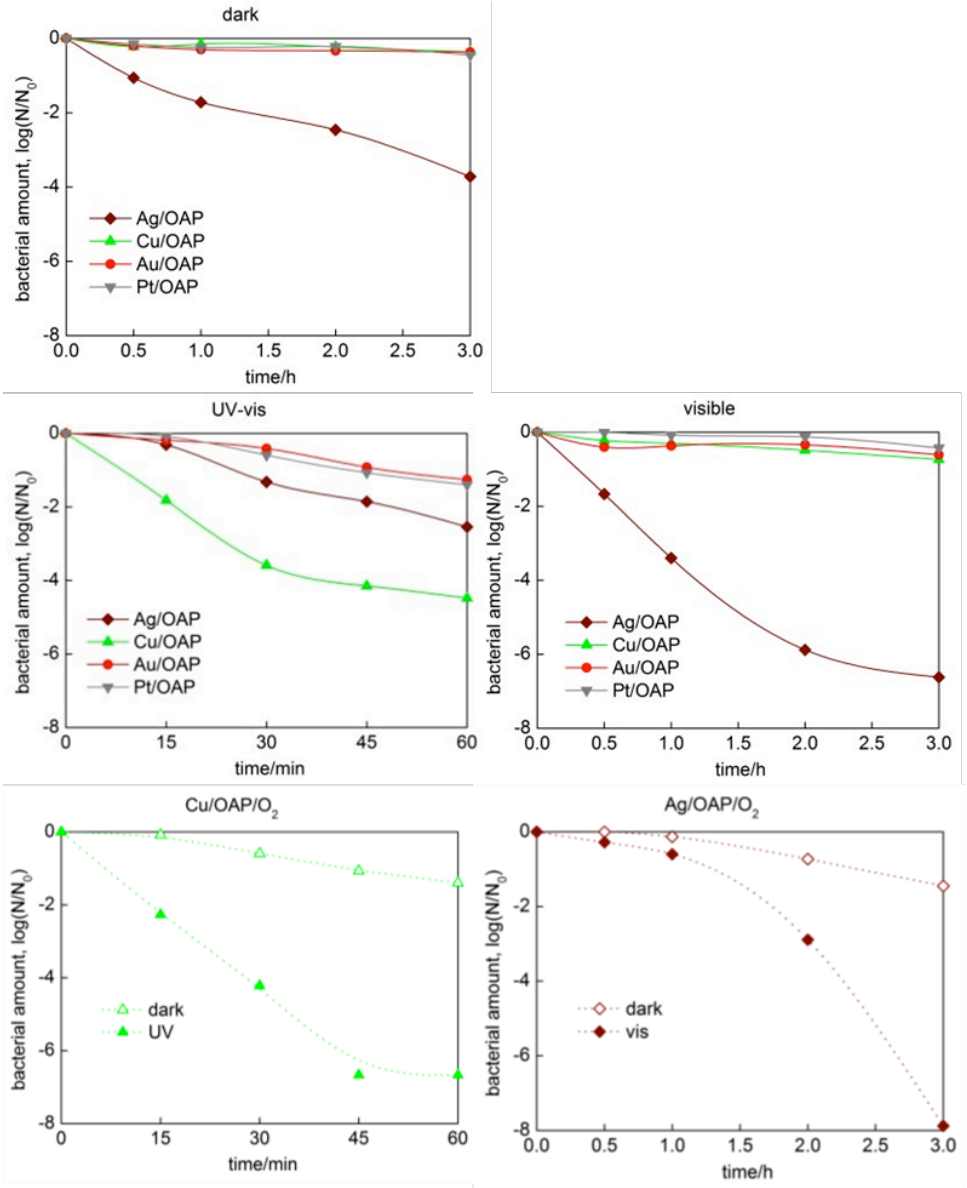


Figure 5.16. Antibacterial activity of OAPs modified with metals: (top-middle) under anaerobic conditions: (top) in the dark, (middle, left) under UV/vis ($\lambda > 350$ nm), (middle, right) under vis ($\lambda > 450$ nm); (bottom) under aerated conditions: (left) Cu/OAPs/O_2 in the dark and under UV/vis ($\lambda > 350$ nm), (right) Ag/OAPs/O_2 in the dark and under vis ($\lambda > 450$ nm).

Copyright © 2018, Copyright Clearance Center, Inc., Creative Commons Attribution License (CC BY), All rights reserved

Antifungal properties in the dark and under visible irradiation was investigated and obtained data are shown in **Figure 5.17**. Similar to antibacterial properties, only Ag/OAPs showed antifungal activities in the dark and under irradiation. These results were quite surprising for me since the preliminary study for commercial titania samples indicated higher antifungal properties of Au than Ag modified sample under visible light irradiation. It is known that properties of metals differed significantly when deposited on various titania supports,[80] and therefore different antimicrobial properties are obtained for different supports of metals. Interestingly, Ag/OAP/O_2, which showed the highest antibacterial properties under visible light irradiation (**Figure 5.16**, bottom, right) was practically inactive against fungi. It is highly possible that different mechanism is responsible for inactivation of fungi and bacteria, and therefore larger sizes and different shapes of Ag NPs prepared under aerated conditions are not harmful for fungi. It is also probable that longer irradiation time should be applied to activate photocatalyst than in the case of bacteria suspension. Further study on explanation of mechanism and clarification of recommended properties are presently under study.

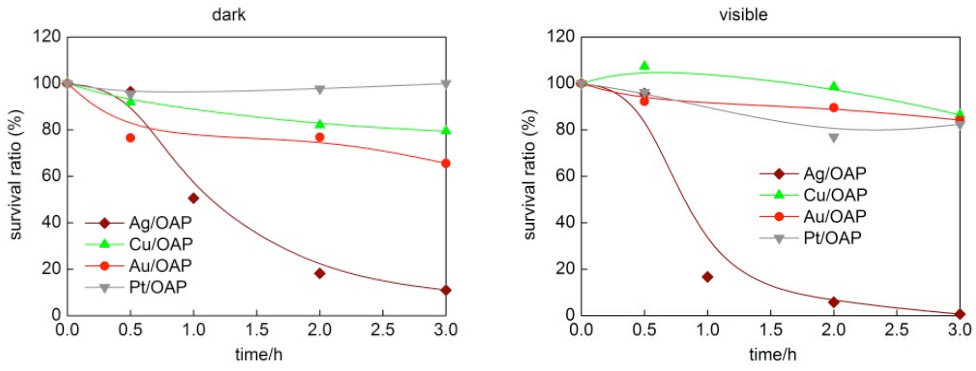


Figure 5.17. Antifungal (against *C. albicans*) activity of OAP modified with NMs under anaerobic conditions: (left) in the dark and (right) under vis (λ > 450 nm).

Copyright © 2018, Copyright Clearance Center, Inc., Creative Commons Attribution License (CC BY), All rights reserved

5.4. Summary

It was found that titania photocatalysts could be efficiently used as antifungal agent for various strains of fungi. Its activity was confirmed under irradiation and in the dark. It was shown that properties of titania were crucial for antifungal action. Though polymorphic forms of titania (anatase and rutile), isolated from commercial P25 photocatalyst, had similar surface properties (crystalline size), their activity highly differed, possibly due to slight difference in band-gap energy and thus ability of photoabsorption of more photons by rutile phase. In addition, it was shown that purification of isolated phases could result in slight change of their surface properties, i.e., particle aggregation, removal and/or adsorption of chemical species, which resulted in significant change in their antifungal properties. It must be pointed that also differences in fungal structure influenced resultant antifungal properties, and thus for example growth of strains of *P. boydii* (ZUT25) and *A. versicolor* (ZUT13) was highly inhibited by titania and light, but growth of ZUTST was stimulated by titania presence. It is important to remind that different fungi had different demand for water and nutrient, and thus adsorbed water and some impurities (e.g., F^-, Na^+, HOO^-) on titania surface could either inhibit or stimulate their growth. Another important finding is that even when mycelium growth was similar, the sporulation and mycotoxin generation was highly inhibited by light and titania presence.

Modification of titania with noble metals resulted in high enhancement of photocatalytic and antimicrobial activities. It was found that kind of metal and preparation method significantly influenced resultant properties and thus activities of photocatalysts. Surface of photocatalysts prepared under aerobic conditions were enriched with oxygen and thus their photocatalytic activity for oxidative decomposition of acetic acid was much higher than that prepared under anaerobic conditions. Oxidation states of Pt and Au (mainly

zero-charged) did not differed significantly by preparation method, and only surface of photocatalyst was enriched with hydroxyl groups. Whereas, the surface of less noble metals was mainly positively charged, especially Cu, although deposited as zero-valent (violet color), was fast oxidized under ambient environment. In contrast, silver existed in both metallic (brown color of LSPR) and oxides forms.

Antibacterial properties of bare titania under UV/vis correlated with their photocatalytic activities for decomposition of acetic acid and dehydrogenation of methanol, suggesting that properties of photocatalyst are crucial, i.e., low recombination of charge carriers on faceted anatase nanoparticles (OAP) of preferential distribution of shallow than deep electron traps. Enhanced antimicrobial properties of Ag/OAP under vis irradiation in comparison to dark activity indicated that plasmon resonance of Ag was responsible for Ag/OAP activation. The highest antibacterial activity of Cu/OAP under UV/vis irradiation correlated with the highest activity for acetic acid decomposition under UV/vis, suggesting prolongation of charge carriers by possible heterojunction mechanism between two semiconductors, i.e., Cu_xO/TiO_2. Further study on explanation of mechanism and clarification of the best properties of photocatalysts are presently under investigation for possible application of metal modified titania for environmental purification.

5.5 References

1. Hoffmann, M. R.; Martin, S. T.; Choi, W. Y.; Bahnemann, D. W., *Chem Rev* **1995,** *95* (1), 69-96.
2. Zhang, J. F.; Smith, K. R., *British Medical Bulletin* **2003,** *68*, 209-225.
3. Ammann, H. M., M*Mycotoxin Research* **2005,** *21* (3), 157-163.
4. Landrigan, P. J.; Schechter, C. B.; Lipton, J. M.; Fahs, M. C.; Schwartz, J., *Environmental Health Perspectives* **2002,** *110* (7), 721-728.
5. Chung, K. F.; Pavord, I. D., *Lancet* **2008,** *371* (9621), 1364-1374.
6. Millman, A.; Tang, D. L.; Perera, F. P., *Pediatrics* **2008,** *122* (3), 620-628.
7. Thomas, V. G.; Guitart, R., *Environmental Policy and Governance* **2010,** *20* (1), 57-72.
8. van Grinsven, H. J. M.; ten Berge, H. F. M.; Dalgaard, T.; Fraters, B.; Durand, P.; Hart, A.; Hofman, G.; Jacobsen, B. H.; Lalor, S. T. J.; Lesschen, J. P.; Osterburg, B.; Richards, K. G.; Techen, A. K.; Vertes, F.; Webb, J.; Willems, W. J., *Biogeosciences* **2012,** *9* (12), 5143-5160.
9. Beulke, S.; van Beinum, W.; Suddaby, L., *Integrated Environmental Assessment and Management* **2015,** *11* (2), 276-286.
10. Hyvarinen, A.; Meklin, T.; Vepsalainen, A.; Nevalainen, A., *International Biodeterioration & Biodegradation* **2002,** *49* (1), 27-37.
11. Wheatley, R. E., *Antonie Van Leeuwenhoek International Journal of General and Molecular Microbiology* **2002,** *81* (1-4), 357-364.
12. Artursson, V.; Finlay, R. D.; Jansson, J. K., *Environmental Microbiology* **2006,** *8* (1), 1-10.
13. Hogan, D. A.; Vik, A.; Kolter, R., *Molecular Microbiology* **2004,** *54* (5), 1212-1223.
14. Boonchan, S.; Britz, M. L.; Stanley, G. A., *Applied and Environmental Microbiology* **2000,** *66* (3), 1007-1019.
15. Corvini, P. F. X.; Schaffer, A.; Schlosser, D., *Applied Microbiology and Biotechnology* **2006,** *72* (2), 223-243.
16. Congeevaram, S.; Dhanarani, S.; Park, J.; Dexilin, M.; Thamaraiselvi, K., *J Hazard Mater* **2007,** *146* (1-2), 270-277.
17. Arslan, I.; Balcioglu, I. A.; Tuhkanen, T., *Environmental Technology* **1999,** *20* (9), 921-931.
18. Kowalska, E.; Janczarek, M.; Hupka, J.; Grynkiewicz, M., *Water Science and Technology* **2004,** *49* (4), 261-266.
19. Barbeni, M.; Minero, C.; Pelizzetti, E.; Borgarello, E.; Serpone, N., *Chemosphere* **1987,** *16*, 2225-2237.
20. Artuna, E.; Hupka, J., H*Cent Eur J Public Health* **2000,** *8 Suppl*, 88-89.
21. Mozia, S.; Tomaszewska, M.; Morawski, A. W., *Desalination* **2006,** *190* (1-3), 308-314.

22. King, C. H.; Shotts, E. B., Jr.; Wooley, R. E.; Porter, K. G., *Applied and Environmental Microbiology* **1988,** *54* (12), 3023-33.

23. Mokrini, A.; Ousse, D.; Esplugas, E., *Water Science and Technology* **1997,** *35* (4), 95-102.

24. Tomova, D.; Iliev, V.; Rakovsky, S.; Anachkov, M.; Eliyas, A.; Puma, G. L., *J Photoch Photobio A* **2012,** *231* (1), 1-8.

25. Bahnemann, D.; Cunningham, J.; Fox, M. A.; Pelizzetti, E.; Pichat, P.; Serpone, N., *Aquatic and Surface Photochemistry* **1994**, 261-316.

26. Duffy, J. E.; Anderson, M. A.; Hill, C. G., Jr.; Zeltner, W. A., *Ind Eng Chem Res* **2000,** *39* (10), 3698-3706.

27. Sanchez-Oneto, J.; Mancini, F.; Portela, J. R.; Nebot, E.; Cansell, F.; de la Ossa, E. J. M., *Chem Eng J* **2008,** *144* (3), 361-367.

28. Legrini, O.; Oliveros, E.; Braun, A. M., *Chemical Reviews (Washington, DC, United States)* **1993,** *93* (2), 671-98.

29. Malato, S.; Blanco, J.; Richter, C.; Curco, D.; Gimenez, J., *Water Science and Technology* **1997,** *35* (4, Oxidation Technologies for Water and Wastewater Treatment), 157-164.

30. Nakata, K.; Fujishima, A., *J Photoch Photobio C* **2012,** *13* (3), 169-189.

31. Hashimoto, K.; Irie, H.; Fujishima, A., *Japanese Journal of Applied Physics Part 1-Regular Papers Brief Communications & Review Papers* **2005,** *44* (12), 8269-8285.

32. Ohtani, B., *Phys Chem Chem Phys* **2014,** *16* (5), 1788-1797.

33. Hay, S. O.; Obee, T.; Luo, Z.; Jiang, T.; Meng, Y. T.; He, J. K.; Murphy, S. C.; Suib, S., *Molecules* **2015,** *20* (1), 1319-1356.

34. Pichat, P., *J Adv Oxid Technol* **2010,** *13* (3), 238-246.

35. Pottier, A.; Chaneac, C.; Tronc, E.; Mazerolles, L.; Jolivet, J. P., *J Mater Chem* **2001,** *11* (4), 1116-1121.

36. Fujishima, A.; Zhang, X. T.; Tryk, D. A., *Surface Science Reports* **2008,** *63* (12), 515-582.

37. Zubkov, T.; Stahl, D.; Thompson, T. L.; Panayotov, D.; Diwald, O.; Yates, J. T., Jr., *J. Phys. Chem. B* **2005,** *109* (32), 15454-15462.

38. Takeuchi, M.; Sakamoto, K.; Martra, G.; Coluccia, S.; Anpo, M., *J. Phys. Chem. B* **2005,** *109* (32), 15422-15428.

39. Allen, N. S.; Edge, M.; Sandoval, G.; Verran, J.; Stratton, J.; Maltby, J., *Photochem Photobiol* **2005,** *81* (2), 279-290.

40. Folli, A.; Pade, C.; Hansen, T. B.; De Marco, T.; Macphee, D. E., *Cement and Concrete Research* **2012,** *42* (3), 539-548.

41. Matsunaga, T.; Tomoda, R.; Nakajima, T.; Wake, H., *FEMS Microbiology Letters* **1985,** *29* (1-2), 211-214.

42. Guillard, C.; Bui, T. H.; Felix, C.; Moules, V.; Lina, B.; Lejeune, P., *Comptes Rendus*

Chimie **2008,** *11* (1-2), 107-113.

43. Zhao, J.; Yang, X. D., *Building and Environment* **2003,** *38* (5), 645-654.

44. Markowska-Szczupak, A.; Ulfig, K.; Morawski, W. A., *Catal Today* **2011,** *161* (9), 249-257.

45. Bekbolet, M.; Araz, C. V., *Chemosphere* **1996,** *32* (5), 959-65.

46. Byrne, J. A.; Dunlop, P. S. M.; Hamilton, J. W. J.; *Molecules* **2015,** *20* (4), 5574-5615.

47. Mitoraj, D.; Janczyk, A.; Strus, M.; Kisch, H.; Stochel, G.; Heczko, P. B.; Macyk, W., *Photochemical & Photobiological Sciences* **2007,** *6* (6), 642-648.

48. Foster, H. A.; Ditta, I. B.; Varghese, S.; Steele, A., *Applied Microbiology and Biotechnology* **2011,** *90* (6), 1847-1868.

49. Rincon, A. G.; Pulgarin, C., *Applied Catalysis, B: Environmental* **2003,** *44* (3), 263-284.

50. Maneerat, C.; Hayata, Y., *International Journal of Food Microbiology* **2006,** *107* (2), 99-103.

51. Chen, F. N.; Yang, X. D.; Wu, Q., *Building and Environment* **2009,** *44* (5), 1088-1093.

52. Thabet, S.; Weiss-Gayet, M.; Dappozze, F.; Cotton, P.; Guillard, C., *Appl Catal B-Environ* **2013,** *140*, 169-178.

53. Thabet, S.; Simonet, F.; Lemaire, M.; Guillard, C.; Cotton, P., *Applied and Environmental Microbiology* **2014,** *80* (24), 7527-7535.

54. Markowska-Szczupak, A.; Janda, K.; Wang, K.; Morawski, W. A.; Kowalska, E., *Cent. Eur. J. Public Health* **2015**, in press.

55. Neas, L. M.; Dockery, D. W.; Burge, H.; Koutrakis, P.; Speizer, F. E., *American Journal of Epidemiology* **1996,** *143* (8), 797-807.

56. Pelaez, M.; Nolan, N. T.; Pillai, S. C.; Seery, M. K.; Falaras, P.; Kontos, A. G.; Dunlop, P. S. M.; Hamilton, J. W. J.; Byrne, J. A.; O'Shea, K.; Entezari, M. H.; Dionysiou, D. D., *Appl Catal B-Environ* **2012,** *125*, 331-349.

57. Zaleska, A., *Recent Patents on Engineering* **2008,** *2*, 157-164.

58. Asahi, R.; Morikawa, T.; Ohwaki, T.; Aoki, K.; Taga, Y., V*Science* **2001,** *293* (5528), 269-271.

59. Mitoraj, D.; Kisch, H., *Angewandte Chemie International Edition* **2008,** *47* (51), 9975-9978.

60. Sakthivel, S.; Janczarek, M.; Kisch, H., *J. Phys. Chem. B* **2004,** *108* (50), 19384-19387.

61. Bledowski, M.; Wang, L. D.; Ramakrishnan, A.; Khavryuchenko, O. V.; Khavryuchenko, V. D.; Ricci, P. C.; Strunk, J.; Cremer, T.; Kolbeck, C.; Beranek, R., *Phys Chem Chem Phys* **2011,** *13* (48), 21511-21519.

62. Dozzi, M. V.; Selli, E., *J Photoch Photobio C* **2013,** *14*, 13-28.

63. Georgieva, J.; Sotiropoulos, S.; Armyanov, S.; Philippidis, N.; Poulios, I., *Journal of*

Applied Electrochemistry **2011,** *41* (2), 173-181.

64. Li, G. Y.; Nie, X.; Gao, Y. P.; An, T. C., *Appl Catal B-Environ* **2016,** *180*, 726-732.

65. Serpone, N.; Maruthamuthu, P.; Pichat, P.; Pelizzetti, E.; Hidaka, H., *Journal of Photochemistry and Photobiology, A: Chemistry* **1995,** *85* (3), 247-55.

66. Kowalska, E.; Remita, H.; Colbeau-Justin, C.; Hupka, J.; Belloni, J., *J. Phys. Chem. C* **2008,** *112* (4), 1124-1131.

67. Herrmann, J. M.; Disdier, J.; Pichat, P., *Chemical Physics Letters* **1984,** *108* (6), 618-622.

68. Sclafani, A.; Mozzanega, M. N.; Pichat, P., *Journal of Photochemistry and Photobiology, A: Chemistry* **1991,** *59* (2), 181-9.

69. Hai, Z. B.; El Kolli, N.; Uribe, D. B.; Beaunier, P.; Jose-Yacaman, M.; Vigneron, J.; Etcheberry, A.; Sorgues, S.; Colbeau-Justin, C.; Chena, J. F.; Remita, H., *J. Mater. Chem. A* **2013,** *1* (36), 10829-10835.

70. Ohtani, B.; Osaki, H.; Nishimoto, S.; Kagiya, T., *J Am Chem Soc* **1986,** *108* (2), 308-10.

71. Macyk, W.; Burgeth, G.; Kisch, H., *Photochemical & Photobiological Sciences* **2003,** *2* (3), 322-328.

72. Memming, R.; Schroeppel, F., *Chemical Physics Letters* **1979,** *62* (2), 207-10.

73. Pedraza-Avella, J. A.; Lopez, R.; Martinez-Ortega, F.; Paez-Mozo, E. A.; Gomez, R., *Journal of Nano Research* **2009,** *5*, 95-104.

74. Martin, M. V.; Villabrille, P. I.; Rosso, J. A., *Environ Sci Pollut R* **2015,** *22* (18), 14291-14298.

75. Qamar, M.; Merzougui, B.; Anjum, D.; Hakeem, A. S.; Yamani, Z. H.; Bahnemann, D., *Catal Today* **2014,** *230*, 158-165.

76. O'Regan, B.; Grätzel, M., *Nature* **1991,** *353*, 737.

77. Tian, Y.; Tatsuma, T., *J Am Chem Soc* **2005,** *127* (20), 7632-7637.

78. Ingram, D. B.; Linic, S., *J Am Chem Soc* **2011,** *133*, 5202-5205.

79. Cushing, S. K.; Li, J. T.; Meng, F. K.; Senty, T. R.; Suri, S.; Zhi, M. J.; Li, M.; Bristow, A. D.; Wu, N. Q., *J Am Chem Soc* **2012,** *134* (36), 15033-15041.

80. Kowalska, E.; Mahaney, O. O. P.; Abe, R.; Ohtani, B., *Phys. Chem. Chem. Phys.* **2010,** *12* (10), 2344-2355.

81. Priebe, J. B.; Radnik, J.; Lennox, A. J. J.; Pohl, M. M.; Karnahl, M.; Hollmann, D.; Grabow, K.; Bentrup, U.; Junge, H.; Beller, M.; Bruckner, A., *Acs Catal* **2015,** *5* (4), 2137-2148.

82. Chen, X.; Zhu, H.-Y.; Zhao, J.-C.; Zheng, Z.-F.; Gao, X.-P., *Angew. Chem. Int. Ed.* **2008** *47*, 5353-5356.

83. Kowalska, E.; Rau, S., *Recent Patents on Engineering* **2010,** *4* (3), 242-266.

84. Dantigny, P.; Guilmart, A.; Bensoussan, M., *International Journal of Food Microbiology* **2005,** *100* (1-3), 187-196.

85. Ohtani, B.; Azuma, Y.; Li, D.; Ihara, T.; Abe, R., *Trans. Mater. Res. Soc. Jpn.* **2007,** *32*, 401-404.

86. Ohno, T.; Sarukawa, K.; Matsumura, M., *J. Phys. Chem. B* **2001,** *105* (12), 2417-2420.

87. Zielińska-Jurek, A.; Kowalska, E.; Sobczak, J. W.; Lisowski, W.; Ohtani, B.; Zaleska, A., *Appl. Catal. B: Environ.* **2011,** *101* (3-4), 504-514.

88. Reszczynska, J.; Grzyb, T.; Sobczak, J. W.; Lisowski, W.; Gazda, M.; Ohtani, B.; Zaleska, A., *Appl Surf Sci* **2014,** *307*, 333-345.

89. Calvo, A. M.; Wilson, R. A.; Bok, J. W.; Keller, N. P., *Microbiology and Molecular Biology Reviews* **2002,** *66* (3), 447-459.

90. Paz, Y.; Heller, A., *Journal of Materials Research* **1997,** *12* (10), 2759-2766.

91. Kurtoglu, M. E.; Longenbach, T.; Gogotsi, Y., *International Journal of Applied Glass Science* **2011,** *2* (2), 108-116.

92. Fujishima, A.; Rao, T. N., *Proceedings - Indian Academy of Sciences, Chemical Sciences* **1997,** *109* (6), 471-486.

93. Boumaaza, B.; Benkhelifa, M.; Belkhoudja, M., *International Journal of Microbiology* **2015,** *2015*, Article ID 57626.

94. Yang, G. D.; Jiang, Z.; Shi, H. H.; Jones, M. O.; Xiao, T. C.; Edwards, P. P.; Yan, Z. F., *Appl Catal B-Environ* **2010,** *96* (3-4), 458-465.

95. Hurum, D. C.; Gray, K. A.; Rajh, T.; Thurnauer, M. C., *J. Phys. Chem. B* **2005,** *109* (2), 977-980.

96. Zielinska-Jureka, A.; Wei, Z.; Wysocka, I.; Szweda, P.; Kowalska, E., *Appl Surf Sci* **2015,** *353*, 317-325.

97. Kowalska, E.; Wei, Z.; Karabiyik, B.; Herissan, A.; Janczarek, M.; Endo, M.; Markowska-Szczupak, A.; Remita, H.; Ohtani, B., *Catal Today* **2015,** *252*, 136-142.

98. Kowalska, E.; Abe, R.; Ohtani, B., *Chem Commun* **2009,** (2), 241-243.

99. Muniz-Miranda, M.; Gellini, C.; Simonelli, A.; Tiberi, M.; Giammanco, F.; Giorgetti, E., *Applied Physics a-Materials Science & Processing* **2013,** *110* (4), 829-833.

100. Kowalska, E.; Janczarek, M.; Rosa, L.; Juodkazi, S.; Ohtani, B., *Catal Today* **2014,** *230*, 131-137.

101. Kowalska, E.; Yoshiiri, K.; Wei, Z.; Zheng, S.; Kastl, E.; Remita, H.; Rau, S.; Ohtani, B., *Appl. Catal. B: Environ.* **2015,** *178*, 133-143.

102. Mendez-Medrano, M. G.; Kowalska, E.; Lehoux, A.; Herissan, A.; Ohtani, B.; Bahena, D.; Briois, V.; Colbeau-Justin, C.; Rodriguez-Lopez, J.; Remita, H., *The Journal of Physical Chemistry C* **2016,** *120*, 5143-5154.

103. Luna, A. L.; Valenzuela, M. A.; Colbeau-Justin, C.; Vazquez, P.; Rodriguez, J. L.; Avendano, J. R.; Alfaro, S.; Tirado, S.; Garduno, A.; De la Rosa, J. M., *Applied Catalysis*

a-General **2016,** *DOI: 10.1016/j.apcata.2015.10.044*.

104. Ito, T.; Yamaguchi, H.; Masumi, T.; Adachi, S., *Journal of the Physical Society of Japan* **1998,** *67* (9), 3304-3309.

105. Siuzdak, K.; Sawczak, M.; Klein, M.; Nowaczyk, G.; Jurga, S.; Cenian, *Phys Chem Chem Phys* **2014,** *16* (29), 15199-15206.

106. Jensen, H.; Soloviev, A.; Li, Z. S.; Sogaard, E. G., *Appl Surf Sci* **2005,** *246* (1-3), 239-249.

107. Yu, J. G.; Zhao, X. J.; Zhao, Q. N., *Thin Solid Films* **2000,** *379* (1-2), 7-14.

108. Nie, R. F.; Wang, J. H.; Wang, L. N.; Qin, Y.; Chen, P.; Hou, Z. Y., *Carbon* **2012,** *50* (2), 586-596.

109. Scott, J.; Irawaty, W.; Low, G.; Amal, R., *Appl Catal B-Environ* **2015,** *164*, 10-17.

110. Hwang, S.; Lee, M. C.; Choi, W., *Appl Catal B-Environ* **2003,** *46* (1), 49-63.

111. Yousef, A.; El-Halwany, M. M.; Barakat, N. A. M.; Al-Maghrabi, M. N.; Kim, H. Y., *J Ind Eng Chem* **2015,** *26*, 251-258.

112. Chiarello, G. L.; Aguirre, M. H.; Selli, E., *Journal of Catalysis* **2010,** *273*, 182-190.

113. Kowalska, E.; Wei, Z.; Karabiyik, B.; Janczarek, M.; Endo, M.; Wang, K.; Rokicka, P.; Markowska-Szczupak, A.; Ohtani, B., *Advanes in Science and Technology* **2014,** *93*, 174-183.

114. Linsebigler, A. L.; Lu, G.; Yates Jr., J. T., *Chem. Rev.* **1995,** *95*, 735-758.

115. Hope, G. A.; Bard, A. J., *J. Phys. Chem.* **1983,** *87*, 1979-1984.

116. Arai, T.; Horiguchi, M.; Yanagida, M.; Gunji, T.; Sugihara, H.; Sayama, K., Reaction *J Phys Chem C* **2009,** *113* (16), 6602-6609.

117. Barreca, D.; Fornasiero, P.; Gasparotto, A.; Gombac, V.; Maccato, C.; Montini, T.; Tondello, E., *Chemsuschem* **2009,** *2* (3), 230-233.

118. Reszczynska, J.; Grzyb, T.; Wei, Z. S.; Klein, M.; Kowalska, E.; Ohtani, B.; Zaleska-Medynska, A., *Appl Catal B-Environ* **2016,** *181*, 825-837.

119. Szczepankiewicz, S. H.; Colussi, A. J.; Hoffmann, M. R., *J. Phys. Chem. B* **2000,** *104* (42), 9842-9850.

120. Rtimi, S.; Baghriche, O.; Sanjines, R.; Pulgarin, C.; Bensimon, M.; Kiwi, J., *J Photoch Photobio A* **2013,** *256*, 52-63.

121. Rtimi, S.; Sanjines, R.; Pulgarin, C.; Houas, A.; Lavanchy, J. C.; Kiwi, J., *J Hazard Mater* **2013,** *260*, 860-868.

122. Ghadimkhani, G.; de Tacconi, N. R.; Chanmanee, W.; Janaky, C.; Rajeshwar, K., *Chem Commun* **2013,** *49* (13), 1297-1299.

123. Qiu, X. Q.; Miyauchi, M.; Sunada, K.; Minoshima, M.; Liu, M.; Lu, Y.; Li, D.; Shimodaira, Y.; Hosogi, Y.; Kuroda, Y.; Hashimoto, K., *Acs Nano* **2012,** *6* (2), 1609-1618.

124. Irie, H.; Kamiya, K.; Shibanuma, T.; Miura, S.; Tryk, D. A.; Yokoyama, T.; Hashimoto,

K., *J. Phys. Chem. C FIELD Full Journal Title:Journal of Physical Chemistry C* **2009,** *113* (24), 10761-10766.

125. Davies, R. L.; Etris, S. F., *Catal Today* **1997,** *36* (1), 107-114.

126. Franci, G.; Falanga, A.; Galdiero, S.; Palomba, L.; Rai, M.; Morelli, G.; Galdiero, M., *Molecules* **2015,** *20* (5), 8856-8874.

127. Rai, M.; Kon, K.; Ingle, A.; Duran, N.; Galdiero, S.; Galdiero, M., *Applied Microbiology and Biotechnology* **2014,** *98* (5), 1951-1961.

128. Choi, O.; Hu, Z. Q., *Environ Sci Technol* **2008,** *42* (12), 4583-4588.

129. Li, J. Y.; Dennehy, J. J., *Applied and Environmental Microbiology* **2011,** *77* (19), 6878-6883.

130. Rtimi, S.; Giannakis, S.; Sanjines, R.; Pulgarin, C.; *Appl Catal B-Environ* **2016,** *182*, 277-285.

131. Benabbou, A. K.; Derriche, Z.; Felix, C.; Lejeune, P.; Guillard, C., *Appl Catal B-Environ* **2007,** *76* (3-4), 257-263.

132. Bui, T. H.; Felix, C.; Pigeot-Remy, S.; Herrmann, J. M.; Lejeune, P.; Guillard, C., *J Adv Oxid Technol* **2008,** *11* (3), 510-518.

Chapter VI

Concluding remarks

6.1 Summary and conclusions

Although studies on titania photocatalysis has started more than a century ago, and habe been intensified during last four decades (after discovery of "Honda-Fujishima effect"), there are still many non-answered questions concerning the reason of high/low activity of some titania photocatalysts and the clarification of key-factors of high activity. It is known that similar to catalytic reactions in the dark, small crystallite sizes and large specific surface area are responsible for high photocatalytic activity. However, in the case of photocatalysis, photoabsorption properties and intrinsic properties of distribution of electron traps (governing electron migration and recombination with hole) are very crucial. Moreover, interactions between various phases in particular titania samples are also possible and could not be neglected. Therefore, one of the highest photocatalytic activities of titania P25 in various photocatalytic reactions (both oxidation and reduction), which could not be simply explained by its surface properties (large, but not the largest specific surface area; small, but not the smallest crystallite sizes; large, but not the largest crystallinity), has been often reported as a result of synergistic effect of co-existence of two crystal phases: anatase and rutile. Authors have suggested a charge transfer between two phases (usually electrons from anatase to rutile), which should cause retardation of charge carriers' recombination. However, in these reports, there have been either no direct proof for such transfer or crystalline phases were not obtained from original P25. Therefore, one can say there is no direct proof for this hypothesis of synergetic effect of anatase and rutile in mixed-phase titania resulting in enhancement of photocatalytic activity. The previous report from Ohtani laboratory confirmed this statement by checking the photocatalytic activities for four photocatalytic reactions (oxidative decomposition of acetic acid, oxidative decomposition of acetaldehyde in air, dehydrogenation of methanol, O_2 liberation from a deaerated solution of silver sulfate) of four titania samples: P25, anatase (isolated from P25), rutile (isolated from P25 and R-P25 (re-built P25 from two isolated phases). It was shown that intrinsic activities of anatase and rutile were responsible for high activity of P25, but not anatase-rutile heterojunction. However, in the case of methanol dehydrogenation, higher activity of P25 and R-P25 could

suggest the possibility of some synergetic effect between both crystalline phases. Therefore, in this thesis this system has been studied in detail. It should be pointed out that for hydrogen evolution, the presence of co-catalyst (here, platinum nanoparticles) is necessary, and thus the properties of Pt NPs should influence the overall photocatalytic activity. In addition, various studies on P25 did not consider high non-uniformity of this sample (even samples taken from the same box could very in composition) and the presence of amorphous phase (only anatase to rutile ratios were reported). To overcome this problem in this thesis, homogenization of P25 sample was performed, and all other studies were performed for uniform P25 sample to avoid the influence of heterogeneity on data interpretation (e.g., higher activity for acetic acid decomposition with higher content of anatase). Moreover, it should be also pointed out that isolation methods by chemical dissolution, used for separation of crystalline phases, have also some shortcomings, i.e., the possibilities of formation of some impurities (from chemical reagents) on the surface of isolated phases. Therefore, the efforts on non-chemical methods of phase separations, i.e., physical isolation by vibration and sonication, have been also carried out in this thesis. However, till now the chemical isolation has seemed to be the most efficient, and thus main data of this thesis are shown for this method. To avoid the influence of the impurities adsorbed on titania surface (from isolation process), post-treatment operations have been applied. It was found that alkali washing and calcination were efficient for removal of adsorbed species on titania surface.

The photocatalytic activity tests for the reaction system of methanol dehydrogenation for purified isolated phases clearly showed that rutile phase was responsible for high photocatalytic activity of P25. Therefore, it could be concluded that high activity of P25 was not caused by anatase-rutile heterojunctions, but due to intrinsic high activity of rutile phase, probably resulting from its better photoabsorption properties than that of anatase (narrower band-gap resulting in bathochromic shift of absorption edge). Action spectrum analyses indicate that rutile was platinized first, and its presence resulted in higher photocatalytic activity. The study on the influence of Pt-loading amount, resulting in maximum photocatalytic activity for much smaller content of platinum for isolated phases than that for

P25, suggested that post-treatment operations caused aggregation of titania particles, lowering the necessary amount of platinum deposits (one Pt deposit was sufficient on one particle/aggregate to enable photocatalytic reaction). Therefore, it was concluded that the interparticle electron transfer (IPET) between titania NPs inside one aggregate proceeded. This hypothesis was confirmed for P25 calcined sample at the same conditions as isolated phases resulting in lowering of necessary Pt-loading amount. This study is probably, the first confirmation of the IPET among the same particles (anatase or rutile), named here HOMO-IPET.

As mentioned before, the properties of platinum deposits are crucial for reaction of methanol dehydrogenation. Photodeposition method, used here, is very convenient and fast, and results in preferential electronic-contact between titania and Pt since photogenerated electrons directly reduce platinum cations on the surface of titania. However, it should be pointed out that photodeposition is very fast (in the case of platinum), and thus often aggregation of Pt deposits is observed, which could result in lowering of photocatalytic activities (one large Pt aggregate on one titania NP resulting in co-existence with some bare titania samples with poor activity). This was clearly shown in the study on Homo-P25 and other titania sample — faceted anatase particles (octahedral anatase particles, OAPs) with very high photocatalytic activity for oxidative decomposition of acetic acid and low activity for methanol dehydrogenation. It was found that slowing the photodeposition rate (by changing the photodeposition conditions, e.g., in the initial presence of O_2 in the system as an electron scavenger) resulted in preparation of non-aggregated Pt deposits. This method was also successfully applied for other noble-metals, such as gold, silver and copper resulting in preparation of noble metal-modified titania samples possessing various properties, and thus different photocatalytic and antimicrobial properties.

Obtained photocatalysts, i.e., HomoP25, isolated titania (anatase and rutile; without and with post-treatment at various conditions) and faceted anatase modified with noble metals were tested for various possible environmental applications, such as decomposition of organic compounds, evolution of hydrogen and inactivation of microorganism (bacteria and fungi).

Plasmonic photocatalysts (titania modified with NPs of noble metals) showed high photocatalytic activity for decomposition of both organic compounds and microorganisms at broad range of irradiation (UV and vis). Modification photodeposition method proved to be efficient way to prepare photocatalysts with various surface properties, and thus different resultant photocatalytic activity. Moreover, it was found that even bare titania could be efficiently used as antifungal agent for various strains of fungi. It was shown that properties of titania were crucial for antifungal action. Rutile showed higher antifungal properties under irradiation, possibly due to better photoabsorption properties, and thus ability of photoabsorption of more photons than anatase (similar to methanol dehydrogenation). In addition, it was shown that purification of isolated phases could result in slight change of their surface properties, i.e., particle aggregation, removal and/or adsorption of chemical species, which resulted in significant change in their antifungal properties. It should be mentioned that also differences in fungal structure influenced resultant antifungal properties, and thus for example growth of strains of *Pseudallescheria boydii* and *Aspergillus versicolor* was highly inhibited by titania and light, but growth of *Stachybotrys chartarum*, was stimulated by titania presence. It is important to remember that different fungi had different demand for water and nutrient, and thus adsorbed water and some impurities (e.g., F^-, Na^+, HOO^-) on titania surface could either inhibit or stimulate their growth. Another important finding is that even when mycelium growth was similar, the sporulation and mycotoxin generation was highly inhibited by light and titania presence.

6.2 Future aspects

Purified chemical isolation is efficient method for separation of crystalline phases, but original amorphous titania cannot be obtained. Moreover, chemical etching results in change of surface properties, such as particle aggregation. Although, particle aggregation allows me to find Homo-IPET effect, pure single titania phases (anatase, rutile and amorphous)—the same as that in P25, could not be prepared. Therefore, other methods should be developed, e.g., physical methods. Although, my study on sonication-enhanced vibration showed its inefficiency for phase separation, I have already started another method, e.g., light-assisted separation, which seems prospective. I would like to obtain original amorphous phase from P25 by this method, and then to prove that this phase (or IPCT between amorphous-anatase-rutile) is not responsible for exceptionally high activity of P25. Moreover, I do believe that this method could be used by others for phase separation.

Another aim of my future study is connected with titania platinization. I would like to prove that platinum is deposited preferentially on rutile by TEM observations and in the presence of other precursors of platinum. Moreover, I would like to clarify how loading amount influence this preferential deposition. Consequently, I wonder if this phenomenon is valid also for other mixed-phase titania photocatalysts (or only for P25) to prove/reject that preferential platinization could be caused by Hetero-IPET (electron transfer from anatase to rutile).

Moreover, there is still a lot of work to be done on titania photocatalytic application, i.e., to obtain efficient and cheap photocatalysts with broad range of use. Although, plasmonic photocatalysts are efficient, especially against microorganisms (due to photocatalysis and "dark" activity of noble metals), cheaper materials should be developed, e.g. F-modified titania (as unpurified rutile in my study) and self-doped titania (able to work under IR). There are also some unsolved issues for microbiological tests, e.g., one of the most important task is to develop quantitative and qualitative analyses of generated mycotoxin.

6.3 Published papers

PhD thesis:

1. Wang, K.; Wei, Z.; Ohtani, B.; Kowalska, E., Interparticle electron transfer in methanol dehydrogenation on platinum-loaded titania particles prepared from P25. *Catal. Today*, 303 (2018) 327-333.
2. Wei, Z.; Kowalska, E.; Wang, K.; Colbeau-Justin, C.; Ohtani, B., Enhanced photocatalytic activity of octahedral anatase particles prepared by hydrothermal reaction. *Catal. Today*, 280 (2017) 29-36.
3. Wei, Z.; Endo, M.; Wang, K.; Charbit, E.; Markowska-Szczupak, A.; Ohtani, B.; Kowalska, E., Noble metal-modified octahedral anatase titania particles with enhanced activity for decomposition of chemical and microbiological pollutants. *Chem. Eng. J.*, 318 (2017) 121-134.
4. Wei, Z. S.; Rosa, L.; Wang, K.; Endo, M.; Juodkazis, S.; Ohtani, B.; Kowalska, E., Size-controlled gold nanoparticles on octahedral anatase particles as efficient plasmonic photocatalyst. *Appl. Catal. B-Environ.* 206 (2017) 393-405.
5. Markowska-Szczupak, A.; Wang, K.; Rokicka, P.; Endo, M.; Wei, Z. S.; Ohtani, B.; Morawski, A. W.; Kowalska, E., The effect of anatase and rutile crystallites isolated from titania P25 photocatalyst on growth of selected mould fungi. *J. Photochem. Photobiol. B-Biol.*, 151 (2015) 54-62.

Other research:

6. Endo, M.; Wei, Z.; Wang, K.; Karabiyik, B.; Yoshiiri, K.; Rokicka, P.; Ohtani, B.; Markowska-Szczupak, A.; Kowalska, E., Noble metal-modified titania with visible light activity for decomposition of microorganisms, *Beilstein J. Nanotech*., in press.
7. Endo, M.; Janczarek, M.; Wei, Z.; Wang, K.; Markowska-Szczupak, A.; Ohtani, B.; Kowalska, E., Bactericidal Properties of Plasmonic Photocatalysts Composed of Noble-Metal Nanoparticles on Faceted Anatase Titania, *J. Nanosci. Nanotech.*, in press.
8. Zheng, S. Z.; Wang, K.; Wei, Z. S.; Yoshiiri, K.; Braumuller, M.; Rau, S.; Ohtani, B.; Kowalska, E., Mono- and Dual-modified Titania with a Ruthenium(II) Complex and Silver Nanoparticles for Photocatalytic Degradation of Organic Compounds. *J. Adv. Oxid. Technol.*, 19 (2016) 208-217.
9. Hirakawa, H.; Katayama, M.; Shiraishi, Y.; Sakamoto, H.; Wang, K.; Ohtani, B.; Ichikawa, S.; Tanaka, S.; Hirai, T., One-pot synthesis of imines from nitroaromatics and alcohols by tandem photocatalytic and catalytic reactions on Degussa (Evonik) P25 titanium dioxide. *ACS Appl Mater Interf.*, 7 (2015) 3797-806.
10. Markowska-Szczupak, A.; Janda, K.; Wang, K.; Morawski, A. W.; Kowalska, E., Effect of water activity and titania P25 photocatalyst on inactivation of pathogenic fungi-contribution to the protection of public health. *Cent. Europ. J. Public Health*, 23 (2015) 267-271.

Acknowledgement

I would never have been able to successfully finish this Ph.D thesis without the guidance of my supervisor, Professor Ewa Kowalska, also professor Bunsho Ohtani. And also help from my girlfriend as well as support from my family.

First of all, I would like to express my deepest gratitude to Prof. Ewa Kowalska for his extensive guidance on my research work: from the topic of this thesis, experiments, to the writing of this thesis. Her immense knowledge, rigorous attitude and tireless teaching greatly benefited me. I would like to thank her for the advice her provided on both research as well as life in general. Besides my supervisor, I would like to thank Bunsho Ohtani, professor of graduate school of environmental science at Hokkaido University, who often discuss with me on science thinking and gave me this great opportunity for studying in Japan since 2011. In addition, I am grateful to all professors from graduate school of environmental science at Hokkaido University, for their help on scientific research study. Last but not least, a special thanks to my parents and my girlfriend for supporting me spiritually throughout writing this thesis. I would not be in the position where I am now without their love, encouragement and understanding.

the end

Feb. 2018 in Sapporo